ISTANBUL TECHNICAL UNIVERSITY ★ GRADUATE SCHOOL OF SCIENCE ENGINEERING AND TECHNOLOGY

HYDRODYNAMIC BEHAVIOUR OF DESALINATION BRINE DISCHARGES IN THE MARINE ENVIRONMENT

Ph.D. THESIS

Bilge BAŞ

Department of Coastal Sciences and Engineering

Coastal Sciences and Engineering Programme

FEBRUARY 2015

ISTANBUL TECHNICAL UNIVERSITY ★ GRADUATE SCHOOL OF SCIENCE ENGINEERING AND TECHNOLOGY

HYDRODYNAMIC BEHAVIOUR OF DESALINATION BRINE DISCHARGES IN THE MARINE ENVIRONMENT

Ph.D. THESIS

Bilge BAŞ
(517072005)

Department of Coastal Sciences and Engineering

Coastal Sciences and Engineering Programme

Thesis Advisor: Asst. Prof. Dr. Şafak N. ERTÜRK BOZKURTOĞLU
Co-advisor: Prof. Dr. M. Sedat KABDAŞLI

FEBRUARY 2015

İSTANBUL TEKNİK ÜNİVERSİTESİ ★ FEN BİLİMLERİ ENSTİTÜSÜ

YOĞUN ATIKSUYUN DENİZ ORTAMINDAKİ HİDRODİNAMİK DAVRANIŞININ İNCELENMESİ

DOKTORA TEZİ

Bilge BAŞ
(517072005)

Kıyı Bilimleri ve Mühendisliği Anabilim Dalı

Kıyı Bilimleri ve Mühendisliği Programı

Tez Danışmanı: Yrd. Doç. Dr. Şafak N. ERTÜRK BOZKURTOĞLU
Eş Danışman   : Prof. Dr. M. Sedat KABDAŞLI

ŞUBAT 2015

Bilge BAŞ, a **Ph.D.** student of ITU **Graduate School of Science Engineering and Technology** student ID **517072005**, successfully defended the **thesis/dissertation** entitled "**HYDRODYNAMIC BEHAVIOUR OF DESALINATION BRINE DISCHARGES IN THE MARINE ENVIRONMENT**", which she prepared after fulfilling the requirements specified in the associated legislations, before the jury whose signatures are below.

Thesis Advisor :	**Asst. Prof. Dr. Şafak N. ERTÜRK BOZKURTOĞLU** Istanbul Technical University	....
Co-advisor :	**Prof. Dr. M. Sedat KABDAŞLI** Istanbul Technical University	....
Jury Members :	**Prof. Dr. Cem AVCI** Boğaziçi University	....
	Assoc. Prof. Dr. Yeşim ÇELİKOĞLU Yıldız Technical University	....
	Asst. Prof. Dr. Necati Erdem ÜNAL Istanbul Technical University	....
	Prof. Dr. İzzet ÖZTÜRK Istanbul Technical University	....
	Prof. Dr. Cem GAZİOĞLU Istanbul University	....

Date of Submission : 25 December 2014
Date of Defense : 06 February 2015

To my family

&

to the memory of my grandmother and aunt

FOREWORD

As the first words of this thesis, I want to thank to supporters of this study and my life through the years.

Lastly, I would like to thank to Zeynep Çetecioğlu Gürol, Şeyma Çay Çınar and Çinel İşlek Güncü for their valuable friendship and existence in my life through the years.

TABLE OF CONTENTS

ABBREVIATIONS

2D   **:** 2 Dimensional
3D   **:** 3 Dimensional
ADV   **:** Acoustic Doppler Velocimeter
ED   **:** Electrodialysis
LDA   **:** Laser Doppler Anemometry
LIF   **:** Laser Induced Fluorescence
MED   **:** Multi Effect Distillation
MF   **:** Microfiltration
MSF   **:** Multistage Flash
NF   **:** Nanofiltration
NTU   **:** Nephelometric Turbidity Units
PIV   **:** Particle Image Velocimetry
RO   **:** Reverse Osmosis
SST   **:** Shear Stress Transport
SWRO   **:** Seawater Reverse Osmosis
UF   **:** Ultrafiltration
VC   **:** Vapor Compression
ZLD   **:** Zero Liquid Discharge

LIST OF SYMBOLS

A	: Wave amplitude
B_0	: Initial buoyancy flux
b_0	: Buoyancy flux per diffuser length
$b_{1/2}$	: Half-width
b	: Dense layer width
C	: Measured concentration of substance
C_0	: Effluent salt concentration
C_a	: Ambient salt concentration
C_T	: Temperature correction factor
c_g	: Group velocity
D_{dif}	: Diffusion coefficient
D	: Discharge port diameter
d	: Water depth
E	: Entrainment
E_w	: Total wave energy
F_d	: Densimetric Froude number
F_w	: Wave Froude number
g	: Gravitational acceleration
g_0'	: Reduced gravitational buoyancy
H_A	: Ambient water depth
H_{max}	: Maximum wave height
H_{mean}	: Mean wave height
H_{min}	: Minimum wave height
H_{rms}	: Root-mean-square wave height
H/L	: Wave steepness
H_s	: Ambient layer depth
h	: Layer thickness
h_0	: Distance of discharge port to the bottom
k	: Wave number
k_a	: Wave number corresponding to peak wave period
L	: Wave length
L_0	: Deep water wavelength
L_D	: Diffuser lengh
L_m	: Overall length scale
l_a	: Crossflow-stratification length scale
l_b	: Wave buoyancy length scale
$l_{b'}$	: Slot plume-stratification length scale
l_M	: Momentum-buoyancy length scale
l_m	: Wave momentum length scale
l_{m1}	: Slot jet-crossflow length scale
$l_{m'}$	: Slot jet-stratification length scale

$\mathbf{u'}, \mathbf{w'}$	**:** Velocity fluctuation
$\mathbf{V}$	**:** Volume
$\mathbf{w_e}$	**:** Entrainment velocity
$\mathbf{x,y,z}$	**:** Cartesian coordinates
$\mathbf{X}$	**:** Salinity
$\mathbf{X_0, Y_0}$	**:** Coordinates of discharge point
$\mathbf{X_b, Y_b}$	**:** Coordinates of bottom of the discharge line
$\mathbf{X_e}$	**:** Front position of dense layer
$\mathbf{X_i}$	**:** Location of the impingement point
$\mathbf{X_m}$	**:** Location of terminal rise
$\mathbf{X_n}$	**:** Length of near-field
$\mathbf{Y_c}$	**:** Vertical coordinate of bottom of the flume
$\mathbf{y_L}$	**:** Thickness of bottom layer
$\mathbf{Z_a}$	**:** Height of the mid-point between the free surface and jet orifice
$\mathbf{Z_m}$	**:** Maximum centerline rise height
$\mathbf{Z_t}$	**:** Maximum terminal rise height
$\mathbf{z_0}$	**:** Distance between the discharge point and the bottom
$\mathbf{Z_{max}}$	**:** Maximum visual rise
$\mathbf{Z_t}$	**:** Terminal rise height
β	**:** Buoyancy difference
β_g	**:** Expansion coeffcient of glass
$\varepsilon_x, \varepsilon_y, \varepsilon_z$	**:** Turbulent mixing coefficients
μ	**:** Dynamic viscosity
η	**:** Water surface elevation
η_0	**:** Water surface level at the discharge point
ρ	**:** Density of seawater
ρ_0	**:** Effluent density
ρ_a	**:** Ambient density
θ	**:** Jet inclination
θ_c	**:** Bottom slope
ν	**:** Kinematic viscosity

LIST OF TABLES

LIST OF FIGURES

xxiv

xxv

HYDRODYNAMIC BEHAVIOUR OF DESALINATION BRINE DISCHARGES IN THE MARINE ENVIRONMENT

SUMMARY

Brine is a dense effluent sourced from desalination plants that produce drinking and industrial water by seperating salt content of seawater or groundwater. Discharge of brine to the surface waters via outfalls is the most common method of brine disposal because of generally being the most feasible method.

In this study, hydrodynamic behaviour of brine discharges under regular wave effect was analysed experimentally in three different configurations.

In the first part of the experimental study, mixing of a stagnant salt layer with the effect of waves was considered. Measured vertical salinity profiles and calculations showed that the external wave energy added to the water column caused rising of potential energy which was observed in the form of thicker salt layers.

In the second part of the experimental study, a single port, horizontal brine discharge was taken into consideration. It was determined that the wave motion cause oscillation of discharged jet and shifted its impingement point to the bottom compared to stagnant ambient water. It was determined that discharge direction to wave propagation is an important parameter which effects shape, thickness and propagation speed.

In the third part of the experimental study, inclined dense jet ($45°$ ve $60°$) discharge was analysed under regular wave conditions. It was determined that wave motion affects terminal rise height and impingement point of dense jets. In addition, propagation rate of dense layer in transitional zone was under the effect of wave motion. It was determined that the wave motion contributed to the propagation with its horizontal velocity component. The results for stagnant ambient were confirmed this finding, too.

In addition to experimental studies, widely used entrainment models (CORMIX, UM3 and JETLAG) for brine discharges evaluated in the context of multiport brine discharges. It was determined that, mentioned models give meaningful results in the case of not merging jets with large port spaces between them. Otherwise, they are not compatible with experimental data.

Lastly, two simple programmes, that roughly simulate density current spreading, were developped as a pre-design tool.

YOĞUN ATIKSUYUN DENİZ ORTAMINDAKİ HİDRODİNAMİK DAVRANIŞININ İNCELENMESİ

ÖZET

20. yüzyılın ortalarında endüstriyel tuzdan arındırma Dünya'daki çeşitli ülkelerde uygulanmaya başlanmış ve bu tarihten itibaren başta Körfez ülkeleri olmak üzere bazı kurak ülkelerin kentsel, tarımsal ve endüstriyel faaliyetlerinin gelişiminde önemli bir faktör haline gelmiştir. Ülkemizde de bölgesel olarak içme ve kullanma suyu sıkıntıları yaşanmakta ve mevcut yüzey sularının arıtılarak kullanılması da bu sıkıntıları gidermek amacıyla uygulanmaktadır.

Tuzdan arındırma tesisleri özellikle kurak bölgeler için oldukça önemli olan su sorununu çözmeleri nedeniyle çevresel olarak zararlı olmadıkları izlenimini uyandırsalar da inşaat ve işletme aşamalarında çevreye önemli derecede olumsuz etkileri olan tesislerdir. Yakıt tüketimi, kullanılan kimyasallar, kıyı alanı kullanımı, görüntü ve gürültü kirliliği, atık üretimi ve hava ve su emisyonları bakımından bu tesisler ağır sanayi tesisleri olarak değerlendirilebilirler.

Tuzluluk oranı yüksek yüzey ve yeraltı sularının arıtılması işlemi sonucunda içerisinden suyu alınmış, daha yüksek tuzluluk oranına sahip ve dolayısıyla daha yoğun bir atıksu (brine) atık olarak ortaya çıkmaktadır.

Özellikle deniz suyunun tuzdan arındırılması sonucu oluşan yoğun atıksuyun denize deşarjı en az maliyetli yöntem olması nedeniyle tercih edilmektedir. Alındığı konuma yakın bir bölgeden sadece daha tuzlu olarak deşarj edilen deniz suyunun zararlı olmayacağı yaygın kanısına rağmen yoğun su deniz ortamında ciddi olumsuz etkilere yol açmaktadır. Deniz ortamına deşarj edilen yoğun atıksu, deniz suyu ile deşarj edilen yoğun su arasındaki yoğunluk farkı nedeniyle deniz tabanında bir tabaka oluşturur. Bu nedenle yoğun atıksu özellikle bentik organizmalar üzerinde etkilidir. Bu etkinin derecesi tesisin ve deşarj edilen tuzlu suyun özelliklerine, tesisin bulunduğu deniz alanının fiziksel özellikleri (batimetri, hidrodinamik özellikler, kıyının morfodinamik yapısı, vb.) ve biyolojik durumuna bağlıdır. Yoğun atıksu deşarjı yeterli karışımın olmadığı durumlarda sudaki çözünmüş oksijen seviyesinin azalmasına, kullanılan yönteme bağlı olarak deşarj noktası çevresinde su sıcaklığının artmasına ve ayrıca bulanıklığın artmasına neden olmaktadır.

Bu tez çalışmasında yoğun atıksuların deniz ortamındaki davranışı deneysel ve sayısal olarak farklı koşullar için incelenmiştir. Çok fazla olmamakla birlikte yoğun atıksuyun durgun su ve akış mevcut olan ortama deşarjı ile ilgili laboratuvar çalışmaları mevcuttur. Ancak literatürde dalga etkisi altında yapılmış laboratuvar çalışmaları oldukça azdır. Bu çalışmanın büyük kısmını, yoğun atıksuyun çeşitli konfigürasyonlardaki deşarjının düzenli dalga etkisi altındaki davranışı ile ilgili deneysel çalışma oluşturmakta olup, söz konusu çalışmalar üç ayrı kısımda gerçekleştirilmiştir.

Birinci kısım deneysel çalışmada, durgun haldeki bir tuzlu su tabakasının düzenli dalga etkisinde davranışı incelenmiştir. Dalga-tabaka etkileşiminin başlangıcında,

tuzlu su tabakası ile alıcı ortam ara yüzünün dalga etkisiyle dalga formunu aldığı ve daha sonra karıştığı belirlenmiştir. Uygulanan farklı deney süreleri sonucunda, deneyin başlangıcında oluşturulan tuzluluk tabakasının kanal içindeki düşey dağılımı tuzluluk probu kullanılarak ölçülmüştür. Elde edilen tuzluluk tabakası ölçümleri deney sonucunda tabakanın ulaştığı potansiyel enerji miktarının hesaplanmasında kullanılmıştır. Potansiyel enerjinin yanı sıra, deneylerde üretilen dalga enerjisi de hesaplanmıştır. Gerçekleştirilen deneysel çalışmada sisteme verilen dalga enerjisinin tabandaki tuzlu su tabakasının düşey yönde karışımına neden olduğu ortaya konulmuştur. Sınırlı sayıda gerçekleştirilen deneyler sonucunda, potansiyel enerjinin dalga enerjisine oranının dalga dikliği ile artan bir eğilime sahip olduğu da belirlenmiştir.

Gerçekleştirilen ikinci set deneylerde, yatay olarak tabandan belirli yükseklikte deşarj edilen bir yoğun atıksu jetinin dalga ile aynı ve zıt yönlerde deşarjını inceleyen deneyler gerçekleştirilmiştir. Söz konusu deneylerde, dalga hareketinin deşarj edilen jetin salınımına ve tabana etki noktasının lokasyonunu ötelediği belirlenmiştir. Deşarj edilen jet zamanla deney kanalının tabanında bir yoğun tabakanın oluşumuna neden olmuştur. Aynı çalışmada, deneyler sırasında kaydedilen video görüntülerinden alınan anlık görüntüler ERDAS görüntü işleme ve coğrafi bilgi sistemi kullanılarak RGB kümeleme yöntemi ile işlenmiştir. Görüntü işleme öncesinde AutoCAD programı kullanılarak resimler üzerindeki bilinen uzaklıklar kullanılarak ölçekleme işlemi gerçekleştirilmiş ve distorsiyonlar giderilmiştir. Görüntü işleme çalışması sonucunda deşarj edilen jetlerin alanları ve ilerleme hızları belirlenmiştir. Elde edilen ilerleme hızı değerleri incelendiğinde dalga ilerlemesine zıt olarak deşarj edilen yatay jetin aynı yöndeki deşarj durumuna göre daha hızlı ilerlediği belirlenmiştir. Tabanda yapılan tuzluluk ölçümleri dalga yönüne zıt yönde yapılan deşarjın seyrelme açısından daha avantajlı olduğunu göstermiştir. Ayrıca, karşılaştırma amacıyla yapılan durgun su şartlarındaki deneyler de dalga etkisinin seyrelmeye olumlu yöndeki etkisini bir kez daha ortaya koymuştur.

Literatürde durgun su koşulları için yapılan çalışmalarda alıcı ortama açılı olarak deşarj edilen yoğun atıksu jetleri ile daha yüksek seyrelme değerlerine ulaşıldığı gözlenmiştir. Bu nedenle, yapılan üçüncü kısım deneysel çalışmada 45° ve 60° açı ile deşarj edilen yoğun atıksuyun düzenli dalga koşullarındaki davranışı incelenmiştir. Deneylerde 4 farklı geçiş derinliği Stokes dalgası kullanılmıştır. Söz konusu deneylerde, dalga hareketinin jetin maksimum yükselme noktası ve etki noktasını etkilediği belirlenmiştir. Durgun suya yapılan deşarj ile en belirgin fark, dalga ortamındaki jetin maksimum noktasının dalga hareketi ile aynı fazda salınan dalgalarla yapılan deneyler, dalga yüksekliği azaldıkça jetin davranışının durgun ortamdaki davranışına benzer hale geldiğini göstermektedir. Ayrıca, dalga hareketinin deşarj noktasından hemen sonra jet yörüngesinde sapmaya neden olduğu da tespit edilmiştir. 60° deşarj açısı için bu davranış daha belirgindir.

Deney videolarından alınan anlık görüntüler iki farklı aşamada bu çalışma için yazılan MATLAB programı kullanılarak işlenmiş ve görüntülerden jet davranışı ile ilgili sayısal veri elde dilmiştir. Görüntü işleme çalışmasının birinci aşamasında jetin maksimum yükselme noktası (Z_t) ve jet etki noktası (X_i) ele alınan jet geometrik parametreleridir. Aynı zamanda, deşarj noktası ve jetin tepe noktası hizasındaki su yüzeyi değeri de yine görüntü işleme sırasında ölçülmüştür. Elde edilen maksimum yükselme noktası-zaman serisi grafikleri söz konusu parametrenin durgun ortamdan farklı olarak dalga hareketi etkisiyle belirli bir ortalama değer etrafında salındığını göstermiştir. Ayrıca, elde edilen su yüzeyi (η_0)-zaman serisi deşarj edilen yoğun jetin kanal içerisinde dalga ile aynı fazda ilerlediğini göstermiştir. 60° deşarj açısı ile

yapılan deneylerde elde edilen maksimum yükselme değerleri 45° deşarj açısı ile gerçekleştirilen deneylerdekinden daha yüksektir. Jet etki noktasının ölçümü görüntünün kanal tabanı kısmındaki renk yoğunluğu nedeniyle kesin olarak ölçülememiştir. Bu nedenle, ölçüm yapılabilen görüntülerde elde edilen değerlerin ortalaması veri olarak dikkate alınmıştır.

Jetin çarpma noktasından sonra yakın-alan ile uzak-alan arasındaki geçiş bölgesinde ilerlemesi de ikinci aşamada incelenen parametredir. Bu kısımda, ilerleyen yoğun tabakanın uç noktasının (X_e) konumu incelenen temel parametredir. Ayrıca, deşarj noktası ve tabakanın uç noktası hizasındaki su yüzeyi değeri de yine görüntü işleme sırasında ölçülmüştür. Görüntü işleme yöntemiyle belirlenen yoğunluk akıntısının uç noktasının zaman içerisindeki lokasyonu ile ilerleme hızları belirlenmiş ve dalga hareketinin yatay hızının ilerleme yönünde etkin olduğu belirlenmiştir. Maksimum yükselme noktasına benzer şekilde, ölçülen ilerleme ve su yüzeyi değerleri tabandaki yoğun tabakanın dalga ile aynı fazda ilerlediğini göstermiştir. Deneyler sırasında, yoğun jetin maksimum yükselme noktasında Vectrino II hız ölçüm cihazı kullanılarak hız ölçümü yapılmıştır. Bu yöntem ile elde edilen veri korelasyon değerine göre filtrelenmiş; bu işlemin ardından ise verideki gürültüyü gidermek için filtreleme işlemi yapılmıştır. Durgun ve dalganın mevcut olduğu koşullarda alınan hız ölçümleri, yatay ve düşey hız bileşenlerinin dalga hareketinden etkilendiğini ortaya koymuştur. Jetin karışım özelliklerinin ölçülmesinde oluşan ekipman sıkıntısı nedeniyle hız ölçümlerinin daha ileri işlenmesi gerçekleştirilmemiştir.

Çalışmanın sayısal kısmında, yoğun atıksuların yakın-alan yayılımının modellenmesinde kullanılan integral modellerinin (CORJET, UM3 ve JETLAG) çok noktalı deşarj sistemleri ile deşarj edilen yoğun atıksuyun modellenmesinde uygunlukları değerlendirilmiştir. Bu amaçla çeşitli yoğun atıksu deşarjı senaryoları oluşturulmuştur. Oluşturulan senaryolarda yoğun atıksu, alıcı ortam ve deşarj sistemi özelliklerinin tümü sabit tutulmuş, tek değişken parametre olarak deşarj noktaları arasındaki uzaklık (s) alınmıştır. Model sonuçlarını değerlendirmek için, literatürde yer alan deneysel bir çalışmada elde edilmiş olan ampirik denklemler kullanılmıştır. Bu amaçla aynı senaryo parametreleri için beklenen sonuçlar ampirik denklemleri kullanılarak hesaplanmış ve model sonuçları ile karşılaştırılmıştır. Etki noktası seyrelme değeri, etki noktası konumu and maksimum yükselme noktası karşılaştırma parametreleri olarak seçilmiştir. Yapılan çalışma sonucunda JETLAG modelinin çok noktalı deşarj sistemlerini tek noktalı deşarj sistemleri ile aynı şekilde modellediği görülmüştür. Bu nedenle sonuçlarda dikkate alınmamıştır. CORMIX ve UM3 modellerinin ise söz konusu modellerin yeterli deşarj noktası uzaklığında tek noktalı deşarj ile aynı şekilde modelleme yapabildiği belirlenmiştir. Deşarj noktaları arasındaki uzaklığın dar olup, jetlerin birleşmesi durumunda ise her üç model de deneysel çalışma ile uyumlu sonuçlar vermemektedir.

Yoğun atıksu başlangıç momentumu etkisini yitirdikten sonra uzak alanda ortam ile kendisi arasındaki yoğunluk farkı nedeniyle tabanda yoğunluk akıntısı şeklinde yayılmaktadır. Çalışmanın son kısmında, yoğunluk akıntılarının 2-boyutlu ve 3-boyutlu yayılımını uzaklık boyunca modelleyen iki program yazılmıştır. Programlar çeşitli kabuller ile basitleştirilmiş yoğunluk akıntılarını temsil eden denklemleri 4. derece Runge-Kutta metodunu kullanarak çözmektedir. Programda alıcı ortamdaki akıntı ve dalga koşulları, batimetri, vb. özellikler dikkate alınmamıştır. Bu nedenle, oluşturulan programlar oldukça kaba sonuçlar vermekte olup, deşarj sistemlerinin ön dizayn aşamasında oluşacak tabakanın özelliklerinin basitçe belirlenebilmesi amacıyla oluşturulmuştur. Ancak, daha ileri aşamada ileri modelleme teknikleri kullanılması gereklidir.

1. INTRODUCTION

1.1 Purpose of The Thesis

Desalination plants have an increasing usage worldwide due to rising water demand of increasing population and industry. Especially in arid areas, it is used as an effective method for water scarcity problems.

The main principle of desalination systems is separating the salt content of source water, which may be seawater or groundwater, from water content. At the end of the desalination process, remaining high salt content water is produced as wastewater that should be disposed. This wastewater is named as brine and its composition highly depends on the desalination method used and content of source water.

For the disposal of brine, most common method is marine disposal, which is generally the most feasible method to apply. Due to increasing number of coastal desalination plants, marine disposal of brine took attention of various studies, which are about different aspects of the topic such as brine dispersion in the marine environment, outfall structures, environmental impacts of brine on marine organisms and environmental legislations.

The purpose of this thesis is determining hydrodynamic characteristics of brine in the marine environment focusing on ambient wih water waves. In general, studies related to dense effluent discharges are about characteristics of them under stagnant ambient or currents. However, the number of studies analyzing effect of water waves is very few. With this study, it was aimed to contribute to literature data related to mixing of dense effluents under regular wave conditions through some experimental studies. Besides, some simple numerical studies executed about multiport discharges and far-field mixing of brine.

1.2 Context of The Thesis

Motivation for the study is to determine effect of water waves on behavior of dense effluents in the marine environment. By this aim, it was targeted to define this effect experimentally in the laboratory conditions with the help of deterministic parameters. In addition some other studies were executed related brine discharge modelling.

In this context, in Chapter 2, general information related to desalination technology, brine, its composition and disposal techniques is presented. After this, a summary of environmental impacts of seawater reverse osmosis plants (SWRO) plants are given.

In Chapter 3, main definitions related to the study are presented as a guide to the parameters used.

In Chapter 4, hydrodynamic behaviour of discharged dense effluents in near-field region was analysed mainly as two parts as the single port and multiport discharges of brine.

In Chapter 5, a brief literature review related to hydrodynamic behaviour of discharged dense effluents in the far-field region (gravity currents) is given.

In Chapter 6, experimental studies executed in this study are presented in three parts: Mixing of a salt layer with regular wave effect, horizontal discharge of dense jets and finally inclined discharge of dense jets.

In Chapter 7, two simple numerical modelling studies are presented. In this part, firstly applicability of the some commercial mixing zone models (CORMIX, UM3, JETLAG) for multiport brine discharges was evaluated. In the second part, a practical simulation tool prepared for far-field spreading of dense effluents is presented.

In Chapter 8, a general conclusion of this study and recommendations for future studies related to the topic are given.

2. DESALINATION PLANTS, BRINE AND ENVIRONMENTAL IMPACTS

2.1 Desalination Plants

Research and development studies related to application, costs of investment and processing has been executed since the beginnings of desalination industry. With these studies, different desalination systems were developed to produce water with required quality by using brackish water and seawater.

Main principle of these methodologies is the separation of dissolved material (salt, etc.) content in the feed water by using energy (Figure 2.1).
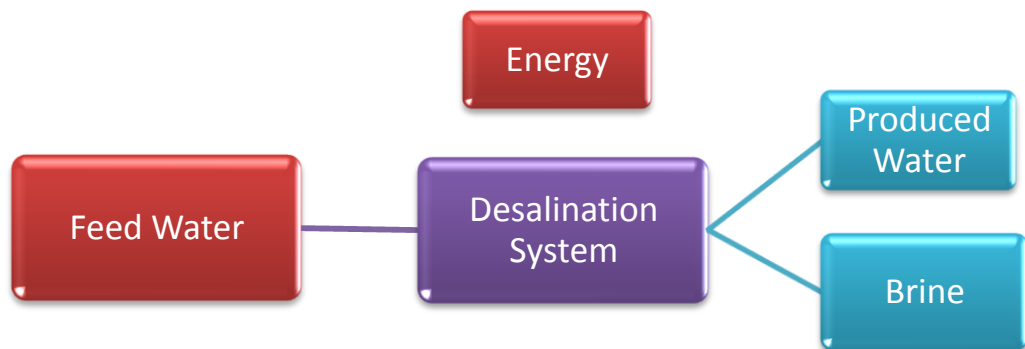
Figure 2.1 : Desalination systems.

In the following sections, a brief information will be given related to different desalination systems, which can mainly be classified as thermal and membrane systems. Later, a comparison of all systems mentioned will be given as a summary including features and worldwide construction ratios.

2.1.1 Thermal systems

Thermal systems were especially used at the inception of desalination industry before the invention of membrane technologies. These systems use thermal power for separation of dissolved materials from feed water by evaporation followed by distillation. Mostly known thermal desalination systems are Multistage Flash (MSF),

Multi Effect Distillation (MED) and Vapor Compression (VC) systems (Frenkel, 2010).

2.1.1.1 Multistage Flash (MSF) systems

MSF systems are constituted of vaporization and condensing units which are connected to each other. In these systems, feed water is heated under pressure prevents boiling before entering the first unit. In the first unit, some part of it is instantaneously boiled by cutting out the pressure and the vapour is sent to condensation unit to obtain desalinated water. The amount of evaporated water has a linear correlation with the temperature difference between process units. Remaining feed water is passed to the second unit where the same process repeats (Figure 2.2). MSF systems have 10-20% recovery ratios for seawater desalination (U.S. Department of the Interior, 2003).
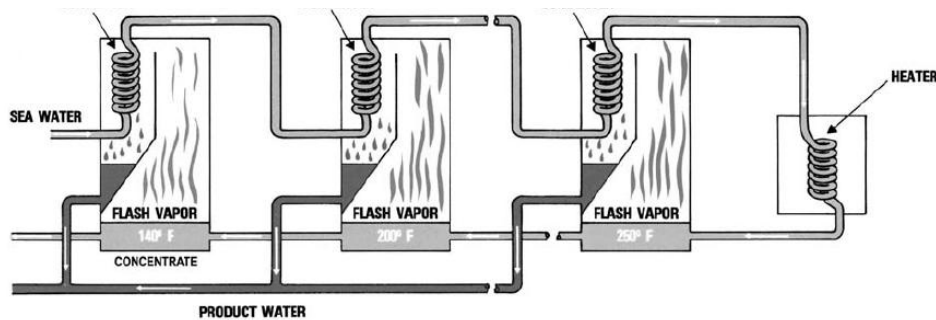
Figure 2.2 : Flow chart of a MSF system (U.S. Department of the Interior, 2003).

2.1.1.2 Multi effect distillation (MED) systems

Multi Effect Distillation (MED) systems are analogous to MSF systems except for their evaporation and heat transfer mechanism. In these systems, input water is sprayed on top of the tubes including vapour. Heat transfer between input water and vapour forms additional vapour which is also a heat source (Figure 2.3). The main advantage of these systems is lower operation temperature which also means lower energy and material costs (Rajagopalan, 2011).
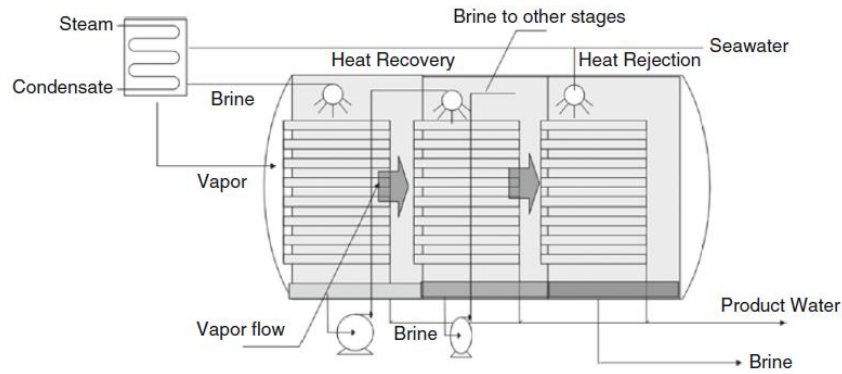
Figure 2.3 : Flow chart of a MED system (Rajagopalan, 2011).

2.1.1.3 Vapour Compression (VC) systems

By using vapour compression (VC) methodology, it is possible to desalinate seawater with recovery ratios of nearly 50%. VC systems can be examined in two groups depending on the compression mechanism used. In mechanical vapour compression (MVC) systems, compression is provided by the help of a compressor with electricity or diesel motor while the mechanism is producing vapour by heat transfer from compressed vapour in thermo-vapour compression (TVC) systems (Figure 2.4). Main operating principle of these systems is compression of vapour which becomes a heat source by the effect of compression and produced water at the end of the process. VC systems operate at 46.1-101.7 °C temperature range (U.S. Department of the Interior, 2003).
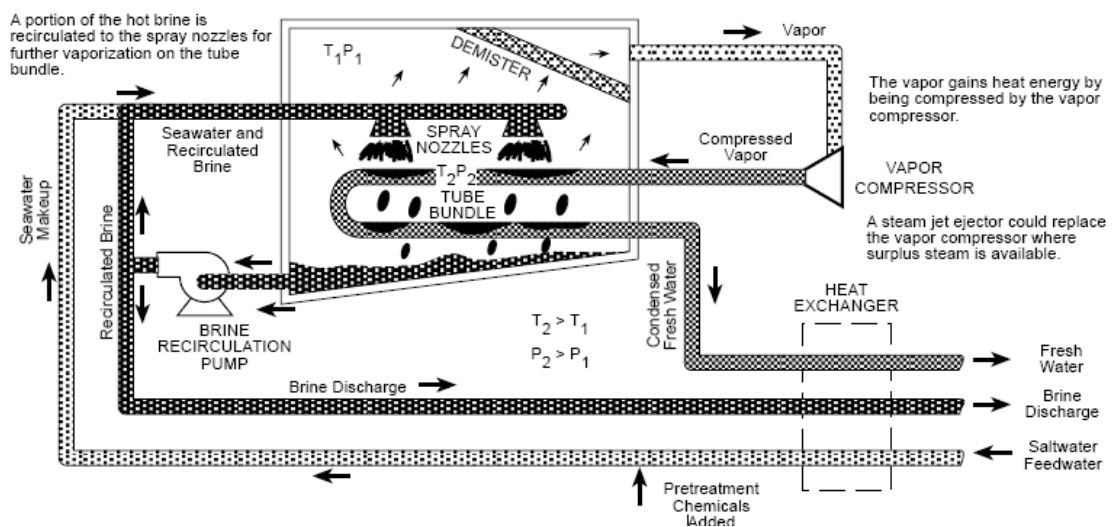
Figure 2.4 : Flow chart for vapour compression systems (Buros, 2000).

2.1.2 Membrane systems

In membrane systems, brackish water/ seawater is desalinated via a membrane system which separates salt content without any phase modification of intake water which means less energy consumption. This is one of the reasons of increasing use of membrane systems in desalination industry.

Membrane systems can be classified according to their pore sizes. Filtration ranges of membrane systems comparative with conventional filtration are presented in Figure 2.5. As the pore size decreases, target of membrane system decreases, too. As it can be seen in the figure, reverse osmosis is the most advanced filter system with the smallest pore size compared to other membrane systems. The values for pore sizes in this figure differ in some references which can be related to developing membrane industry and variation of membrane types. However, ranking is constant.
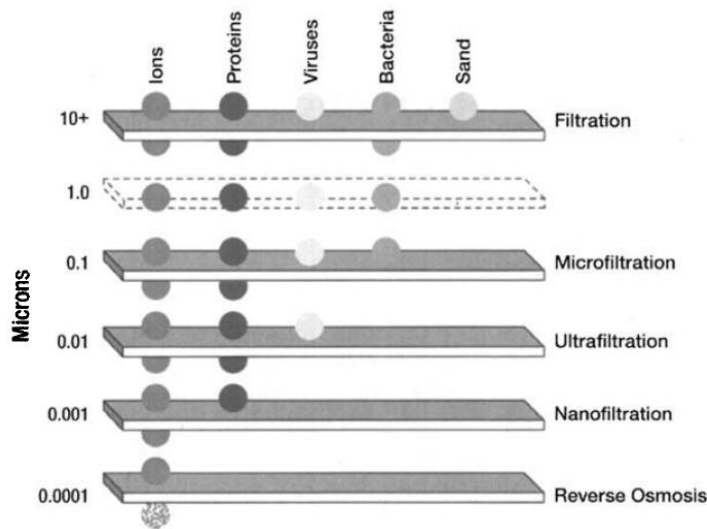
Figure 2.5 : Filtration ranges of membrane systems.

Efficiency of a membrane system can be measured by the term 'recovery rate, (R)' which is defined as the ratio of product flow rate (Q_P) to feed flow rate (Q_F) and concentrate flow rate (Q_C) (Ladewig & Asquith, 2012):

$$R = \frac{Q_P}{Q_F} = \frac{Q_P}{Q_C + Q_P} \qquad (2.1)$$

2.1.2.1 Reverse Osmosis (RO)

Reverse osmosis (RO) is based on separation of dissolved solids from water by using a semi-permeable membrane and applying pressure against natural osmotic pressure

(Figure 2.6). As the osmotic pressure increases with high total dissolved solids (TDS) content, the required pressure for these systems is higher for seawater desalination than for brackish water desalination. Operating pressure range is 680-4150 kPa for brackish water treatment and 5500-8250 kPa for seawater treatment (Kenna & Zander, 2000). While recovery rate for brackish water RO systems is 65-90%, this value is 40-65% for seawater RO systems due to the higher salt content of feed water (Voutchkov et al., 2011). In RO systems, the amount of energy required for production of 1 m^3 water from seawater is nearly 2.6-5.3 kWh which is higher for seawater with higher salinity concentration and lower temperature (AWWA, 2011).
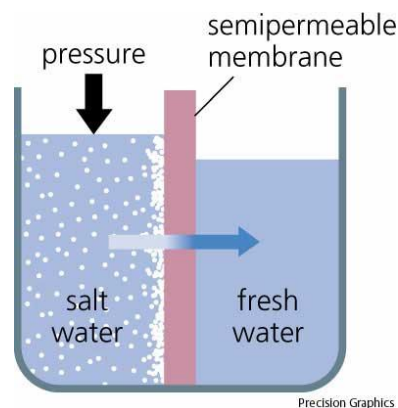
Figure 2.6 : Reverse osmosis (RO) process (Url-1).

2.1.2.2 Electrodialysis (ED) systems

Electrodialysis systems are the second most common membrane technology for desalination after RO systems. In ED systems, high voltage is used to separate anions & cations in the feed water through a membrane and derive desalinated water (Valero et al, 2011). This method is especially used for desalination of brackish water rather than seawater. It is feasible to use ED technology for brackish water including TDS concentration lower than 10000 mg/L due to the high cost of electricity used (U.S. Department of the Interior, 2003).

2.1.2.3 Microfiltration (MF) and Ultrafiltration (UF) systems

Microfiltration (MF) systems are used for removal of particles with dimensions of 0.1 to 0.5 microns while ultrafiltration (UF) is used for screening particles from 0.005 to 0.05 microns. These methods are low pressure systems and usually used as a pretreatment stage before other membrane systems such as RO and ED with an increasing amount of usage in desalination systems (Frenkel, 2010). Operating

pressure values are lower than 680 kPa for both of the systems. Recovery rates are 90-98% and 85-95% for MF and UF systems, respectively (Kenna & Zander, 2000).

2.1.2.4 Nanofiltration (NF) systems

Nanofiltration (NF) is also named as "membrane softening" due to removal of hardness and dissolved organic compounds removal. NF are high pressure systems which operates at 350-1050 kPa pressure range, lower than RO processes (Kenna & Zander, 2000). Its range of screening is from 0.0005 to 0.001 microns (Frenkel, 2010).

2.1.3 Comparison of different desalination technologies

In general, membrane systems are advantageous compared to thermal systems in several aspects. The major one is not using thermal energy to operate the system which reduces amount of used energy, fuel and related air pollutant emissions. Amount of fuel consumption for 1 m^3 desalted seawater is 1500 MJ at MSF systems and 37.5 MJ at RO systems. Again, for unit volume of water, 8.18 kg and 2.05 kg CO_2 produced at MSF and RO desalination plants, respectively (Darwish et al, 2013). The surface area required for construction of the desalination plant is also smaller for membrane systems compared to thermal ones. Membrane systems are consisted of non-metal and stainless steel parts and so the corrosion amount is considerably lower than corrosion rates of thermal systems. Another advantage of membrane systems is that formation of trihalomethanes, which are halogenated hydrocarbons from chlorination, is almost not observed during these processes despite it is an important impact of MSF systems (Lattemann & Höpner, 2008). In addition, chlorination load is very high at MSF systems which results in carcinogenic effects on marine organisms and very low at RO systems due to applied de-chlorination process (Darwish et al, 2013).

Whole of these advantages elucidate higher and increasing usage of membrane systems worldwide. As shown in Figure 2.7, ~60% of 16000 desalination plants worldwide are RO type desalination systems (IDA, 2012). Ratio of RO type desalination systems in Turkey is higher compared to worldwide distribution with 96.3% percentage (Figure 2.8) (IDA, 2011).
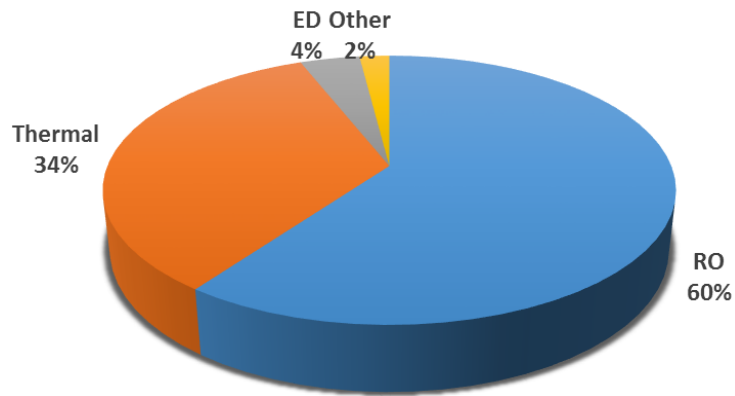
Figure 2.7 : Distribution of worldwide desalination plants according to type (IDA, 2012)
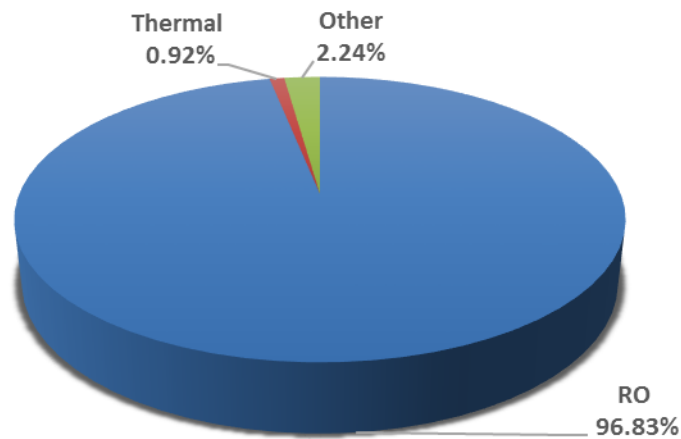
Figure 2.8 : Distribution of desalination plants in Turkey according to type (IDA, 2012).

2.2 Reverse Osmosis Systems

This section will be focusing on reverse osmosis (RO) systems with further details due to the reason being the fundamental issue of this study.

Main phases of a typical RO system is pretreatment of intake water (using biocide, coagulants, antiscaling, antifoaming chemicals), membrane process (treatment with membranes) and post treatment (aeration, degasification, pH adjustment, addition of corrosion control chemicals, fluoridation and disinfection). A simple flow chart of RO systems including main steps and material flow is presented in Figure 2.9 (AWWA, 2007; Lattemann, 2003). In Figure 2.10, a flow chart of a seawater reverse osmosis (SWRO) plant in Tampa Bay, Florida is also presented.
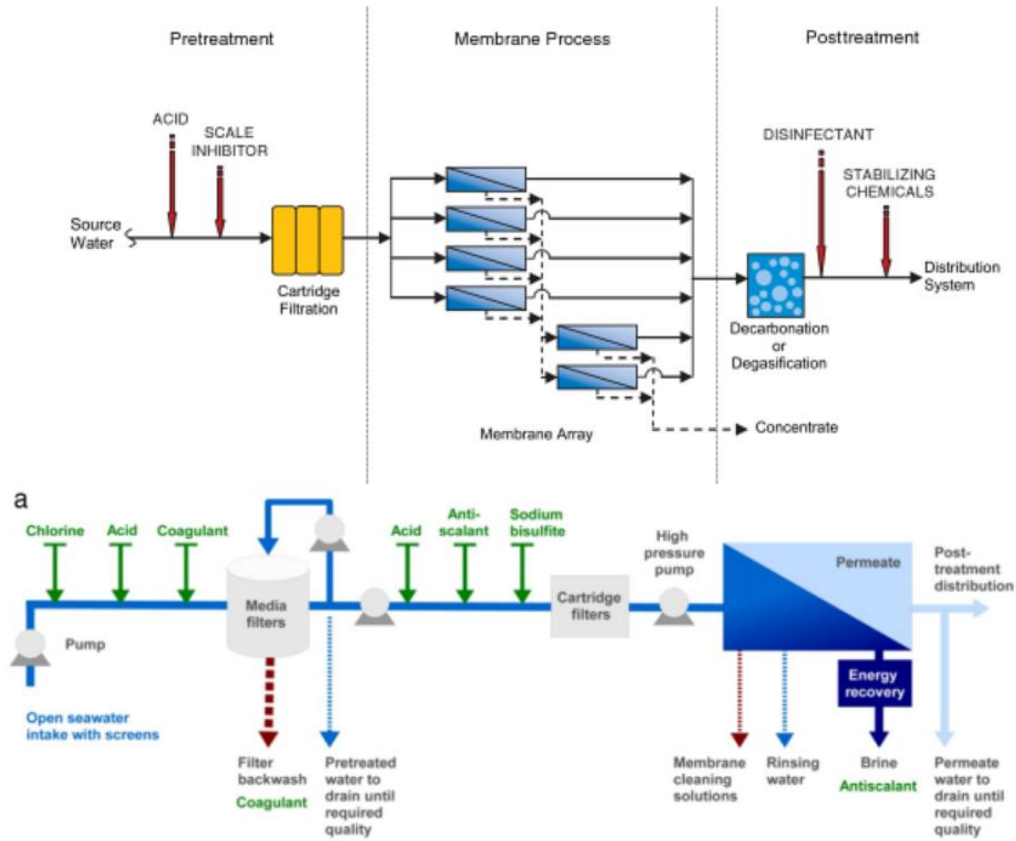
Figure 2.9 : Reverse osmosis (RO) flow chart (AWWA, 2007; Darwish et al., 2013).
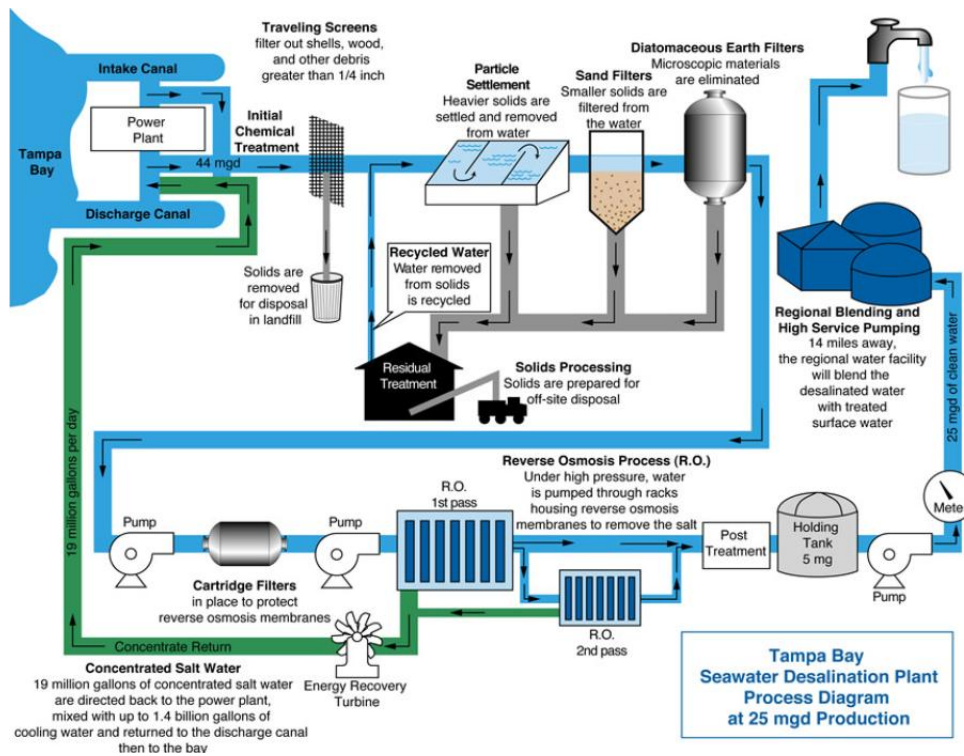
Figure 2.10 : Flow chart of a SWRO plant in Tampa Bay, Florida (Url-2).

2.2.1 Pre-treatment of intake water

Before reaching the membrane system, seawater is pre-treated by different methods depending on the raw water characteristics. Pre-treatment processes are vital for adequate operation and sustainability of RO systems.

By this way, undesired material in seawater such as dissolved solids, algae, etc. are eliminated. At the end of pre-treatment steps, seawater is conditioned in a form that is suitable for membrane process. In Table 2.1, limit values of parameters of seawater features for RO membranes are presented. Particulate, colloidal matter and micro-organisms have tendency of accumulating on RO membranes and prevent the process. In the table, The Silt Density Index (SDI) is a scale which is used for evaluation of fouling potential of seawater for membranes.

Table 2.1: Seawater quality requirement for RO systems (Gaid, 2011).

Parameter	Limit recommended up stream RO membrane
Iron	$<50 \mu g/L$
Manganese	$<20 \mu g/L$
Turbidity	<0.5 NTU
Suspended solids	<1 mg/L
SDI	<4 (95% of time)
Algae	<100 u/L
Chlorophyll	$<2 \mu g/L$
Organic substances (Dissolved Organic Carbon, DSO)	<2 mg/L
Hydrocarbons	<0.1 mg/L

Pre-treatment applications include screening, biocide addition, coagulation & flocculation and filtration processes each of serving removal of different parameters from feed water. In Figure 2.11, different options for pre-treatment steps are given. As it can be seen from the figure, the main difference is the type of filtration system which is applied following flocculation step (Gaid, 2011). In the following paragraphs, brief information will be given about each pre-treatment step.

Screening: As the first step, seawater enters the system through a screen which is capable of holding big materials.

Biocide addition: After screening of seawater, some chemicals added as a measure for biofouling which is the accumulation of microorganisms on membrane system, forming a bio-film mixed with suspended solids and corrosion products and making the system dysfunctional.

Coagulation and flocculation: Particulate, colloidal matter and micro-organisms have tendency of accumulating on RO membranes and prevent the process. In the case of desalinating seawater with high suspended solids, algae, organic matter and oil content only filtration is not enough to comply required quality for membrane system. In that case, coagulation& flocculation, which is a conventional chemical treatment process, and following filtration is applied by the aim of removing suspended materials in seawater (Gaid, 2011).
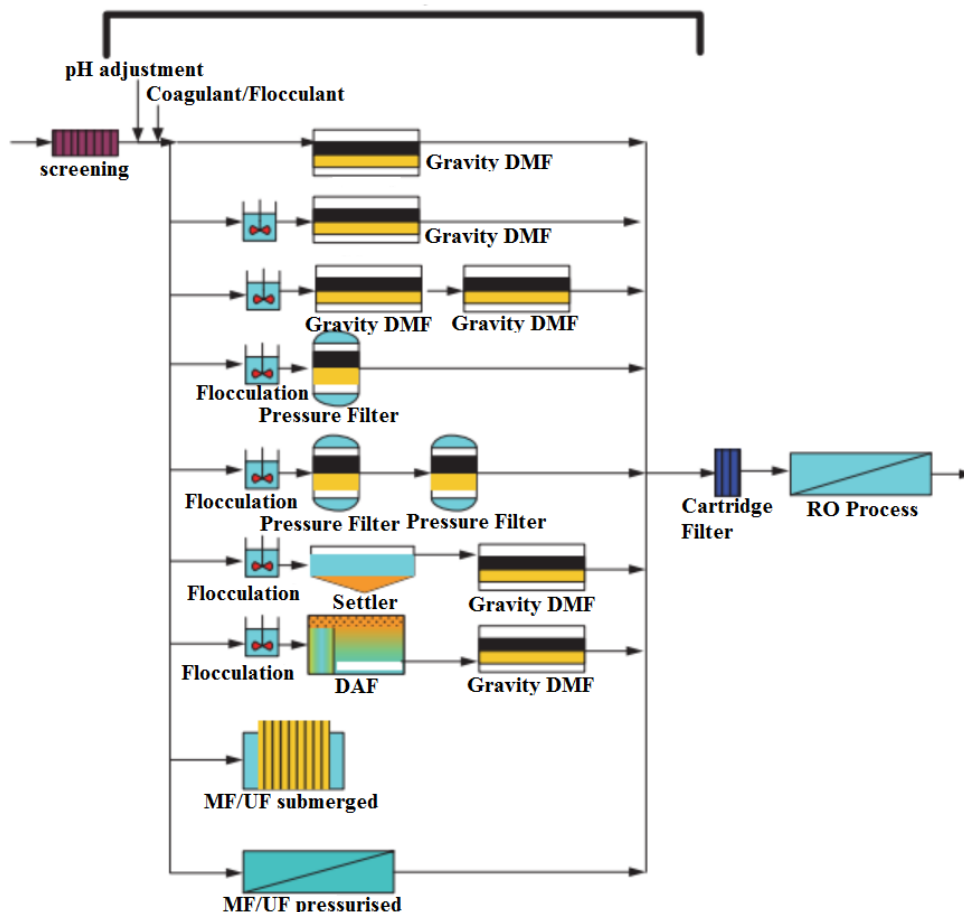
Figure 2.11 : Pre-treatment options for RO systems (Gaid, 2011).

Coagulation process is a water treatment process which includes adding chemicals (coagulants) which form coagulants in water and traps unwanted particles inside. Flocculation is a solid-liquid separation process during which coagulants are removed from seawater.

Filtration: Main purpose of filtration process is to separate particles which are bigger than 10 microns. If the seawater quality is good, pre-treatment step may only include filtration. In other case, media filtration is applied following coagulation & flocculation process. Media filters can be made of single media (sand) and dual

media (sand & anthracite) which are preffered for seawater having SDI values of lower than 10 and 25, respectively. Also, depending on the water quality, filtration can be executed in two stages. In some cases, ultrafiltration or nanofiltration can be used instead of media filtration (Figure 2.11) (Gaid, 2011). Usage of ultrafiltration and nanofiltration prior to seawater RO systems has increasing usage because of eliminating need of coagulation. However, cleaning and maintanence need of these systems are higher (Lattemann, 2010).

Other applications: In addition to applications above, antiscalants are added to the process as a measure for scale formation (Lattemann, 2003).

2.2.2 Membrane process

During the operation phase, RO membranes should be washed using some chemicals to prevent fouling problem due to silt and microorganisms. After cleaning, membranes are disinfected and rinsed with fresh water (Lattemann, 2010).

2.2.3 Post treatment

Treatment stages after feed water passed through membrane systems is called post treatment process which includes advanced treatment of desalted water and sometimes brine. Post treatment includes aeration, degasification, pH adjustment, addition of corrosion control chemicals, fluoridation and disinfection. Aeration and degasification are applied by the aim of removing unwanted gases as a final treatment step. Corrosion control products and alkaline chemicals are added to the permate water because produced water has potential of being corrosive due to including almost no minerals and so no alkalinity. In addition, disinfection chemicals and fluoridation is applied for providing disinfected water especially. Disinfection is obligatory with legislations in the case of permate would be use as municipial drinking water (Lattemann, 2003).

2.3 Brine and Its Composition

Brine is the concentrated waste stream sourced from desalination plants whose main characteristic is the high salinity content. After taking out of the water from feed water by using desalination systems and producing water of required quality, the remaining concentrated water arises as wastewater which should be disposed.

The characteristics of brine mainly depends on intake water features, recovery rate of the system, type of desalination process and type and amount of chemicals used. As stated before, recovery rates 30-70% for seawater RO systems and 65-90% for brackish water RO systems.

This section will be focusing on reverse osmosis (RO) systems with further details due to the reason being the fundamental issue of this study.

2.3.1 Chemical characteristics of brine

Main feature of brine is its high concentration of salts concentrated by the membrane system. Differences may be observed due to the chemicals added during pretreatment, membrane and post-treatment stages as mentioned before. Also, as well as chemicals, brine also can include organic materials and metals sourced from feed water. In addition, corrosion is another source of metal content of reverse osmosis brine.

2.3.1.1 Salinity

High salinity is the most distinctive feature of brine. At the end of the RO process, water with very low concentrations of dissolved solids and brine which has similar characteristics to the source water except added process chemicals and high dissolved solids content (1.2-3 times higher compared to source values) (Vanhems, 1992).

Salinity content of brine firstly depends on type of desalination system and content of feed water used.

Brine composition can be calculated by using feed water components and R of the system as below (Ladewig & Asquith, 2012):

$$TDS_{brine} = TDS_{feed\,water}\left(\frac{1}{1-R}\right) - \frac{R \times TDS_{produced\,water}}{100(1-R)} \qquad (2.2)$$

TDS$_{produced\,water}$ may be omitted in the equation and so the equation for calculating brine composition is:

$$TDS_{brine} = TDS_{feed\,water}\left(\frac{1}{1-R}\right) \qquad (2.3)$$

By using this equation, concentration factor (CF), which is a measure of concentration of brine, can be calculated as below:

$$CF = \frac{TDS_{feed\,water}}{TDS_{brine}} = \left(\frac{1}{1-R}\right) \qquad (2.4)$$

As it can be seen from the equations, higher recovery rates will ended up with more concentrated brine with smaller amounts.

In Table 2.2, feed water and brine composition values of a SWRO plant in Canary Islands are presented (Zimmerman, 1999). As it can be seen, brine with 63800 mg/L salinity value was produced from seawater with 38951 mg/L salinity. As TDS amount in brine increases, amount of hardness and conductivity also increases. In addition, CF for each parameter is presented at the same table.

Table 2.2: Seawater quality requirement for RO systems (Zimmerman, 1999).

Parameter	Seawater (mg/L)	Brine (mg/L)	Concentration Factor (CF)
Ca^{++}	962	1583	1.64
Mg^{++}	1021	1909	1.87
Na^{+}	11781	19346	1.64
K^{+}	514	830	1.61
NH_4^{+}	0.004	0.005	1.25
HCO_3^{-}	195	256	1.31
SO_4^{2-}	3.162	5.548	1.75
Cl^{-}	21312	43362	2.03
F^{-}	1.5	1.9	1.26
NO_3^{-}	2.6	4	1.54
PO_4^{-}	0.08	0.4	5
NO_2^{-}	0.03	0.05	1.67
Total Hardness ($CaCO_3$)	6600	11800	1.78
Total Salinity (TDS)	38951	63840	1.64
Fe^{+++}	0.04	0.05	1.25
Al^{+++}	0.001	0.007	7
pH	6.33	6.26	-
Conductivity (μS)	46200	75300	-

2.3.1.2 Dissolved oxygen (DO)

Because of high salinity concentration in brine, amount of dissolved oxygen (DO) is relatively low. In addition, dechlorination process causes lower DO values (Lattemann & Höpner, 2003).

2.3.1.3 pH

pH of brine depends on the chemicals and their amount used through desalination processes.

2.3.1.4 Chemicals

General overview of RO flow chart is presented in the previous chapter. Various chemicals are used through the reverse osmosis process and these chemicals are also included in brine generated as a waste. These chemicals vary in type and amount depending on feed water quality, system capacity and user preference. Generally, chemicals for RO systems can be classified as biocides, antiscalants, antifoulants and disinfectants. In addition, some corrosion products may be present (Figure 2.12). Also, membrane cleaning is executed using different chemical solutions.
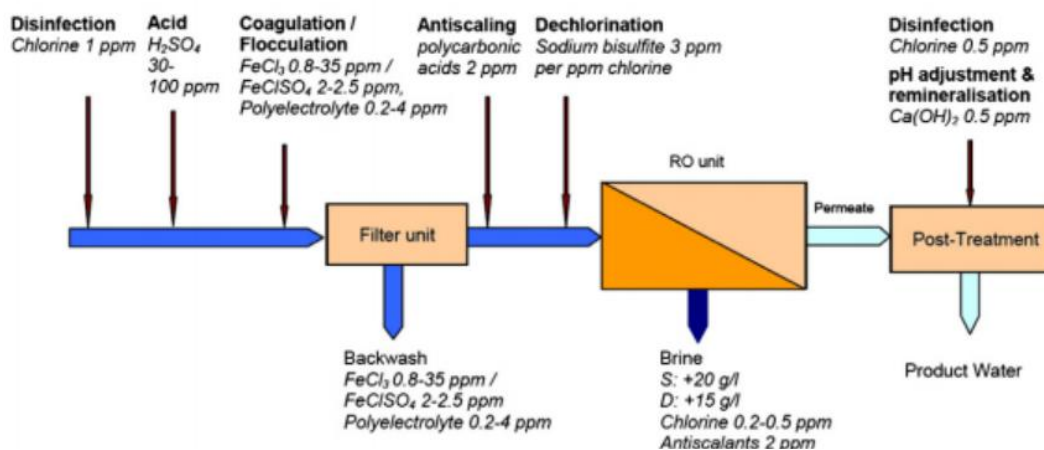
Figure 2.12 : Chemicals and dosages in RO systems (Darwish et al., 2013).

Biocides: Chlorine is the most common chemical which is used for preventing biofouling. Chlorine is harmful for RO membranes; so feed water is dechlorinated with using sodium bisulfite after chlorination. Due to this reason, amount of chlorine

in brine is very low (Lattemann, 2008). Other disinfectants which are used in RO plants are chloramine and copper sulphate (Lattemann & Höpner, 2003).

Coagulation and flocculation: Most common chemicals used for this process are ferric chloride ($FeCl_3$) and ferrous sulphate ($FeSO_4$) salts (Lattemann, 2008). Also, aluminium sulphate ($Al_2(SO_4)_3$), aluminium chlorohydrate (ACH) and polyaluminium chloride (PACl) are other chemicals being used (AWWA, 2007).

Efficiency of coagulant & flocculant salts are pH dependent and sulphuric acid and hydrochloric acid are used for pH adjustment (Lattemann, 2008).

In addition, various types of polyelectrolytes are used for enhancing the process and increasing treatment efficiency (Lattemann, 2008).

Amount of coagulants and polyelectrolytes depends on the suspended solid content of seawater which change in a range of <1 and 30 mg/L and 0.2-4 mg/L for coagulants and polyelectrolytes, respectively.

Membrane cleaning: Alkaline solutions are used for removing silt deposits and biofilms during membrane cleaning. Also, acidic solutions are used for metal oxides and scaling. In addition, various types of detergents or oxidants are used during cleaning process (Lattemann, 2008). Formaldehyde (with 5-10 ml/L recommended dosage of 0.5-1% solution), isothiazole (with 20 ppm recommended dosage of 1.5% solution), sodium dodecylbenzene sulfonate (recommended usage of 25% of cleaning solution), sodium dodecylsulfate (Na-DSS) (recommended dosage of 1.2 mg/L), ethylenediamine tetraacetic acid (EDTA) and sodium perborate are some of the cleaning agents used in this process (Lattemann, 2008).

After cleaning, membranes are disinfected by using chemicals (chlorine, hydrogen peroxide or formaldehyde) and rinsed with fresh water. This washing water includes whole cleaning chemicals and generally first wash water disposed to sewer, not into the brine. The residues from onward washings may be present (Lattemann, 2008).

Scale control: In RO type desalinaton systems, calcium carbonate formation is observed. Sulphuric or hydrochloric acid solutions and antiscalant chemicals are used for prevention. Polyphosphates (most widely Sodium hexametaphosphate, SHMP) widely used antiscalants in RO systems since early times of desalination industry. Also, polymer antiscalants (polycarboxylic acids, polyacrylics and others) began to be used by developing chemical industry (Lattemann and Höpner, 2003). Acid

solutions applied with 20-100 mg/L concentration to feed water while this value is 1-2 mg/L for antiscalant chemicals (Lattemann, 2008).

Corrosion products: In RO brine, iron, nickel, chromium and molybdenum can be present due to the corrosion. However, their amount is too low as trace materials because of using non-metal and stainless steel equipments in RO systems.

2.3.2 Physical characteristics of brine

As stated previously, characteristics of brine mainly depends on the type of desalination method used and its operational conditions besides intake water characteristics. Physical features of SWRO brine are presented below.

2.3.2.1 Temperature

RO is a membrane type desalination system and so the temperature of brine generated will be almost the same as intake water. Temperature difference between feed water and brine may be sourced from distant depths of intake and outfall structures.

2.3.2.2 Density

Due to high salt content, density of brine would be higher than feed water. Density values of brine can be calculated using different equations published. Due to being able to calculate for a wide range of salinity and temperature using just one equation, equation set of El-Dessouky and Ettouney (2002) was chosen to calculate density of brine in this study similar to Bleninger et al (2009). In the mentioned equation set, salinity and temperature are the input values to calculate density of seawater (ρ):

$$\rho = 10^3(A_1F_1 + A_2F_2 + A_3F_3 + A_4F_4) \tag{2.5}$$

$$B = ((2)(X)/1000 - 150)/150 \tag{2.6}$$

$$G_1 = 0.5 \tag{2.7}$$

$$G_2 = B \tag{2.8}$$

$$G_3 = 2B^2 - 1 \tag{2.9}$$

$$A_1 = 4.032219G_1 + 0.115313G_2 + 3.26 \times 10^{-4}G_3 \tag{2.10}$$

$$A_2 = -0.108199G_1 + 1.571 \times 10^{-3}G_2 - 4.23 \times 10^{-4}G_3 \tag{2.11}$$

$$A_3 = -0.012247G_1 + 1.74 \times 10^{-3}G_2 - 9 \times 10^{-6}G_3 \tag{2.12}$$

$$A_4 = 6.92 \times 10^{-4}G_1 - 8.7 \times 10^{-5}G_2 - 5.3 \times 10^{-5}G_3 \tag{2.13}$$

$$B = ((2)(T) - 200)/160 \tag{2.14}$$

$$F_1 = 0.5; \; F_2 = A; \; F_3 = 2A^2 - 1; \; F_4 = 4A^3 - 3A \tag{2.15}$$

Here, X is the salinity value (ppm) and T is the temperature (°C). Calculation method is valuable for 0≤X≤160000 ppm and 10≤T≤180°C.

In Table 2.3, an example of calculation results of brine for different temperature and salinity values are given. For the calculation, effluent temperature assumed same with the ambient water due to the fact that RO is an membrane process.

Table 2.3: Characteristics of brine for calculated according to El-Dessouky and Ettouney (2002).

Salinity (ppt)	Temperature (°C)	Density (kg/m³)	Kinematic Viscosity (m²/s)
70	20	1051.1	1.1121x10⁻⁶
70	15	1052.7	1.2529 x10⁻⁶
70	14	1053.0	1.2843 x10⁻⁶
70	13	1053.3	1.3170 x10⁻⁶
70	12	1053.5	1.3510 x10⁻⁶
70	11	1053.8	1.3864 x10⁻⁶
70	10	1054.1	1.4232 x10⁻⁶
69	15	1051.9	1.2505 x10⁻⁶
68	15	1051.2	1.2482 x10⁻⁶
67	15	1050.4	1.2460 x10⁻⁶
66	15	1049.6	1.2437 x10⁻⁶
65	15	1048.8	1.2414 x10⁻⁶
60	15	1045	1.2304 x10⁻⁶
60	15	1045	1.2304 x10⁻⁶

2.3.2.3 Viscosity

Effluent kinematic viscosity value can be calculated using the equation set below (El-Dessouky and Ettouney, 2002) related to dynamic viscosity (μ) calculation in which chosen salinity and temperature values were used:

$$\mu = (\mu_W)(\mu_R) \times 10^{-3} \tag{2.16}$$

$$Ln(\mu_W) = -3.79418 + 604.129/(139.18 + T) \tag{2.17}$$

$$\mu_R = 1 + AX + BX^2 \tag{2.18}$$

$$A = 1.474 \times 10^{-3} + 1.5 \times 10^{-5}T - 3.927 \times 10^{-8}T^2 \tag{2.19}$$

$$B = 1.0734 \times 10^{-5} - 8.5 \times 10^{-8}T + 2.23 \times 10^{-10}T^2 \tag{2.20}$$

$$v = \mu/\rho \tag{2.21}$$

Here, X is salinity value (gm/kg) and T is the temperature (°C). Calculation method is valuable for 0≤X≤130 gm/kg and 10≤T≤180°C.

In Table 2.3, an example of calculation results of brine for different temperature and salinity values is given.

2.3.2.4 Turbidity

Turbidity is a measure of amount of fine particulate matter in the water. Nephelometric Turbidity Units (NTU) is used as the measure of turbidity. Turbidity of brine is slightly higher than the feed water. Typical turbidity for SWRO systems given as 8 NTU for a 5 NTU feed water by Whiting (2012).

2.4 Brine Disposal Methods

Brine is a waste stream which should be disposed with the most appropriate methodology depending on various conditions. Location of desalination plant (coastal/inland), brine characterictics and amount affect the choice of brine disposal method. In addition, cost of disposal method is one of the most important parameters. Depending on the methodoloy chosen, brine disposal constitutes 5%-33% of total cost of desalination (Ahmed et al, 2001).

Surface water discharge, deep well injection, land application, evaporation ponds and zero liquid discharge (ZLD) techniques are the mostly used methodologies for disposing brine (Younos, 2005).

Usage of surface water discharge is the most common method for coastal desalination plants due to its feasibility. Direct discharge of brine to the surface waters at the shore is generally observed at the old desalination projects through where marine pollution accompanies (Einav, 2003). Submerged discharge of brine is more effective to obtain adequate rates of mixing (Jirka, 2008).

In Figure 2.13a, usage of brine disposal methods for municipal desalination systems in USA is given with graphics to give an idea of quantative distribution of methods. As it can be seen, surface discharge is the most common way of concentrate disposal for whole desalination methods used. The plants are categorized also according to their capacities and construction dates in Figures 2.13b and c, respectively.
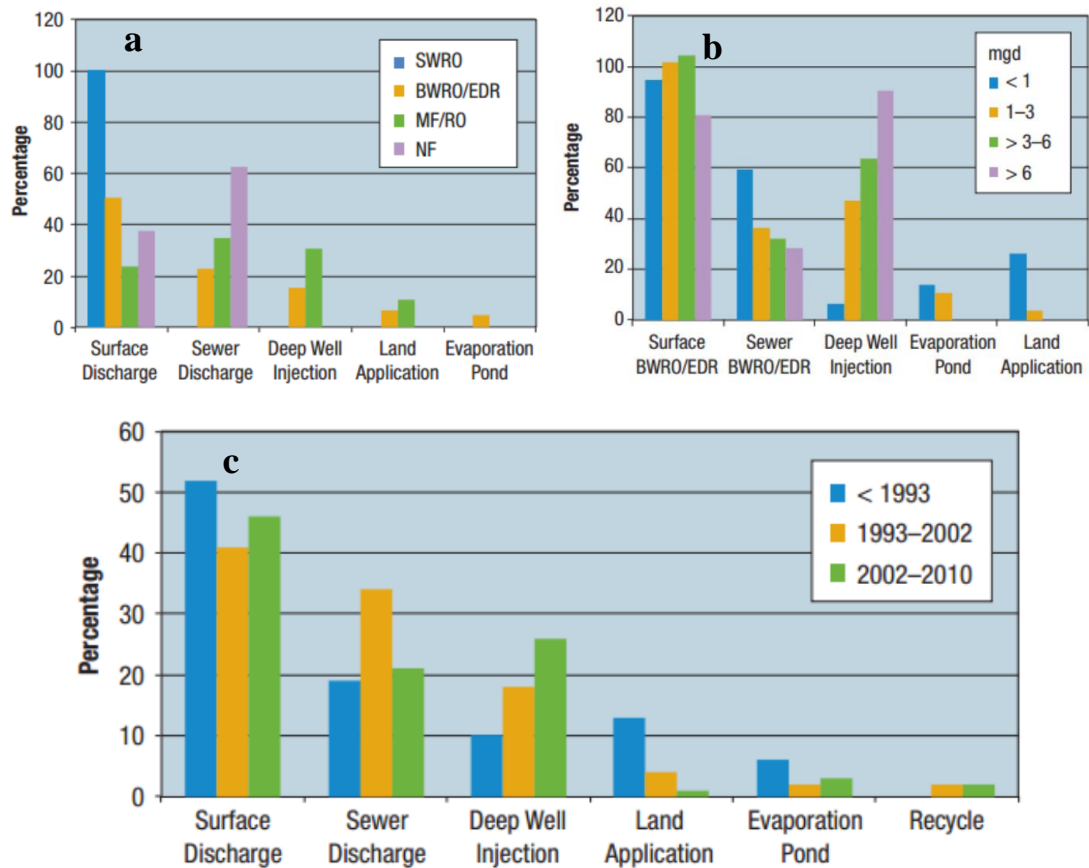
Figure 2.13 : Distributon of brine disposal methodologies of municipal desalination plants in USA according to a) type of membrane process used, b) capacity of plant, c) whole desalination methodologies (Mickley, 2012).

Some general information related to brine disposal methods is given below. Advantages and disadvantages of these methods are also given as a table which is adapted from SOL-BRINE Project Deliverable (2012) (Table 2.4).

Surface water discharge: The most common method of brine disposal is discharge to surface waters (freshwater, rivers and coastal waters) via outfalls. In addition to single discharge of brine, there are examples of combined discharge methods in which the brine is combined with other wastes such as direct discharge with an existing wastewater plant outfall, concentrate discharge into sewage system and discharge through an existing power plant outfall (Voutchkov, 2011).

Deep well injection: Deep well injection is pumping desalination brine into underground aquifers that are not used for drinking water. Due to the geological conditions, this method is not a very common one. Isolation of these aquifers is a very important concern due to the fact that it is possible to loose drinking water

sources in the case of leaks (Younos, 2005). This method is applied for large desalination plants (>1 mgd) due to economic feasibility (Sethi, 2006).

Land application: Land application which is not a very common method of brine disposal, is implemented by spray irrigation, infiltration trenches and percolation ponds (Younos, 2005). With this method, brine is reused in the areas where its high salinity does not cause negative impacts. The applicability of this method depends on land availability, salinity tolerance of existing plants, percolation capacity of the land and also groundwater standards (Sethi, 2006).

Evaporation Ponds: Evaporation ponds are used for disposal of desalination brine by evaporating it in a constructed pond where the salt content remains after the process. This method is applied in the regions with warm climate with high evaporation rates (Younos, 2005). Evaporation ponds are good alternatives for removal of brine sourced from inland desalination plants where it is not possible to dispose it into surface waters and in arid and semi-arid areas where there is high solar energy potential (Ahmed et al., 2000). These plants are used as industrial salt production facilities (Ravizky and Nadav, 2007).

Zero liquid discharge (ZLD) techniques: In these methods, brine is concentrated with different techniques and its phase is converted from liquid to solid. ZLD techniques are used as the last solution for brine disposal in the case of other methodologies cannot be applied due to their high cost and possible environmental impacts of solid waste disposal into landfills (Younos, 2005; Sethi 2006).

Near-zero liquid discharge (near ZLD): In this method, brine is concentrated by using heaters, deaerators and vapour compression techniques. It is converted into a slurry form (5% of produced brine) and remaining (95% of produced brine) is recovered as distillate water with <10 mg/L TDS content. The slurry part may be further concentrated as ZLD technique or converted into sludge in settling ponds (Younos, 2005).

Table 2.4: Advantages and disadvantages of brine disposal methods (SOL-BRINE, 2012).

Disposal Method	Advantages	Disadvantages
Direct surface water discharge	✓ Natural processes promote degradation ✓ Can accommodate large volumes ✓ Water body promotes dilution ✓ Low cost ✓ High dilution rates in the water body, possible dilution and blending with power plant discharge	− Dilution depends on local hydrodynamic conditions − Good knowledge, monitoring and planning programs of receiving waters are required Limited natural assimilation capacities cause adverse impacts on marine environment if exceeded − Thermal pollution, reduction of dissolved oxygen in receiving waters, eutrophication, toxicity, pH increase, damage of biota
Discharge to a sewage treatment plant	✓ Lowers the BOD of the resulting effluent ✓ Dilutes the brine concentrate ✓ Uses existing infrastructure	− Can inhibit bacterial growth − Can hamper the use of the treated sewage for irrigation due to the increase in TDS and salinity of the effluent − Overload the existing capacity of the sewage treatment plant while diminish its usable hydraulic capacity
Deep well injection	✓ Viable for inland plants with small volumes of brine ✓ No marine impact expected	− Cost efficient only for larger volumes − Needs a structurally isolated aquifer − Increases the salinity of groundwater
Land applications	✓ Can be used to irrigate salt tolerant species ✓ Viable for inland plants with small volumes of brine ✓ No marine impact expected	− Requires large areas of land − Suitable for smaller discharge flows − Can affect the existing vegetation − Can increase the salinity of groundwater and underlying soil − Storage and distribution system needed

Table 2.4 (continued) : Advantages and disadvantages of brine disposal methods (SOL-BRINE, 2012).

Disposal Method	Advantages	Disadvantages
Evaporation ponds	✓ A viable option for inland plants in highly arid regions ✓ Possible commercial salt exploitation ✓ No marine impact expected ✓ Low technological and managing efforts	– Expensive option – Risk of underlying soil and groundwater pollution – Needs dry climates with high evaporation rates – Requires large areas of land with a level terrain – Needs regular monitoring
Brine concentrators/Zero liquid Discharge	✓ Can produce zero liquid discharge ✓ Can commercially exploit concentrate ✓ Recovery of salt and minerals ✓ No marine impact expected	– Expensive – High energy consumption – Production of dry solid waste – precipitates
Mixing with the cooling water discharge	✓ Achieve dilution of both effluents prior to discharge ✓ Combined outfall reduces the cost and environmental impacts of building two outfalls ✓ Necessary to reduce salinity if disposing in fresh water bodies	– Dependent on the presence of a nearby thermal power plant
Mixing with the sewage treatment effluent	✓ Achieve dilution of brine effluent prior to discharge ✓ Does not overload the operational capacity of sewage treatment plant ✓ Use of existing infrastructure ✓ Necessary to reduce salinity if disposing in fresh water bodies	– The brine could enhance the aggregation and sedimentation of sewage particulates that can impact benthic organisms and interfere with the passage of light in the receiving water body

Except previously mentioned disposal methodologies of brine, there are also new developing techniques which aim minimizing brine amount, concentration of its content and also recovering some chemicals for reuse (El-Naas, 2011; Jibril and Ibrahim, 2001).

2.5 Environmental Impact of Desalination Plants and Brine Outfalls

Even they evoke the impression of being not harmful for the environment due to solving the water scarcity problem in arid regions, desalination plants have negative impacts for the environment during their construction and operation phases. These plants may be evaluated as heavy industrial plants due to fuel consumption, chemicals used, coastal area usage, visual and noise pollution, waste production and air and water emissions (Höpner and Windelberg, 1996).

Environmental impacts of desalination plants were analysed in different aspects in the literature. In this chapter, a summary of literature review will be presented focusing on impacts on the marine environment due to disposal of brine to the sea.

2.5.1 Marine environment

In this chapter, environmental impacts of desalination plants on the marine environment will be presented briefly under the titles of water quality, marine organisms and sediments.

2.5.1.1 Water quality

Discharged brine affects the water quality of the marine environment. The degree of mentioned effect is related to characteristics of outfall system (length, depth, distance of location from the shore, structure, etc.) and hydrodynamic features of the receiving environment besides chemical composition of the brine itself.

In the conditions of not adequate mixing, brine discharge causes increase in salinity and decrease in dissolved oxygen (DO) levels, increase in water temperature depending on desalination method used and also turbidity (Gleick et al., 2006; Raventos et al., 2006). For example, Tigne RO Plant outfall in Malta caused increase in salinity levels up to 58 psu by discharging brine with a 62‰ salinity content (Falzon and Gingeil, 1990).

In addition to salinity values, concentrations of chemicals in the contents of brine increase in the receiving environment. Dupavillon & Gillanders (2009) determined elevated amounts of Ba, Ca, K, Sr and Mg close to the desalination outfall in Point Lowly, Australia with their field study. Besides changing seawater quality, pollution of groundwater with the chemicals and cleaning agents is a possible environmental

effect of brine discharges in the case of reaching underlying aquifers (Ahmed et al., 2001).

2.5.1.2 Marine organisms

Discharged brine constitutes a dense layer at the sea bottom due to its negative buoyancy compared to seawater. Because of this reason, it is especially effective on benthic organisms. Degree of this impact depends on features of desalination plant, brine composition, physical (bathymetry, hydrodynamic properties, morphological structure of the coasts, etc) and biological characteristics of the marine environment (Fernández-Torquemeda et al., 2005). Effect of brine on marine organisms is mainly related to increasing salinity levels. While some of the species have the capability of living in high salinity conditions, some of them are negatively impacted or even can not survive. Especially organisms that are in the larvae stage, eggs or juveniles are more sensitive to salinity.

Besides the ecotoxicological effects of discharged brine, construction and existence of outfall structure also has negative effects for the marine environment. Placement of outfall system cause deterioration of marine organisms and entrainment of them into the discharged effluent (Gordon et al., 2012).

Studies on ecotoxicological impacts of discharged brine on marine organisms may be organized in two groups as laboratory salinity tolerance studies and field studies at the vicinity of brine outfallares and control areas. Most of these studies are about the effect of salinity but there are also studies concerning the effect of chemicals in brine content (Levy et al., 2007). Studies which are only directly related to impacts of brine are presented here due to the high number of studies investigating salinity tolerance in laboratory conditions.

Argyrou (1999) determined that the discharge of brine from Dhekelia and Larnaca SWRO plants in Republic of Cyprus caused damages to macrobenthic marine organisms especially at the discharge point (cited in WL│Delft Hydraulics et al., 2004).

Del-Pilar-Ruso et al., (2007) investigated effect of brine discharge on soft bottom infaunal communities in a desalination outfall area in Alicante, Spain. With this field study which continues in a two year period, they determined that salinity values of 39 ppt caused change in soft bottom communites (Polychaeta, Crustacea and

Mollusca to nematodes) at test points which are close to the outfall. At the same location, it was determined that the discharge was the source of decrease of abundance, richness and diversity of the soft bottom Polychaeta assemblage communities at the discharge point. Response of species was different to brine discharges as Ampharetidae, Nephtyidae and Spionidae were sensitive and Paraonidae was resistant species for brine (Del-Pilar-Ruso et al., 2009).

Riera et al. (2011) investigated effect of proximity of macrobenthic fauna to discharge point with a field study near Las Burras desalination plant, Gran Canaria. Analysis of collected samples, which are from 0, 15 and 30 m away from the discharge point, showed the different abundance, structure and diversity of examined species.

Yoon & Park (2011a) investigated ecotoxicological effects of brine on marine organisms of various trophic levels. According to this study, brine effect on marine organisms differs with some parameters such as adaptation capacity, exposure time, environments of inhabitation and origin of species, etc. The importance of site specific environmental monitoring before and after construction of brine outfalls was emphasized as the results of the executed experimental study.

Yoon and Park (2011b) executed marine bioassays of three phytoplankton, macroalgea, zooplankton and one fish species for discharges of Chuja Desalination Plant outfall in South Korea. The authors determined that chlorine and membrane cleaning materials caused higher acute toxicity levels rather than salinity. In general, determined limit salinity value for tested organisms was ~40 ppt. For chlorine concentration of 2.5 mg/L, olive flounder juvenile survival rate was 20% and this ratio increased to 100% for higher concentrations. For membrane cleaning solution concentrations of 19, 37.5, 75, 150, 300 mg/L survial rates were 80%, 100%, 80%, 40%, respectively.

Dupavillon and Gillanders (2009) investigated possible impacts of a planned desalination plant in Point Lowly, Spencer Gulf, Australia which is a semi-enclosed bay and spawning area of Australia cuttlefish (*Sepia apama*). In this context, existence of eggs of mentioned fish and water quality were determined at 9 points in the area. In addition, salinity tolerance of *Sepia apama* was tested in laboratory conditions. Spencer Gulf is an inverse estuary with natural high salinity values (about

40-43 psu). By this study, it was concluded that Australian cuttlefish could not tolerate high salinity and trace chemicals of brine. Salinity values of ~45‰ had effected number of embryos and caused perishing. For this reason and also considering effect of construction, it was decided that the outfall structure should be located according to locations of spawning and the study should be developed by analysing adult cuttlefish behaviour. Another observed negative impact is immigration of fish to offshore waters where their chances of living reduce due to increasing competition (Malcangio and Petrillo, 2011).

Seagrass reaction to hypersaline brine discharges was also studied in various field studies. *Posidonia oceanica* is a seagrass to the Mediterranean Sea which is protected with international (EU Legislation, 'Appendix I – Strictly protected flora species' of Berne Convention on the Conservation of European Wildlife and Natural Habitats 19.09.1979;   Barcelona Protocol Concerning Specially Protected Areas and Biological Diversity in the Mediterranean, 10.06.1995) and national legislations. It is listed in IUCN Red List as an endemic species (Url-3).

Fernández-Torquemada et al. (2005) presented a field study related to brine outfall of Alicante SWRO in Spain. During the study, spatial distribution of salinity on the surface and bottom, temperature and salinity profiles, density of echinoderms and division and mortality rates of *Posidonia oceanica* meadows were monitored to determine effects of brine discharge. For the first year of operation of the desalination plant, it was observed that brine discharge did not cause regression of meadows, however, affected the vitality of them negatively. Echinoderms, which are very sensitive to salinity changes are chosen as indicator due to this reason. They were totally vanished in the vicinity of the discharge point. They were still alive at the north of the desalination plant due to the flow conditions in the region.

In another study, effect of increasing salinity for survivor of *Posidonia oceanica* under effect of brine discharge was determined through laboratory and field tests (Latorre, 2005).

Gacia et al. (2007) made a 6-year survey on two Posidonia oceanica meadows whose location were chosen as one is exposing to outfall of a groundwater desalination plant and the other is not far away and not affected. Measurement which are executed two times a year (June and February) due to seasonal changes showed

the analysed species was very sensitive to brine discharges. The reason for this situation stated as high salinity ratios and eutrophication resourced from agricultural drainage water. The threshold value of salinity for *Posidonia oceanica* is determined as 39.3 psu.

Garrote-Moreno et al. (2014) made a controlled, one month field study during which they planted a seagrass species (*Cymodocea nodosa*) at four locations, of two are close to the discharge point and the others are control locations. Effect of brine discharge on the planted seagrass was observed in the form of decrease in growth, fewer number of leaves and mortality. In the same study, it was stated that this negative impact was higher during the tests conducted at higher temperature which is compatible with some previous studies (Fernández-Torquemada and Sánchez-Lizaso, 2011).

In some field studies, no negative impact of brine discharge observed on marine communities. Tomasko et al. (2000) did not detect any noticable effect of brine discharge on *Thalassia testudium*, which is a seagrass species, micro-epifauna, pelagic fish and corals. Talavera and Queseda-Ruiz (2001) investigated the situation of the marine area near a desalination outfall in Canary islands which is the habitat of seagrasses (*Cymodocea nodosa* and *Caulerpa prolifera*) on sandy seabeds. According to their observations, seegrass communities were in good condition and were not affected from brine discharge.

van der Merwe et al. (2014) examined physiology of Red Sea corals (*Fungia granulosa*) under increasing salinity conditions with an in-situ study ongoing 29 days. According to this study, it was found out that F. granulosa is a resistant species to salinity variation. The authors stated that the reason for this detection might be acclimation of the coral to high salinity values of Red Sea.

In Table 2.5, quantitative results of mentioned studies presented according to trophic level of marine organism analysed and threshold values of salinity.

Alkalinity of seawater is defined as total number of equivalents of calcium carbonate. In addition to existing studies, impact of increasing alkalinity due to discharge of brine on marine organisms needs to be elucidated with future studies (Danoun, 2007).

Table 2.5: Salinity threshold values for various marine organisms (adapted and modified from Bhpbilliton, 2009).

Common Name	Scientific Name	Response & Limit Value	Study Type	Source
Sea bream juvenile	Pagrus major	<45‰, no effect; 50‰, colour darkening after 30 minutes and 25% fatality after 24 hours; 70‰, lethal within 1 hour	Laboratory	Iso et al. (1994) (cited in Bhpbilliton, 2009)
Marbled flounder (eggs)	Pseudopleuronectes yokohamae	31-60 g/L, hatchability successful but delayed with increasing salinity; 70 g/l, hatchability 0%	Laboratory	
Marbled flounder (larvae)	Pseudopleuronectes yokohamae	<50 g/L, no observable effect; >50 g/L, lethal after six days; 60-100 g/L, number of dead larvae increased in shorter periods of time	Laboratory	
Littleneck Clams	*Venerupis (Ruditapes) philippinarium*	<50 g/L, no measurable effect; 60-70 g/L, impaired behaviour observed	Laboratory	
Seagrass	*Halophila johnsonii*	30 g/L, optimum growth; >40 g/L, reduced growth; >50 g/L, reduced photosynthetic activity; >60 g/L, increased mortality		Fernández -Torquemada et al. (2005)
Seagrass	*Posidonia oceanica*	39.3 psu		Gacia et al. (2007)
Seagrass	*Posidonia oceanica*	38.5 psu in more than 25% of measurements, 40 psu in more than 5% of measurements		Sánchez-Lizaso et al, (2008)
Australia cuttlefish	*Sepia apama*		Laboratory & Field	Dupavillon and Gillanders (2009)
Seagrass	*Zostera noltii*	41 psu		Fernandez-Torquemada and Sánchez-Lizaso (2006)
Seagrass	*Cymodocea nodosa*	39.5 psu in more than 25% of measurements, 41 psu in more than 5% of measurements		Spanish Ministry of Environment (cited in Palomar & Losada, 2011)
Seagrass	*Posidonia oceanica*	40 psu, mortality of 27% of the plants; 45 psu, mortality of 50% of the plants; 50 psu, mortality of 100% of the plants in 15 days; reduced growth rates for salinities higher than 38 psu	Laboratory & Field	Latorre (2005)

2.5.1.3 Sediments

Heavy metal concentration in the marine sediments is an important parameter affecting bioaccumulation in marine organisms. As stated before, various metals are included in RO brine such as iron, nickel, chromium and molybdenum. These metals accumulate in the sediment even if they are in low concentrations in the discharged brine and this causes negative impacts on marine organisms (Lattemann & Höpner, 2008).

Sadiq (2002) analysed 50 sediment samples from a marine area near a small scale desalination plant near Ras Tanajib Eastern Province, Saudi Arabia. According to the analysis results, it was found out that measured heavy metal concentrations (Mercury, Barium, Cadmium, Cobalt, Chromium, Copper, Iron, Manganese, Nickel, Phosphorus, Lead, Titanium, Vanadium, Zinc,) were higher for the samples which were taken close to the discharge point. With the prepared contour maps of concentrations, it was obvious that the most important effect was in the first 200 m distance from the discharge point but elevated values of heavy metals were visible in distances of kilometers following the plume movement.

Lin et al. (2011) executed a field study in Taiwan on sediment pollution sourced from desalination plant discharges. The authors detected that the concentrations of heavy metals, especially Cu and Zn, in marine sediments and bivalve samples are directly related to brine discharges.

2.5.2 Air quality

Desalination plants are the source of important amount of air pollution. The main air pollution source in RO plants are related to high amount of electric energy usage during the operation phase. Other usages of electricity include electric usage for manufacturing and transportation of the products and also construction of the plant in the project location (Lior, 2013). For a middle-sized RO plant (25000 m^3/day), energy demand is 5 kWh/m^3 which corresponds to 125,000 kW h/day consumption (Lattemann & Höpner, 2008). It was determined with an Life Cycle Assessment (LCA) study that the contribution of materials and disposal to greenhouse gases is 10% while operation phase takes the major role with 90% contribution (Raluy et al., 2006; Raluy et al., 2004). Produced amount of CO_2 and other greenhouse gases (as CO_2-e) are calculated in the range of 0.73-7.80 kg/m^3 and 0.98-1.31 kg/kWh CO_2-e

for various RO plant with different capacities (125000-2700000 m^3/d) and electricity usages (2.3-4.7 kWh/m^3) (Lior, 2013).

2.5.3 Noise pollution

Besides the noise generated during construction of the plant, SWRO plants cause noise pollution at their operation phases due to usage of high-pressure pumps and energy turbines. Due to the high level of noise, large desalination plants should be located far from residential areas. Also, mitigation methods for noise impact should be applied (Einav et al., 2002). Chavand and Evenden (2010) presented their study related to noise modelling of a large SWRO plant (150 billion litres of intake water a year) which was executed as a pre-construction study in Australia. In this study, possible noise impacts of the planned plant is modelled by using a software by taking into consideration of types and powers of the pumps used, buildings, background noise level measurements, topography and ground absorption effects and meteorological conditions. It was found out that estimated internal sound pressure levels varies between 76-101 dB(A) and plant would be capable of complying with the 37dB(A) limit noise level at the outside.

2.5.4 Coastal area usage and visual pollution

Large SWRO plants cause wide areas of coastal usage and also visual pollution in coastal areas (Figure 2.14). A large desalination plant with 100 million m^3/year capacity requires an area of ~4050 m^2. In addition, construction of these plants into coastal areas totally changes the function of coastal areas into industrial zones (Einav et al., 2002). Thus, they should be evaluated in detail through coastal zone management plants before taking decision of construction.

Figure 2.14 : Some photos of various SWRO plants from the world a) Barcelona desalination plant, Spain (Url-4), b) Perth desalination plant, Australia (Url-5), c) Southern Seawater Desalination Plant, Binningup WA (Url-6), d) Ashkelon desalination plant, Israel (Url-7).

3. DEFINITIONS AND GOVERNING EQUATIONS

In this chapter main definitions and governing equations and parameters related to near and far field spreading of discharged brine will be presented. Here, it is aimed to give an introduction to the topic before specific literature review.

3.1 Main Definitions

Receiving Water: Receiving water is the water body where the effluents are discharged. These waters may be rivers, lakes, estuaries or open coastal areas.

Effluent: A liquid or gaseous waste stream that flow outs from somewhere.

Concentration: Concentration is the amount of a substance in a mixture which has the dimension of mass divided by volume such as mg/L, kg/m^3, µg/L, mol/L, etc.

Salinity: It is the amount of dissolved solids in seawater.

Dilution: Decrease of concentration of a substance in a mixture. Dilution (S) of a pollutant in a water body may be defined with the equation below where C_a is the ambient concentration, C_0 is the effluent concentration and C is the is the measured concentration of the substance considered (Fischer et al., 1979):

$$S = \frac{C_0 - C_a}{C - C_a} \qquad (3.1)$$

Jet: Flows that are driven by only momentum fluxes.

Plume: Flows that are driven by only buoyancy fluxes.

Buoyant jet: Flows that are driven by both of momentum and buoyancy fluxes.

Near-field region: The region where the initial momentum is the preaviling parameter for the mixing processes.

Far-field region: The region where the receiving environment features are effective on the mixing processes.

Transition region: The region where the receiving environment features are effective on the mixing processes.

Densimetric Froude number (F_d): It is the ratio of inertial forces to buoyancy forces.

Reynolds number (Re): Reynolds number (Re) is the ratio of inertial forces to viscous forces in a flow and it is used for classifying the flow regime as laminar or turbulent.

Gravity (density) current: It is a horizontal flow which is driven by density difference.

Entrainment: Entrainment is entering of ambient flow into the gravity current by generated shear at density interface and bottom effect.

Dispersion: It is the scattering of particles by the combined effect of shear and transverse diffusion.

3.2 Mixing and Transport Processes and Main Equations Governing Brine Discharge

In this part, a brief information related to mixing and transport mechanisms will be given containing main equations. For modelling brine discharges, some assumptions are made to simplfy analyzing the flow behavior: Incompressible flow, Reynolds decomposition, Boussinesq approximation, various turbulence closure models (Boussinesq turbulent viscosity theory, k-ε turbulence closure, etc.) and neglection of molecular diffusion (Palomar and Losada, 2011).

Molecular diffusion: Despite molecular diffusion is neglected in most of studies related to mixing of dense effluents, it will explained here because of being the main concept of mixing and transport. Molecular diffusion is the scattering of particles or a cloud of pollutants by random motions which are governed by material properties such as type, temperature, etc. from high concentration regions to lower concentration regions. Fick's law of diffusion (Fischer et al., 1979) defines molecular diffusion (Fischer et al., 1979):

$$q = -D_{dif}\nabla C \qquad\qquad (3.2)$$

$$q = -D_{dif}\left(\frac{\partial C}{\partial x} + \frac{\partial C}{\partial y} + \frac{\partial C}{\partial z}\right) \qquad \text{(3.3)}$$

Here, q is the solute mass flux vector with the components in three dimensions (q_x, q_y, q_z); C is the concentration and D_{dif} is the diffusion coefficient. D_{dif} is generally order of 2.10^{-9} m^2/s for water solutions (Socolofsky and Jirka, 2005).

By using Fick's law, diffusion eqution in three dimensions can be defined with Eq. 3.4 in vector notation and Eq. 3.5 in Cartesian coordinates (Fischer et al., 1979):

$$\frac{\partial C}{\partial t} = D_{dif}\nabla^2 C \qquad \text{(3.4)}$$

$$\frac{\partial C}{\partial t} = D_{dif}\left(\frac{\partial^2 C}{\partial x^2} + \frac{\partial^2 C}{\partial xy^2} + \frac{\partial^2 C}{\partial z^2}\right) \qquad \text{(3.5)}$$

Other mixing mechanisms may be explained by using the same analogy with diffusion equation.

Equation of continuity: Flow rate into a control volume must be equal to the flow rate of the outflow that is defined by continuity equation. Continuity equation is given with the following equations in vector notation (Eq. 3.6) and in Cartesian coordinates (Eq. 3.7) (Fischer et al., 1979):

$$\frac{\partial \rho}{\partial t} + \nabla(\rho V) = 0 \qquad \text{(3.6)}$$

$$\left(\frac{\partial \rho}{\partial t} + \frac{\partial \rho u}{\partial x} + \frac{\partial \rho v}{\partial y} + \frac{\partial \rho w}{\partial z}\right) = 0 \qquad \text{(3.7)}$$

Equation of conservation of momentum: Conservation of momentum equation is based on Newton's second law of motion. It is stated in vector notation (Eq. 3.8) and in Cartesian coordinates (Eq. 3.9-11) (Fischer et al., 1979):

$$\frac{\partial V}{\partial t} + (V.\nabla)V = \rho g - \frac{1}{\rho}\nabla p + \upsilon\nabla^2 V \qquad \text{(3.8)}$$

$$\rho\left(\frac{\partial u}{\partial t} + u\frac{\partial u}{\partial x} + v\frac{\partial u}{\partial y} + w\frac{\partial u}{\partial z}\right)$$
$$= -\frac{\partial p}{\partial x} + \rho g_x + \mu\left(\frac{\partial^2 u}{\partial x^2} + \frac{\partial^2 u}{\partial y^2} + \frac{\partial^2 u}{\partial z^2}\right) \qquad \text{(3.9)}$$

$$\rho\left(\frac{\partial v}{\partial t} + u\frac{\partial v}{\partial x} + v\frac{\partial v}{\partial y} + w\frac{\partial v}{\partial z}\right)$$
$$= -\frac{\partial p}{\partial y} + \rho g_y + \mu\left(\frac{\partial^2 v}{\partial x^2} + \frac{\partial^2 v}{\partial y^2} + \frac{\partial^2 v}{\partial z^2}\right) \qquad \text{(3.10)}$$

$$\rho \left(\frac{\partial w}{\partial t} + u \frac{\partial w}{\partial x} + v \frac{\partial w}{\partial y} + w \frac{\partial w}{\partial z} \right)$$
$$= -\frac{\partial p}{\partial z} + \rho g_z + \mu \left(\frac{\partial^2 w}{\partial x^2} + \frac{\partial^2 w}{\partial y^2} + \frac{\partial^2 w}{\partial z^2} \right) \tag{3.11}$$

Advection: Transport of particles or a pollutant cloud due to mean motion of the fluid flow. In the nature, advection and diffusion occurs simultaneously. If two components analyzed separately, total rate of mass transport (flux) (q) through a unit area can be defined with Eq. 3.12 (Fischer et al., 1979):

$$q = uC + \left(-D_{dif} \frac{\partial C}{\partial x} \right) \tag{3.12}$$

If this definition is placed into continuity equation, it takes the form of 'advection-diffusion equations as below (Fischer et al., 1979):

$$\frac{\partial C}{\partial t} + \frac{\partial}{\partial x} (\nabla u C) = D_{dif} \nabla^2 C \tag{3.13}$$

$$\frac{\partial C}{\partial t} + u \frac{\partial C}{\partial x} + v \frac{\partial C}{\partial y} + w \frac{\partial C}{\partial z} = D_{dif} \left[\frac{\partial^2 C}{\partial x^2} + \frac{\partial^2 C}{\partial y^2} + \frac{\partial^2 C}{\partial z^2} \right] \tag{3.14}$$

Turbulent diffusion: Turbulent diffusion is the scattering of particles or a cloud of pollutants by turbulence properties. Previously given advection-diffusion equation is defined for laminar flow conditions. Transport equation under turbulent flow conditions is defined as below considering turbulence parameters (Fischer et al., 1979):

$$\frac{\partial C}{\partial t} + u \nabla C = \nabla(\varepsilon \nabla C) \tag{3.15}$$

$$\frac{\partial C}{\partial t} + u \frac{\partial C}{\partial x} + v \frac{\partial C}{\partial y} + w \frac{\partial C}{\partial z}$$
$$= \frac{\partial}{\partial x} \left(\varepsilon_x \frac{\partial C}{\partial x} \right) + \frac{\partial}{\partial y} \left(\varepsilon_y \frac{\partial C}{\partial y} \right) + \frac{\partial}{\partial z} \left(\varepsilon_z \frac{\partial C}{\partial z} \right) \tag{3.16}$$

where $\varepsilon_x, \varepsilon_y, \varepsilon_z$ are turbulent mixing coefficients analogous to diffusion coefficient. Turbulent mixing coefficients are higher than molecular diffusion coefficients.

Equation of state: Equation of state is the equation which defines density of an incompressible fluid in terms of salinity, temperature and pressure. For seawater , it

is defined as below by UNESCO (1981) where S is the salinity (psu) and T is the temperature (°C):

$$\rho(T,S) = 999.842594 + 6.793952 \cdot 10^{-2}T - 9.09529 \cdot 10^{-3}T^2 - 1.120083 \cdot 10^{-6}T^4 + 6.536332 \cdot 10^{-9}T^5 + (0.824493 - 4.0899 \cdot 10^{-3}T + 7.6438 \cdot 10^{-5}T^2 - 8.2467 \cdot 10^{-7}T^3 + 5.3875 \cdot 10^{-9}T^4)S + (-5.72466 \cdot 10^{-3} + 1.0227 \cdot 10^{-4}T - 1.6546 \cdot 10^{-6}T^2)S^{1.5} + 4.8314 \cdot 10^{-4}S^2$$

(3.17)

4. HYDRODYNAMIC BEHAVIOUR OF DISCHARGED DENSE EFFLUENTS IN THE MARINE ENVIRONMENT

A discharged dense jet moves towards the sea bottom due to its high density compared to the receiving environment. After impinging to the sea bottom, it constitutes a dense layer and goes forward (Younos, 2005; Ruiz-Mateo et al., 2008) (Figure 4.1). Discharged brine causes turbulence formation and undergoes mixing due to its kinetic energy even if the receiving water is stagnant (near-field).
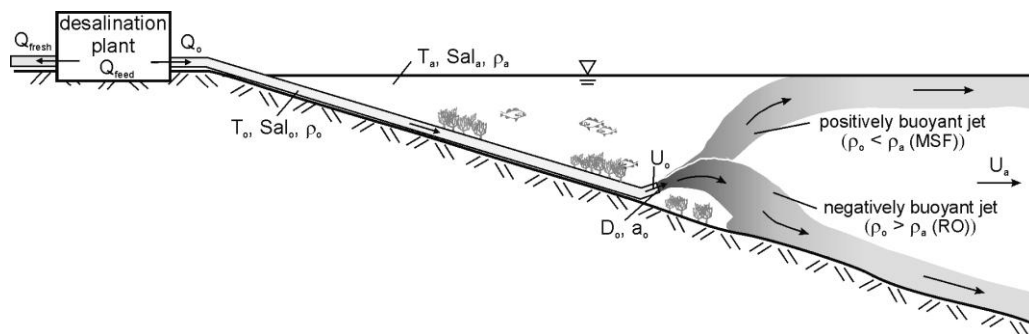
Figure 4.1 : Hydrodynamic behaviour of brine in the marine environment (Url-8).

Hydrodynamic behaviour of brine can be analysed mainly in two regions as near-field and far-field region, respectively. In the near-field region, initial conditions are effective on behaviour of discharged jet such as initial momentum and buoyancy and discharge system geometry. In addition, if the discharge is distant from the sea bottom, existing potential energy contributes to the mixing. The degree of first mixing increases with kinetic energy, surface area of receiving water and also with kinetic energy of discharged brine.

In the far-field region, receiving environment conditions dominates the fluid behaviour such as currents, waves, bottom topography, etc. The region between near-field and far-field regions is called the intermediate field where both initial and environmental factors are effective. Whole of these mentioned regions have different time and spatial scales and flow behavior (Figure 4.2).
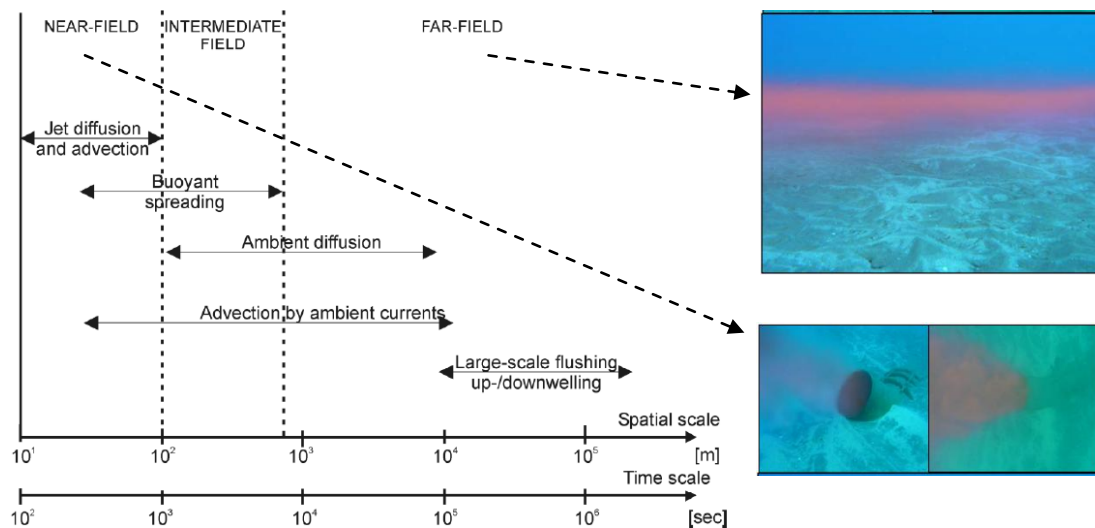
Figure 4.2 : Temporal and spatial scales for mixing processes (Fischer et al., 1979). (Photos are from a dye study for a brine outfall in Maspolamas beach, (Palomar and Losada, 2011)).

In far field region, discharged brine constitutes a dense layer that spreads following the bathymetry. Far field region can be defined as the region where receiving environment characteristics are predominant and the initial conditions are not effective on the mixing (Vaselali and Vaselali, 2009; Url-8). As the flow develops, the width of the discharged brine expands due to spreading and loses its thickness. After that, a transitional zone forms between the dense layer and the receiving environment. Under the transition layer, a dense layer lies down conserving its characteristics such as salinity, temperature, density, etc. until its disappearance. In the case of a stratified receiving environment and the brine layer is in a layer with the same density itself, it leaves the bottom and move ahead horizontally as an interflow (Ruiz-Mateo et al., 2008).

Besides near-field characteristics, content and dimensions of brine plume spreading in far-field region were the main interest of various studies especially for determining impact of outfalls in the marine environment. These studies were executed as measurement of salinity and temperature values at different distances from the outfall to determine extent of the plume and its ultimate concentration values. These types of studies are very helpful for case specific evaluation of environmental impacts besides being a guideline for the future studies.

In Table 4.1, a summary of some field studies related to brine discharges is given. As it can be seen from the table, discharged brine spreads in distances of hundreds of

meters or kilometers away form the discharge point. During this spreading, salinity difference reduces to 2 ppt, 1 ppt and 0.5 ppt above receiving environment salinity values as it propagates on the sea bottom.

Table 4.1 : Extent and intensity of brine plumes in receiving water surrounding desalination plant outfalls (adapted and modified from Roberts et al., 2010).

Author	Capacity (ML/d)	Discharge (ML/d)	Salinity of Brine (ppt)	Location	Habitat	Plume extension and intensity
Abdul-Wahab, 2007	92.4	NR	37.3	Muscat, Oman	Soft sediments	Returned to background levels within approximately 100 m of outlet
Abdul-Wahab, 2007	191	NR	40.11	Muscat, Oman	Soft sediments	Appeared to return to background levels 980 m from outlet
Altayaran and Madany, 1992	106	288	51	Sitra Island, Bahrain	Soft sediments	Salinity of receiving water reach 51 ppt, relative to reference areas of 45 ppt, plume extended at least 160 m from discharge. Temperature also affected, discharged at 10-15ºC above ambient, receiving water up to 7º C above ambient harbour basin
Talavera and Ruiz, 2001	25	17	75.2	Canary Islands, Spain	Sub-tidal rocky reef	2 ppt above background on the seabed and 1 ppt on the surface within the 20 m of the outlet; similar to background levels at 100 m.
Einav et al., 2002	NR	NR	NR	Dhkelia, Cyprus	NR	Above background 100-200m from outlet, occasionally as high as 60 ppt.
Fernandez-Torquemeda et al., 2005	50	75	68	Alicante, Spain	Seagrass and soft sediments	0.5 ppt above ambient for up to 4 km from outlet along the seafloor
Malfeito et al., 2005	28	NR	44	Javea, Spain	Seagrass and soft sediments	Slightly above background up to 300 m from the outlet
Raventos et al., 2006	60	33	60[a]	Blanes, Spain	Seagrass and soft sediments	At background levels within 10 m of outlet. No apparent measurement or analysis of salinity
Del-Pilar-Ruso et al., 2007	50	65	68	Alicante, Spain	Soft sediments	2.6 ppt above ambient within 300 m of outlet; 1 ppt within 600m; similar to background at 1300 m.
Safrai and Zask, 2008	274	600	42	Ashkelon, Israel	NR	Approximately 2 ppt above ambient within 400 m of outlet, <1 ppt above ambient within 4000 m of the outlet
Sadhwani et al., 2005	25	NR	75	Canary Islands, Spain	Soft sediments	75 ppt effluent diluted to 38 ppt within 20 m of outlet, no details given as to background salinity
Gacia et al., 2007	NR	2	60	Formentera, Balearic Islands, Spain	Seagrass and soft sediments	5.5 ppt above background 10 m from outlet; 2.5 ppt at 20 m; 1 ppt at 30 m; not measured any further than this
Lin et al., 2013	NR	1.5		Penghu County, Taiwan	Soft sediments	differences in salinity among monitoring sites were consistently less than 2 ppt through the seasons

*NR: Not recorded

4.1 Single Port Discharges

In this part, firstly, main definitions and governing parameters related to single port discharges of dense effluents are presented. This information is followed by experimental and numerical studies in the literature.

4.1.1 Definitions and governing parameters

The parameters controlling hydrodynamic behavior of dense jets can be classified as effluent parameters, receiving ambient parameters and discharge system parameters, respectively.

Effluent parameters are salt concentration of the effluent (C_0), density of the effluent (ρ_0), kinematic viscosity of the effluent (ν), discharge velocity (U_0) and discharge flow rate (Q_0).

Receiving environment parameters are salt concentration of the ambient (C_a), density of the ambient (ρ_a), ambient water depth (H_A) and ambient flow velocity (U_a).

Discharge system parameters are the discharge port diameter (D), the discharge (θ) angle, the maximum terminal rise height (Z_t), the maximum centerline rise height (Z_m), the location of the impingement point (X_i), the length of near field (X_n), the impact point dilution (S_i), the near-field dilution (S_n) and the thickness of bottom layer (y_L).
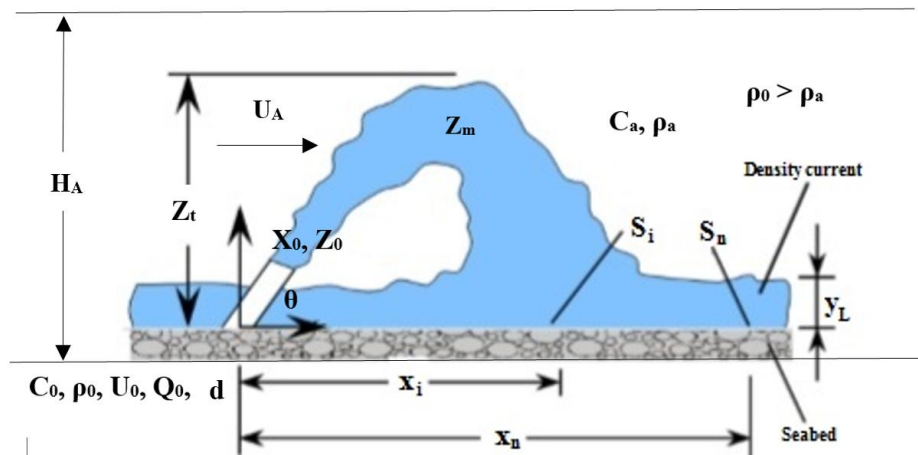
Figure 4.3 : Geometric features of a negatively buoyant jet (Adapted and modified from Roberts et al., 2010).

For a round jet, initial flow rate (Q_0), momentum flux (M_0) and buoyancy flux (B_0) are the main parameters wich define the jet behavior (Fischer et al., 1979; Roberts et al, 1997).

$$Q_0 = \frac{1}{4}\pi D^2 u \tag{4.1}$$

$$M_0 = \frac{1}{4}\pi D^2 u^2 \tag{4.2}$$

$$B_0 = g\left(\frac{\Delta\rho_0}{\rho}\right)Q = g_0'Q \tag{4.3}$$

Here, g_0' is the reduced gravity due to different buoyancy of the effluent compared to receiving environment.

Thus any jet parameter can be defined using these three, dimensional quantities:

$$y_t = f(Q, M, B) \tag{4.4}$$

And if the jet has an inclination (θ), this equation takes the form of:

$$y_t = f(Q, M, B, \theta) \tag{4.5}$$

By using these values, two characteristic length scales may be defined as below (Fischer et al., 1979; Roberts et al, 1997):

$$l_Q = \frac{Q}{M^{\frac{1}{2}}} = \sqrt{A} \tag{4.6}$$

$$l_M = \frac{M^{\frac{3}{4}}}{B^{\frac{1}{2}}} \tag{4.7}$$

Flux-momentum length scale, l_Q, is the distance over which it can be concluded that volume flux of entrained ambient water developped into equal initial volume flux. For more far distances from the discharge point, initial volume flux is dynamically unimportant. Momentum-buoyancy length scale, l_M, is the distance where buoyancy generated momentum is approximately equal to the initial momentum flux. For more far distances from the disharge point, initial momentum leaves its control to buoyancy flux. However, it is important to state that momentum flux is always an important parameter for negatively buoyant jets due to the different directions of buoyancy and jet momentum (Roberts et al., 1997).

According to dimensional analysis study by various authors (Fischer et al.,1979; Roberts et al., 1997), ratio of mentioned length scales formed a non-dimensional parameter which is called as the jet Richardson number (Ri_0) where F_d is the densimetric Froude number (F_d) (Fischer, et al., 1979):

$$Ri_0 = \frac{l_Q}{l_M} = \frac{QB^{\frac{1}{2}}}{M^{\frac{5}{4}}} = \left(\frac{\pi}{4}\right)^{\frac{1}{4}}\left(\frac{g_0{}'D}{w^2}\right) = \left(\frac{\pi}{4}\right)^{\frac{1}{4}}\frac{1}{F_d} \tag{4.8}$$

$$F_d = \frac{u_0}{\sqrt{g_0{}'D}} \tag{4.9}$$

These parameters are indications of domination of momentum and buoyancy forces on the jet which can be used to evaluate if the jet behaviour is jet-like ($1 < F_d < \infty$), plume-like ($F_d < 1$) or non-buoyant jet ($F_d \rightarrow \infty$) (Yongping, 2006).

l_M ve l_Q may be stated as a function of F_d:

$$l_M = \left(\frac{\pi}{4}\right)^{1/4}.DF_d \tag{4.10}$$

$$l_Q = \left(\frac{\pi}{4}\right)^{1/2}.D \tag{4.11}$$

In the light of these expressions, governing non-dimensional parameters for dense jet flow are obtained as the following equations which were widely used in various experimental and parametric studies related to the topic (Cipollina et al., 2005; Palomar et al., 2010, etc.):

$$\frac{y_t}{DF} = C_1; \frac{X_i}{DF} = C_2; \frac{X_m}{DF} = C_3; \frac{y_L}{DF} = C_4; \frac{S_t}{F} = C_5; \frac{S_i}{F} = C_6 \tag{4.12}$$

Here, C_1, C_2, C_3, C_4 and C_5 are empiric coefficients.

These non-dimensional parameters are valid for hydrodynamic analysis of negatively buoyant jet flow in stagnant receiving environment.

Yongping (2006) executed a dimensional analysis for positively buoyant vertical jets under irregular waves with Jonswap spectrum. In this study, the author included a wave-induced characteristic velocity (u_w) which is dependent on wave height, wave peak period (T_p) and water depth to take into consideration the effect of waves on jet behaviour:

$$u_w \approx \frac{\pi H_{rms}}{T_p} \frac{\cosh(k_a Z_a)}{\sinh(k_a h)} \tag{4.13}$$

Here, Z_a is the height of the mid-point between the free surface and jet orifice and k_a is the wave number corresponding to peak wave period.

In the mentioned study, following dimensionless quantities were obtained:

$$\emptyset = f(u_w, M_0, B_0, Q_0, z) \tag{4.14}$$

By using these main parameters, some non-dimensional parameters were developped as below (Yongping, 2006):

$$\emptyset = f(\frac{z}{Q_0/M_0^{1/2}}, \frac{z}{Q_0^{3/4}/B_0^{1/2}}, \frac{u_w}{M_0/Q_0}) \tag{4.15}$$

$$\emptyset = f(\frac{z}{l_Q}, \frac{z}{l_M}, \frac{u_w}{u_0}) \tag{4.16}$$

or

$$\emptyset = f(\frac{z}{M_0^{1/2}/u_w}, \frac{z}{B_0/u_w^3}, \frac{Q_0}{M_0^{5/4}/B_0^{1/2}}) \tag{4.17}$$

$$\emptyset = f(\frac{z}{l_m}, \frac{z}{l_b}, F_0) \tag{4.18}$$

$$l_w = l_m^{1/2} l_b^{1/2} = \frac{M_0^{1/4} B_0^{1/2}}{u_w^{1/2}} \tag{4.19}$$

$$\frac{l_w}{l_b} = (\frac{l_m}{l_b})^{1/2} = \frac{u_w M_0^{1/4}}{B_0^{1/2}} = (\frac{4}{\pi})^{1/4} \frac{u_w}{\sqrt{\frac{\rho_a - \rho_0}{\rho_0} d}} = 1.062 F_w \tag{4.20}$$

$$F_w = \frac{u_w}{u_0} F_0 \tag{4.21}$$

$$\emptyset = f(\frac{z}{l_w}, F_0, F_w) \tag{4.22}$$

Here, l_w is the characteristic wave momentum-buoyancy length scale which is a combination of wave momentum length scale (l_m) and wave buoyancy length scale (l_b). As it can be seen in Eq. 4.20, it is a function of wave Froude number (F_w) which is a measure of ratio of wave effect and buoyancy flux. Thus, any parameter related to negatively buoyant jets can be explained as a function of the non-dimensional parameters below (Yongping, 2006):

$$\emptyset = f(\frac{z}{l_w}, F_0, F_w) \tag{4.23}$$

In addition to parameters above, horizontal wave momentum flux ratio (R_M) may be added as a parameter to analyze jets under wave effect which is used for non-buoyant horizontal jets in the literature (Mori and Chang, 2003).

$$R_M = \frac{gkA^2}{2u_0{}^2} \qquad \qquad \textbf{(4.24)}$$

Here, k is the wave number, A is the wave amplitude and u_0 is the initial jet velocity. In the mentioned study, R_M was stated as the determining parameter for jet oscillation behavior classification in three regions: Type 1 region, symmetrical oscillation and continuous centerline ($R_M < 0.04 - 0.05$), Type 2 region, asymmetrical oscillation and continuous centerline ($0.05 < R_M < 0.2$) and Type 3 region, asymetrical oscillation and discontinuous centerline ($R_M > 0.2$).

4.1.2 Stagnant ambient

Experimental studies examining behaviour of dense jets in stagnant receiving environment include vertical, horizontal and inclined jets (Turner, 1966; Zeitoun et al., 1970, Roberts, 1987; Roberts et al., 1997, etc.). First studies were limited due to rough measurement methods and included only values of impingement point, maximum height distances and sometimes dilution values at these points. By the development of new measurement techniques, the quality and content of experimental studies related to dense jets were developed as well (Roberts et al., 1997; Tian and Roberts, 2003).

Experimental studies examining behaviour of dense jets in stagnant receiving environment include vertical, horizontal and inclined jets (Turner, 1966; Zeitoun et al., 1970, Roberts, 1987; Roberts et al., 1997, etc.). First studies were limited due to rough measurement methods and included only values of impingement point, maximum height distances and sometimes dilution values at these points. By developing of new measurement techniques, the quality and content of experimental studies related to dense jets also developed, too (Roberts et al., 1997; Tian and Roberts, 2003).

A dense jet with a vertical component of momentum flux rises to a maximum point (Z_m) and falls onto itself and spreads on the bottom as a density current (Roberts et al., 1997). Negative buoyancy acts in the opposite way with initial momentum flux and the jet falls with the effect of negative buoyancy after the terminal point (Lee and Chu, 2003) (Figure 4.4).
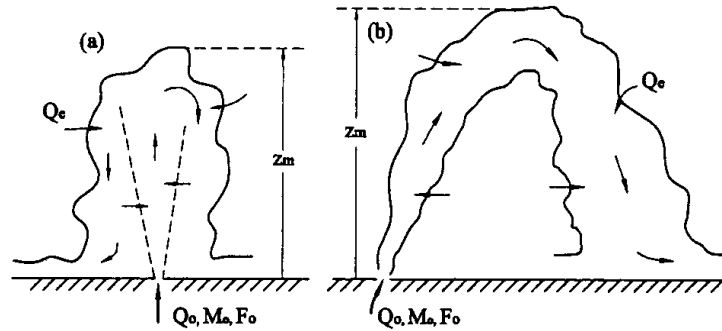
Figure 4.4 : Discharged jet with vertical momentum flux (Lee and Chu, 2003).

Horizontal momentum component of an inclined dense jet provides drawing away of wastewater from source point (Pincince & List, 1973). 60° is determined as the most suitable discharge angle for dense jets providing highest dilution ratios (Zeitoun et al., 1972; Roberts et al., 1997). However, the study by Zeitoun has variable and non-realistic results due to the measurement technique used (Roberts and Toms, 1981; Jirka, 2008).

Cipollina et al. (2005) investigated characteristics of inclined dense jets with 30°, 45° and 60° vertical angles in stagnant receiving environment. For the experiments, authors used NaCl solutions with 1.055, 1.098 ve 1.179 kg/m^3 density values. Densimetric Froude number range was 30-120. In this experimental study, authors measured geometrical features of the dense jets without dilution measurement. Maximum rise level, impact point distance and jet centreline maximum coordinates were the parameters they measured. According to their findings, these geometrical parameters were proportional to F (Table 4.2).

Another study about inclined dense jets was executed by Roberts et al. (1997) in which salt water jets discharged with a 60º horizontal angle and investigated by using LIF system with CCD cameras and microconductivity probes. Using instantaneous and time-averaged LIF images, geometrical characteristics and dilution values were measured during that study. Instantaneous LIF images showed that there were local concentration gradients and patchiness of concentration distribution which were decreasing after the impact point. Also, time-averaged images showed that additional mixing occurred after the impact point which leads ultimate dilution values 60% higher than the impact point dilution (Figure 4.5).

x/DF$_d$
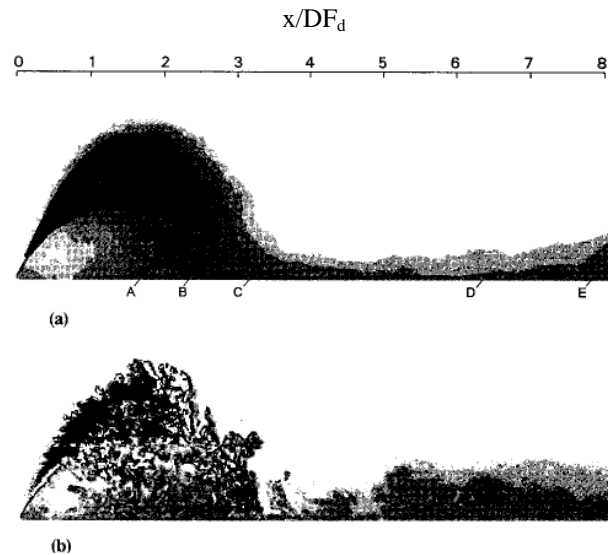
Figure 4.5 : LIF images of dense jet, a) Time-averaged image, b) Instantaneous image (Roberts et al, 1997).

In that study, hydrodynamic behaviour of a discharged inclined dense jet was explained by using measured dilution values and concentration fluctuations. According to concentration values, concentration fluctuations were greatest at the impact point and they collapsed after that point due to established stable density profile. These values are used to define the location of the end of mixing zone at which concentration fluctuation falls to 5%. Ampiric equations obtained with this study are presented at Table 4.2. Differently, Kikkert et al. (2007) used both Light-Attenuation (LA) and LIF techniques for examining inclined dense jets in stagnant environment.

In their study, Papakonstantis et al. (2011a,b) experimentally investigated inclined (45°, 60°, 75°, 80°, 85°, 90°) dense jets for a range of densimetric Froude numbers (7.5-59.2) in stagnant environment. In the mentioned experiments, main geometrical characteristics (Papakonstantis et al., 2011a) and concentration characteristics (Papakonstantis et al., 2011b) of discharged jets are presented in dimensionless form (Table 4.2).

Shao and Law (2011) experimentally investigated mixing behaviour of inclined dense jets with 30° and 45°. Using LIF and PIV systems, they were capable of determining concentration and velocity distributions of spreaded jet besides its geometric features. An important part of this study was investigating the effect of bed proximity, which is defined by z_0/D ratio or bed proximity parameter (z_0/L_M), on characteristics of inclined dense jets. Here z_0 is the distance between the discharge

51

point and the bottom, D is the port diameter and L_M is the jet/plume characteristic length scale. When a jet is discharged close to a impermable bed, it has a tendency of attaching the bed depending on the space between them. This process is named as Coanda effect and important for mixing of inclined dense jets because of causing reduced mixing and increasing salinity concentrations at the sea bottom.

Geometrical features and dilution were found to be dependent on densimetric Froude number similar to previous studies. Related experimental coefficients are given in Table 4.2. Impingement point locations were determined from obtained concentration profile data as the point where the concentration value reaches to a maximum value from zero and drops after a short distance. Minimum dilution at the impact point were independent of discharge angle. In addition, dilution ratios were comparable after the impingement point which shows that discharge with high Froude numbers was not advantageous and lower ones may be chosen after making an optimization study (Shao and Law, 2011).

Cross-sectional concentration profiles of jets showed that upper part of the jet was compatible with the Gaussian distribution and lower part deflected from normal distribution with an increasing amount as getting far away from the nozzle. After the impingement point, concentration profiles were converted into wall-jet pattern (Figure 4.6a) (Shao and Law, 2011).

Cross sectional velocity profiles for various downstream locations were also obtained from the velocity data. As it can be seen from the figure, close to upstream they are consistent with the Gaussian distribution and start to deflect from it after a distance. Similar to concentration profiles, velocity profiles turned into wall-jet pattern after the impingement point (Figure 4.6b) (Shao and Law, 2011).
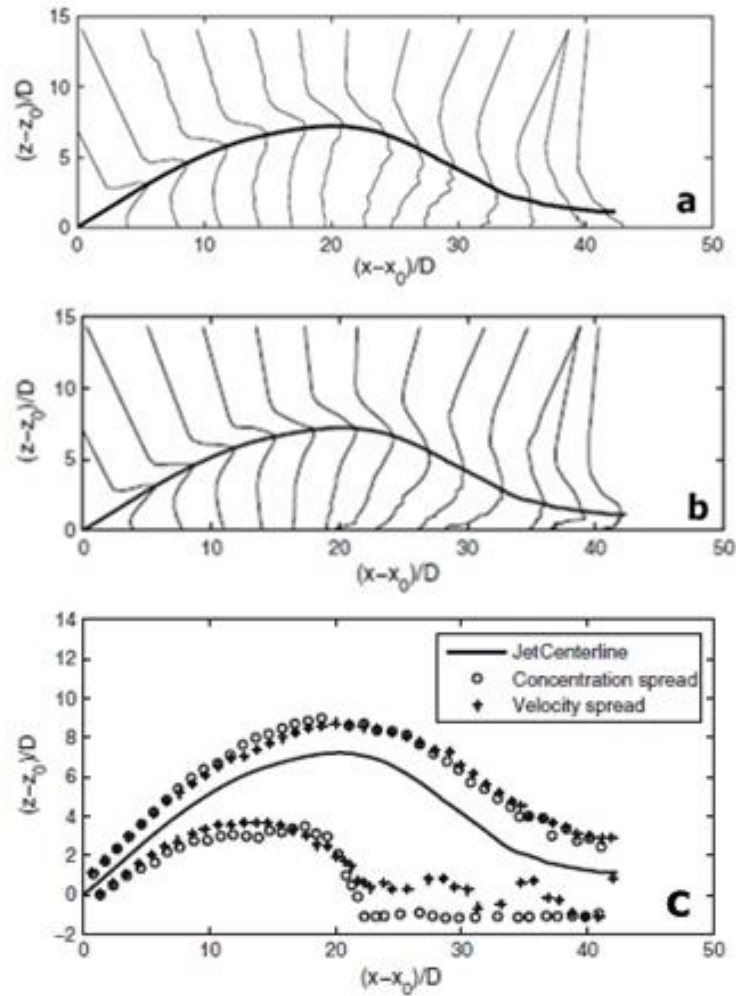
Figure 4.6 : Cross-sectional axial a) concentration, b) velocity distribution at various downstream locations, c) comparison (Shao, 2011).

When these profiles are examined by superposing them, concentration and velocity profiles were almost identical for the upper part of the jet which fits the Gaussian distribution. For the lower part, concentration spread was overestimated and for the upper layer it was under estimated. However, the figure clearly shows lower spread formed due to buoyancy induced instability (Figure 4.6c) (Shao and Law, 2011).

For the effect of bed proximity, it was found out that the controlling parameter was z_0/L_M and not z_0/D. Lower inclination (30°) resulted in significant bed proximity effect for $z_0/L_M<0.2$ while at 45° having very little effect. For 30° discharge angle, horizontal location of centerline peak was shifted downstream for $z_0/L_M<0.2$. However, its value and terminal rise height were similar to less bed proximity effect ($z_0/L_M>0.2$). Effect of boundary was also observed at centerline peak minimum dilution values at the tests with boundary effect as slighltly lower dilution of jets compared to the ones with no boundary effects. However, dilution coefficients for

45° inclined dense jets were almost the same for the tests with and without boundary effect. For the impact dilution, the values were lower at tests with boundary effect and 30° discharge angle which was elucidated with reduction of overall distance from the nozzle. However, no difference was observed in the presence and absence of boundary effect for the tests with 45° discharge angle (Shao and Law, 2011).

Lai and Lee (2012) developed the previous studies of inclined dense jets by taking into consideration of new discharge angles (15°, 30°, 38°, 45°, 52° and 60°) for a range of densimetric Froude number 10-40 using LIF and PIV methodologies.

Propagation of dense jet is classified in three stages as intial stage, transition stage and developed stage depending on time-mean average concentration data from LIF system (Figure 4.7). Initial stage (x/D ≤20 where x is the streamwise coordinate) defined as the region where concentration profile is well-aproximated with the Gaussian distribution. In the transition stage, jet partly (lower part) goes out from the Gaussian profile developing until terminal rise height and preserves this form in the developed stage before impinging on the bottom which shows that buoyancy-driven instabilization fades out after the terminal rise height (Lai and Lee, 2012).

In the same study, it was shown that the jet centreline trajectory which is determined by using transverse concentration maximum values is seriously effected by the jet discharge angle. Visual terminal rise was defined as 0.25 C_{max} and this value is used also for determining maximum visual rise (Z_{max}) value. It is found out that dimensionless terminal rise height (Z_{max}/F_d) was dependent on discharge angle and densimetric Froude number and for F_d>25, it reaches to an asymptotic value for an angle of discharge. In addition, centerline rise height (Z_m), location of terminal rise (X_m) and impingement (return) point location (X_i) were determined (Table 4.2) (Lai and Lee, 2012).
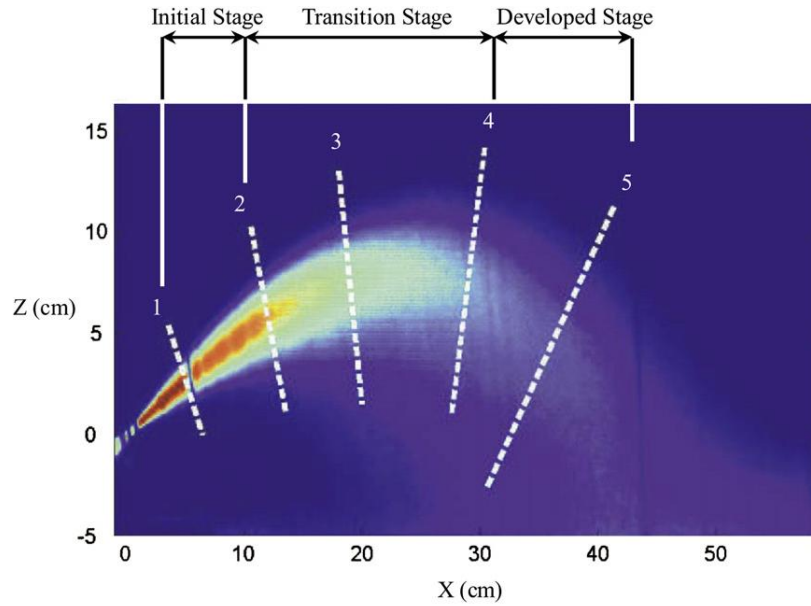
Figure 4.7 : Inclined dense jet development in stagnant environment
(Lai and Lee, 2012).

Dilution values at terminal rise height and impact point were also dependent on discharge angle and densimetric Froude number. $F_d > 20$ is the value at which dimensionless terminal rise height dilution (S_t/F_d) reached a constant value of 0.45 for the discharge angles 38°-60° and 0.27 for 15°. For the impact point (S_i/F_d), 1.06 and 0.43 were the asymptotic values for the discharge angles 38°-60° and 15°, respectively. By using these values, dilution ratio ($R_s = S_i/S_t$) was defined with the value of ≈1.5-2.7 and tendency of increase for increasing vertical discharge angles (Lai and Lee, 2012).

Centerline velocity (U_m) decays due to jet spreading and negative buoyancy in a discharged dense jet. Measured U_m values showed that negative buoyancy effect is not so serious for the decay of centerline velocity (U_m) until terminal rise height. Decay behaviour was closely compatible with the trend for pure jets defined by Fischer et al. (1979). Analysis of turbulence structure at vertical concentration of jet showed the occurrance of jet detrainment as an uplifted inner profile. It was also found that vertical and horizontal concentration turbulent intensity (C_{rms}/C_m) profiles at terminal rise were similar for all discharge angles. While vertical values had a peak value at $r/bg_c = -0.76$ decreasing towards higher values of r/bg_c, horizontal profiles had two peaks at ±0.76. The peak values increased with increasing vertical angle. Measured turbulence intensity values were higher than a pure jet in stagnant environment (Lai and Lee, 2012).

Table 4.2 : Experimental results for geometrical characteristics of inclined dense jets (Modified from Lai and Lee, 2012).

		15°	30°	38°	45°	52°	60°
Maximum terminal rise height (Z_t/DF_d)	Lai & Lee (2012)	0.44	0.95	1.20	1.58	1.69	2.08
	Papakonstantis et al. (2011b)	-	-	-	1.59	-	2.15
	Papakonstantis and Christodoulou (2008)	-	-	-	1.59	-	2.16
	Shao and Law (2010)	-	-	-	1.47	-	-
	Kikkert et al. (2007)	0.52/0.52	1.17/1	-	1.61	-	2.43/2.04
	Cipollina et al. (2005)	-	1.08	-	1.61	-	2.32
	Lindberg et al. (1994)	-	-	-	1.56	-	2.16
	Roberts et al. (1999)	-	-	-	-	-	1.93
	Roberts and Toms (1987)	-	-	-	-	-	2.08
	Zeitoun et al. (1970)	-	1.15	-	1.43	-	2.04
Centerline rise height at Z_{max} (Z_m/DF_d)	Lai & Lee (2012)	0.21	0.65	0.87	1.19	1.34	1.64
	Papakonstantis et al. (2011a)	-	-	-	1.17	-	1.68
	Ferrari and Querzoli (2010)	-	-	-	1.19	-	1.67
	Shao and Law (2010)	-	0.66	-	1.14	-	-
	Kikkert et al. (2007)	0.21/0.21	0.68/0.54	-	1.07	-	1.71/1.46
	Cipollina et al. (2005)	-	0.79	-	1.17	-	1.77
Horizontal location at Z_m (X_m/DF_d)	Lai & Lee (2012)	1.22	1.95	1.95	2.09	1.87	1.78
	Shao and Law (2010)	-	1.54	-	1.69	-	-
	Kikkert et al. (2007)	1.47/1.22	1.84/1.75	-	1.81	-	1.75/1.56
	Cipollina et al. (2005)	-	1.95	-	1.80	-	1.42
Horizontal distance from source to return point (X_i/DF_d)	Lai & Lee (2012)	2.41	3.18	3.19	3.34	2.87	2.84
	Papakonstantis et al (2011a)	-	-	-	3.16	-	2.75
	Ferrari and Querzoli (2010)	-	-	-	3.03	-	2.67
	Shao and Law (2010)	-	3.00	-	3.33	-	-
	Kikkert et al. (2007)	2.53/2.13	3.40/3.07	-	3.2	-	2.8
	Nemlioglu & Roberts (2006)	-	3.3	-	3.2	-	3.4&3.1
	Cipollina et al. (2005)	-	3.03	-	2.82	-	2.25
	Roberts et al. (1997)	-	-	-	-	-	2.40

Table 4.2 (continued) : Experimental results for geometrical characteristics of inclined dense jets (Modified from Lai and Lee, 2012).

		15°	30°	38°	45°	52°	60°
Minimum dilution at terminal rise (S_t/F_d)	Lai & Lee (2012)	0.27	0.40	0.45	0.45	0.47	0.44
	Papakonstantis et al. (2011b)	-	-	-	0.52	-	0.56
	Shao and Law (2010)	-	0.62	-	0.46	-	-
Minimum dilution at X_i (S_i/F_d)	Roberts and Toms (1987)	-	-	-	-	-	0.37
	Zeitoun et al. (1970)	-	0.36	-	0.42	-	0.56
	Lai & Lee (2012)	0.43	0.82	0.99	1.09	1.10	1.07
	Papakonstantis et al (2011b)	-	-	-	1.55	-	1.68
	Shao and Law (2010)	-	1.45	-	1.26	-	-
	Roberts and Toms (1987)	-	-	-	-	-	1.03
Minimum dilution at X_i (S_i/F_d)	Papakonstantis et al. (2011b)	-	-	-	0.52	-	0.56
	Shao and Law (2010)	-	0.62	-	0.46	-	-
	Roberts and Toms (1987)	-	-	-	-	-	0.37
	Zeitoun et al. (1970)	-	0.36	-	0.42	-	0.56
	Lai & Lee (2012)	0.43	0.82	0.99	1.09	1.10	1.07
	Papakonstantis et al (2011b)	-	-	-	1.55	-	1.68

4.1.3 Wavy ambient

Studies on discharged jets in the literature are mostly focused on discharge into a stagnant or flowing environment. There are some studies related to wave conditions, however most of them investigated positively/neutrally jet interaction with the waves.

First study on inclined negatively buoyant jets under wave effect is an experimental study by Ferrari and Querzoli (2006) using LIF methodology to determine concentration profiles of released jets. In the mentioned study, both jet and wave characteristics were variable parameters and experimental data were analysed depending on the wave phase for which one wave period were divided into 8 phases. Temporal evoluation of negatively buoyant jet under regular wave conditions was determined in three phases as jet deflection, transition region and developed region, which is same as the study of Hwung et al. (1994) related to horizontal positively buoyant jets.

Deflection region is the region where initial momentum of the jet is effective on flow behaviour and jet protects its shape. In that region, it was observed that the upward oscillation was larger than the downward one. In the transition region, this oscillation becomes clearer as the effect of momentum decreases against the growing influence of wave motion. It was also observed that jet divides into two branches in that region if the wave motion was strong enough. In the developed region, these branched jets form a single unit again by reaching stable characteristics. This behaviour was also observed with the concentration measurements at the maximum rise height and return point. Concentration profiles have bifurcation at maximum rise height and changes through the wave phases and this behaviour was not observed at the return point.

Lin and others (2013) executed an experimental study on the horizontal, neutrally, positively and negatively buoyant jets under regular wave conditions. In that study, statistical flow and turbulence characteristics of jets were determined with regard to wave phases by using 2D-PIV method. Generated waves were regular waves with 3 cm height and 1 s period. Measured area was for a range of $40 \leq x/D \leq 60$ at which five cross-sections of velocity maps are obtained. Mean velocity values were determined by averaging 1320 instantaneous velocity data. Also, some tests were done without any discharge to determine wave particle velocities. Some experiments were done without discharge to have the ability of measuring the wave particle velocities. Negative buoyancy was 2% which was generated by using salt solution.

The results provided with that study were examined mainly in two parts as potential core region and near field region of the discharged jet. In the potential core region, oscillation and centreline velocity decay was observed from mean velocity profiles in which wave velocities were removed to have a better understanding of jet behaviour (Figure 4.8). According to the calculated turbulence properties, it was found out that the difference between neutrally and negatively buoyant jets were small compared to the difference between jets with/without waves. So, it was elucidated that buoyancy was not an effective parameter and waves are the predominant factor affecting jet properties in that region (Lin et al., 2013).

In the near-field region, jets are under the effect of jet momentum which decreases with distance from the jet as it gets wider, slower and skewed due to buoyancy effect. Similar to potential region, mean velocity profiles were produced also for the near-

field region. Because of the jet was oscillating, different mean velocity profiles obtained for neutrally buoyant jets. However, mentioned differences were little compared to tests with stagnant environment and almost symmetrical. In the near field region, oscillaton of negatively buoyant jet was again obvious (Figure 4.8c,d). Also, negatively buoyant jets were wider at the wave conditions with an 82% higher value than neutrally buoyant ones. This result was evaluated by the authors as an indication of that the wave dispersion was more effective than the negative buoyancy for the buoyancy value in the experiments (Lin et al., 2013).

Experimental results showed that the buoyancy not only affected the flow velocties but also the turbulence area in the near-field region. According to the calculated turbulence properties (turbulence intensity and Reynolds stresses values), negatively buoyants jets were slightly different than the neutrally buoyant jets for the stagnant environment. However, increase of width and magnitude of turbulence properties were observed for the tests with regular wave conditions. Averaged magnitudes of fluctuations ($(u'^2)^{\frac{1}{2}}$ and $(w'^2)^{\frac{1}{2}}$) increased 35% and 37% for negatively buoyant jets, respectively. In addition, 2D mean kinetic energy ($MKE_{2D} = [(u)^2 + (w)^2]/2$), turbulent kinetic energy ($TKE_{2D} = [(u')^2 + (w')^2]/2$) and total energy ($MKE_{2D} + TKE_{2D}$) values on the jet centreline plane were calculated by integrating velocity and turbulence intensity values through the water depth. Average values of calculated energy parameters were higher (MKE_{2D}:30% and TKE_{2D}:11%) in stagnant conditions compared to neutrally buoyant jets. In the wave conditions, MKE_{2D} value decreased (19%) while TKE_{2D} increased (18%) which leads to a total energy decrase of 13% by the wave dispersion. This low rate of change of the energy compared to neutrally buoyant jets (43%) related to energy from buoyancy which compensates energy decrease by the wave-enhanced mixing and diffusion.
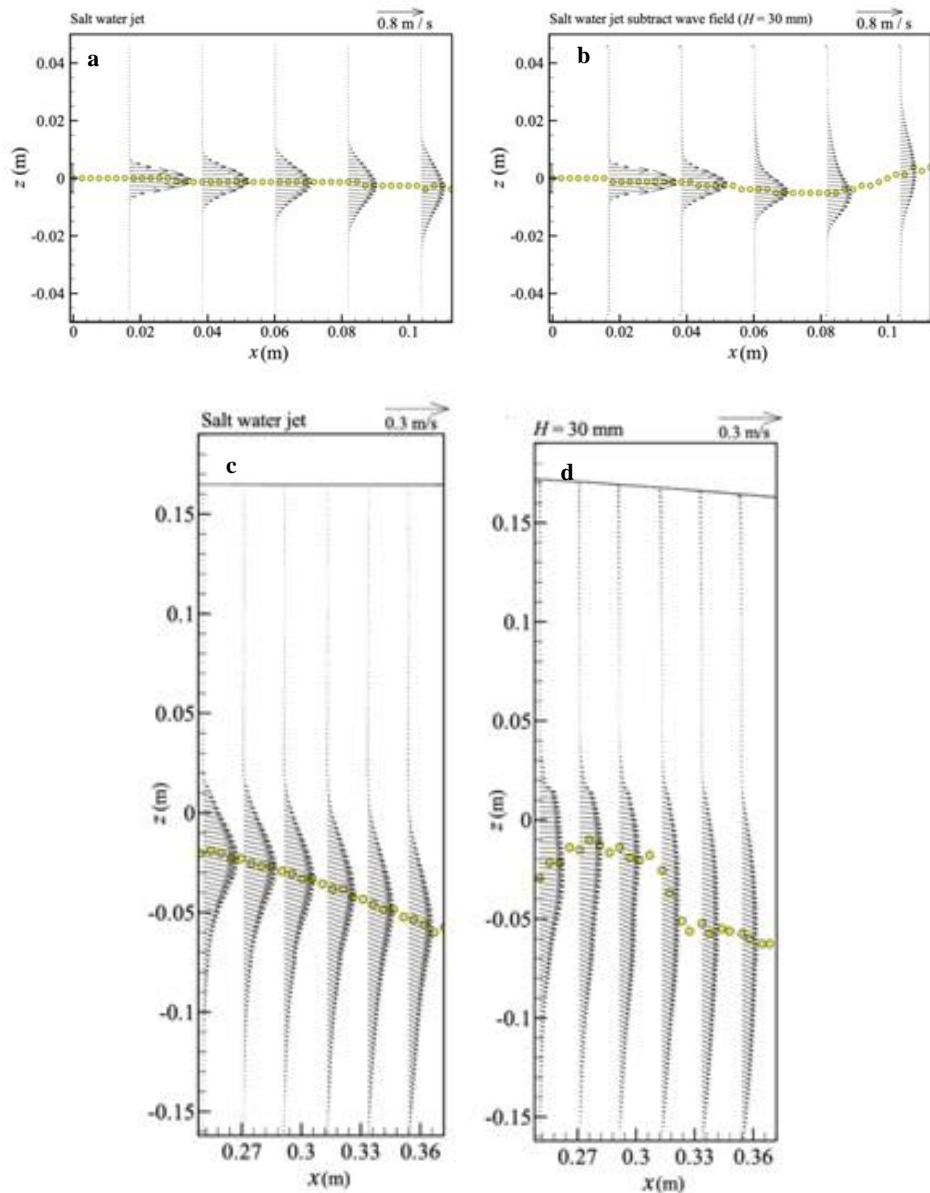
Figure 4.8 : Cross sectional velocity profiles of horizontal negatively buoyant jets a) Potential core region, without waves, b) Potential core region, with waves, c) Near field region without waves, d) Near field region, with waves (Lin et al., 2013).

According to the calculated eddy viscosity (v_t) values, increase of v_t was 5% for the stagnant conditions and 43% for the wave conditions compared to neutrally buoyant jets in the potential core region. In the near-field region, magnitudes were not so different from neutrally buoyant jets. However, v_t profiles were wider and skewed due to the buoyancy effect under stagnant conditions. In regular waves, difference between neutrally buoyant and negatively buoyant jets increased (2.2 times higher than stagnant environment) by the means of eddy viscosity owing to the wave dispersion (Lin et al., 2011).

Also, calculation of turbulent kinetic energy budget showed that waves contributed to turbulence properties significiantly. Profiles of advection, production and combined diffusion and dissipation components of the turbulent kinetic energy budget had higher values (0.5%) and widths compared to neutrally buoyant jets in stagnant environment. Also, they were skewed due to the buoyancy. For the wave conditions, profiles were again higher and wider than neutrally buoyant jets. Also, effect of waves were clear at the production profiles with 1.4 times higher values of production component compared to stagnant conditions for negatively buoyant jets. Diffusion and dispersion profile, which has 2.1 times higher values than the stagnant conditions, was also another proof of wave effect (Lin et al., 2011).

In addition to experimental studies, in a field study in Alicante, Spain, effect of wind and waves on discharged brine was investigated through the measurement of wind, wave, current and salinity values at a point which was outside of the surf zone. In this study, considered desalination plant outfall was a nearshore plant and the effluent was diluted with seawater due to existence of nearby *Posedonia oceanica* meadows. It was determined that wave height and duration of the storm was the reason of reduction of near bottom salinity values.

4.1.4 Single port systems numerical modelling

Numerical models that are used for modelling the behaviour of brine discharge can be classified as simple length scale models based on dimensional analysis, entrainment models and CFD models (Palomar and Losada, 2011).

4.1.4.1 Entrainment models

In the length scale models, the number of independent variables is reduced by considering the predominant parameters for the situation. In this method, relationship between the chosen independent parameters is built up by using main flux magnitudes (Q_0, M_0 and B_0) by which the length scales are formed to define the flow characteristics (Palomar and Losada, 2011).

Integral models are common tools for modelling jets and gravity currents because of being a simple and effective way of solving jet and plume problems (Fischer et al., 1979). In these models, equations to be solved are integrated through the cross-section to have simpler, ordinary differential equations and solved by numerical

methods. In this method, the receiving water is assumed as infinite and boundary interactions are neglected. For this reason, data gathered by these models is valuable for the region before the impingement point. So, these models are used for near-field region modelling. Integral models do not take into consideration mixing after the impingement point (Palomar et al., 2012a). Increase in the dilution ratio between impingement point and the end of near-field region is determined as 60% during the experiments of Roberts et al. (1997). Also, Coanda effect is another parameter that they neglect.

Most common integral models that are used for modelling dense jets are CORJET module of CORMIX software, JetLag module of VISJET software and UM3 module of VISUAL PLUMES software. When these models were compared with experimental data, lower values of measured data were obtained (Palomar et al., 2012b). CORJET is a 3D integral model that is used for modelling jets without interaction of any boundaries (Loya-Fernández et al., 2012). VISJET simulates positively and negatively buoyant jets in the near-field region considering effluent properties, discharge geometry and ambient conditions and the interaction with the boundaries is out of scope of that software (Palomar et al., 2012a). UM3 is also a 3D model for simulating one-point and multiple submerged jets. It is a Lagrangian model and is based on projected-area-entrainment (PAE) hypothesis. A jet is assumed to be conical and it is considered that jet velocity and pollutant concentration will decrease with entrained receiving environment fluid (Lee and Chu, 2003).

4.1.4.2 CFD models

Hydrodynamic models are the most common way of modelling wastewater outfalls. However, they have some limitations such as coupling near and far field models, calibration difficulties and long run times (Palomar and Losada, 2011). In the literature, there are several studies modelling dense jets discharged to stagnant receiving environment. Vafeidou et al. (2002) examined numerically a dense jet discharged to stationary environment by using 3D CFX-5 model and compared their results with experimental data. According to this study, difference between initial and final rises is 20%. In addition, it is found out that initial and final rise heights were proportional to F_d for the whole discharge angles (0°, 10°, 20°, 45°, 60°).

Model results were compatible with Bloomfield and Kerr (2002) for 0°-45° discharge angle interval. For 30° discharge angle, terminal rise height values were lower than the experimental data (Roberts, et al., 1997) which leads underpredicted values for impingement point distance and dilution ratios. Vafeidou et al. (2005) expressed that they generally obtained compatible results with experimental data. In that study, Boussinesq approximation was used, all density terms were accepted constant except buoyancy and a source term was added to the momentum equation:

$$S_M = (\rho - \rho_\alpha)g \qquad\qquad (4.25)$$

Density difference in that equation was defined as a function of concentration:

$$\rho - \rho_\alpha = \rho_\alpha \alpha C \qquad\qquad (4.26)$$

Here, ρ is the local density, ρ_α is the density of the receiving water and C is the concentration which corresponds to the local density assuming the initial concentration was zero and α is a constant. In this study, Shear Stress Transport (SST) model which was a combination of k-ε ile k-ω models was used for turbulence closure.

Oliver et al. (2008) also used CFX model to simulate discharged brine from desalination plant with the same condition with Vafeidou et al. (2005) by using two approaches. In the first approach, k-ε model, which is present in CFX model, was used and some calibrations were made by adjusting the turbulent Schmidt number as the second approach. In this study, different discharge angles (15°, 30°, 45°, 60°) were under consideration. By this study, more accurate results were obtained compared to integral model predictions and analytical solutions and they were compatible with the experimental data gathered by Kikkert et al. (2007). There were some differences between the standard and modified models especially for some bulk parameters such as tracer spread and dilution; however two models were not so different in general.

Seil and Zhang (2010) modelled dense jets bu using FLUENT 6.23.6 software which solves Reynolds-averaged Navier–Stokes equations. In this study, the software was modified through using Renormalization group (RNG) k-ε turbulence model of Yakhot and Orszag (1986) and Yakhot et al. (1992) with SST k-ω turbulence model of Menter (1994). In addition, SST k-ω turbulence model was calibrated with regard to experimental data obtained by Roberts et al. (1997). When compared to

experimental data, it is seen that the model gave very close results for 1≤x/dF≤4 region and good results for 4≤x/DF≤7 region. However, this consistency decreased with distance from the discharge point and results did not simulate turbulence decay after the impingement point. Same results were also valid for comparison with other experimental data (Nemlioglu and Roberts, 2006). In addition, RNG k-ε turbulence model gave dilution values which were half of the experimental data.
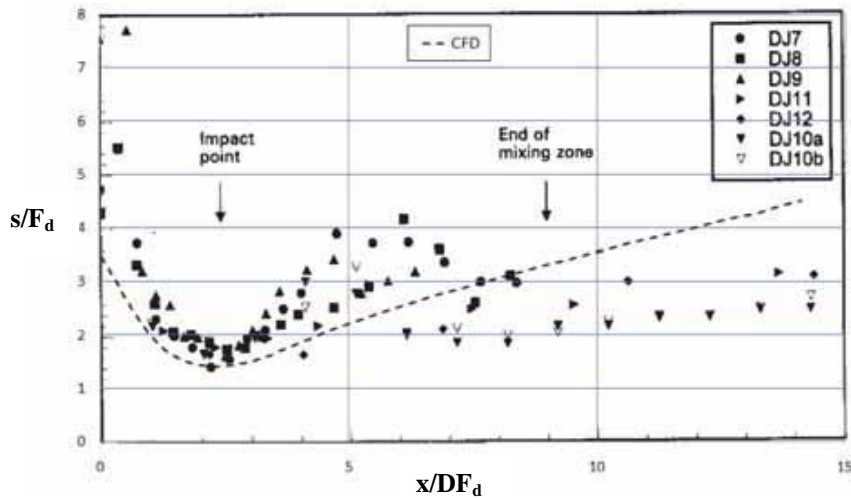
Figure 4.9 : Comparison of modified SST k-ω turbulence model with experimental data of Roberts et al. (1997) (Seil and Zhang, 2010).

4.2 Multiport Discharges

Multiport diffuser usage for brine outfalls, which may be constructed for a new desalination plant or as a renovation of an existing near shore discharge system, is the choice when the mixing capacity of near-shore zone is not sufficient for the salinity discharge load. By this way, adequate mixing of discharged brine is achieved constructing long diffuser lines designed with hydrodynamic modeling studies for site-specific conditions. In addition, it is possible to contain higher capacity desalination plants and locating them more freely. However, the main disadvantage of this method is obviously higher costs (WaterUse, 2011).

Multiport discharge systems consist of a diffuser line with closely spaced ports/nozzles from which the effluent is discharged. In addition, various types of diffuser ports can be placed with different openings and shapes. Ports may be directly installed on the diffuser line or riser may be used when it is needed to bury the pipeline below the seabottom or check valves can be used. There are different

types of multiport diffusers used for effluent discharges depending on arrangement of ports on the diffuser line. Some of them are given in Figure 4.10.
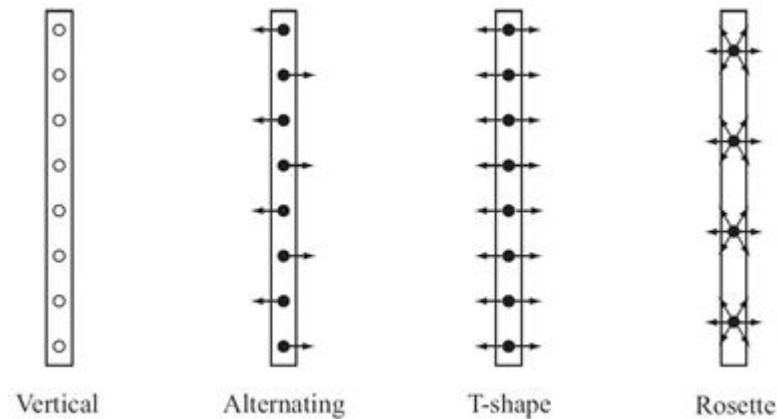
Figure 4.10 : Some multiport diffuser types.

In vertical type multiport diffusers, diffusers are placed on the diffuser line with space between them. In alternating diffusers, each diffuser in a line is towards the opposite direction. T-shape diffusers include two diffusers at a point, each of them looking at opposite sides. Rosette type diffusers discharge effluent via discrete risers, each one including 4-8 ports for effluent discharge. Besides these arrangements, there are also many distinctive configurations of ports.

Brine was mostly discharged with single port diffusers at the beginning of the desalination industry. Due to increasing awareness of possible negative impacts of brine discharge of the marine environment, the number of constructed multiport outfall systems for brine discharges is increasing. Some examples of brine outfall systems with different types of multiport discharge systems are given in Figure 4.10. In Perth desalination plant in Australia, brine is discharged with conventional line type diffusers which consists of a line diffuser with uniformly spaced ports on one side (Marti et al., 2011). Gold Coast Seawater Desalination Plant in Southeast Queensland, Australia is another example of a multiport diffuser system which is used for discharging 67 ppt brine to the marine environment (WaterUse, 2011). Brine outfall system in Sydney is an example of rosette-type diffuser systems with 4 diffusers (s=25 m, n=4) used for brine discharge (Tarrade et al., 2010).

Figure 4.11 : Some examples of multiport discharge outfall constructions, a) alternating diffuser (WaterUse, 2011), b) T-shape diffuser (CEDEX), c) rosette type diffuser (Roberts et al., 2010).

4.2.1 Hydrodynamic behaviour

In this chapter, a literature review related to hydrodynamic behaviour of multiport discharge systems will be presented. Various researchers studied merging of multiple jets mostly for positively buoyant discharges (domestic wastewater, cooling water discharges). However, the number of studies concerning the multiport brine discharge systems is very limited. Because of that, after giving general concept for multiport outfall systems, the studies related to positively buoyant effluents will be given and multiport brine discharge studies will follow.

Main flux variables for multiport diffuser discharges can be described by using line source parameters which are flux values (q, flow rate; m, momentum flux and b, buoyancy flux) for unit length of diffuser. By using the total flow rate (Q_T) and diffuser length (L_D) values, these fluxes are defined as below (Roberts et al., 2010):

$$q_0 = \frac{Q_T}{L_D}, \qquad m_0 = u_0 q \quad , \qquad b_0 = g_0' q \qquad \textbf{(4.27)}$$

Here, u_0 is discharge velocity and g_0' is the reduced gravitational buoyancy.

4.2.1.1 Line type (conventional) multiport diffusers

Similar to Tian and Roberts (2004), Abessi and Roberts (2014), investigated the effect of port space on mixing behaviour of multiple discharge systems but taking into consideration of brine effluent discharge. In their experimental work with 3DLIF method, they executed experiments for a wide range of densimetric Froude number (F) ($12 < F_d < 40$) and nozzle numbers (1, 4, 7 and 22) which were at one or two sides of the diffuser line with a $60°$ angle to the horizontal. In this study, densimetric Froude number is included in dimensionless port spacing parameter (s/DF_d) due to the fact that F is the leading parameter for dense effluent mixing. The range of port spacing in the experimental setup was $0.44 < s/DF_d < 12$. Here d is the nozzle diameter.

As the result of their study, Abessi and Roberts (2014) found out that for point plume region (s/DF>2), data related to computed geometrical features of discharged jets (y_t, X_i and X_n) is compatible with predicted asymptotic solutions ($s/DF_d\gg1$), corresponding to the single port jet case, which is not valid for closer port spaces, due to formation of merging. Another important finding is that these geometrical features decrease as the port space gets smaller which is contrary to the first prediction of the authors according to dimensional analysis.

Closer port spaces cause lower impact point dilution (S_i) and near-field dilution (S_n) values which are lower (~20%) for two-side discharge compared to one-sided configuration. Besides, development of dilution from the impact point to the end of the near-field was ~60% for non-merged jets and 20% for merged jets due to the merging process. The reason for that case is elucidated with combined merging and Coanda effect by the means of literature related to positive and negative buoyant jets. Coanda effect cause more rapid and sharp bending of discharged jet which ends up with re-entrainment of the descending jet, shorter trajectories and narrower external surfaces leading to lower dilution values. This effect also excited by merging which constitutes an almost impermeable wall that prevents entrainment. This was clearly seen from experimental images as the full and empty spaces under the inclined jets for merging and non-merging jets, respectively (Figure 4.12). Filled cavity caused lower entrainment rates at closer port spacing values (Abessi and Roberts, 2014).

So, s/DF_d>~2 value is defined as the appropriate dimensionless port space value to prevent Coanda and merging effects and obtain high dilution ratios.
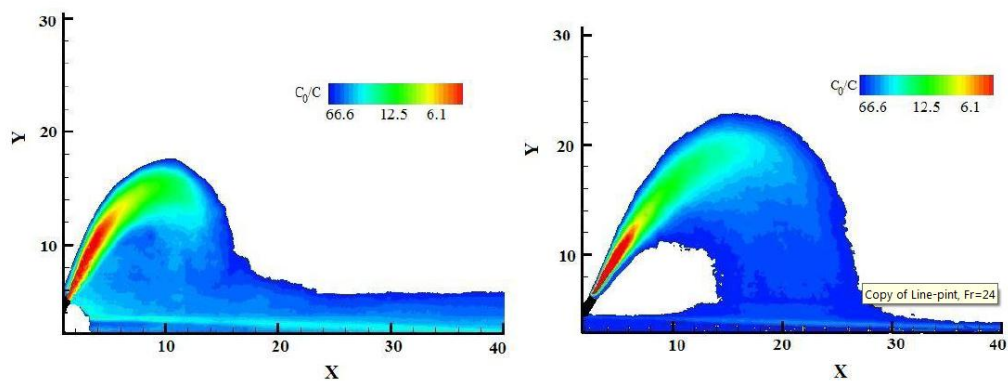
Figure 4.12 : Coanda effect and merging a)line source, $s/DF_d\approx1$, b) point source, $s/DF_d\approx12$ (Abessi and Roberts, 2014).

In Table 4.3, measured geometrical features and dilution values are given related to the mentioned study. As it can be seen from the table, for s/DF_d>0.2, the coefficients

of point plume behaviour is similar to Roberts et al. (1997) stated for single dense jets. Besides, the table presents field study data obtained by Miller et al. (2011) at the Perth Stage1 outfall which is a diffuser line with equally spaced 40 nozzles at one side. These results are consistent with the results of Abessi and Roberts (2014) and also with results of Roberts et al. (1997).

Marti et al. (2011) executed a field study near the multiport diffuser of Perth Seawater Desalination Plant, Australia. The outfall system consisted of a 160 m long diffuser line including 40 equally spaced ports installed with a 60° discharge angle. Measured dilution values of this study are also given in Table 4.3.

4.2.1.2 Rosette type multiport diffusers

Tarrade et al. (2010) executed a physical modelling study of two desalination plant outfalls with rosette type diffusers. In their study, they examined various parameters (number of risers, number of nozzles, spacing between nozzles, different arrangements, nozzle diameter, vertical angle of nozzles, flow rate, etc.) which are effective on brine mixing. Experiments included test of 1 or 2 risers with 3,4,5,6,9,12 nozzles placed with an angle of 30°, 45°, 50°, 55° or 60°. Experiments were executed under stagnant receiving environment conditions. Some examples of different configurations can be seen in Figure 4.13.
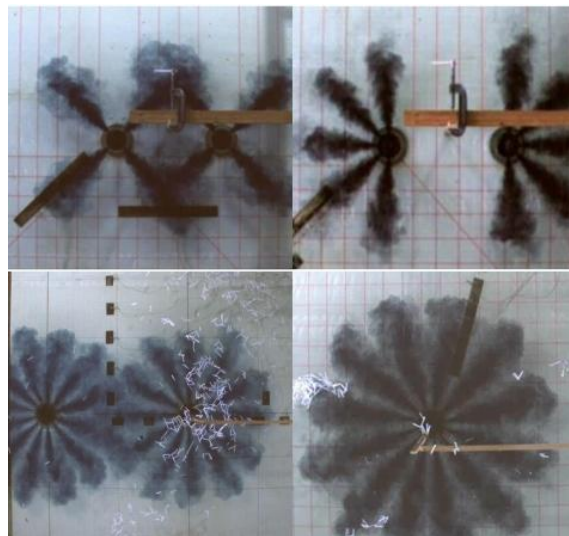
Figure 4.13 : Plan views of different experimental configurations
(Tarrade et al., 2010).

Their results were compatible with the previous experimental studies on single dense jets for X_i, S_i and y_t values. Some of non-dimensional experimental results of Tarrade et al. (2010) for S_i are given in Table 4.3. As it can be seen, good agreement

was observed for S_i values with the existing literature coefficients (Roberts et al., 1997; Papakonstantis et al., 2011) for single point discharges of dense jets. However, merging between dense jets reduced mixing in the range of 14-35 % for different configurations which is argued from comparison of S_i values along a merging plume centreline between two risers and a single plume centreline. Deepending on this measurement, it was concluded that the volume of surrounding water for entrainment, which can be provided with high water depth and adequate spacing between jets, is an important parameter for high dilution values.

The difference between different configurations determined that 4 nozzles with 90° between them was the configuration with little reduction in dilution from a single jet. However, the dilution value was lower for the configuration with 6 nozzles with 60° between them and it reached to very low values for the configurations with nozzles more than 6 (Miller, 2011).

Table 4.3 : Empirical equations related to multiport brine discharges to stagnant receiving environments.

Line Type Diffusers

Source	Parameter	Point Plume $(s/dF_d \sim > 2)$	Line Plume $(s/dF_d < \sim 2)$
Abessi & Roberts (2014)	Terminal rise height (y_t)	$\dfrac{y_t}{DF} = 2.2$	$\dfrac{y_t}{DF} = 1.9(\dfrac{s}{DF})^{1/2}$
	Location of the impact point (X_i)	$\dfrac{x_i}{DF} = 2.4$	$\dfrac{x_i}{DF} = 2.0(\dfrac{s}{DF})^{1/2}$
	Length of near field (X_n)	$\dfrac{x_n}{DF} = 9.0$	$\dfrac{x_n}{DF} = 6.0(\dfrac{s}{DF})^{1/2}$
	Dilution at the impact point (S_i) (one-side discharge)	$\dfrac{S_i}{F} = 1.6$	$\dfrac{S_i}{F} = 0.9(\dfrac{s}{DF})$
	Dilution at the end of near-field (S_n) (one-side discharge)	$\dfrac{S_n}{F} = 2.6$	$\dfrac{S_n}{F} = 1.1(\dfrac{s}{DF})$

Source	Parameter	Transition Region $(s/dF_d \sim 1.3)$	
Marti et al. (2011)	Dilution at the impact point (S_i)	$\dfrac{S_i}{F} = 1.7$	
	Dilution at the end of near-field (S_n) (one-side discharge)	$\dfrac{S_n}{F} = 2.7$	

Rosette Type Diffusers

Source	Parameter	Θ (°)	Single Plume	Merging Plumes
Tarrade et al. (2011)	Dilution at the impact point (S_i)	60	$\dfrac{S_i}{F} = 1.54$	$\dfrac{S_i}{F} = 1.14$
		45	$\dfrac{S_i}{F} = 1.02$	$\dfrac{S_i}{F} = 0.86$
		45	$\dfrac{S_i}{F} = 1.17$	$\dfrac{S_i}{F} = 1.02$

4.2.2 Multiport outfall systems numerical modelling

In that section, general information will be given about the modelling methods that are used to simulate multiport outfall systems.

4.2.2.1 Empirical and length scale models

Dimensional analysis is the mainstay of empirical and length scale models. These models classify flows according to the length scales which are defined by dimensional analysis and gives the jet/plume properties as output using semi-empirical equations and coefficients that belong to the determined flow class. Main

software of this type modelling is CORMIX2 and DHYDRO about which a brief information will be given in following.

CORMIX2 and DHYDRO

Brine discharges with multiport outfall systems can be modelled by using CORMIX2 and DHYDRO modules of CORMIX software. CORMIX2 is an empirical and length scale model which is used for modelling discharge of positively/negatively buoyant effluents from multiport outfalls. Unidirectional, fanned, alternating ports and risers with multiple ports are the outfall configurations which can be modelled by CORMIX2. DHYRO is the module which is capable of simulating single and multiport discharges and surface discharge of brine and sediments in unbounded (bounded laterally on one side only) coastal environments.

In this section, main features of CORMIX2 and DHYDRO will be described by using the information in "User Manual" of the software (Doneker and Jirka, 2007) followed by information about its usage for multiport brine discharges (Palomar et al., 2012a).

Geometrical features: Plan and cross-sectional views of a multiport outfall system are given in Figure 4.14 to define the main geometrical features of the system.
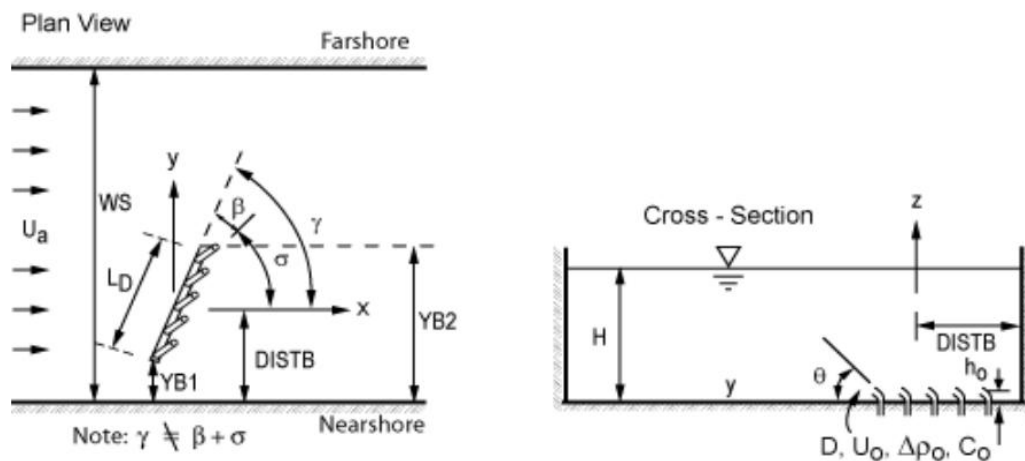
Figure 4.14 : Geometric definition of multiport discharges
(Doneker and Jirka, 2007).

Types of multiport discharges: Multiport discharge systems can be classified into to three classes such as unidirectional, staged and alternating diffusers. Unidirectional diffusers are the type which has nozzles pointing in a horizontal direction, almost perpendicular to the diffuser line ($\beta \cong 90°, \theta_0 = 0 - 90°$).

71

This type of diffusers produce net momentum input in the receiving water which ends up with strong currents and direct negative impact on benthic organisms. Staged diffusers have nozzles again pointing in a horizontal direction, but almost parallel to the diffuser line ($\beta \cong 0°, \theta_0 = 0°$). This type of diffuser also provides a directed momentum input leading formation of strong currents.

Alternating diffusers have nozzles that are placed as every following nozzle points an opposite horizontal direction ($\beta \cong \mp 90°, \theta_0 = undefined$). This type of diffusers do not produce direct momentum input into the receiving water and so they have less negative impact on the benthic environment.

Length scales used: Length scales used in CORMIX2, which are different from the ones in CORMIX1, are based on "equivalent slot diffuser concept". These length scales can be listed as slot jet/plume transition length scale ($l_M = m_0/j_0^{\frac{2}{3}}$), slot jet-crossflow length scale ($l_{m1} = m_0/u_a{}^2$), slot jet-stratification length scale ($l_{m'} = m_0{}^{1/3}/\varepsilon^{1/3}$), slot plume-stratification length scale ($l_{b'} = j_0{}^{1/3}/\varepsilon^{1/2}$) and crossflow-stratification length scale ($l_a = u_a/\varepsilon^{1/2}$). l_M, defines the distance at which jet-plume transition occurs in a uniform stagnant ambient. l_m, shows the distance at which a jet in a crossflow is advected by the cross flow. $l_{m'}$ and $l_{b'}$ are the scales of the point at which a jet and a plume is affected by the linear stratification in the receiving environment, respectively. l_a is the vertically upward/downward flotation distance beyond which a plume is strongly advected by crossflow.

Flow classification: As mentioned above, flows of negatively buoyant effluent discharge with multiport diffusers are classified for the simulation of outfalls by CORMIX2. These flow classes are coded with the letters MNU and numbers. Totally, there are 14 flow classes for negatively buoyant multiport discharges which are divided in two main classes as stable (deep water conditions, MNU1-6) and unstable (shallow water conditions, MNU7-14) (Figure 4.16 and 4.17). For that main and first classification, the equation below is used as the criteria. When the value of this equation is <1, flow is classified as deep-layer flow, otherwise it is classified as shallow-layer flow:

$$\frac{|l_M|(1 + \cos^2 \theta)^2}{H_s} + \frac{|l_M|}{l_m} \sin \gamma \qquad \textbf{(4.28)}$$

Stable, deep-layer flows are divided into two categories as strong buoyancy (MNU1-2) and weak buoyancy flows (MNU3-6). As it can be seen from the flow chart for flow class determination (Figure 4.16), the criteria for this step is the ratio of l_M and ambient layer depth (H_s). If $l_M/H_s < 0$, strong buoyancy will be effective and the effluent will not interact with the water surface (MNU1-2). After that, the condition to be controlled is the l_m/H_s ratio to decide if the effect of crossflow is weak ($l_m/H_s > 0$) (MNU1) or strong ($l_m/H_s < 0$) (MNU2).

In other case, in which $l_M/H_s > 0$, buoyancy will be weak and the momentum will be the effective parameter (MNU3-6) which also indicates that the geometric features of the multiport diffuser system are effective on the flow conditions. Due to the type of discharge system flow chart is divided into two branches at this step: alternating and unidirectional diffusers. For alternating diffuser system flow behaviour is the same with MNU2. For the unidirectional diffusers, classification criteria is to determine if the effective parameter is momentum & buoyancy or crossflow. For that purpose, the ratio of l_M and overall length scale (L_m) is used. If $l_M/L_m < 0$, the flow has a weak deflection (MNU3) and in other case ($l_M/L_m > 0$), strong deflection is observed (MNU4). For the staged diffusers L_M/L_m ratio is the criteria to evaluate relative impact of ambient velocity. For $L_M/L_m < 0$, weak deflection (MNU5) and for $L_M/L_m > 0$ strong deflection (MNU6) are observed.
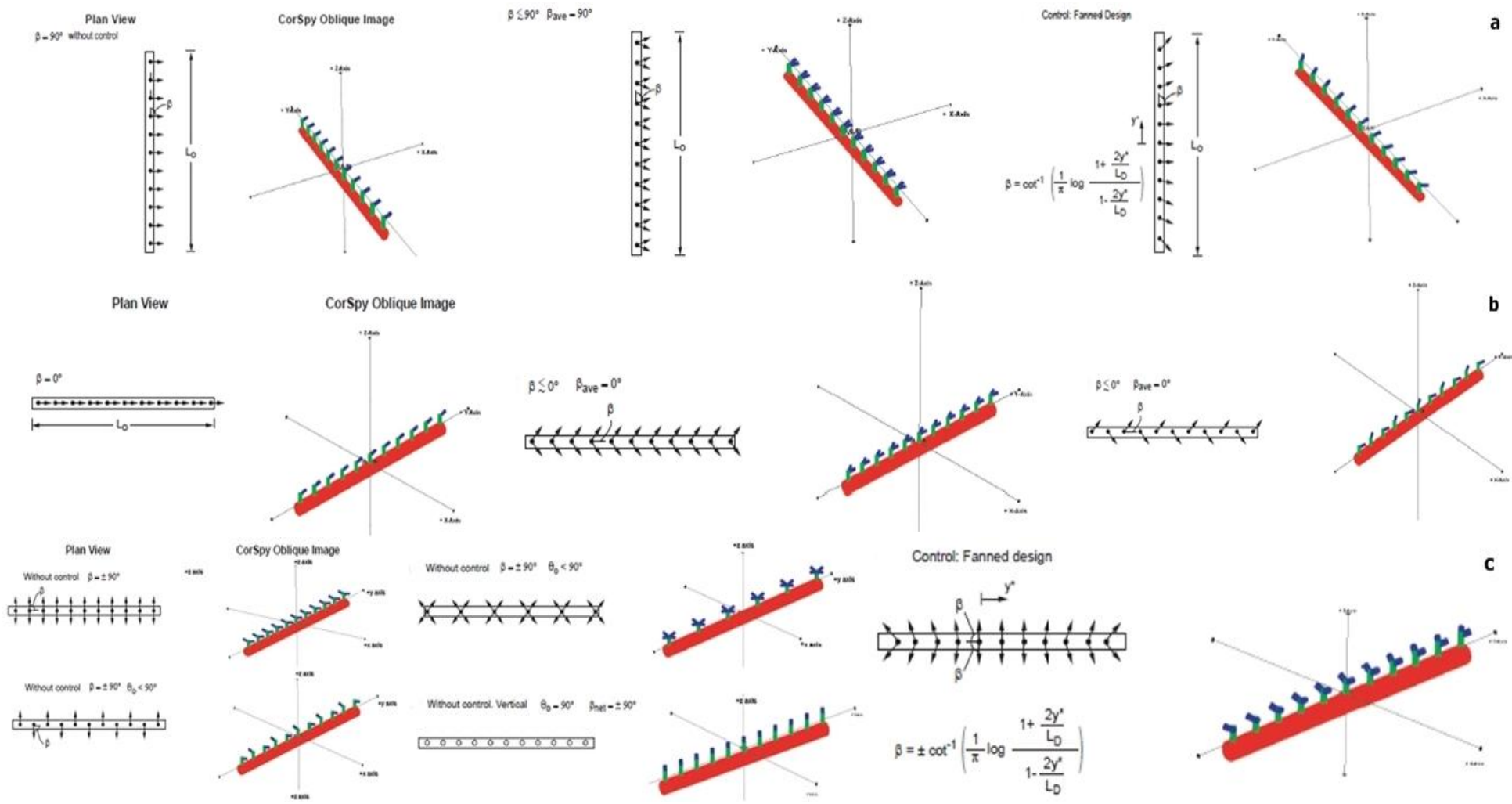
Figure 4.15 : Types of multiport diffusers, a) Unidirectional diffusers, b) Staged diffusers, c) Alternating diffusers (Jirka and Akar, 1991) in CORMIX2.
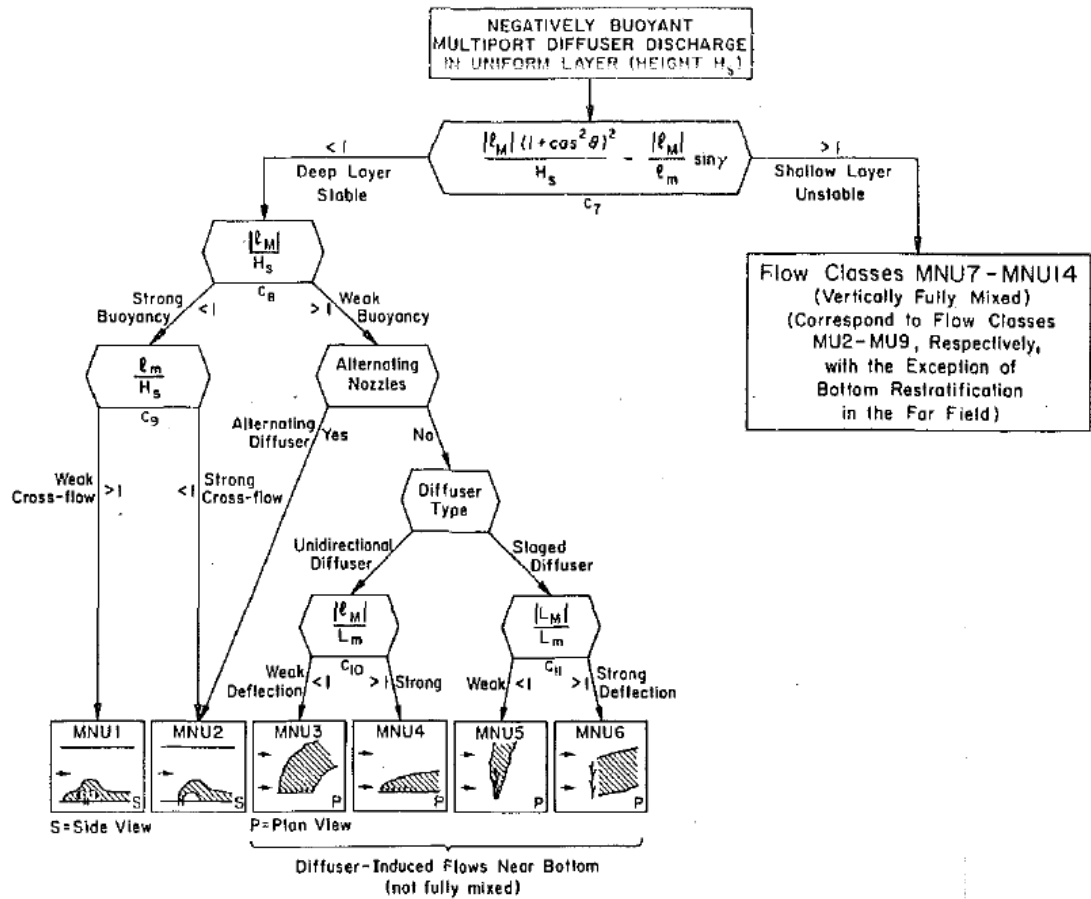
Figure 4.16: Flow classes for negatively buoyant multiport diffuser discharged in CORMIX2 for deep-water conditions (Jirka and Akar, 1991).

Unstable, shallow-layer discharges are fully mixed at the vicinity of the discharge points similar to positively buoyant multiport discharge flows with exception of bottom restratification in the far field region due to their tendency to sink at the bottom because of negative buoyancy (MNU7-14).

As it can be seen from the flow chart for flow class determination (Figure 4.17), the criteria for this step is the diffuser type. For the unidirectional diffusers with alignment angles (γ) >45°(perpendicular), flow class is MNU7. If γ < 45° (parallel), l_m/H_s ratio is the criteria to decide if the weak current ($l_m/H_s > 1$) (MNU8) or strong current ($l_m/H_s < 1$) (MNU9) is observed. For the staged diffusers, procedure is the same. MNU10 and MNU11 are the flow classes at which weak and strong currents are observed, respectively. In the case of alternating diffuser usage, flow is classified according to only their alignment angle: MNU13 with perpendicular discharge (γ > 45°) and MNU14 with parallel discharge (γ < 45°).
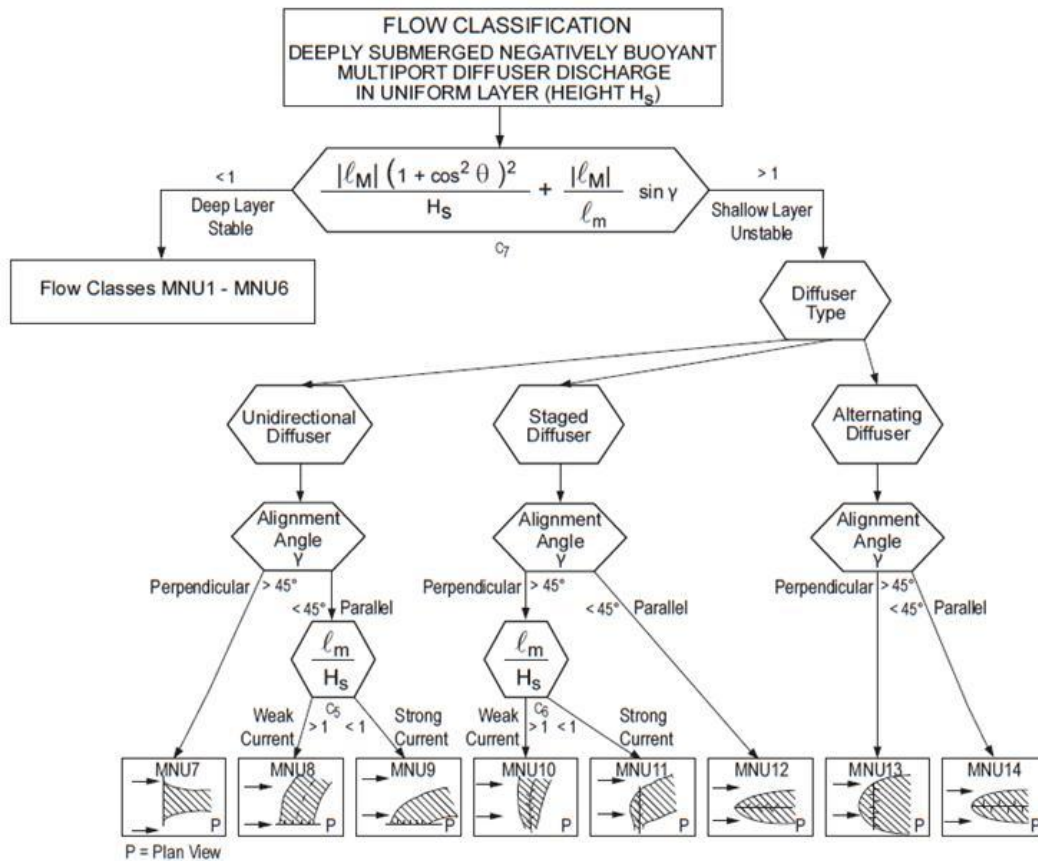
Figure 4.17 : Flow classes for negatively buoyant multiport diffuser discharged in CORMIX2 for shallow-water conditions (Jirka and Akar, 1991).

For more detailed analysis of discharged jets, CORJET, which is a post-processing module in CORMIX software, can be used. CORJET can be used for stable flow classes; so it can be used for modelling flow classes of MNU1-6 for negatively buoyant discharges. Additional information related to CORMIX will be given below.

Input data: CORMIX2 has a user interface which lets user entering data sets under various tabs: "Project", "Effluent", "Ambient", "Discharge" and "Mixing Zone". There are also two additional tabs "Output" and "Processing". Differently in DYHDRO module, a density calculator is inserted for brine effluents. In that calculator, ambient/effluent density is calculated using entered temperature and salinity values. Calculation is executed based two different equations (One Atmosphore International Equation of State of Seawater by UNESCO (1980) and Seawater Density Equation by El-Dessouky and Ettouny (2002) which can be chosen by the user.

Evaluation for brine discharges: CORMIX2 have some main assumptions when producing results for multiport discharge cases. For the mentioned assumptions first criteria is the merging of the jets. If the programme does not detect a merging between jets, it uses same length scales and semi-empirical formulas in CORMIX1. In the other case, it uses different assumptions such as equivalent slot diffuser concept and emprical formulas.

In the equivalent slot diffuser concept, it is assumed that all the discharging nozzles are a line slot discharging with the total discharge rate. In addition, for some discharge configurations with discharge points on two sides, it prompts totally wrong results for negatively buoyant effluents (Figure 4.18). The reason for that is that these dense jets have momentum and buoyancy fluxes in opposite ways and they fall down separately instead of merging (Palomar et al., 2012a).
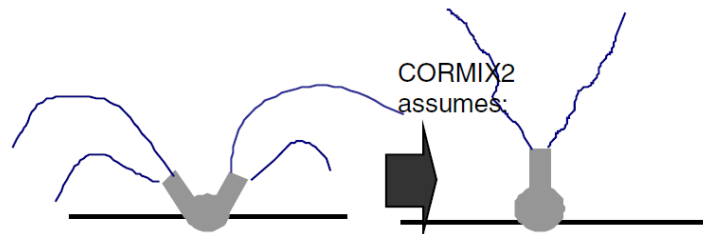
Figure 4.18 : Simulation of brine discharge from the two sides
(Palomar et al., 2012a).

If CORMIX2 does not detect merging between jets, it is insensitive to nozzle spacing, since the discharge corresponds to single port jets.

In the case of jet merging, CORMIX2 (through CORJET module) applies the assumption of equivalent slot diffuser for unidirectional diffusers and all jets discharged from multiple ports are assumed as a line slot discharge. Dilution values decreases slightly with decreasing port space. Also, the programme gives the same results for scenarios with different multiport configurations due to the assumptions made (Palomar et al., 2012a).

4.2.2.2 Entrainment models

Entrainment models are used for jet and plume modelling which are named after using integration of conservation equations over jet cross-sections.

Entrainment models can be classified in two types as Eulerian and Lagrangian according to the definition of the control volume used. Most common entrainment models used for brine discharge modelling are CORJET, UM3 and JETLAG.

CORJET

CORJET is an Eulerian integral model simulating submerged single and multiport buoyant jets in unbounded receiving environment. The programme makes the assumption of Gaussian profile of discharged jets.

Merging of discharge of jets from multiport diffusers is determined by CORJET when the plume diameter calculated from Gaussian profile is equal to distance between ports. So, the programme takes the merging as a one point process and assumes the jet as a 2D line plume from that point (Davis, 1999).

Input data: Input data is similar to CORMIX1 and CORMIX2 which is through a user interface with different tabs. CORJET has 3 tabs as "Project" (Project name), "Ambient" (ambient temperature, salinity, flow velocity, etc.) and "Discharge" (effluent temperature, salinity, velocity, angle, diffuser features, etc.) through which related parameters entered into the program as input.

In CORJET, the only discharge configuration that can be simulated is equally spaced unidirectional jets with same diameters and discharge angles which is different from CORMIX2.

Evaluation for brine discharges: CORJET is sensitive to vertical angle (θ) and discharge velocity and it is less sensitive to density differences considering the real desalination plant values. While simulating multiport diffusers, CORJET is insensitive to port space when it is wide enough that merging doesn't occur. In the case of merging, this sensitivity is not high for different port spaces. Coanda effect is also an important parameter that should be considered and it can't be modelled by CORJET. Thus, it is recommended that not to simulate jets with a possibility of Coanda effect occurrence ($\theta < 30°$ and $h_0 = 0$ m) where h_0 is the distance of discharge port to the bottom. Since another deficiency of program is not being capable of detecting jet upper surface and so the water surface interaction, it is recommended to that the user should determine the jet-surface interaction and not consider the following calculations (Palomar and Losada, 2011).

3D Updated Merge (UM3)

UM3 is one of five moduls of Visual Plumes modeling software. It is a Lagrangian type integral model which includes time integration and has a coordinate system moving with the plume. In the plume, distribution of properties in a slice of the plume is assumed as constituting a top-hat profile (Davis, 1999).

The model is based on projected-area-entrainment (PAE) hypothesis which elucidates forced entrainment into the plume discharged. This hypothesis assumes that there is only inflow (ambient water entrainment) and the plume is steady-state. So, plume outer boundary remains same and the elements travel in that plume boundary with time. PAE includes a cross-current term corresponding to third-dimension which provides simulation of single port discharges in three-dimension and multiport discharges less detailed by splitting that parameter to whole jets discharged (Frick et al., 2003).

Mentioned ambient entrainment is constituted of two parts as forced entrainment (Ea) and Taylor-type aspiration entrainment (Eα), respectively (Davis, 1999).

In the case of merging of the jets from a multiport diffuser, volume of slice and both forced and aspiration entrainment is modified due to the fact that decreasing exposed entrainment surface is affected on these parameters (Davis, 1999).

In UM3, the only discharge configuration that can be simulated is equally spaced unidirectional jets with same diameters and discharge angles.

Input data: Visual Plumes has a user interface which lets user entering data sets under various tabs: "Diffuser" (port diameter, port elevation, vertical angle, horizontal angle, number of ports, port spacing, acute mixing zone, chronic mixing zone, port depth, effluent flow, effluent salinity, effluent temperature, effluent concentration), "Ambient" (measurement depth or height, current speed, current direction, ambient salinity, background concentration, pollutant decay rate) and "Special Settings" (text and graphic output options).

Evaluation for brine discharges: UM3 is sensitive to vertical angle (θ) and discharge velocity and it is less sensitive to density differences compared to CORJET again for considering realistic desalination plant values. While simulating multiport diffusers, UM3 has low sensitivity to port space when merging of jets occur. UM3 is

not capable of detecting impact point of jet at surface and bottom (Palomar et al., 2012a).

Coanda effect is also an important parameter that should be considered and it can't be modelled by UM3. Thus, it is recommended that not to simulate jets with a possibility of Coanda effect occurrence ($\theta < 30°$ and $h_0 = 0$ m) (Palomar and Losada, 2011).

JETLAG

Jetlag is a Lagrangian type integral model which is used for modelling behaviour of jets and plumes in the near field region. It is included in VISJET software which also allows user to model intermediate field by distributed entrainment sink approach (DESA). It is a Windows based model using visualization denser than the other software.

Input data: The program is easily used by entering input data directly on the screen and run the scenarios just with a button. Visualization of simulated system is shown with a large screen in which the user can choose a point to see its characteristics in the near field.

Evaluation for brine discharges: JETLAG is sensitive to vertical angle (θ) and discharge velocity and it is less sensitive to density differences. JETLAG simulates each port on a diffuser line as a single port. Thus, it is not sensitive to merging, port space and diffuser type parameters and it is not appropriate to use it to simulate multiport diffusers (Palomar et al., 2012a).

The program is also insensitive to port height and the minimum port height allowed by the programme is 5 cm which should be considered when simulating diffuser lines on the sea bottom (Palomar et al., 2012a).

Coanda effect is also an important parameter that should be considered and it can't be modelled by JETLAG. Thus, it is recommended that not to simulate jets with a possibility of Coanda effect occurrence ($\theta < 30°$ and $h_0 = 0$ m) (Palomar et al., 2012a).

5. HYDRODYNAMIC BEHAVIOUR OF DISCHARGED DENSE EFFLUENTS IN THE FAR-FIELD REGION (GRAVITY CURRENTS)

In this chapter a brief information on hydrodynamic behaviour of discharged dense effluents in the far field region will be given. Discharged brine behaves as a gravity current in the far-field region. In this context, a literature review of gravity current studies are presented focusing on their hydrodynamical behaviour and effective parameters.

Firstly, a general view of gravity currents produced by lock-exchange technique will be given. This information will be followed by a more detailed literature review related to continuous release gravity currents especially the ones propagating on inclined bottoms.

Gravity currents are flows caused by the gravity when a fluid enters into a fluid of different density and they are mainly horizontal. Flow is driven by the density difference between them and their surrounding environment. Due to this reason they are also called "density currents". Mentioned density difference may be related to temperature difference or different content of flow and ambient. "Multiphase flow" such as turbidity currents which is a combination of sediment and water and "multispecies mixtures" such as mixture of salt and water and gas mixtures are examples of different density cases leading formation of gravity currents (Gerber, 2008). These types of gravity currents are also classified as particle driven and compositional gravity currents, respectively (Ungarish, 2009).

As it is stated before, since it is propagating with the density difference, a gravity current is located in the ambient depending on its density. It may form a more dense bottom current, which is the topic of this study, (Figure 5.1a); a less dense surface current (Figure 5.1b) or as an intrusion of mixed fluid in a stratified environment (Figure 5.1c, d).
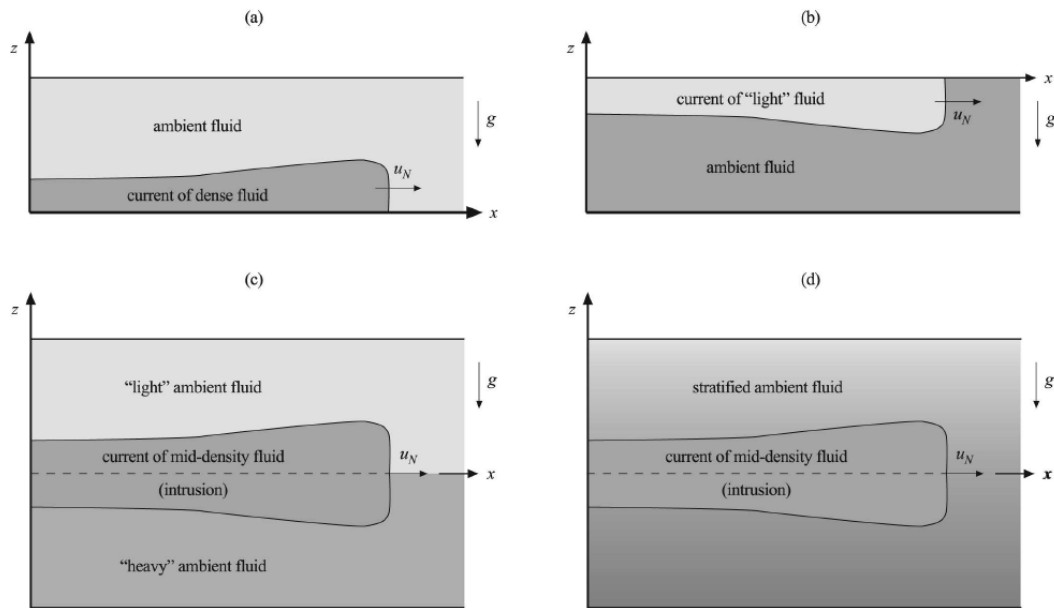
Figure 5.1 : Schematic description of typical gravity current configurations related to density differences, a) bottom current of more dense (heavy) fluid; b) top (surface) current of less dense (light) fluid; c) intrusion of mixed fluid in a sharply stratified ambient; d) intrusion of mixed fluid in a linearly-stratified ambient (Ungarish, 2009).

A typical gravity current consists of mainly two regions which are called head and tail section (Keulegan, 1958; etc.). As it can be seen from Figure 5.2, head section is thicker compared to the tail section and includes billows (which are called Kelvin-Helmholtz instabilities (Britter & Simpson, 1978) and structures called as lobes and chefts. Leading edge of the current is named as nose. Head is followed by the tail section which constitutes of a dense layer and a mixing region on top of it.
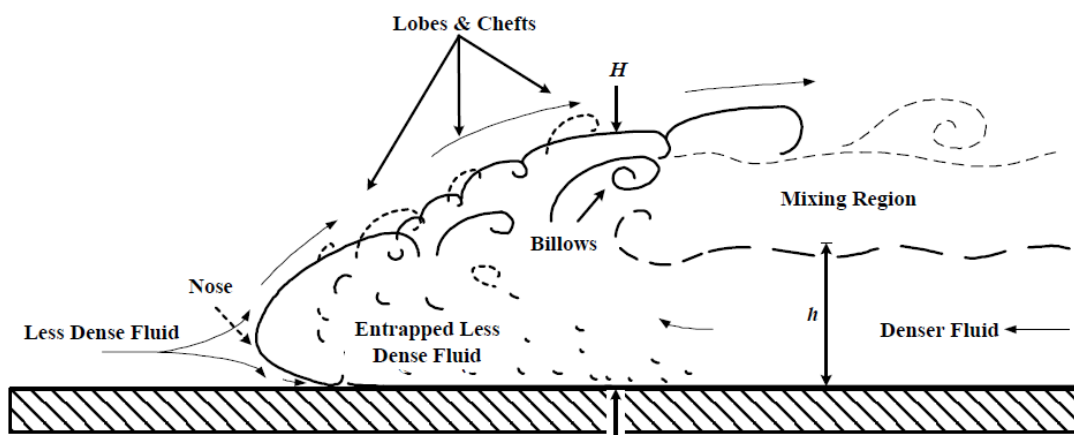
Figure 5.2 : Structure of a gravity current (Mok et al., 2003).

Gravity current flow is an interest of many researchers who executed experimental and numerical studies on their flow behaviour.

Depending on the way of the gravity current is generated, experimental studies related to gravity currents can be examined in two classes as the ones using "lock-release/exchange" method and the ones using "continuous-release" method. In the lock release method, a constant volume of saline solution/sediment is released to an environment in which it propagates with the density difference (Kneller et al., 1999; Buckee et al., 2009; Hallworth et al., 1996, etc.). In continuous-release method, prepared solution simulating gravity current is discharged continuously during the tests. Because of developing technology, experimental instruments used in the literature include intrusive techniques in early stages and non-instrusive techniques in recent past such as laser doppler anemometry (LDA), particle image velocimetry (PIV) and LIF (Kneller et al.,1999; Alahyari & Longmire, 1996; Thomas et al., 2003; Martin and Garcia, 2009, etc.).

Fluid behaviour and so the entrainment mechanisms and mixing are different for these experimental conditions. Hallworth et al. (1996) used lock-exchange technique to model constant-gravity currents. In this study, they also made some experiments to model constant-flux gravity currents. However, their presented results for constant-flux ones was not detailed due to different and more complex behaviour of the flow. In Figure 5.3, a schematical comparison of constant-volume and constant-flux gravity currents prepared by Hallworth et al. (1996) is given. In the lock-exchange experiments head and tail sections were more pronounced than the other in which flow was continuously fed from tail section.

First studies related to gravity currents were executed by Keulegan (1958) using lock-exchange technique. In that study, main structure of a gravity current was defined.

Ellison and Turner (1959) studied turbulent entrainment in stratified flows experimentally and analytically. It was elucidated with this study that a gravity current reaches a steady state after a short time of release and continues flowing with a constant Richardson number (Ri).
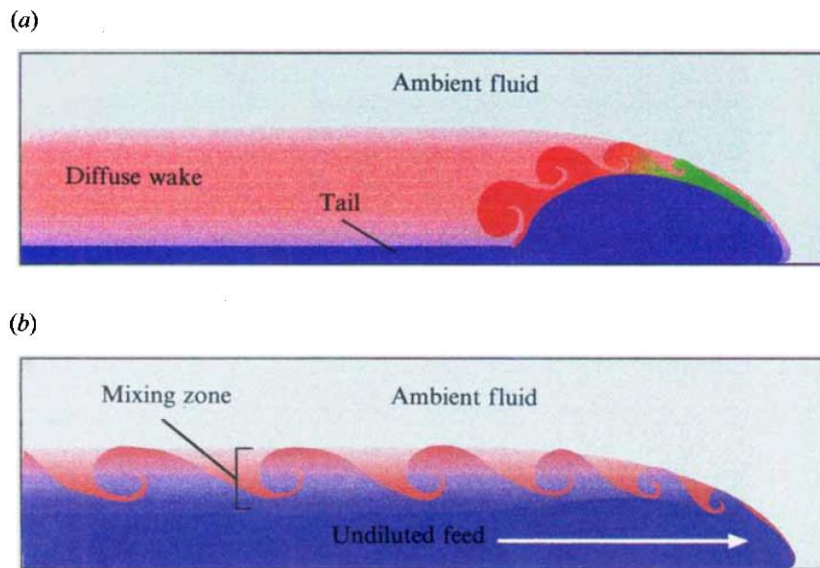
Figure 5.3 : Comparison of entrainment mechanisms and regions for a) constant-volume, b) constant-flux gravity currents (Hallworth et al., 1996).

Britter and Simpson (1978) and Simpson and Britter (1979) experimentally examined behavior of a steady gravity current head. In these studies, existence of shear instabilities (Kelvin-Helmholtz instabilities) and overturning of fluid (lobes and cheft structures) were determined.

Alavian (1986) used thermistor probes for measurement of velocity profiles and conductivity probes for measurement of density of continuously fed gravity currents propagating on an inclined bottom. Besides obtaining velocity and density profiles, effect of bottom slope on behaviour of gravity currents in the means of current shape and entrainment was also evaluated.

Alahyari and Longmire (1996) used PIV technique to measure the velocity field of axisymmetric laboratory currents which were generated by lock-exchange technique.

Garcia and Parsons (1996) investigated continuous-release gravity current fronts using the same experimental technique consisting of a conveyor belt system, LIF and microconductivity probes. In this study, it was found out that low Reynolds numbers (Re) of gravity flow and shallow water depth ended up with lower mixing rates than the ones having higher values of Re and water depth.

Kneller et al. (1999) used LDA technique to measure mean and turbulent flow characteristics of a saline gravity current generated in a lock exchange tank.

In another study using lock-exchange method, PTV technique was used for elucidating the structure of the head of an inertial gravity current (Thomas et al., 2003). In that study, vorticity, shear stress and divergence fields and streamlines were also obtained besides the velocity profiles.

Firoozabadi et al. (2009) experimentally modelled continuous-release gravity currents using Acoustic Doppler Velocimeter (ADV) besides applying a low Reynolds number k–ε model.

Gerber et al. (2011) experimentally investigated continuously released gravity current using Particle image velocimetry scalar (PIV-S) technique. In that study, measured mean and turbulent flow parameters and excess density variance were used to evaluate their numerical model realized by ANSYS CFX software.

In addition to these studies, gravity currents which come across some objects such as obstacles with different shapes, cylinders and aquatic vegetation took attention of researchers.

Yaghubi et al.(2013) experimentally investigated turbidity current behaviour which flows over two sequential triangle shaped obstacles. In this study, they presented measured velocity and concentration profiles by Acoustic Doppler Velocimeter (ADV). For experimental study of Mok et al.(2011), the obstacle was a vertically mounted circular cylinder this time. Tokyay and Constantinescu (2012) and Tokyay et al.(2012) numerically investigated gravity current interaction with a series of identical objects simulating dunes and an array of obstacles interaction, respectively. Hatcher et al. (2000) analytically and experimentally examined drag effect of some metal rod array in which a gravity current flows through. Tanino et al. (2005) made experiments for evaluating gravity current behavior through aquatic canopies.

For a general view (Figure 5.4), behaviour of a gravity current flow which was produced by lock-exchange method and propagating on a horizontal bottom may be analyzed in 3 phases as slumping phase, inertial phase and viscous phase, respectively in time (Hallworth et al., 1996).
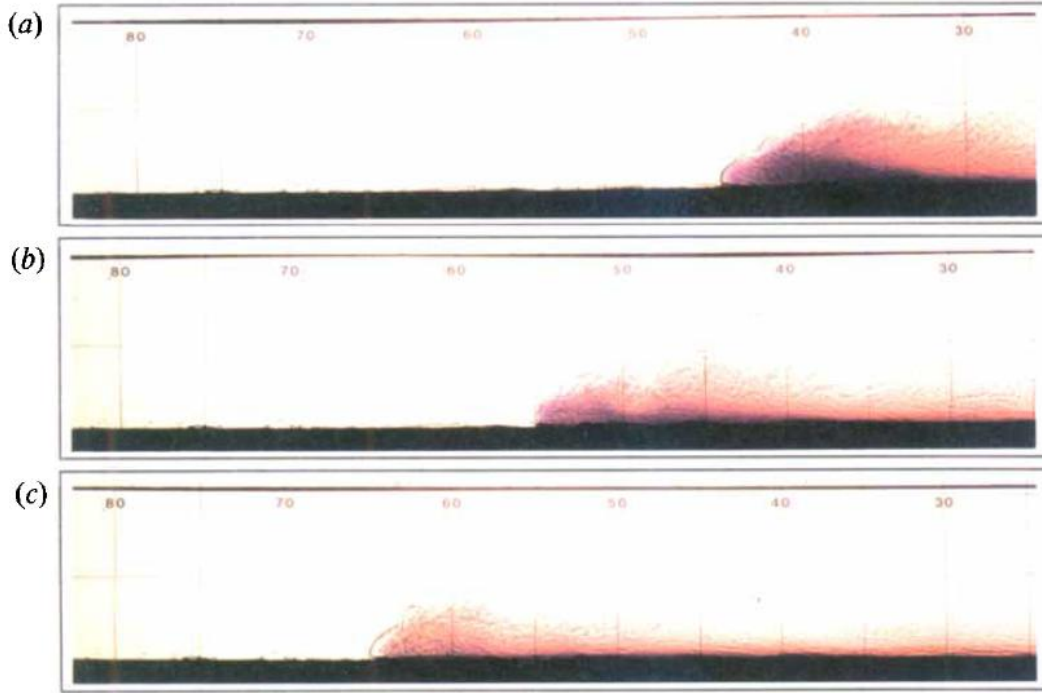
Figure 5.4 : Phases of a propagating gravity current on a horizontal bottom, a) Slumping phase, b) inertia-buoyancy phase, c) head at the position of neutralization (Hallworth et al., 1996).

The criteria for slumping phase is given as that when the ratio of depth of current to total depth is less than 0.075, mentioned phase ends and inertial phase starts (Huppert and Simpson, 1980). For transition from inertial phase to viscous phase, the criteria is determined as below where t_v is the transition time from inertial to viscous phase (Alahyari and Longmire, 1996):

$$t_v = 0.5(\frac{Q}{g'v})^{1/3} \tag{5.1}$$

In the inertial phase, buoyancy forces determine the flow behaviour and their role conveys to viscous forces in the viscous force. Viscosity and rheology of the flowing fluid are very important for transition between these phases and for the flow behaviour. This ends up quite different characteristics of non-viscous (saline, non-cohesive particle laden) and highly viscous (cohesive particle laden) gravity currents (Chowdhury & Testik, 2014).

Ellison and Turner (1959) determined that a dense layer, which was produced by lock-exchange method, flowing down on a bottom slope reached to an equilibrium

state in a short period of time and propagated with a constant Richardson number (Rin) beyond this point which was also observed by Alavian (1986).

In their experimental work, Britter and Simpson (1978) and Simpson and Britter (1979) declared that Kelvin-Helmholtz instabilities which are generated at the gravity current head determines the flow behaviour and mixing of the gravity current propagating on a horizontal bottom.

Gravity currents may have high (higher than 10^3), low (less than 10) or intermediate Reynolds numbers which affect mixing behaviour of them. High Re numbers indicate the turbulent behaviour of the current which generates entrainment of ambient water and dilution (Hallworth et al., 1996) Studies in the literature related to gravity currents include a wide range of Re number.

In their experimental study, Garcia and Parsons (1996) investigated mixing rates at the head of a gravity current which was kept steady by using a movable-bed tank. In that study, dimensionless mixing rate $(g'q_l/U_1^3)$ were used to evaluate mixing in which g' is the reduced gravity, q_l is the discharge per unit width of dense fluid and U_1 is the flow velocity in the channel. According to the results, the scale of tests and Re were effective on mixing characteristics. It was observed that mixing rates were increased with increasing water depth and increasing Reynolds number of gravity current flow. The maximum value of dimensionless mixing rate was 0.3, compatible with Britter and Simpson (1978) and Simpson and Britter (1979), over which the gravity current is deformed.

- *Thickness and lateral spreading*

Thickness of dense layer and its lateral spreading are important parameters for the gravity current flow. Lateral spreading contributes to mixing of gravity current flowing down a slope besides the entrainment at the density interface.

It was determined by Alavian (1986) that initial buoyancy flux and bottom slope were the characterizing parameters for lateral spreading amount of gravity currents. It was found out that lateral spreading increased with increasing buoyancy. For changing bottom slope, lateral spreading rate increased and reached to an almost constant value at different down slope distances for different bottom slopes. It was also measured that ratio of rate of lateral spreading and thickening was three.

Choi and Garcia (2001) developed a spreading law for lateral spreading of gravity currents on inclined slope using their experimental data obtained by image processing. They determined that for the bottom slopes <5°, lateral spreading may be expressed as:

$$u_f = c(\frac{B_0}{b})^{1/3}$$ **(5.2)**

where u_f is the front velocity, B_0 is the buoyancy flux, b is the maximum travel distance in the lateral direction and c is a coefficient which is equal to 1.0 for bottom slopes <5°. As it can be seen from the equation, bottom slope effect on lateral spreading may be ignored for these values.

As the maximum width is a time-dependent paramater, the relationship equation between half-width ($b_{1/2}$) and time (t) below was developed by using experimental data (Choi & Garcia, 2001) which was then used for calculation of lateral spreading for given time for tested bottom slope range (2°-10°):

$$\frac{b_{1/2}}{l_p} = 16.73\ln(1 + 0.022\frac{t}{t_p})$$ **(5.3)**

- *Effect of bottom slope (θ_c)*

Bottom slope is one of the important parameters that affect spreading of dense layer. In the case of gravity currents propagating on a inclined bottom rather than a horizontal bottom, gravitational force is also in subject besides buoyancy, inertia and viscous forces (Chowdhury & Testik, 2014).

In the literature, there are studies which encompassed effect of bottom slope on behaviour of gravity currents (Alavian, 1986; Etling et al, 2000; Choi and Garcia, 2001; Gerber et al, 2011; etc.). For a general view, most of these studies dealt with high bottom slopes. However, in a study of Alavian et al. (1986), it was declared that shape of gravity current flow was dependent on bottom slope and flow rate. It was determined that the flow was subcritical for bottom slopes of ~ <1/10 and observed entrainment was almost negligible for these slope values. In contrast to this, it was observed that the flow behavior varied to supercritical with increasing slope values and this concluded with generation of some interfacial instabilities and related entrainment. In the same study, it was concluded that shape of velocity and density profiles were independent of bottom slope.

88

Choi and Garcia (2011) executed a study with bottom slopes of 2.5°-5°-10°. In that study, they were interested in the effect of bottom slope on lateral spreading of density currents. As it was stated before, it was found that bottom slope effect was negligible for $\theta_c < 5°$. In addition, it was found out that in the buoyancy-dominated region, effect of bottom slope was negligible for density currents spreading on bottom with slopes of 5^0 and 10°.

- *Bottom roughness*

As a result of their experimental study, Hallworth et al. (1996) determined that bottom roughness affect shape of gravity current head due to frictional drag. Fernandez and Imberger (2006) executed a field study in a reservoir having gravity current inflows by using a profiler to measure salinity and temperature. They defined Ri_n related to bottom drag and entrainment rate. According to their findings, increased bottom roughness reduced effect of strafication and endorsed mixing.

Peters and Venart (2000) experimentally investigated effect of bottom roughness on the behaviour of gravity currents compratively with smooth beds. In the mentioned study, LIF methodology was used. By this study, it was found out that roughness elements caused lower initial constant frontal velocities, earlier domination of viscous forces and higher detention of gravity flows in viscous/buoyant regime. It was observed that additional mixing and related deceleration of flow occurred at the gravity current head due to the existence of ambient water between roughness elements.

- *Velocity and density profile*

Velocity and density profiles were measured in different studies for various conditions in the literature to elucidate mixing behaviour of gravity current flow. Simpson and Britter (1979) realized one of earliest measurements of velocity profile of a steady gravity current head on a horizontal bottom using a hot-film probe. Alavian (1986) measured centerline velocity and density profiles of gravity currents on an inclined bottom ($\theta_c = 10°$) by using thermistor probes. Gerber et al. (2011) used PIV technology to obtain velocity data related to a continuous-flux gravity current. Density measurements also realized by using various intrusive and non-intrusive instruments such as taking samples by the help of syphons, conductivity probes and LIF. As the instruments developed by time, more detailed and accurate

measurements of velocity and density profiles executed. Chowdhury and Testik (2014) draw a general scheme for velocity and density profiles of gravity currents in their comprehensive review of gravity current literature (Figure 5.5).
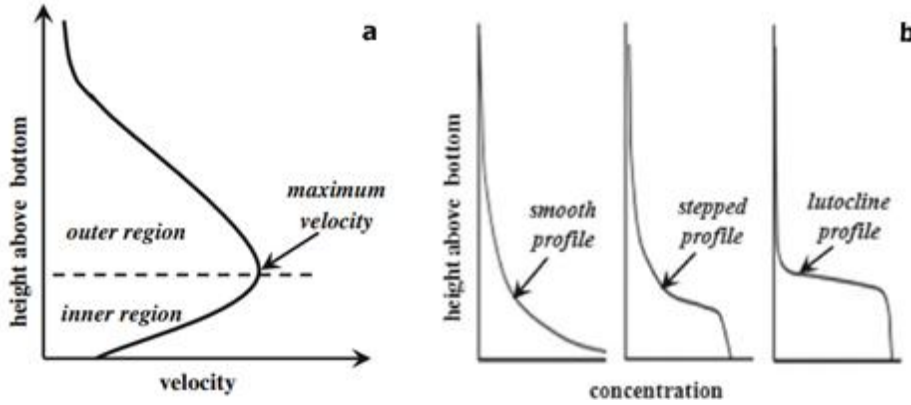
Figure 5.5 : Velocity (a) and concentration (b) profiles of gravity currents (Chowdhury & Testik, 2014).

- *Entrainment*

Entrainment is entering of ambient flow into the gravity current by generated shear at density interface and bottom effect. Entrainment is evaluated by using an entrainment coefficient (E) which shows the rate of entrained water.

Ellison and Turner (1959) developed a theory related to flow of fluids entering into an ambient fluid which has a different density and stagnant/moving with a very low turbulence. According this this theory, flow is in the form of a turbulent thin layer and entrainment, which is the ambient water entered into that layer, is a function of velocity of the layer multiplied with an emprical function, E(Ri). Here, E is called as the entrainment constant and it is a function of flow bulk Ri as below (Ellison & Turner, 1959; Fernandez and Imberger, 2006):

$$E = \frac{w_e}{u} = E(Ri_b)^{-k} \tag{5.4}$$

where bulk Richardson number (Ri_b) is:

$$Ri_b = \frac{g'h}{u^2}\cos\theta = \frac{1}{F_d^2} \tag{5.5}$$

In these equations, w_e is the entrainment velocity, u is the mean underflow velocity, k is a constant (0-3/2), g' is the corrected buoyancy as $g' = g(\rho - \rho_a)/\rho_a$, g is the

gravitational acceleration, h is the depth of flowing layer, α is the bottom slope and F_d is the densimetric Froude number.

In the same study, they obtained entrainment definitions experimentally for surface jets and also a salt underflow for the first time in the literature. By this study, they determined that the saline underflow reaches an equilibrium state after a quick initial phase. During this transition, initial Ri number gradually increase and reaches to an ultimate value (R_n) and remains constant for the rest of the flow (Ellison and Turner, 1959; Fernandez and Imberger, 2006).

Alavian (1986) calculated E by using measured velocity and density profiles in his experimental study, which was about continuosly fed gravity currents on an inclined slope, for different cross sections of the flow by using the equation below:

$$\frac{d}{dx}(UA) = EU(b + 2h) \tag{5.6}$$

Here, U is mean layer velocity; b is the dense layer width and h is the layer thickness. According to results of this study, calculated E was high and then decreased to a constant value as the flow propagates along the slope. For different bottom slopes, it was determined that E increased with increasing bottom slopes and buoyancy flux.

As stated before, Richardson number is an indicator of mixing efficiency of density flow. Energy exchange between dense layer and ambient decreases with increasing Ri which ends up in lower entrainment and mixing rates (Alavian, 1986).

Various definitions of entrainment rate were declared for different conditions in many studies related to gravity currents (Fernandez and Imberger, 2006). Their common point was defining the entrainment rate related to bulk Richardson number for different ranges of it (Fernandez and Imberger, 2006; Chowdhury and Testik, 2014). Differently, Wells et al. (2010) defined E related to turbulence flux, length and velocity scales.

In Table 5.1, entrainment formulas obtained in experimental studies in the literature are given. Figure 5.6 shows plots of mentioned equations in the form of Ri versus E. As it can be seen generally there is an inverse ratio between E and Ri. The reason of different behaviour of some plot lines is probably the experimental method used.

Table 5.1 : Entrainment formulas in the literature (Adapted and modified from Fernandez and Imberger, 2009).

Source	Equation	Validity
Ellison & Turner (1959)	$E = \dfrac{0.08 - 0.1Ri}{1 + 5Ri}$	$Ri < 0.4$
Lofquist (1960)	$E = \dfrac{0.001}{Ri}$	$7 < Ri < 110$
Ashida & Egashira (1977)	$E = \dfrac{0.0015}{Ri}$	No limit
Hebbert et al. (1979)	$E = \dfrac{c_K c_D{}^{3/2}}{Ri - c_s}$	$0.3 < Ri$
Garcia (1985)	$E = \dfrac{0.075}{(1 + 718Ri^{2.4})^{0.5}}$	No limit
Christodoulou (1986)	$E = 0.07$ $E = 0.07Ri^{-1/2}$ $E = 0.02Ri^{-1}$ $E = 0.07Ri^{-3/2}$	$Ri < 0.01$ $0.01 < Ri < 0.1$ $0.1 < Ri < 10$ $Ri > 10$
Parker et al. (1987)	$E = \dfrac{0.075}{(1 + 715Ri^{2.4})^{0.5}}$	No limit
Atkinson (1988)	$E = \dfrac{c_F c_b Ri Pe^{-1/2}}{c_t + Ri}$	No limit
Kessel & Kranenburg (1996)	$E = \dfrac{5.5 * 10^{-3}}{3.6Ri - 1 + \sqrt{(3.6Ri - 1)^2 + 0.15}}$	No limit
Dallimore et al. (2001)	$E = \dfrac{c_K c_D{}^{3/2} + c^*{}_s}{Ri + 10(c_K c_D{}^{\frac{3}{2}} + c^*{}_s)}$	No limit
Princevac et al. (2005)	$E = 0.05Ri^{-0.75}$	No limit

As it can be seen from the Figure 5.6, flow behaviour and entrainment is directly related to Ri. By using the equations above, it is possible to define characteristic values of Ri for various flow conditions: Critical Ri (Ri_c) for critical flow, normal Ri (Ri_n) for normal/equilibrium flow and uniform Ri (Ri_u) for uniform flow (Table 5.2).
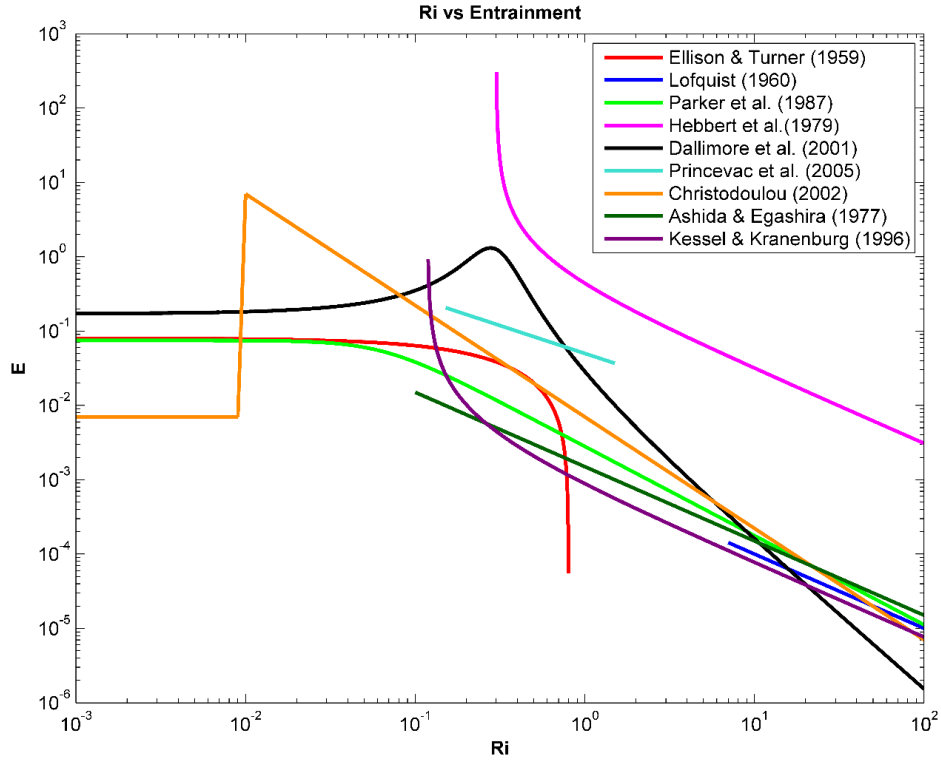
Figure 5.6 : Entrainment and Ri relation determined in different studies.

Table 5.2 : Example Characteristic Richardson numbers for density currents.

Ri	Flow Type	Condition	Equation	Notes
Ri_c	Critical	$\dfrac{dh}{dx} = \pm\infty$	$Ri_c = \dfrac{1}{S_2}$	$Ri > Ri_c$: subcritical flow $Ri < Ri_c$: supercritical flow
Ri_n	Normal/Equilibrium	$\dfrac{dRi}{dx} = 0$	$Ri_n = \dfrac{E + C_d}{S_1 S_0 - \frac{1}{2} S_2 E}$	$E = f(Ri_n) = \text{constant}$ $\dfrac{dh_n}{dx} = E$ $\dfrac{dU}{dx} = 0$ $\beta_n = \dfrac{Ri_n U_n{}^2}{g h_n(x)}$
Ri_u	Uniform	$\dfrac{dh}{dx} = 0$	$Ri_u = \dfrac{2E + C_d}{S_1 S_0 - \frac{1}{2} S_2 E}$	$= -E \dfrac{3 Ri_u}{h_u} \leq 0$ Uniform density currents are not possible.

After spreading for some distance, a density current reaches to an equilibrium flow which is characterized by its constant Richardson number, Ri_n. At this stage, density current thickness increases linearly with entrainment, which corresponds to a decreasing buoyancy difference (β) as it propagates with a constant velocity and dilutes.

Uniform flow is defined as the flow type during which the thickness of dense layer is constant through the distance. However, as it can be seen of the notes for this

condition, this type of flow is impossible to exist due to the reason that the equation showing variation of Ri along distance is only valuable for E=0.

- *Turbulence parameters*

For a general view of mixing of gravity currents, main parameters which are controlling gravity current flow are turbulence, interaction of turbulence and stratification, anisotropy and causes of density differences (Gerber, 2008).

Islam and Imran (2010) made an experimental study using ADV and presented mean velocity, excess fractional density and turbulence structures of saline and particulate density currents which are propagating on horizontal and inclined bottom. Gerber et al. (2011) measured turbulent flow properties (Reynolds stresses, Reynolds fluxes, production of TKE) of a continuous-release gravity current on a horizontal bottom with PIV-S methodology and presented this data comparatively with their numerical modelling results.

6. EXPERIMENTAL STUDY & RESULTS

In this chapter, experimental studies which are executed in the context of this thesis is presented. These studies are realized in 3 parts through which different aspects of the topic are handled.

6.1 Mixing of a Salt Layer Under Regular Wave Effect

In the first part of experimental studies, mixing behaviour of a discharged horizontal dense jet under regular wave conditions was investigated. This study is presented as a conference paper in IMAM 2011 Conference (Bas et al., 2011).

6.1.1 Experimental system

Experiments were conducted in a wave flume with dimensions 22.5 m. x 1 m. x 1 m. in Hydraulics Laboratory of Istanbul Technical University. The wave flume has glass walls for easy observation and a wave generator at one end to produce regular waves with a metal slope behind it to prevent the swash behind it. At the other end of the flume, a sandy beach is established for preventing wave reflection. During the experiments water surface elevation was measured with resistant type wave gauges. Wave data was evaluated with zero-crossing method to obtain the wave height values.

For simulating brine discharges, salt (NaCl) solution with 35 ppt salinity was prepared with freshwater. In this way, same density difference ratio (~0.0256) between the effluent and the receiving environment was provided with the real situation as applied in Ruiz-Mateo et al.'s (2008) study. For the flow visualization, the solution was colored with Ponceau 4R red food dye as trace material.

Experiments were recorded with a Canon Legria HF M36 digital camera. The wave flume is filled with freshwater and depleted, washed and refilled after every two experiment with the same configuration.

Salinity values were measured with salinity/conductivity probes of two WTW MultiLine meters, each one is placed at 0.8 m and 5 m after the discharge point, respectively. Dense jet discharge was implemented from a solution tank at the top of the flume via a plastic tube with 4 mm diameter, 10 cm above the bottom. Schematic diagram of experimental set up can be seen in Figure 6.1.
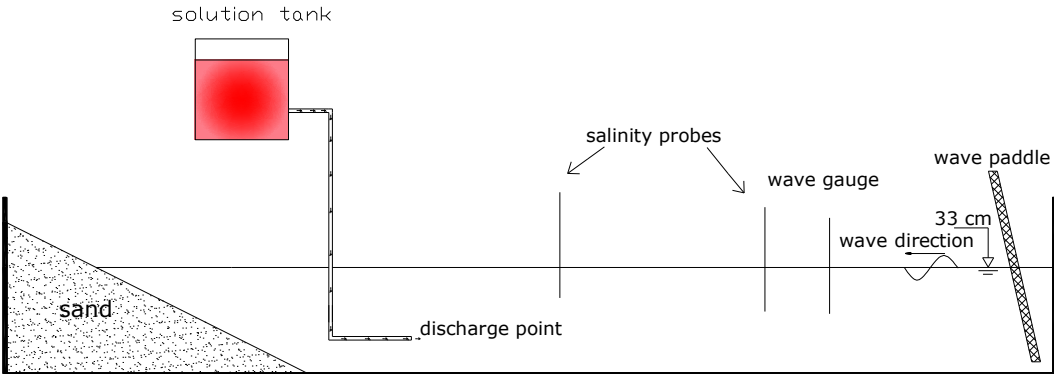
Figure 6.1 : Experimental setup for the tests related to mixing of salt layer.

6.1.2 Experimental procedure

At each test, a uniform density layer (~8 cm thick) is composed along the flume and then different waves were generated to investigate the effect of wave properties on mixing of this dense layer (Figure 6.2). Each characteristic regular wave is applied for 5 and 10 minutes for different tests and the vertical distribution of salinity is measured after each test. Experimental procedure is given at Table 6.1. In each test, water depth was 0.33 m and the waves were transitional water waves with $1/20 < d/L < 1/2$ ratios. Here d is the water depth and L is the wave length calculated according to the linear wave theory:

$$L = \frac{gT^2}{2\pi}\tanh\frac{2\pi h}{L} \qquad (6.1)$$

96
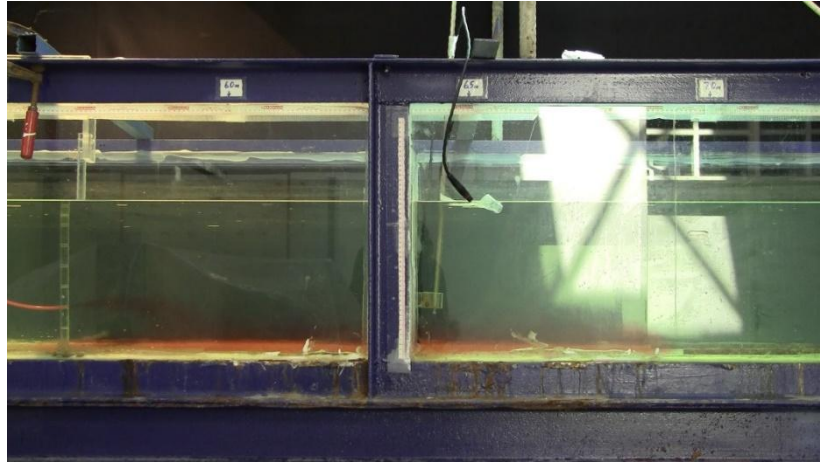
Figure 6.2 : A picture from the experiments showing formation of dense layer.

Table 6.1 : Test procedure.

Test No	Test Duration, t_e (min)	Wave height, H_{mean} (cm)	Mean wave period, T_{mean} (s)
1	5	5.81	0.71
2	10	5.81	0.71
3	5	6.36	0.74
4	10	6.36	0.74
5	5	6.93	0.73
6	10	6.93	0.73
7	5	7.86	0.76
8	10	7.86	0.76

6.1.3 Results

During the experiments, it was seen that the dense layer at the bottom of the wave flume was oscillating with water surface with a phase difference (Figure 6.3). This situation can be explained by pressure differences at the bottom due to the wave motion. In the experiments, wave motion was the main factor affecting mixing of dense layer besides molecular diffusion.

Figure 6.3 : Movement of dense layer with waves.

As it can be seen from the Figure 6.4, wave motion caused mixing of dense layer with fresh water ending in increased water column height with salinity values for the experiment with 5 minutes duration. In the tests for 10 minute wave generation, mixing is increased and salinity layer became thicker. As the wave height increased, salinity profiles became uniform along the whole water column with 0.1 ppt value for the two highest wave height values.

Additionally, wave energy and potential energy exchange for each experiment is calculated by using linear wave theory and vertical salinity profile values, respectively.

For the total wave energy calculation per area for test duration (t_e):

$$E_w = \frac{1}{8} \rho g H^2 \frac{t_e}{L} \tag{6.2}$$

formula is used.

Potential energy can be used as a measure of stratification due to salinity values in the profile and their vertical location in the water column. By this way it is possible to relate the events causing mixing and stratification. In terms of mixing, external kinetic energy added to the water column gives rise to increasing of potential energy due to the lifting of dense fluid at the bottom (Hodges et al., 2006).

According to linear wave theory, the total energy per wave per unit width is:

$$E_w = \frac{1}{8} \rho g H^2 \tag{6.3}$$

and wave energy flux through a unit width is:

$$P = E c_g \tag{6.4}$$

where c_g is the group velocity.

In addition, potential energy (E_p) of the water column can be described as:

$$E_p = g \int_0^h \rho z \, dz \tag{6.5}$$
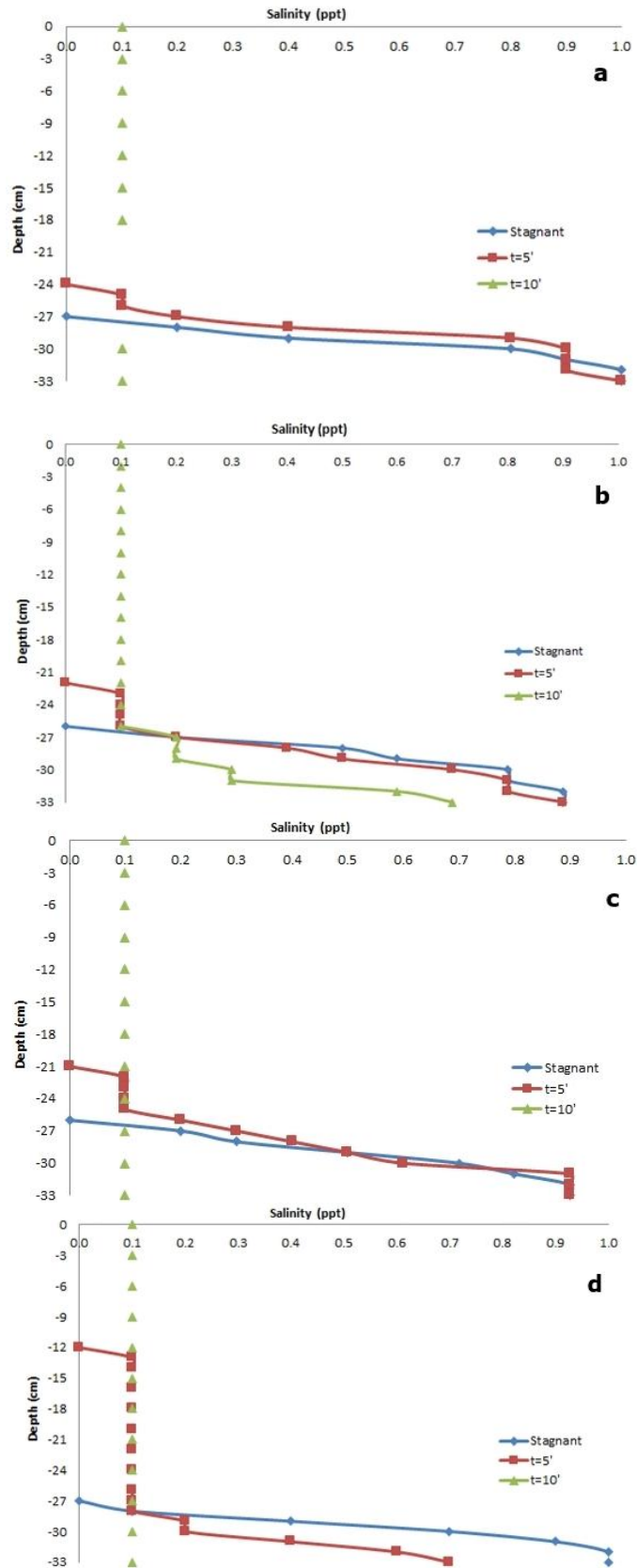
Figure 6.4 : Variation of vertical salinity distribution for the tests a)1-2,b) 3-4, c) 5-6, d) 7-8.

For potential energy calculation, density values were estimated from salinity values. Potential energy of the water column was calculated for the tests 1, 3, 5 and 7 by using potential energy formula for each measurement height. These values can be seen in Figure 6.5 depending on wave steepness (H/L). According to the graphic, ratio of potential energy of the mixed water column to generated wave energy has an increasing trend with wave steepness.
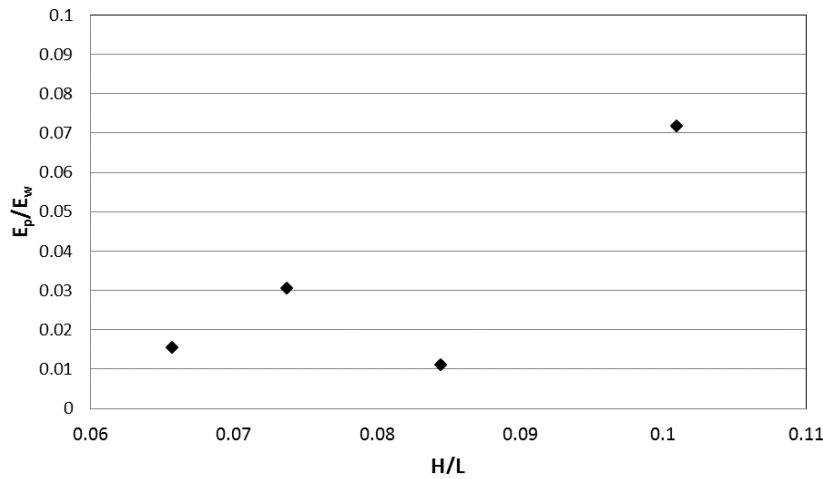
Figure 6.5 : Energy ratio versus wave steepness.

Wave energy can be effective on the vertical mixing of a dense saline layer in transitional wave conditions for our test conditions. In this process, wave energy in the form of kinetic energy is transferred to the water column and causes mixing. At the end of this process, potential energy of the water column increases due to ascending salinity concentrations in the water column. Wave motion is responsible for this situation.

6.2 Horizontal Discharge

In the first part of experimental studies, mixing behaviour of a discharged horizontal dense jet under regular wave conditions was investigated. These tests were executed as the preliminary tests with not sofisticated measurement devices due to existing laboratory conditions. The results were presented in the 16th International Symposium on Environmental Pollution and its Impact on Life in the Mediterranean Region (MESAEP 2011) and published (Bas et al., 2012). In the following section, this study will be presented.

6.2.1 Experimental system

Experimental setup was prepared in a wave flume, which has dimensions of 22.5 m. x 1 m. x 1 m., in ITU Hydraulics Laboratory (Figure 6.6 and 6.7). The wave flume has sidewalls made of glass for the observation of the tests. It is equipped with a piston-type wave-maker which is capable of generating regular waves. For the aim of preventing wave reflection, a sandy beach was formed at the other side and it was covered to prevent mixing of particulate matter into the flume during the experiments. Water depth was 0.33 m for the whole tests because of being the most appropriate value depending on the previous studies executed in the same wave flume.
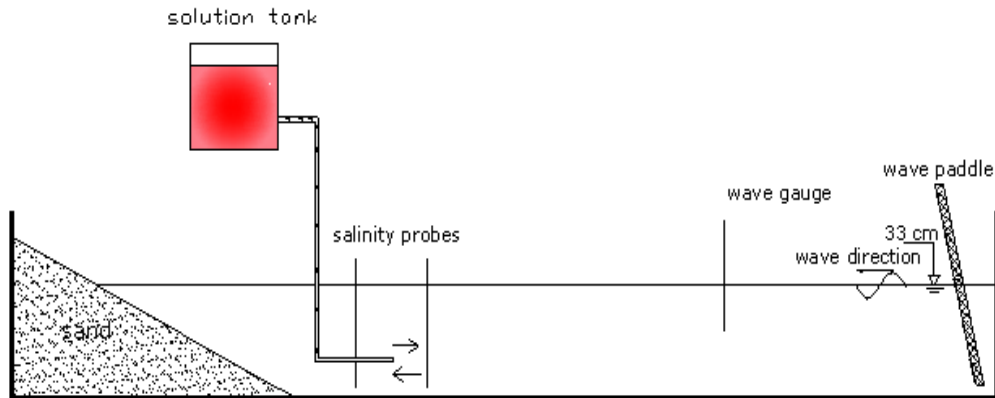
Figure 6.6 : Schematic diagram of the experimental set up.

For the simulation of desalination brine, salt solution was prepared using NaCl, tap water and red food dye (Ponceau 4R) which provides easy following of the flow. Density difference between the salt solution and the wave flume ($\Delta\rho=\rho_0- \rho_a)/ \rho_a$) was kept constant at ≈0.025 for the whole tests (Ruiz Mateo et al. , 2008). Discharge was executed via a plastic tube of 4 mm diameter which is connected to a solution tank placed above the tank. Discharge pipe was mounted horizontally on a plexiglass rod at 10 cm away from the bottom which provides constant bed proximity for the whole tests.

Salinity values were measured during the tests by using two salinity probes of WTW MultiLine measurement device which is an field-type instrument capable of measuring temperature, salinity and conductivity and dissolved oxygen in the water using different measurement probes. WTW Multiline P4 conductivity and salinity probe has a measuring range of 1-1999 μS/cm and 0-70 ppt, respectively. Its

accuracy is ±1% of measured value for conductivity. For salinity, accuracy value is ±0.1 (5-25 °C ambient temperature) or ±0.2 (25-30 °C ambient temperature). It calculates salinity values depending on UNESCO Technical Papers in Science 36 which is about defining conductivity and salinity of oceanic waters. Response time of the instrument for conductivity is stated as >10 seconds.

Mentioned two probes were placed at 56 cm away from the disccharge point at upstream and downstream directions. According to jet/plume transition length scale (l_M) value at this distance discharged dense jet behaves like a plume due to the fact that it is higher than the threshold value of 0.11 m for the test conditions.

A resistant-type wave probe was used for measuring wave parameters.

A light source was placed above the wave flume for enlightening the part of the wave flume where the dense jet was discharged. For minizing reflections on the recorded images, a black curtain was hanged behind the wave flume.
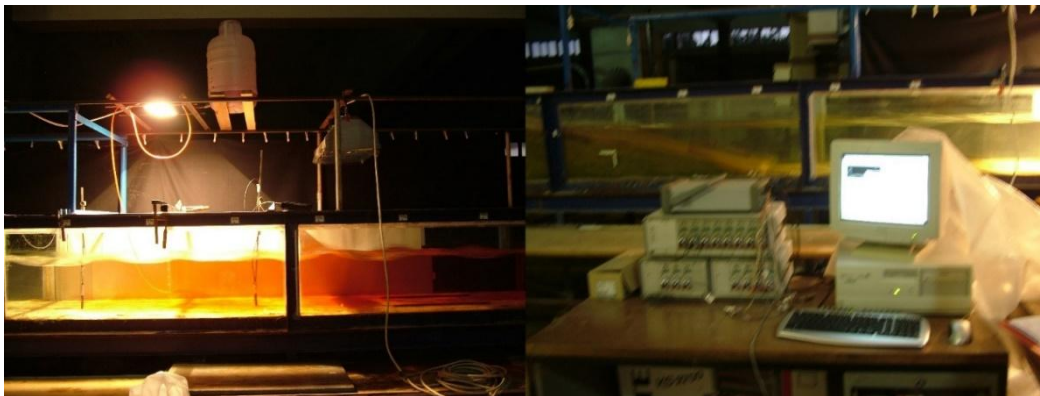
Figure 6.7 : Photos of experimental setup.

6.2.2 Experimental procedure

Before each test, wave flume was cleaned, filled with tap water and wave calibration was done. Before starting discharge of salt solution, firstly wave measurement was realized by the aim of having correct measurement without the effect of salinity.

Salt solution was discharged continuously for 3 minutes in each test. Discharge rate was measured using a chronometer previously then the tests and assumed constant at 0.012 L/s. With these values of $\Delta\rho$ and flow rate, F_d was around 30 for the whole experiments.

All of the tests were recorded by using a Canon Legria HF M36 digital video camera which was placed at one side of the wave flume.

Experiments were conducted in test pairs of same experimental conditions except having different discharge directions; co-directional and opposite directional with waves. In addition, a test was executed with stagnant receiving environment conditions (Table 6.2).

Table 6.2: Test procedure and wave characteristics.

Test No	Discharge Direction Relative to Waves	Mean wave height, H_{mean} (cm)	Mean wave period, T_{mean} (s)	Wave Type
C702	co.	4.19	0.54	deep
O502	opp.			
C501	co.	4.82	0.60	deep
O102	opp.			
C703	co.	6.83	0.68	transitional
O704	opp.			
S601	stagnant	-	-	-

6.2.3 Data evaluation procedure

In this part, used data evelation procedure will be explained in the order of wave data, salinity data and video and images.

6.2.3.1 Wave data

Zero-crossing method was used to process wave data and obtain wave parameters. Wave length values were calculated by iteration using the wave length equation of linear wave theory (Eq. 6.1). (Dean & Dalrymple, 1991).

Calculated wave lengths were used to define classification of generated waves according to water depth (d) as transitional for $1/20 < d/L < 1/2$ and as deep water waves for $d/L \geq 1/2$ (Dean & Dalrymple, 1991). Obtained wave characteristics are given in Table 6.2.

6.2.3.2 Salinity data

As the connection of WTW Multiline P4 to computer for recording the data was unsuccessfull, salinity values were recorded manually by observing the instrument screen and also alive at camera records.

6.2.3.3 Video and images

Recorded video images were used to obtain snapshots with time intervals between for each test. These images were processed to obtain measure distances and area of discharged jet by using ERDAS image processing and geographical information (GIS) software. RGB colour clustering methodology was used to classify pictures into 256 colour classes. By this method, three band of data is compressed in an image which constitutes of only a single band. For this aim, software firstly plots all pixels of an image in 3-D space and then clusters this data depending on user specified numbers of Red (R), Green (G) and Blue (B) sections in each dimension. Option of arranging the number of R, G and B sections allows the user to set the image according to the aim of use which in this case was colouring only the required area (jet) in the images (ERDAS Inc., 1999).

By using AutoCAD software, scaling is done by using known distances on the figure and also distortions were discarded. After this procedure, perimeter of dense jets at the time concerned were digitized to make it ready to measurement. Distances and areas were measured in the GIS environment combining whole the layers. In addition, recorded videos were used to check the salinity time series obtained.

6.2.4 Results

As it is expected, discharged horizontal dense jet followed a horizontal trajectory until it plunges at a point from which it started to move vertically to the bottom because of its negative buoyancy. After impinging to the bottom, it formed a dense layer at the bottom for both stagnant and wave conditions (Figure 6.8). As it can be seen from the images, dense jet oscillated with the effect of waves differently than stagnant conditions (Figure 6.9). When the images at same time interval after discharge moment were compared for stagnant and wave conditions, it was determined that wave action shifted impingement of the dense jet. Oscillation was still present after the impingement point at tests with waves.

| t=3 s | t=8 s | t=11 s | t=19 s | t=24 s |
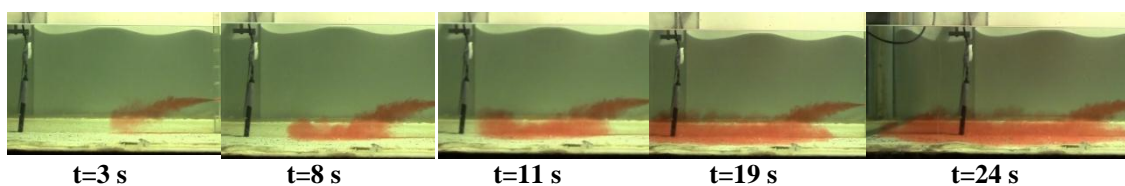
Figure 6.8 : Pictures from the test of discharge to stagnant environment (Test S601).

104

In Figure 6.9, images of a test pair are given in the form of raw photos and processed images for different times. During both co-directional and opposite directional discharges, discharged dense jet oscillates with wave effect and sinks to bottom ending up a dense layer form. However, direction of discharge respect to the waves generated different behaviour of dense jet despite having the same initial conditions. Comparison of images related to the 11th , 19th and 24th second of the tests demonstrated that spreading rate of dense jet with opposite directional discharge was greater than the one with co-directional discharge. In terms of thickness, it was observed that the tests with co-directional discharge had wider areas compared to the ones with opposite directional discharge (Figure 6.9).
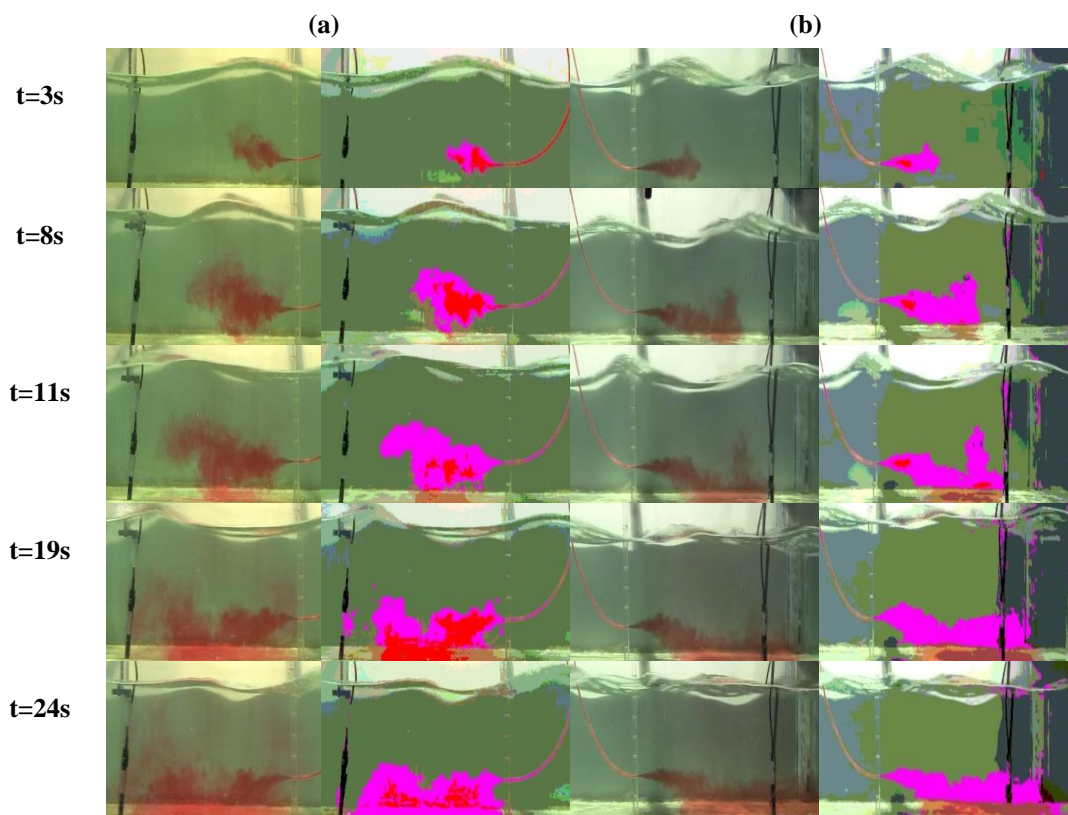
Figure 6.9 : Pictures and processed images showing outer boundaries of spreading area for a) co-directional (C501) discharge, b) opposite directional (O502) discharge.

Cross-sectional area from the processed images of 3rd, 8th, 11th, 19th and 24th seconds are given in Figure 6.10 and Figure 6.11 cumulatively in the form of only outer borders (a) and with coloured image (b). It is quantitatively seen that co-directional discharge generated wider jets in the vertical direction and the jets with opposite directional discharge spreaded more effectively in the horizontal direction which concluded in lower thickness values. Measured values also certified that

observation with end point distance value at 24th seconds is 0.49 and 0.62 m for co-directional and opposite directional discharge cases, respectively (Table 6.3).
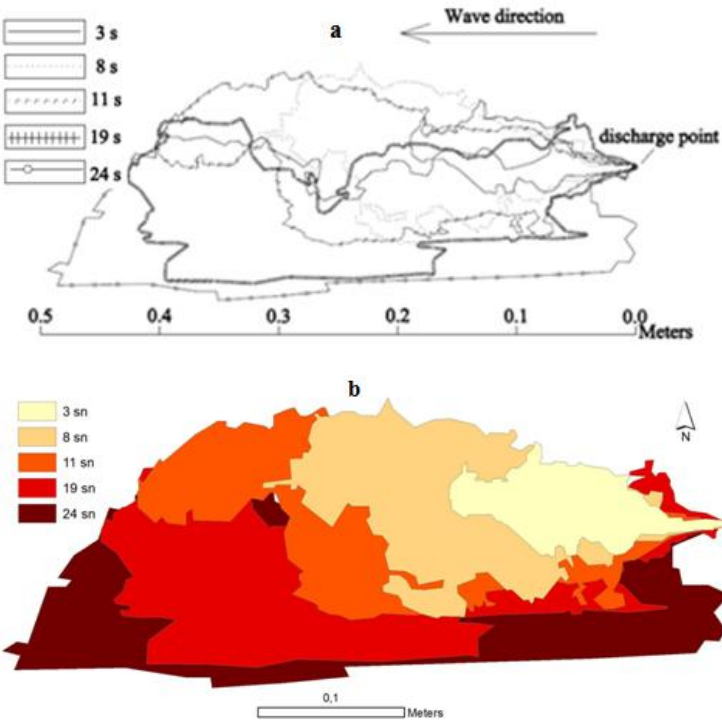
Figure 6.10 : Cross-sectional area in the vertical direction for co-directional discharge (Test C502).
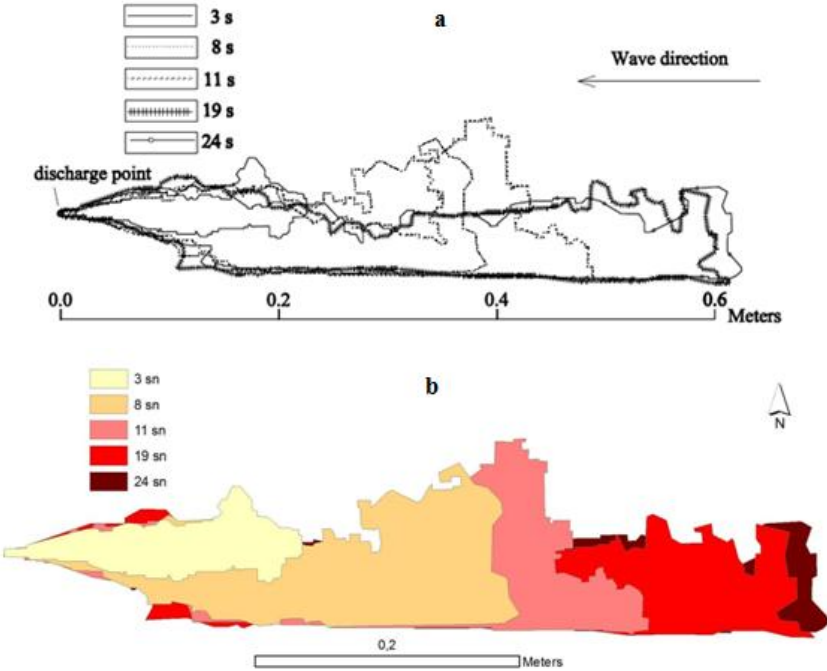
Figure 6.11 : Cross-sectional area in the vertical direction for opposite discharge (Test O501).

Table 6.3: Cross-sectional areas in the vertical direction and distance of the final destinations to the discharge point.

Time (s)	Co-directional discharge		Opposite directional discharge	
	Cross-sectional area in the vertical (m^2)	Horizontal distance to the discharge point (m)	Cross-sectional area in the vertical (m^2)	Horizontal distance to the discharge point (m)
3	0.007	0.19	0.007	0.23
8	0.021	0.30	0.024	0.39
11	0.030	0.40	0.028	0.49
19	0.036	0.43	0.031	0.60
24	0.047	0.49	0.032	0.62

Measured salinity values were used to obtain dilution ratios at the measurement point through the time. Dilution (S) is defined as the ratio of initial salinity (C_0) to measured value of salinity (C) since salinity of water in the wave flume was zero. Time series of dilution values are presented in Figure 6.12 comperatively for each test pairs. As it can be seen, highest dilution values are greater for opposite directional discharge for O102 & C501 test pair (Figure 6.12a) which is also compatible with the second test pair of O502 & C702 (Figure 6.12b). However, it is seen in Figure 6.12c that dilution values were closer for the third test pair (O703 & O704) at which the waves were transitional rather than deep water waves in the other tests. Dilution values in stagnant receiving environment conditions were obviously lower than the tests with opposite directional discharge (Figure 6.12d) This situation is an indication positive effect of regular waves on mixing. However, values were slightly different than the tests with co-directional discharge meanwhile accumulation of saline solution at the observed.
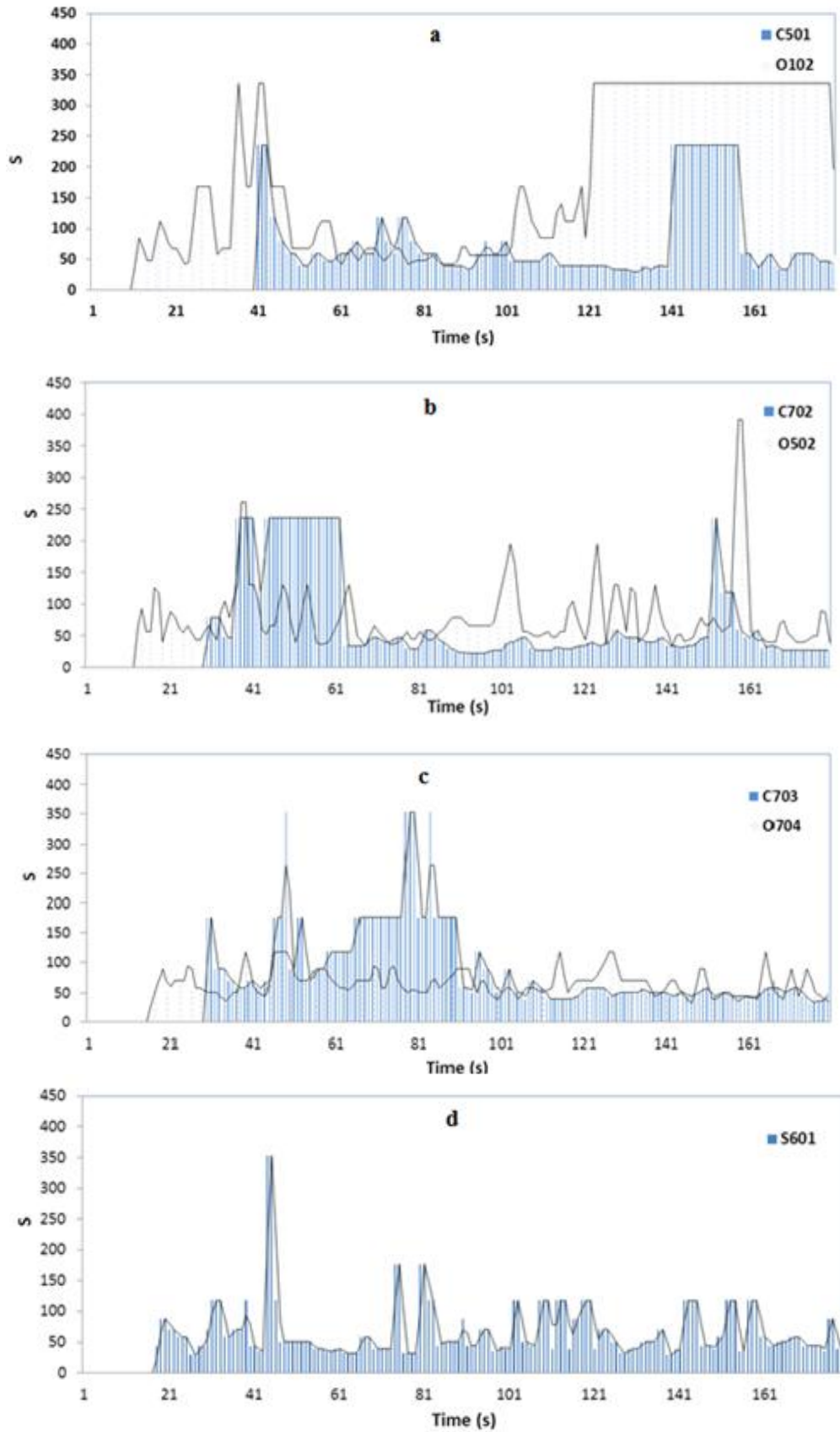
Figure 6.12 : Effect of discharge direction on the dilution (S) values a) Tests C501 and O102, b) Tests C702 and O502, c) Tests C703 and O704, d) stagnant receiving environment (Test O501).

108

In Figure 6.13, same time series are given as a cumulative presentation of whole tests with regular wave conditions and one discharge direction. As it can be seen, dilution rates were higher for the tests with higher wave amplitudes for both cases of direction. When the same figure is analyzed through the time, dilution rates decreased by the time at co-directional discharges and it is vice versa for the opposite directional discharges. This is an inevitable result due to the different spreading behaviour of jets related to their direction with water waves.
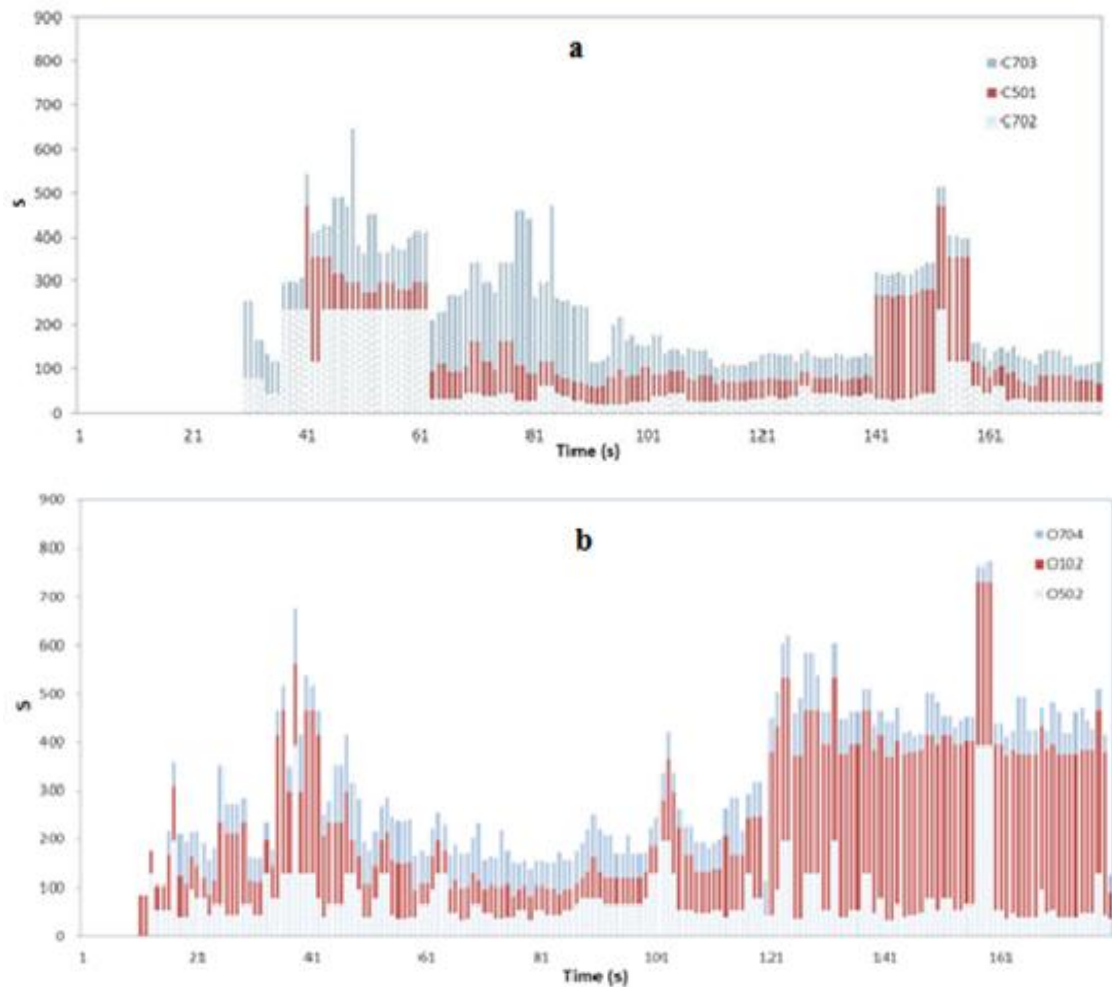
Figure 6.13 : Dilution (S) time series for a) co-directional discharges, b) opposite directional discharges.

As the summary of first tests, it can be concluded that opposite-directional discharge of a horizontal dense jet caused more mixing at the bottom compared to co-directional discharge case. In addition, positive effect of waves on mixing of

mentioned jet was observed for both cases which was more distinctive at opposite directional case.

6.3 Inclined Discharge

In the third part of experimental studies, mixing behaviour of a discharged inclined dense jet under regular wave conditions was investigated.

6.3.1 Experimental setup

A schematic view of experimental setup by which discharge of inclined dense jets under regular conditions was examined is presented by Figure 6.14.
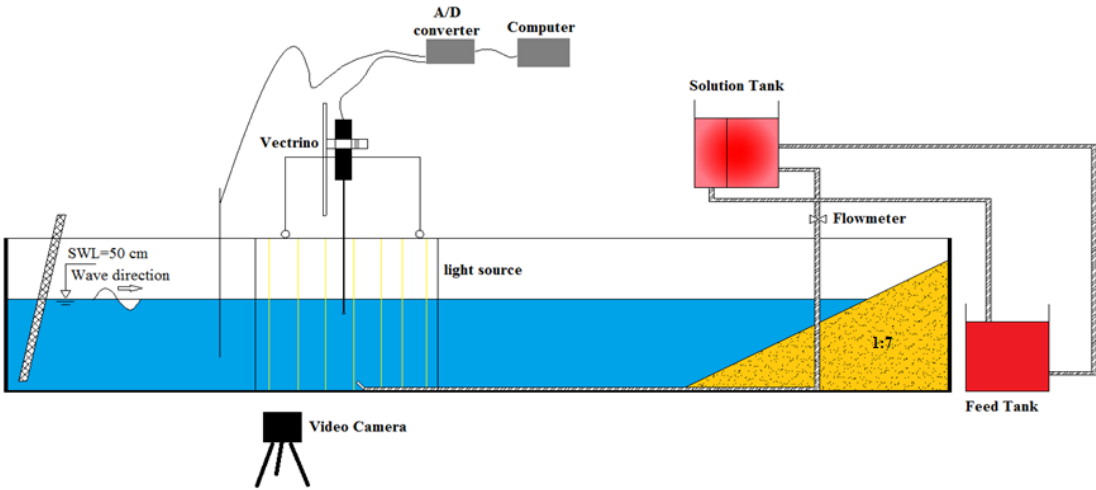
Figure 6.14 : Schematic diagram of the experimental set up.

Experimental study was executed in a wave flume with the dimensions of 24 m x 1 m x 1 m (Figure 6.15). Structural part of the wave flume is made of iron with concrete bottom and it has glass walls at both sides to provide visibility of ongoing experiments inside. At one end of the flume, in the direction of wave propagation, a rubble mound slope (1:7) is constructed to preclude wave reflection. Before placing in the flume, stones were well washed as a measure for impurities in the water.
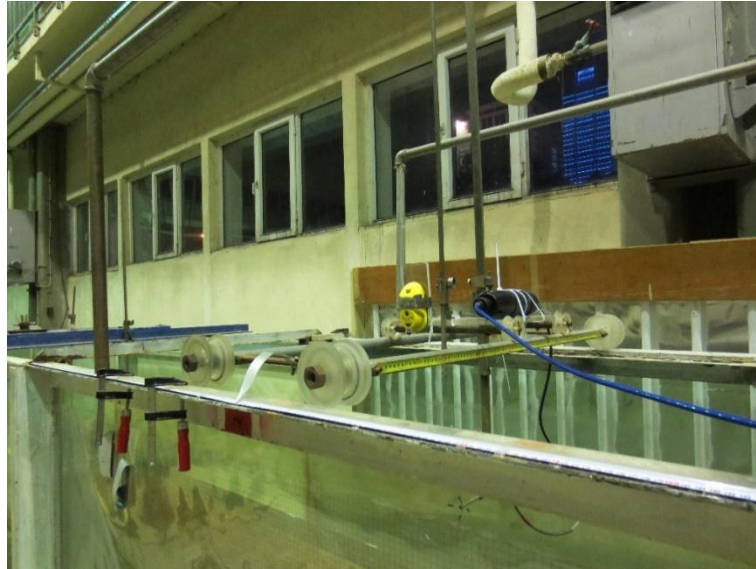
Figure 6.15 : Wave flume.

At the other side, there is a piston-type wave maker which is capable of generating both regular and irregular waves. The wave maker is moved by a motor and controlled by a signal box and computer which are placed besides the wave flume (Figure 6.16).
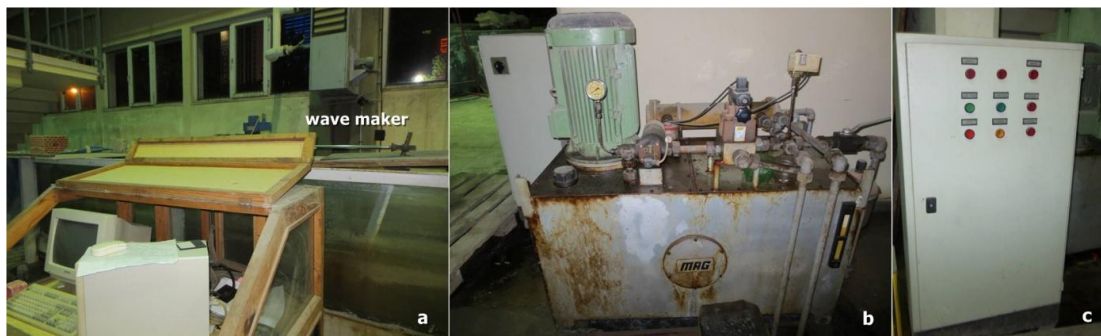
Figure 6.16 : Wave generation system a) wave maker and computer, b) motor, c) control panel.

Prepared salt solutions discharged to the wave flume through a constant head discharge system (Figure 6.17). In that system, a constant head tank is placed above the flume. Salt solutions were prepared in a different tank which was at the same level with wave flume. Salt solution was pumped to constant head tank above via a submersible pump and discharged to wave flume through a pipe with ¾" diameter which was ended with a discharge nozzle placed at the middle of the flume. 2 brass nozzles with different inner diameters (5 and 7 mm) were made in the laboratory to provide inclined discharge of salt solutions.

Figure 6.17 : Discharge system.

Flow rate of discharged salt solution is measured by a FLOWX3 brand electromagnetic flow meter. The reason for choosing electromagnetic type flow meter was using salt solutions which may harm conventional type flowmeters. Electromagnetic flow meters are widely used in the systems in which measurement of seawater flow rate is required. Used flow meter has a measurement range of 0.05-8 m/s and gives instantaneous flow rate and amount of total discharge volume. Discharge rate was regulated using a line valve and a butterfly valve (Figure 6.18).
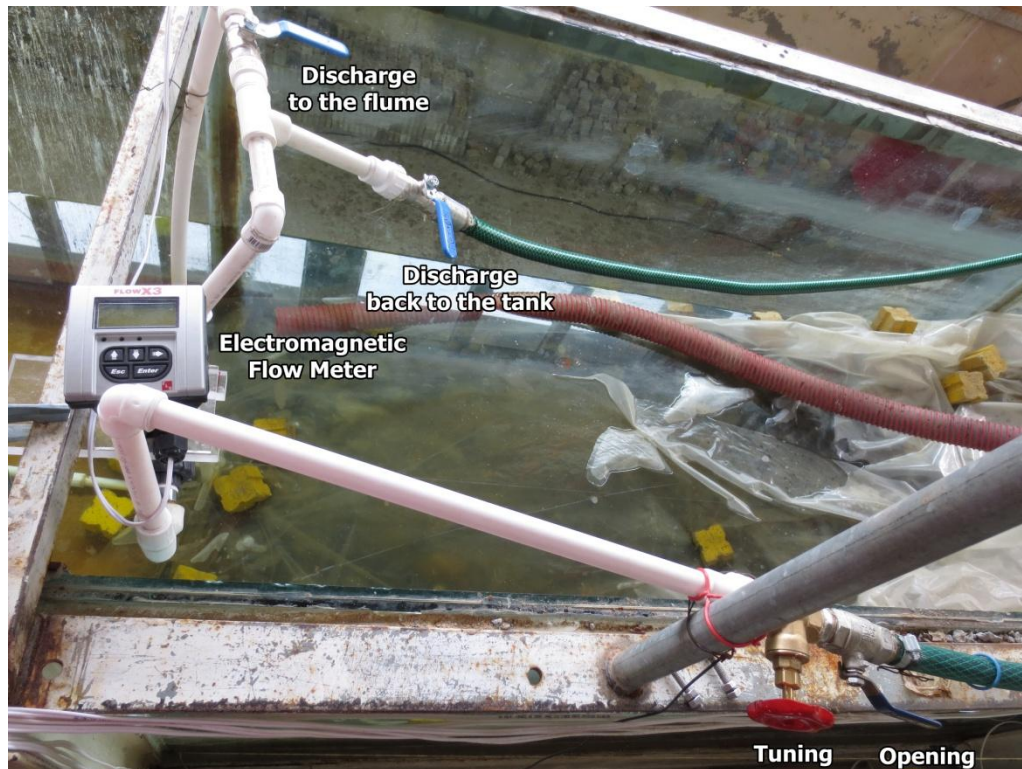
Figure 6.18 : Electromagnetic flowmeter and valves.

6.3.2 Data measurement and recording systems

During the experiments, water surface elevation profile (η) and velocity are measured as time series and recorded. In addition, experiments were recorded with a video camera. Measuring and recording systems used in the experimental system are presented below.

6.3.2.1 Wave measurement

For measuring and recording water surface elevation profile time series two resistance-type wave probes, a wave monitor, an Analog/Digital converter and a computer were used (Figure 6.19).

Wave probes are made of two parallel stainless stell rods which are bounded with plastic parts. Working principle of wave probes is measuring sent electric current between these steel rods which is converted to an output voltage (Volt). The amount of this voltage linearly changes with immersion value of probes in the water. Wave probes are connected to a wave monitor which send and receive electric signals providing linearity of data. Required regulation was done on fron-panel of wave monitor to provide ±10V range for the experiments. During the experiments,

received analog data (Volt) was converted to digital data by using a NI9215 Analog/Digital (A/D) converter and recorded to a computer. LabView Express software was used to record data.

Figure 6.19 : Wave measurement system.

For each experiment, wave calibration was executed to have the relationship between obtained Volt data and corresponding water wave elevation. At each calibration, a calibration graph showing this corelation was prepared (Figure 6.20).

Each calibration graph gives the relation between measured Volt values and corresponding water surface elevation with a linear equation in which y is the water surface elevation, x is the measured Volt value and a and b are the correlation coefficients.

$$y = ax + b \tag{6.6}$$
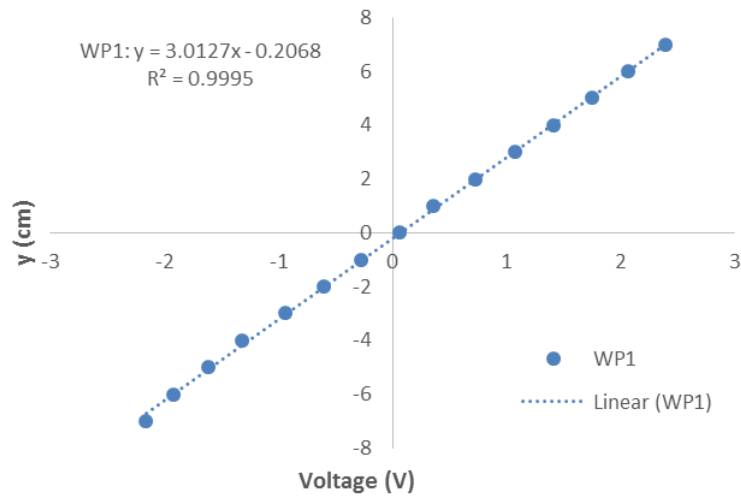
Figure 6.20 : An example wave calibration graph.

Calibration coefficients of calibration graph equations were used produce water surface elevation-time series from measured values for further evaluation of experimental wave characteristics. In Table 6.4, all of the obtained calibration equations are given.

Table 6.4 : Calibration equations of the tests.

Test No	Equation	R^2
W1U145	y = 3.0127x - 0.2068	0.9995
W2U145	y = 3.0661x - 0.3157	0.9999
W3U145	y = 3.0715x - 0.0762	0.9996
W4U145	y = 3.0749x - 0.0052	0.9998
W1U160	y = 3.0634x + 0.1283	1
W2U160	y = 3.0667x + 0.0563	1
W3U160	y = 3.0837x - 0.1097	0.9999
W4U160	y = 3.0675x + 0.0839	1

6.3.2.2 Velocity measurement

Determining mixing characteristics of discharged jet is possible with having mean velocity and turbulence paramaters which are obtained with processing velocity data. In that study, Vectrino II velocimeter was used to measure velocity values in the discharged dense jet.

Vectrino II is an instrument which is capable of measuring three-component velocity (U,V,W) values using Doppler effect with 10 Hz pulse frequency. Vectrino II has a 4-beam downlooking probe which is placed on a body which is connected to a computer via a cable to record measured values (Figure 6.21). Weight of the instrument is 1.2 kg and easy to use in laboratory and field studies.

Differently then the conventional pointwise acoustic doppler velocimeters (ADV), it has capable of measuring velocity up to 35 points in a distance range of 40-70 mm away (Figure 6.22) from the probe with high frequency. Sampling volume diameter is 6 mm and cell size is 1-4 mm. Velocity range and sampling rate ranges of the instrument are 0-3 m/s and 1-100 Hz, respectively.

Vectrino II is suitable for measuring velocity values under turbulent jet flows without disturbing flow structure. Also, it is convenient to use it at a salinity range of 0-60 ppt and a temperature range of -4°-40° C.

Figure 6.21 : Vectrino II instrument and sampling distance.

Vectrino II has its own software for data acquisition through which measurement set up can be done. During the experiments, received analog data (Volt) was converted to digital data by using the same NI9215 Analog/Digital (A/D) converter and

recorded to computer. Measurement conditions are entered and measured data is recorded in own sofware of Vectrino II. Recorded data can be taken as a MATLAB file (.mat) by this software.

6.3.2.3 Video and image recording

Video recording made by using a CanonLegria HF M36 video camera placed side of the wave flume. The section of wave flume, where jet dicharged and video recorded, was covered with a transparent film with 1-cm spaced grids to facilitate obtaining quantitative data from video and images. Also, 10 fluorescent linear bulbs placed in a wooden frame were placed at the other side of the same section to illuminate the view (Abessi et al., 2012). A tracing paper was sticked in front of this light system to distribute light equally for the whole scene (Figure 6.22).
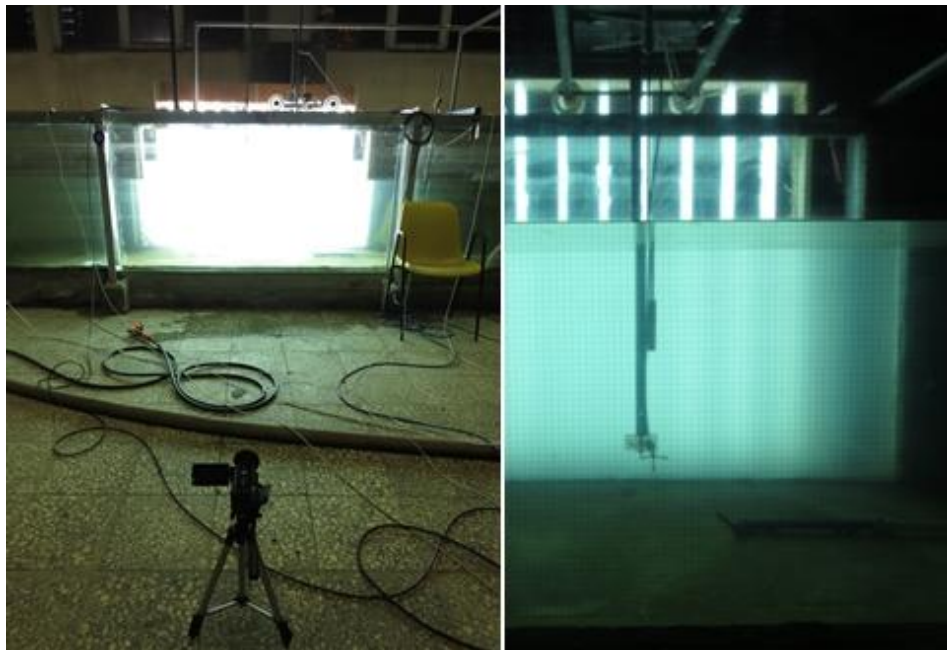
Figure 6.22 : Video recording system.

6.3.3 Experimental procedure and plan

In this part, experimental procedure and plan related to tests analysing inclined jet behaviour under regular waves are presented.

6.3.3.1 Preparation of salt solutions

During the experiments, brine was simulated using salt solutions which are prepared by using salt and tap water (Figure 6.23a). Used salt was NaCl with a density of ~2.17 g/cm^3 (20°C) and solubility value of ~358 g/L (20°C, H_2O) (Tekkim, 2005).

Before each experiment, densities of discharged solution and water in the flume were measured by using hydrometers. Indeed, using digital densimeters with high accuracy are more proper way of making this measurement; however hydrometers were chosen due to the economic reasons (Figure 6.23b).

Figure 6.23 : a) Preparation of salt solutions, b) Hydrometers and measurement.

Hydrometers are instruments that are used to measure specific gravity, which is the ratio of the density of the liquid to the density of water, of liquids by the help of Archimedes' principle. Each hydrometer is produced for a range of density with reference to density of pure water at a definite temperature. Hydrometers can be classified into two groups, constant-volume hydrometers and constant-mass hydrometers (Gupta, 2010).

Constant-mass hydrometers are generally made of glass with a bulb part at one end having a weight inside and scaling section at the other side. Weight material is generally mercury or lead. Scaling systems is a paper ruler on which measurement divisions exist.

In this study, Groiner brand constant-mass type hydrometer were used. Measurement range and accuracy values of them are given in Table 6.5.

Table 6.5 : Features of used hydrometers.

Product Code	Length (mm)	Measuring Range	Product Code	Length (mm)
GR101005	330	0.900-1.000	100	0.001
GR101006	330	1.000-1.100	100	0.001

Measurement was done according to procedure of "ASTM D1429-08 Standard test methods for specific gravity of water and brine" (2008) which includes simple directives for the measurement. For that, salt solution/water was filled into a graduated cylinder and the hydrometer with proper range was submerged carefully for allowing it swim and not to touch walls of the cylinder. Measurement was read after waiting the hydrometer reached to the equilibrium position.

Hydrometer measurement is directly related to temperature. Because they produced according to a reference temperature, it is required to measure temperature of liquid tested. In the case of measurement temperature is different from reference temperature, measurement results are revised using some correction factors. In this study, measured density values corrected according to correction procedure below.

For a thermometer produced for T °C,

$$m = R_h V \tag{6.7}$$

in which m is mass, V is volume and R_h is density. In the case of making the measurement for liquid with different temperature from reference temperature, T, measurement result differs due to volume expansion of the thermometer (Wright, 2008):

$$m = (R_h + C_T)V[1 + \beta_g(T' - T_0)] \tag{6.8}$$

Here, C_T is temperature correction factor, β_g is expansion coeffcient of glass, T_0 is reference temperature according to which hydrometer is produced and T' is the temperature of liquid being measured. In this case, C_T is defined as below (Wright, 2008):

$$C_T = \frac{R_h \beta_g(T' - T_0)}{1 + \beta_g(T' - T_0)} \tag{6.9}$$

β_g is 26×10^{-6} /°C for glass which is too lower than 1 and may be omitted (Wright, 2008):

$$C_T \cong -R_h \beta_g (T' - T_0) \qquad \textbf{(6.10)}$$

After calculating temperature correction according to this equation, it is added to measurement data to obtain final value:

$$\rho = R_h + C_T \qquad \textbf{(6.11)}$$

Density values were also calculated using the equations 2.5-2.10 by El-Dessouky and Ettouney (2002) in which salinity and temperature are the input values to calculate density.

In Table 6.6, measured and calculated values of density values are given. As it can be seen from the table, the percentage difference between measured and calculated values are very low (0.001-0.473%). This provided also the conformation of characteristics of prepared solution in the tests.

Table 6.6 : Measured and calculated density and kinematic viscosity values.

Test No	T_0 (°C)	ρ_0 (Meaasured) (kg/m³)	ρ_0 (Calculated) (kg/m³)	Difference (%)	v (m²/s)	T_a (°C)	ρ_a (Measured) (kg/m³)	ρ_a (Calculated) (kg/m³)	Difference (%)
W1U145	18.8	1024.03	1022.98	0.103	1.07404E-06	19.1	999.02	998.64	0.038
W2U145	19.8	1024.01	1023.98	0.003	1.05179E-06	19.2	1000.02	998.61	0.141
W3U145	20.2	1025.99	1021.91	0.398	1.03808E-06	19.2	995.02	998.61	0.360
W4U145	21.2	1024.97	1023.05	0.187	1.0173E-06	19.5	1000.01	998.53	0.148
SU145	21.3	1025.07	1021.37	0.362	1.01169E-06	19.8	999.01	998.46	0.055
W1U160	22.0	1025.85	1021.01	0.473	9.95416E-07	19.8	1000.01	998.46	0.155
W2U160	21.5	1024.96	1021.53	0.335	1.00753E-06	20.0	1000.00	998.40	0.160
W3U160	22.1	1025.04	1026.48	0.140	1.00418E-06	20.6	999.98	998.24	0.174
W4U160	22.7	1022.93	1025.69	0.269	9.89494E-07	20.3	994.99	998.32	0.334
SU160	23.7	1024.10	1028.40	0.419	9.7384E-07	21.6	996.96	997.97	0.101

6.3.3.2 Experimental plan

Experimental plan which includes a list of experiments with variable parameters is given in Table 6.7. As it can be seen, behaviour of an inclined negatively buoyant jet is examined under stagnant and regular wave conditions. In these experiments, different discharge angles and wave series were changing parameters while the other parameters were constant.

Table 6.7 : Experimental plan.

Exp. No	θ (°)	D (m)	Q_0 (m^3/s)	U_0 (m/s)	M_0 (m^3/s^2)	g' (m/s^2)	B_0 (m^4/s^3)	L_Q (cm)	L_M (cm)	Ri_0	F_d
W1U145	45	0.005	0.00004	2.04	8.15E-05	0.235	9.41E-06	0.44	27.96	0.016	58.86
W2U145	45	0.005	0.00004	2.04	8.15E-05	0.235	9.40E-06	0.44	27.97	0.016	60.10
W3U145	45	0.005	0.00004	2.04	8.15E-05	0.265	1.06E-05	0.44	26.34	0.017	52.94
W4U145	45	0.005	0.00004	2.04	8.15E-05	0.226	9.04E-06	0.44	28.53	0.016	58.95
SU145	45	0.005	0.00004	2.04	8.15E-05	0.220	8.78E-06	0.44	28.94	0.015	57.69
W1U160	60	0.005	0.00004	2.04	8.15E-05	0.206	8.24E-06	0.44	29.87	0.015	57.96
W2U160	60	0.005	0.00004	2.04	8.15E-05	0.211	8.45E-06	0.44	29.51	0.015	58.94
W3U160	60	0.005	0.00004	2.04	8.15E-05	0.260	1.04E-05	0.44	26.60	0.017	58.83
W4U160	60	0.005	0.00004	2.04	8.15E-05	0.303	1.21E-05	0.44	24.65	0.018	55.66
SU160	60	0.005	0.00004	2.04	8.15E-05	0.309	1.24E-05	0.44	24.38	0.018	56.50

6.3.4 Data evaluation procedure

In this section, data evaluation methodology which were executed in this study are presented in three groups as the wave data evaluation, velocity data evaluation and video and image processing, respectively.

6.3.4.1 Wave data

Wave data was saved as Volt-time series and converted into water surface elevation (η)-time series by using calibration equations as stated before. In Figure 6.24, an example η-time series is given.
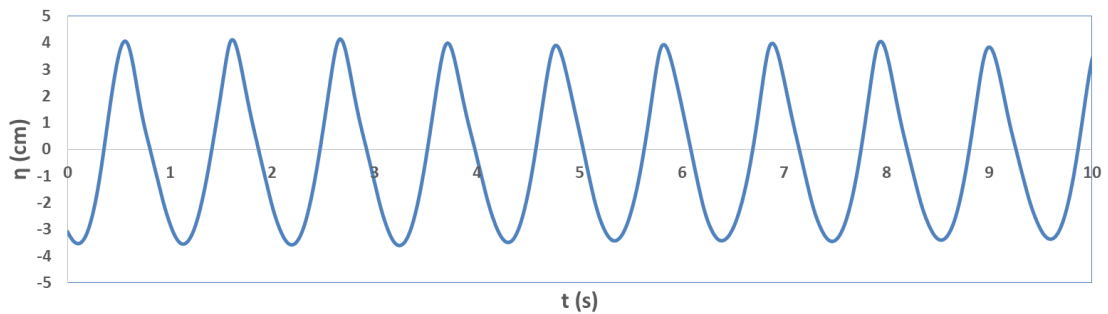
Figure 6.24 : An example water surface (η)-time (t) series (Test W1U145).

After that, each η-time series graph were examined to choose representative part due to the fact that waves became regular after a while of starting the wave paddle.

Wave parameters were obtained by processing η-time series using zero-crossing method. For application of zero-crossing method, a Matlab code, which seperates waves from η-time series, calculates wave characteristics and statistics parameters and writes them into a table, was written.

121

In addition to the mentioned code, wavelength values were calculated iteratively by using a second program written which uses the wave dispersion equation of linear wave theories (Mani, 2011):

$$L = L_0 \tanh \frac{2\pi h}{L} \qquad \text{(6.12)}$$

Here, L_0 is the deep water wavelength which is defined as below:

$$L_0 = \frac{gT^2}{2\pi} \qquad \text{(6.13)}$$

6.3.4.2 Velocity data

Data Quality, filtering and despiking

Velocity data includes points that are not valuable because of low data quality and these points should be detect in the time series and removed. Because of an intermittent time-series is not suitable for calculations, these removed (outlied) points should be replaced also with meaningful values.

Before passing to explain the methodology for velocity data filtering and despiking, it would be better to give the main concepts related to data and data quality. Signal-to-noise ratio (SNR) is the ratio of received signal and it is an indicator of data quality. dB is the unit for SNR. For a appropriate measurement, SNR values expected to be higher than 15. Correlation (COR) is the measure of signal quality as percentage (%) and it an indicator of data accuracy. It is required COR to be as high as possible and filtering the values lower than 40 is recommended for convenient measurement with Vectrino II (Nortek AS, 2013). For measurement of turbulent flow, a COR range of 70-100% is acceptable (Nortek AS, 2013). According this, velocity data that is not in the acceptible limits of COR and SNR values should be filtered to have clean data.

Correlation filter

For filtering velocity data, the points with not acceptable COR and SNR values were filtered. By this aim, a MATLAB code was written. In that stage, each data is filtered for COR values of 40, 50, 60, 70, 80 and 90 with the aim of observing the quality of the recorded data at different measurement points in spatial measuring range of Vectrino II (in 3 cm measuring distance). An example of a correlation filtering is given in Figure 6.25.
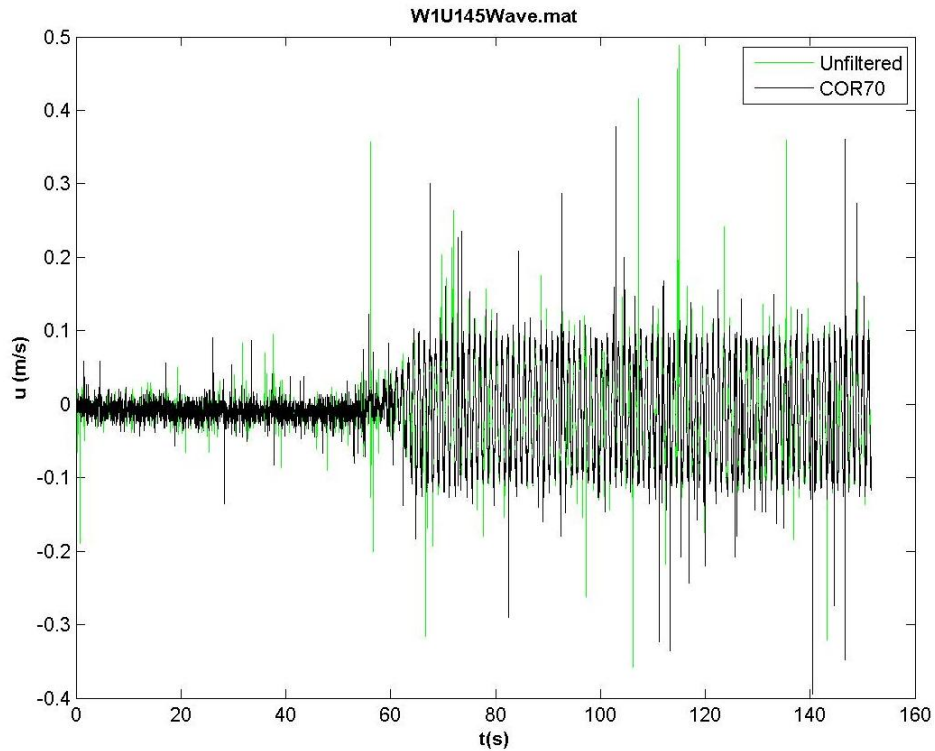
Figure 6.25 : An example of filtered wave series for COR70 (Test W1U145).

Number of outliers and data elimination

For the whole velocit data set which constitutes of 35 points in the measuring range of Vectrino II, a plot which shows percentage of filtered data points for one COR value was plotted. The first plot in Figure 6.26a is an example of this graph for COR 70 value. Also, all of the COR value filtering process on one wave data was united in one plot as the second plot in Figure 6.26b. As it can be seen, inner points have higher quality data compared to the ones at the edge of the meassurement range. This situation was observed for the whole test cases. Due to this reason, middle point of the range was chosen for all tests for further analysing.

According to filtered number of elements, 70 was chosen as the COR value that will be applied for the whole tests. As it can be seen from the example graph in Figure 6.26b, this value is suitable with low percentage of filtered elements in the middle region. After filtration for COR70, filtered points replaced with average value of the first previous and next data points with the help of a MATLAB code written.
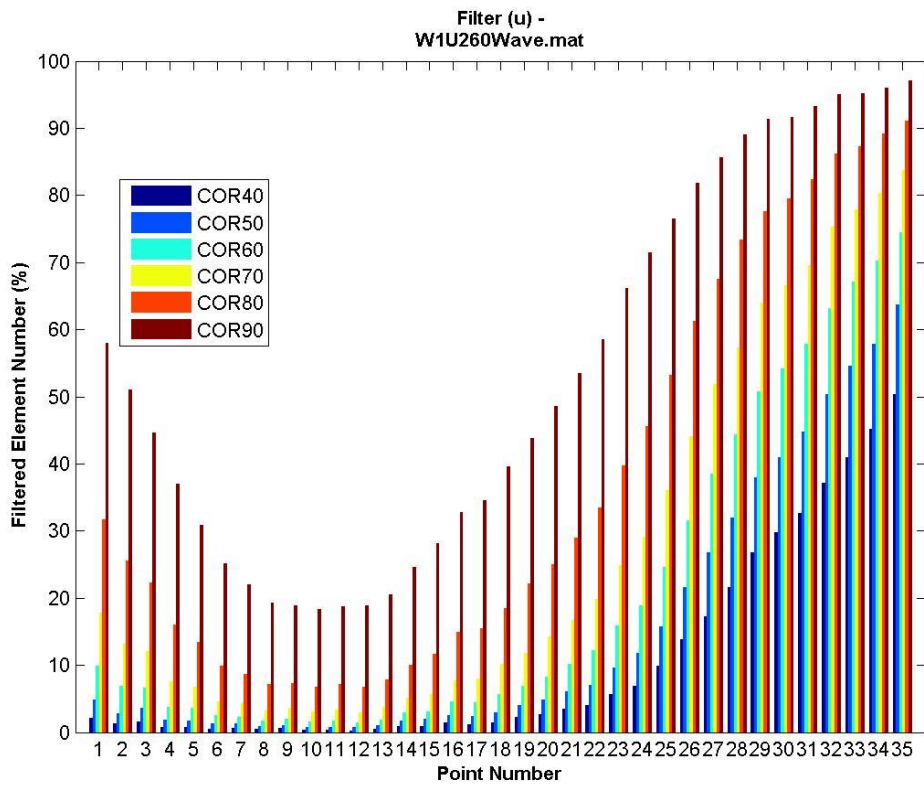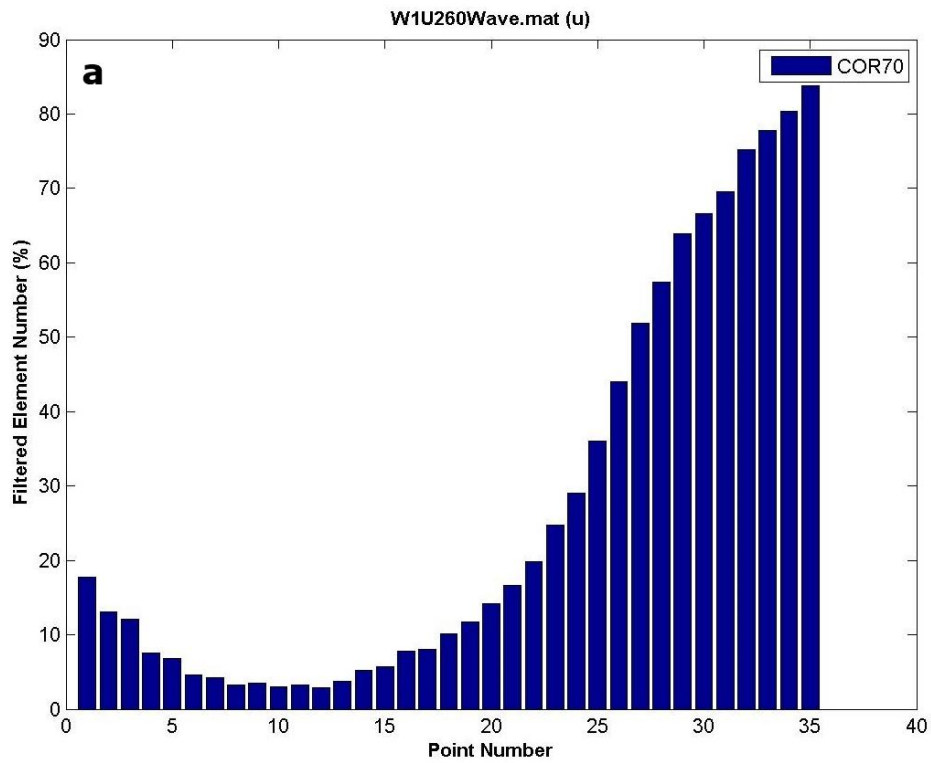
Figure 6.26 : An example graph of filtered element numbers according to COR values a) COR70, b) all COR values tested.

Noise filter

In addition to COR values, noise spikes are also another problem that should be handled. By this aim, a suitable method for filtering obtained velocity data is searched and low pass Butterworth filter (*butter*) and Zero-phase digital filter (*filtfilt*) was used by the help of MATLAB programme. For this process, cutoff frequency was chosen as 0.5 which was in the recommended range ($0.0 < Wn < 1.0$). After this, filtered values were replaced with the value of following data.

6.3.4.3 Video and images

Experimental videos were evaluated by capturing frames from them. Frame capture process was executed by using ImageGrab 5.0.6 software which lets the user to capture frames with required frame or time interval. On each image, instantaneous time at which image was taken was shown by the program. After image capturing with frame interval of 7 frames (~5 fps), these pictures were processed by using bespoke MATLAB codes.

Image proccessing for the experiments was executed in two phases. Before running the main code for each test, some points were determined by using Matlab for 1 image of each test.

At this stage, coordinates of discharge point (X_0 and Y_0) for each experiment were determined by using Matlab. This value is entered as input to the code and showed on the processed images as 'P0'. In addition, the coordinates of discharge device (X_b and Y_b) and the edge of flume (Y_c) were determined on the images (Figure 6.27). These values were entered into main code as input for calculating required distances.
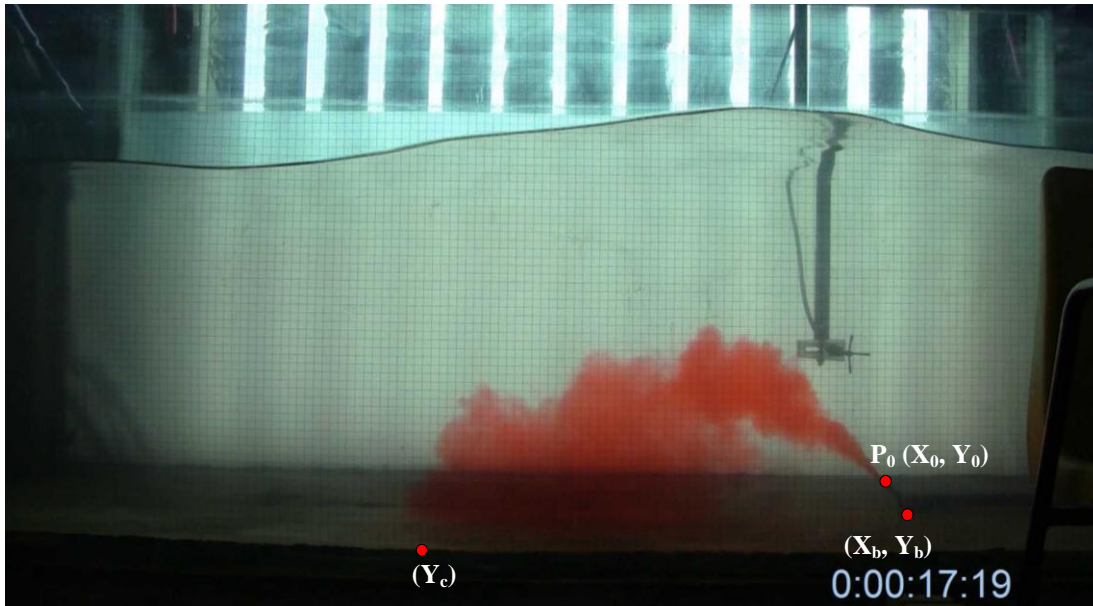
Figure 6.27 : Main coordinates determined for each test before image processing.

As stated before, video camera was placed perpendiculary to the wave flume. However, existence of distortion was checked for each test before doing the image processing by the aim of having correct measurements. Check is executed by measuring lengths of 10 grids for each test at different locations of one image. An example of distortion check was shown by Figure 6.28. For each test, pixel value of 10 different grids were measured. For the whole tests, it was seen that no distortion was observed. Pixel value of 1 cm grid in X and Y directions (Grid Pixel (X) & Grid Pixel (Y)) was decided from known distances on the image for each tests. Thus, conversion factor (CF) which is the ratio of actual value of grid (cm) to pixel value of grid was calculated in the code. If the images were not so straight, they were turned with the code.

126
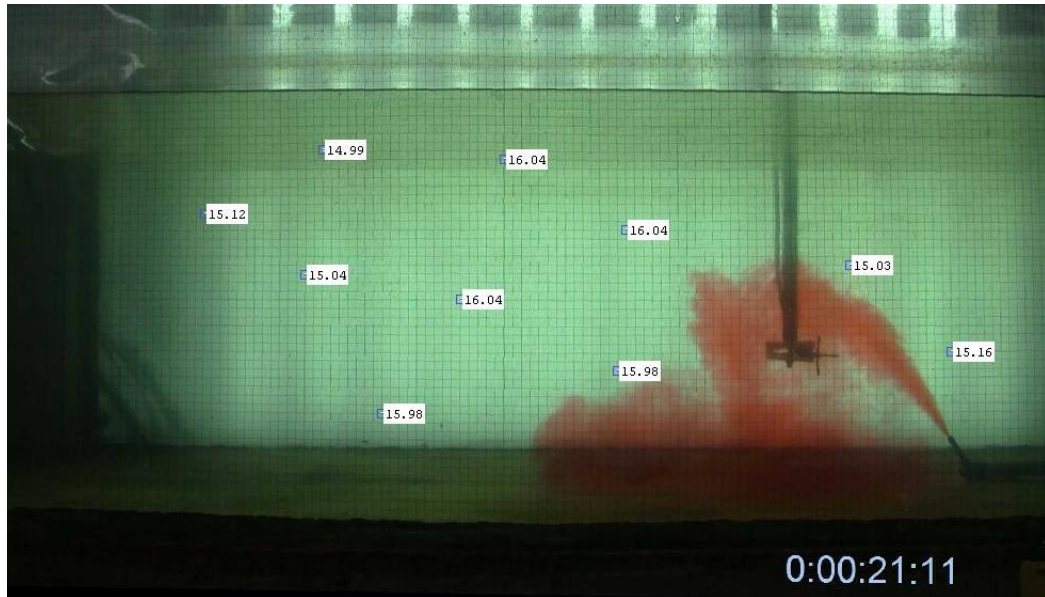
Figure 6.28 : Measuring pixel values of grids (Test SU160).

In the first phase, one-minute videos were taken after the first minute of discharge. By the second code, maximum rise point of the discharged dense jet (Z_t), water surface level at Z_t (η) and discharge point (η_0) were marked on the captured images by the user and saved as pixel values. In addition, impingement point of the jet (X_i) was determined as the point which has the minimum pixel value on a line at the bottom level. By the help of CFs, distance values of these values were calculated and whole variables were written to an Excel file for further processing. In some images, it was obviouss that location of X_i was not determined correctly. So, after completing image processing runs, each processed image was revised and eliminated in the case of wrong defination of impingement point.

An example of a processed image of first part of image processing is shown in Figure 6.29. As it can be seen, image axes was converted into real distances from pixel values by using known grid distance drawn on side of wave flume. On the picture, time stamp is in the format of 'hour:minute:second:frames'.

Whole processed images for first part of image processing study is given with Appendix A. Due to huge number of images, whole images of one test was combined into one image using PhotoScape software (Url-10).
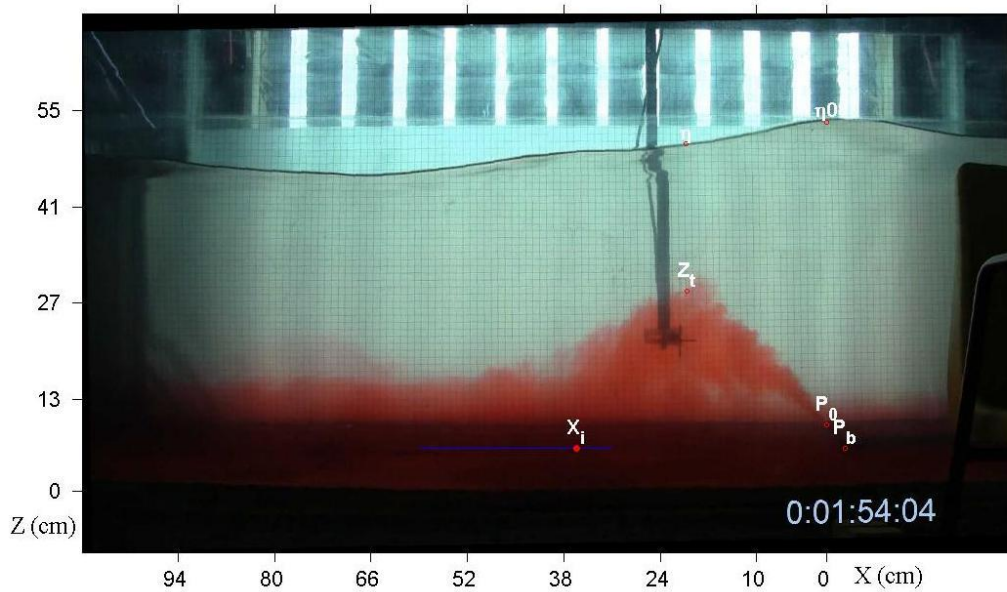
Figure 6.29 : A processed image in Phase 1 of image processing (Test W1U145).

In the second phase, videos for taken for the time interval in which constituted dense layer reached the end of video frame to analyse flow behaviour after impingement point. By the first code, front position of dense layer (X_e), water surface level at the end point of dense current (η) and discharge point (η_0) were marked on the captured images by the user and saved as pixel values. By the help of CFs, distance values of these values were calculated and whole variables were saved into the workspace in cm's.

An example of a processed image of second part of image processing is shown in Figure 6.30. As it can be seen, image axes was converted into real distances from pixel values by using known grid distance drawn on side of wave flume. On the picture, time stamp is in the format of 'hour:minute:second:frames'.

Whole processed images for second part of image processing study is given with Appendix B. Due to huge number of images, whole images of one test was combined into one image using PhotoScape software (Url-10).

128
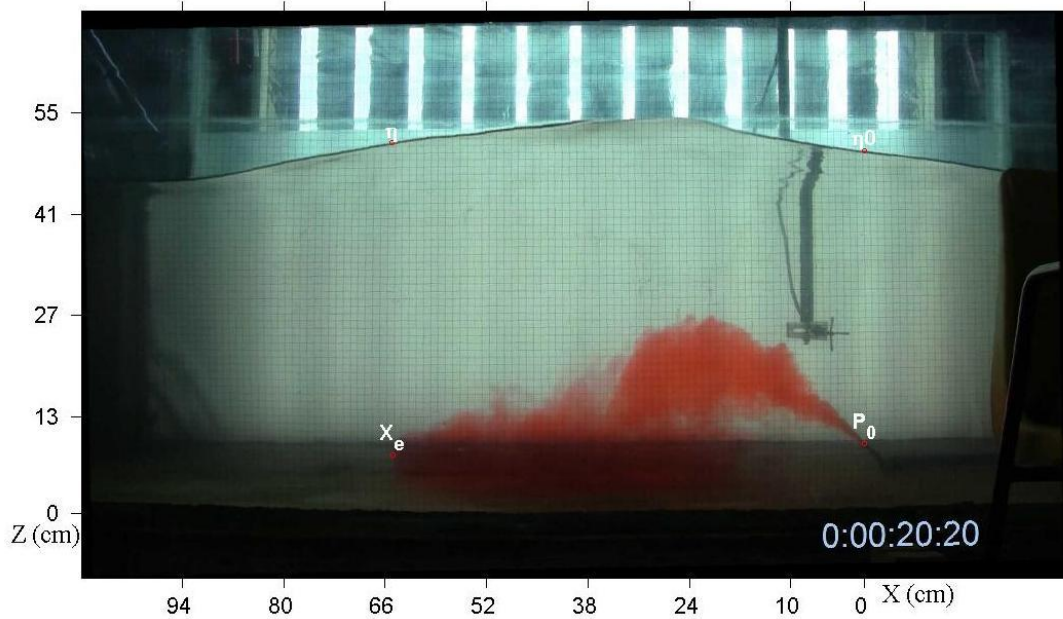
Figure 6.30 : A processed image in Phase 2 of image processing (Test W1U145).

All of Matlab codes were arranged as saving obtained data to the Matlab workspace after image processing. With this method, a shorter duration for image processing was provided. Due to this reason, a third code was written to write saved data (in .mat format) to an main Excel file for further processing.

In Table 6.8, parameters which are used for image processing study is presented.

Table 6.8 : Image processing study procedure and parameters.

Test	# of Images		X_0 (Pixel)	Y_0 (Pixel)	X_b (Pixel)	Y_b (Pixel)	Y_c (Pixel)	Grid Pixel (X)	CF (X)	Grid Pixel (Y)	CF (Y)
	Phase 1	Phase 2									
W1U145	82	258	1544.60	853.26	1584.30	902.26	991.46	14.30	0.0699	14.45	0.0692
W2U145	80	259	1452.30	857.03	1502.20	914.48	1003.80	14.90	0.0671	14.90	0.0671
W4U145	71	259	1580.5	870.95	1625.20	924.92	1005.00	14.50	0.0690	14.50	0.0690
W1U160	123	388	1480.8	849.70	1504.50	924.24	1009.30	15.50	0.0645	15.50	0.0645
W2U160	113	259	1717.00	838.25	1751.00	910.19	997.98	15.5	0.0645	14.3	0.0699
W3U160	83	259	1548.00	851.84	1579.70	923.78	994.87	14.30	0.0699	14.1	0.0709
W4U160	145	259	1607.20	818.78	1635.40	891.66	973.66	15.55	0.0643	15.55	0.0643
SU145	74	259	1577.50	867.70	1621.60	925.48	997.99	14.50	0.0690	14.5	0.0690
SU160	183	259	1738.00	815.59	1763.40	886.96	970.23	15.54	0.0644	15.54	0.0644

6.3.5 Results

In this part, obtained results with three stages of data processing will be presented in the same order: Wave data, velocity data and video and image processing data.

6.3.5.1 Wave data

Calculated wave parameters for each experiment are presented in Table 6.9 and 6.10. As it can be seen from the Table 6.10, four different types of regular waves were used in the tests. In this table, H_{rms}, which is root-mean-square value of obtained wave heights; H_{mean}, which is the average of obtained wave heights; H_{max}, which is the maximum of obtained wave heights; H_{min}, which is the minimum of obtained wave heights; T_{mean}, which is the average of obtained wave periods; T_{max}, which is the maximum of obtained wave periods and T_{min}, which is the minimum of obtained wave periods are presented.

Table 6.9 : Wave characteristics of the experiments (1).

Test No	Wave Serie	H_{rms} (cm)	H_{mean} (cm)	H_{max}	H_{min} (cm)	T_{mean} (s)	T_{max} (s)	T_{min} (s)
W1U145	214	7.3699	7.3678	7.74	6.91	1.058	1.084	1.044
W2U145	412	6.9701	6.9656	7.59	6.21	0.970	0.992	0.948
W3U145	217	6.9169	6.9161	7.11	6.72	1.221	1.236	1.200
W4U145	418	3.1516	3.1503	3.32	2.98	1.261	1.268	1.252
W1U160	214	7.5550	7.5511	8.16	6.97	1.059	1.096	1.016
W2U160	412	6.9169	6.9136	7.50	6.39	0.969	0.992	0.944
W3U160	217	7.1320	7.1307	7.38	6.79	1.221	1.232	1.204
W4U160	418	3.1498	3.1483	3.42	3.00	1.261	1.268	1.256

Water waves can be classified according to their wave lengths relative to the water depth (d) they are generated as deep water waves (d/L>1/2), transitional waves (1/20<d/L<1/2) and shallow water waves (0<d/L<1/20) (CEM, 2002).

In addition to this, water waves can be classified according to the wave theories which are used for explaining their characteristics (CEM, 2002). In Figure 6.33, a graph showing applicability range of various wave theories is shown. As it can be seen, determining parameters are relative water depth (d/gT^2) and wave steepness (H/gT^2). In Table 6.8, some other parameters related to wave characteristics with the classification of produced water waves during the tests are presented. 4 main wave series used in executed tests are also marked on Figure 6.31, with red dots using calculated wave parameters to show their classification in wave theories (Table 6.10).
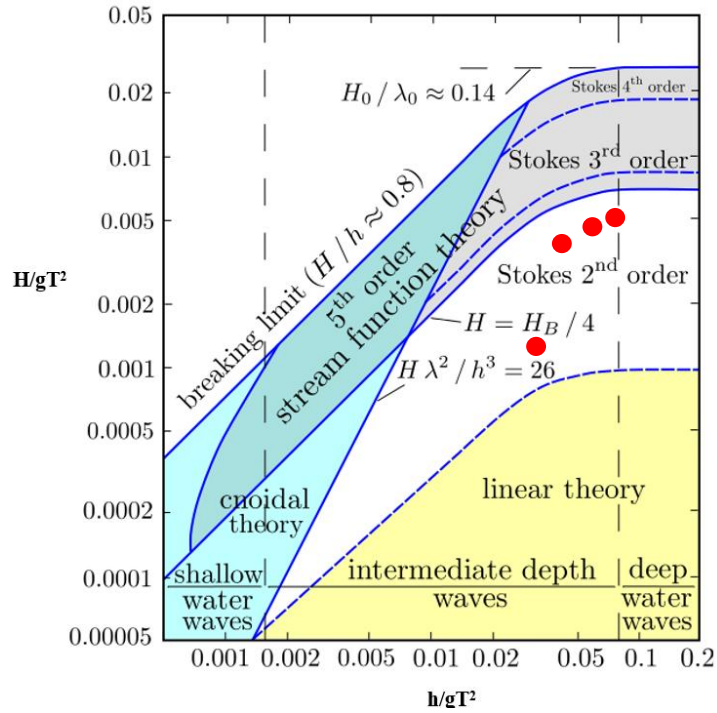
Figure 6.31 : Wave theories (Url-9).

Table 6.10 : Wave characteristics of the experiments (2).

Test No	Wave Serie	L_0 (cm)	L (cm)	d/gT^2	H_{rms}/gT^2	Wave Theory	d/L	Wave Class
W1U145	214	1.7471	1.6676	0.0455	0.0067	Stokes 3	0.300	Transitional
W2U145	412	1.4669	1.4302	0.0542	0.0076	Stokes 3	0.350	Transitional
W3U145	217	2.325	2.1011	0.0342	0.0047	Stokes 3	0.238	Transitional
W4U145	418	2.4816	2.2085	0.0320	0.0020	Stokes 2	0.226	Transitional
W1U160	214	1.7508	1.6706	0.0454	0.0069	Stokes 3	0.299	Transitional
W2U160	412	1.4649	1.4285	0.0543	0.0075	Stokes 3	0.350	Transitional
W3U160	217	2.3273	2.1032	0.0342	0.0049	Stokes 3	0.238	Transitional
W4U160	418	2.4822	2.2089	0.0320	0.0020	Stokes 2	0.226	Transitional

6.3.5.2 Velocity data

In Table 6.11, calculated dimensionless parameters that include wave characteristics are given. In the table, u_w is calculated wave orbital velocity value at the depth of discharge. u_w values were used for the calculation of wave momentum length scale (l_m), wave buoyancy length scale (l_b), wave momentum buoyancy length scale (l_w), F_w and R_M.

Table 6.11 : Velocity related parameters.

Test No	Wave Serie	u_w (m/s)	l_m (m)	l_b (m)	l_w (m)	F_w	R_M
W1U145	214	0.069	0.131	0.029	0.061	2.008	0.00605
W2U145	412	0.052	0.175	0.068	0.109	1.506	0.00631
W3U145	217	0.085	0.107	0.017	0.043	2.325	0.00423
W4U145	418	0.040	0.223	0.137	0.175	1.204	0.00083
W1U160	214	0.071	0.127	0.023	0.054	2.219	0.00634
W2U160	412	0.052	0.175	0.062	0.104	1.587	0.00622
W3U160	217	0.088	0.103	0.015	0.040	2.434	0.00449
W4U160	418	0.041	0.222	0.181	0.201	1.043	0.00083

In Figure 6.32, examples of recorded velocity data is presented. As it can be seen, generated waves were beter for the tests with higher wave height values (W1U145 and W1U160). In Figure 6.33, recorded velocity data at measurement points after discharge started are presented. Stagnant ambient velocity data after discharge are also given in Figure 6.34. Due to the reason that it was not possible to make a velocity profile measurement, in each test velocity data was recorded at only one point around jet maksimum rise height. In the all figures, 15th point in the measurement range is presented.
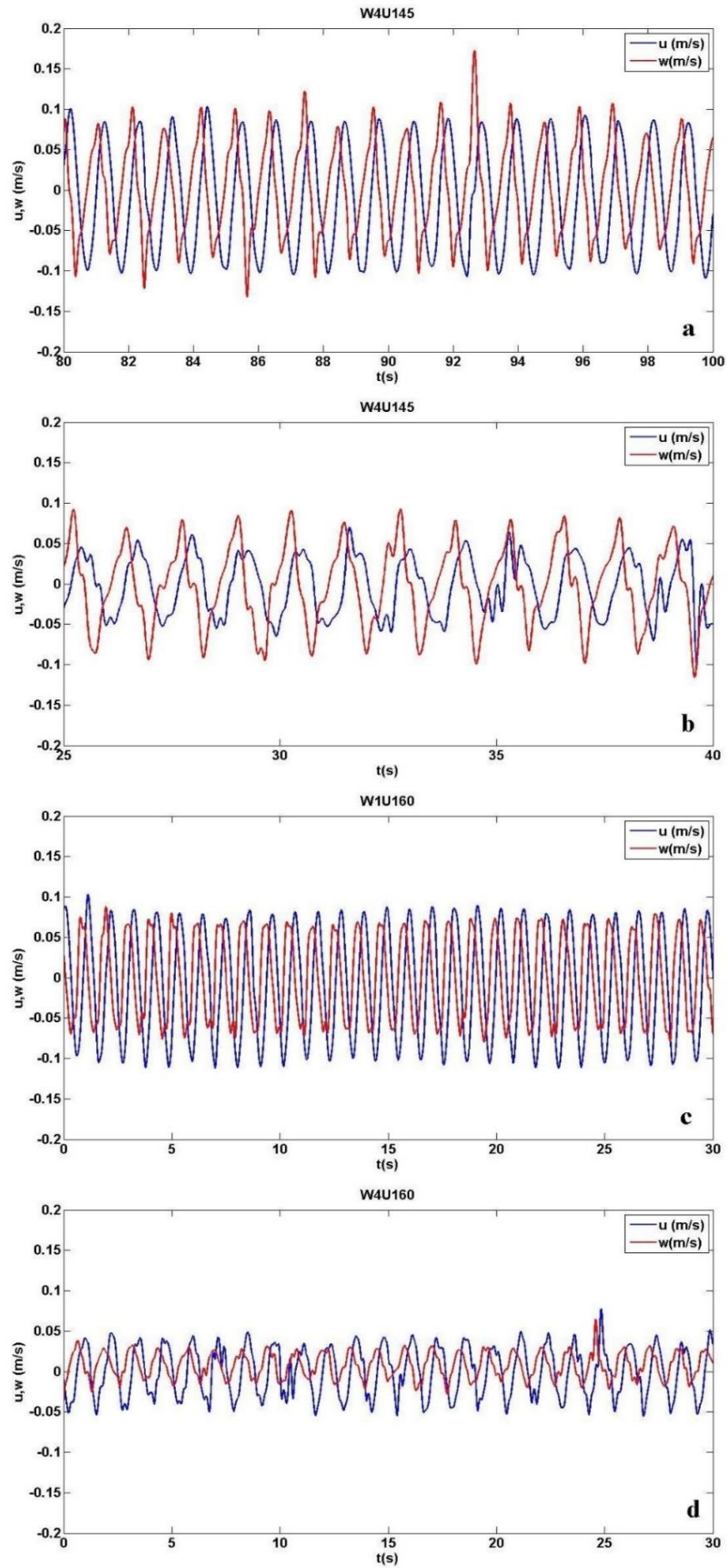
Figure 6.32 : Velocity time series for waves a)Test W1U145, b)Test W4U145
c)TestW1U160, d) W4U160.

133
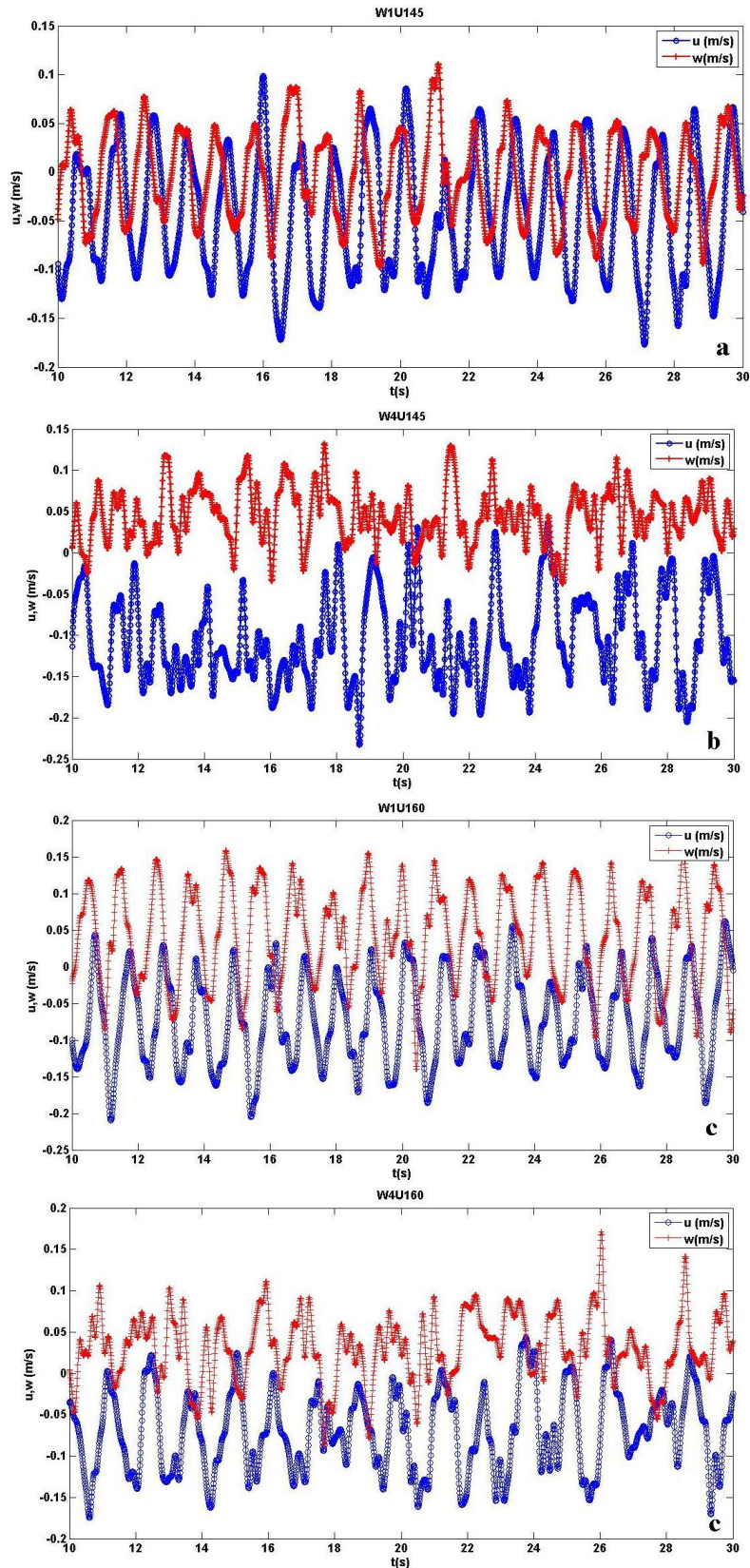
Figure 6.33 : Velocity time series for the tests with waves a)Test W1U145, b)Test W4U145 c)TestW1U160, d) W4U160.
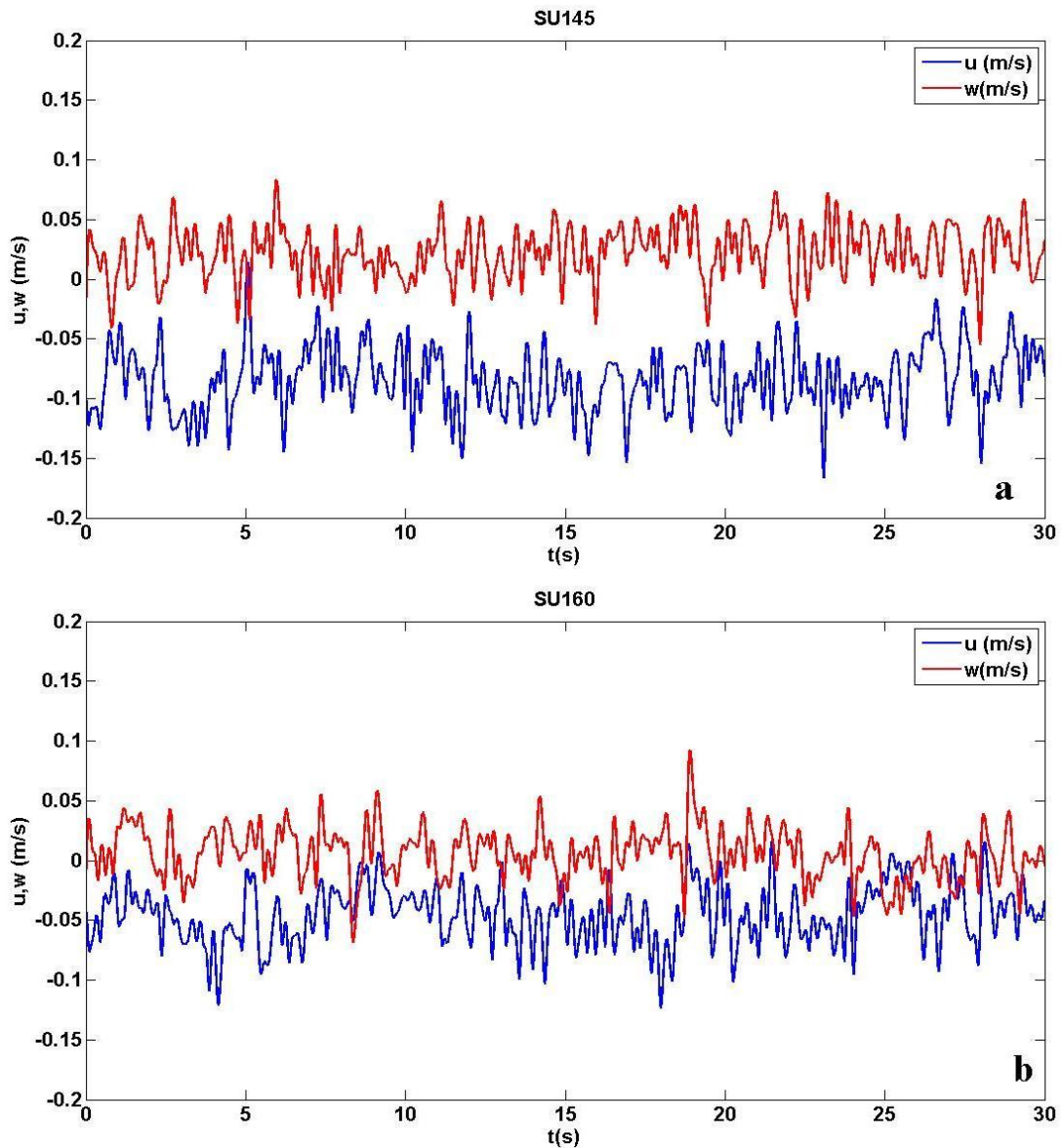
Figure 6.34 : Velocity time series for the tests with stagnant ambient a)Test SU145, b)Test SU160.

6.3.5.3 Video and image processing data

In this part, results of video and image processing studies will be presented in the order of general observation of the flow behaviour followed by image processing.

6.3.5.3.1 General observation

As the first attempt for processing test videos, some general observations from videos will be given here.

It was observed that the inclined dense jets followed a path almost the same with their discharge angles like projectile motion until they rised to their terminal rise

height. After terminal rise point, which was like a stop, dense jets started to fall until their impingement at the bottom. This general behaviour is the same both for wavy and stagnant ambient due to negative buoyancy of discharged solution. However, wave effect caused obvious oscillation of discharged jets. From the videos, it was determined that oscillation movement ended up detention of jet movement compared to stagnant conditions. Due to lack of equipment to measure salt concentrations, it was not possible for determining contribution of this delay to entrainment rates. However, it is pretented that wave action extends the time of jet behavior before impingement which may be conclude in higher entrainment rates and dilution relative to stagnant conditions.

When two tests were compared which have almost the same conditions except the existince of waves, it was observed that water waves affected the shape of inclined dense jet. In Figure 6.35, some experimental photos showing evolution of inclined dense jet through time are presented. As it can be seen, the dimensions of discharged jets are higher in the case of wave existence which corresponds to higher entrainment ratios. Besides, at the outer side of the jets, it can be seen that outside edges are more steady for stagnant ambient conditions. This is valuable for both of the near-field and intermediate regions.

In addition, it was observed that the wave action caused less amount of effluent build up at upstream of the discharge point which is a positive feature not preventing ambient water entrainment into that region.

For comparing test videos with different wave characteristics, it was observed that the flow behaviour becomes more similar to stagnant ambient conditions with decreasing wave height values.
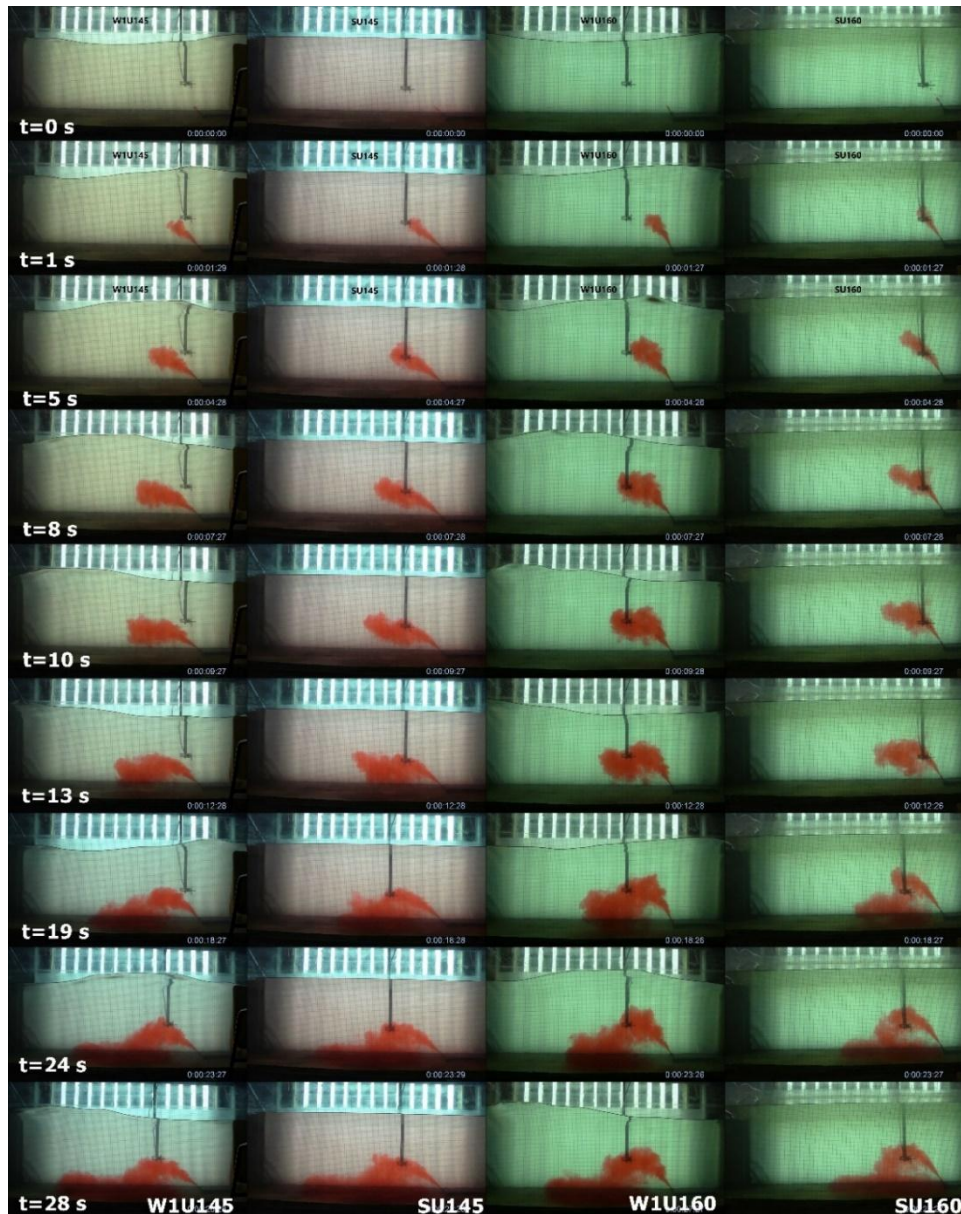
Figure 6.35 : Evolution of discharged inclined dense jet through time (Tests W1U145, SU145, W1U160, SU160).

Another difference of jet behaviour under regular wave effect was the deflection of the jet at the vicinity of the discharge point (in the deflection region) related to wave motion. In the videos, mentioned deflection was more clear for the tests with 60° discharge angles (Figure 6.36).

This behavior was firstly defined by Chyan and Hwung (1993) as a hypothesis that analyzes wave interacted positively buoyant vertical jet behaviour in three different regions as jet deflection region, transition region and developed region from the initial point of discharge, respectively. In the deflection region, jet momentum is the prevailing mechanism in the flow while jet attraction due to jet-wave interaction

becomes effective in the developed jet region (Mossa, 2010). Mentioned regions were also observed by Mossa (2010) and Yongping (2006) for non-buoyant and buoyant vertical jets, respectively. Ferrari and Querzoli (2006) reported the presence of deflection region for negatively buoyant horizontal jets.
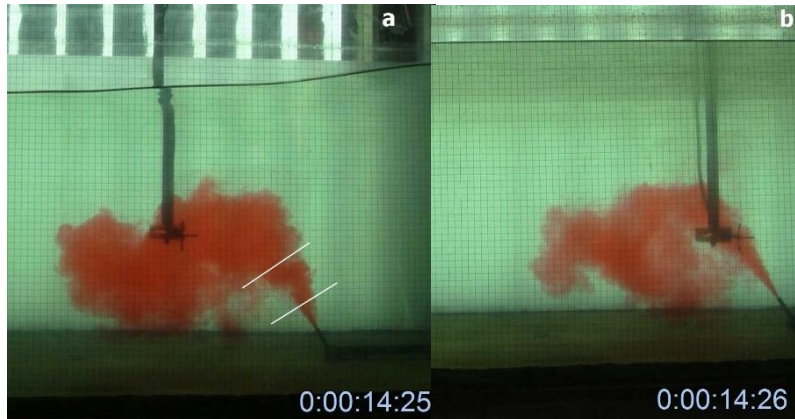
Figure 6.36 : Jet deflection region in jet-wave interaction and jet in stagnant ambient (W1U160, SU160).

In the plan view videos, it was observed that discharged dense jet radially spreads in the wave flume for both wavy and stagnant conditions (Figure 6.37).
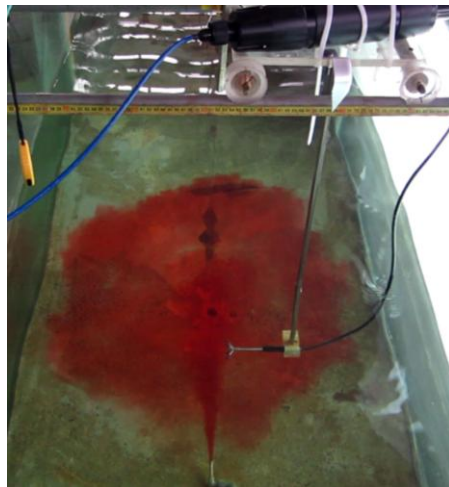
Figure 6.37 : Laterally spreading of inclined dense jet in the wave flume (Test W3U145).

6.3.5.3.2 Image processing

In this part, results of image processing process will be presented in the order of image processing in two phases, each of them including different aspects of the flow. It is important to state that it was considered not to be subjective about choosing the points during image processing. Besides, some of the points are not exactly accurate due to the flow behaviour and the method applied.

138

Phase 1

As it was stated before, in the first phase of image processing terminal rise height (Z_t), water surface level at Z_t (η) and discharge point (η_0) and impingement point of the jet (X_i) were the considered parameters.

Terminal rise height (Z_t)

In Figure 6.38, 6.39 and 6.40 terminal rise height (Z_t) time series determined by image processing are given in seperate graphs. As it can be seen, tests with waves have greater oscillation values compared to stagnant ambient conditions for terminal rise height values. As it can be predicted, Z_t values are higher for the tests with 60° discharge angle compared to the ones with 45° discharge angle. In the figure, mean values are shown with a fixed value for each test to demonstrate the oscillation behavior. As shown, maximum rise height fluctuated along the mean value. For stagnant conditions, terminal rise height values were almost constant as expected. Calculated mean and standard deviation values of the considered parameters are also presented in Table 6.12.

Table 6.12: Image processing data, Phase 1.

Test No	Z_{t_mean} (cm)	σ_{Zt} (cm)	X_{i_mean} (cm)	σ_{Xi} (cm)	Z_{t_mean}/D -	$\sigma_{Zt/D}$ -	X_{i_mean}/D -	$\sigma_{Xi/D}$ -
W1U145	17.85	1.27	39.68	3.85	35.69	2.54	79.36	7.70
W2U145	16.42	0.95	36.10	2.11	32.84	1.90	72.20	4.22
W4U145	20.49	1.30	47.91	1.55	40.97	2.59	95.82	3.11
W1U160	22.68	1.67	36.92	0.71	45.37	3.34	73.84	1.42
W2U160	26.48	1.86	38.26	3.19	52.96	3.73	76.53	6.39
W3U160	24.81	1.97	37.97	3.64	49.63	3.93	75.94	7.27
W4U160	22.90	1.22	37.65	0.87	45.81	2.45	75.30	1.74
SU145	16.93	0.59	43.92	1.78	33.85	1.17	87.84	3.55
SU160	19.20	0.57	35.00	1.33	38.40	1.14	70.00	2.67
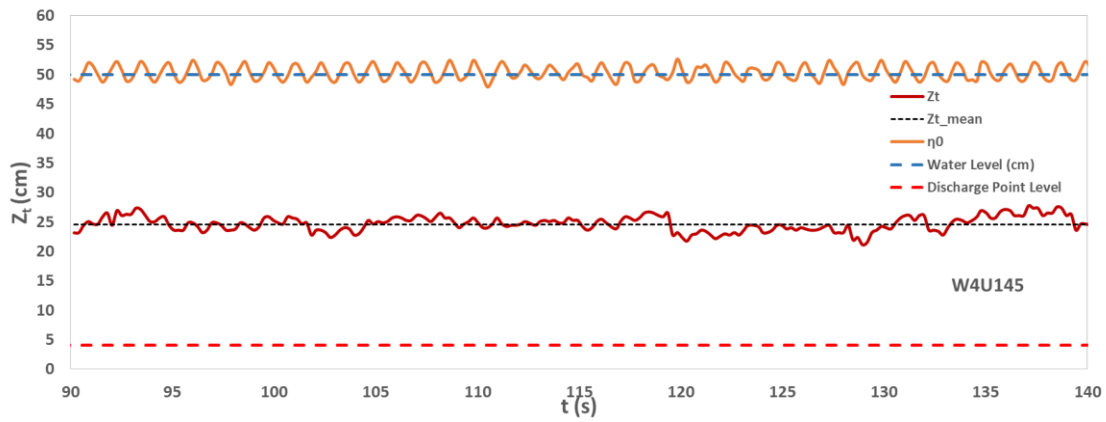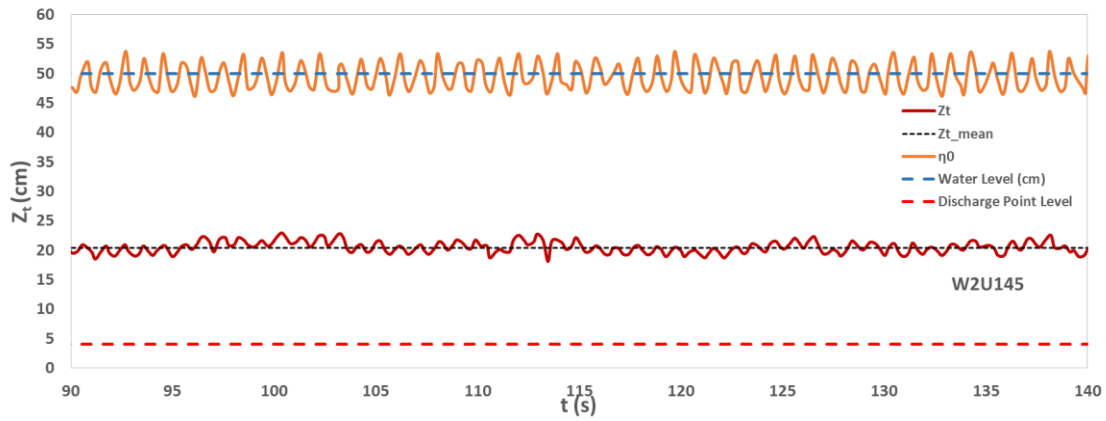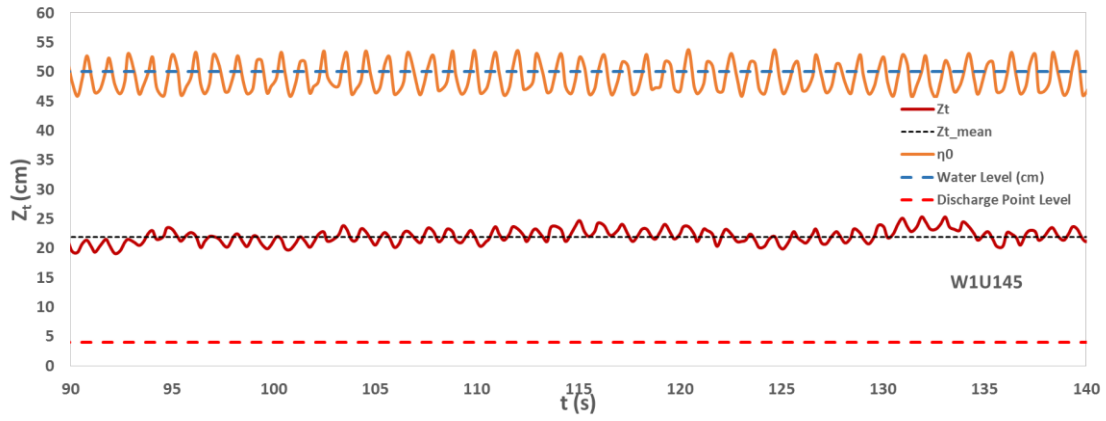
Figure 6.38 : Measured terminal rise height time series, for tests with waves (θ=45°).
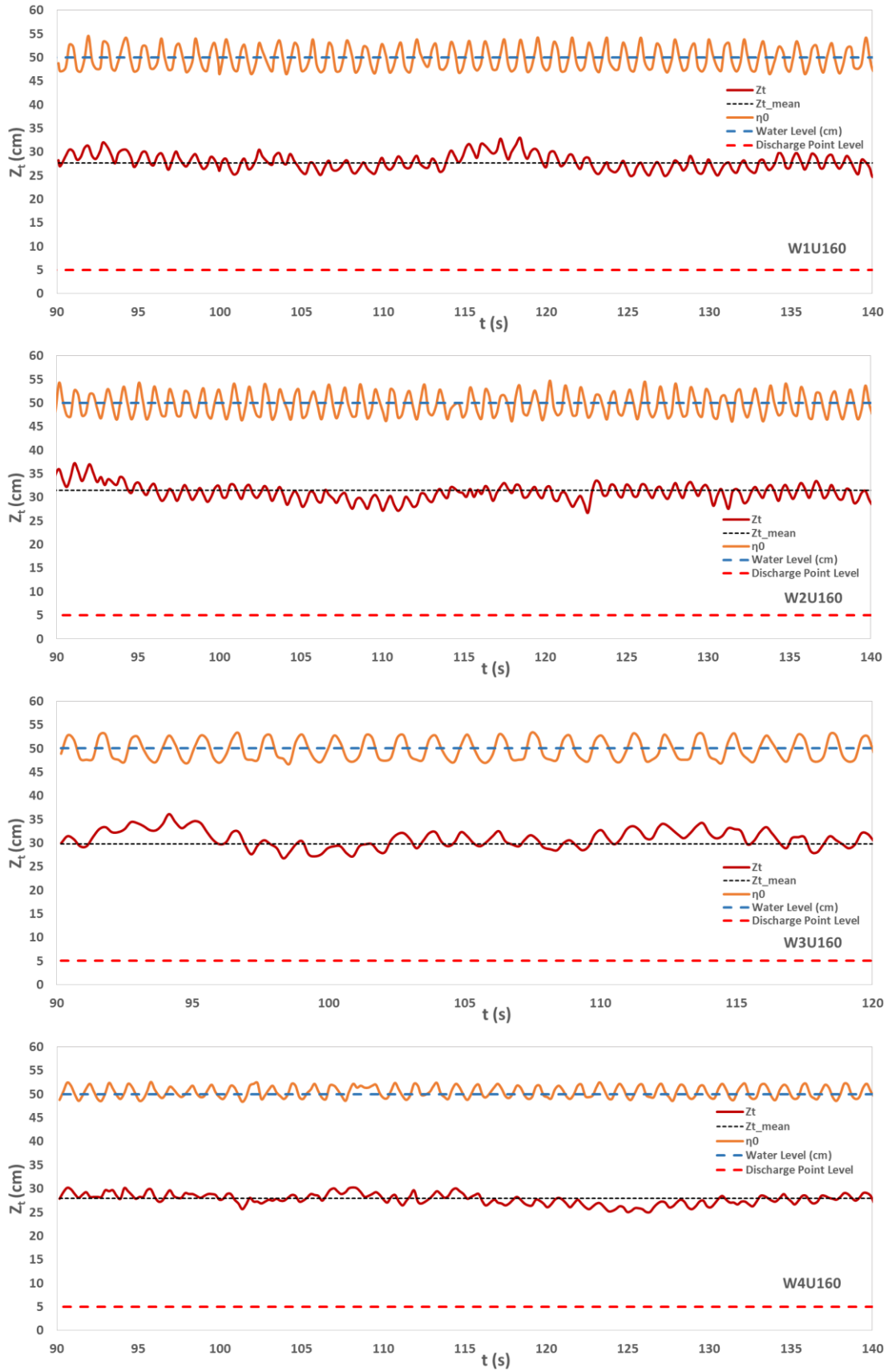
Figure 6.39 : Measured terminal rise height time series, for tests with waves (θ=60°).
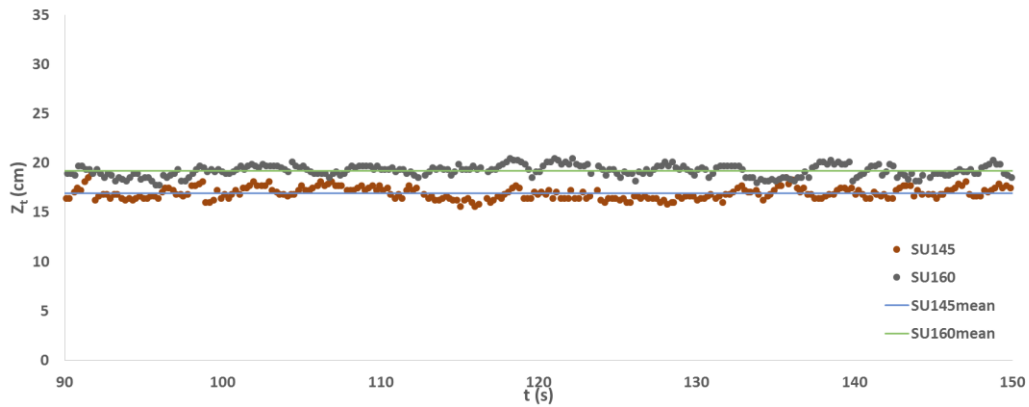
Figure 6.40 : Measured terminal rise height time series, for tests with stagnant ambient (θ=45°, 60°).

In Figures 6.41 and 6.42, a deeper look to the terminal rise height (Z_t) time series is presented. In this figure, only 10 s data is given with the addition of water surface profile (η_0). For the whole tests, it was clear that the discharged jet propagated with the same phase with the water waves.

In Figures 6.43, 6.44 and 6.45, normalized terminal rise height and discharge angle (θ), wave Froude number (F_w) and wave steepness (H_{rms}/gT^2) relationships are presented by using mean values of measured parameters.
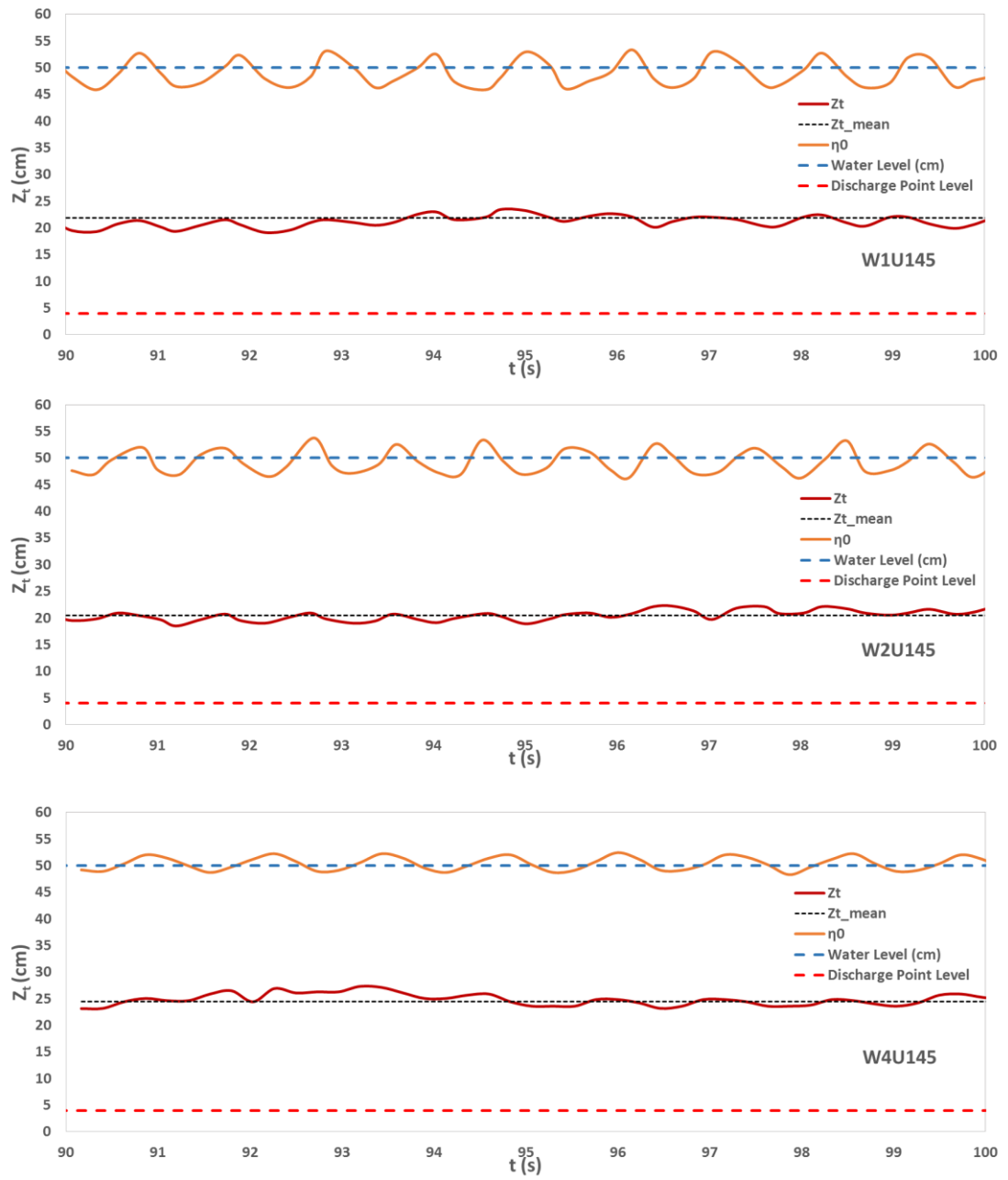
Figure 6.41 : Terminal rise height along wave propagation
(Tests with waves, θ=45°).
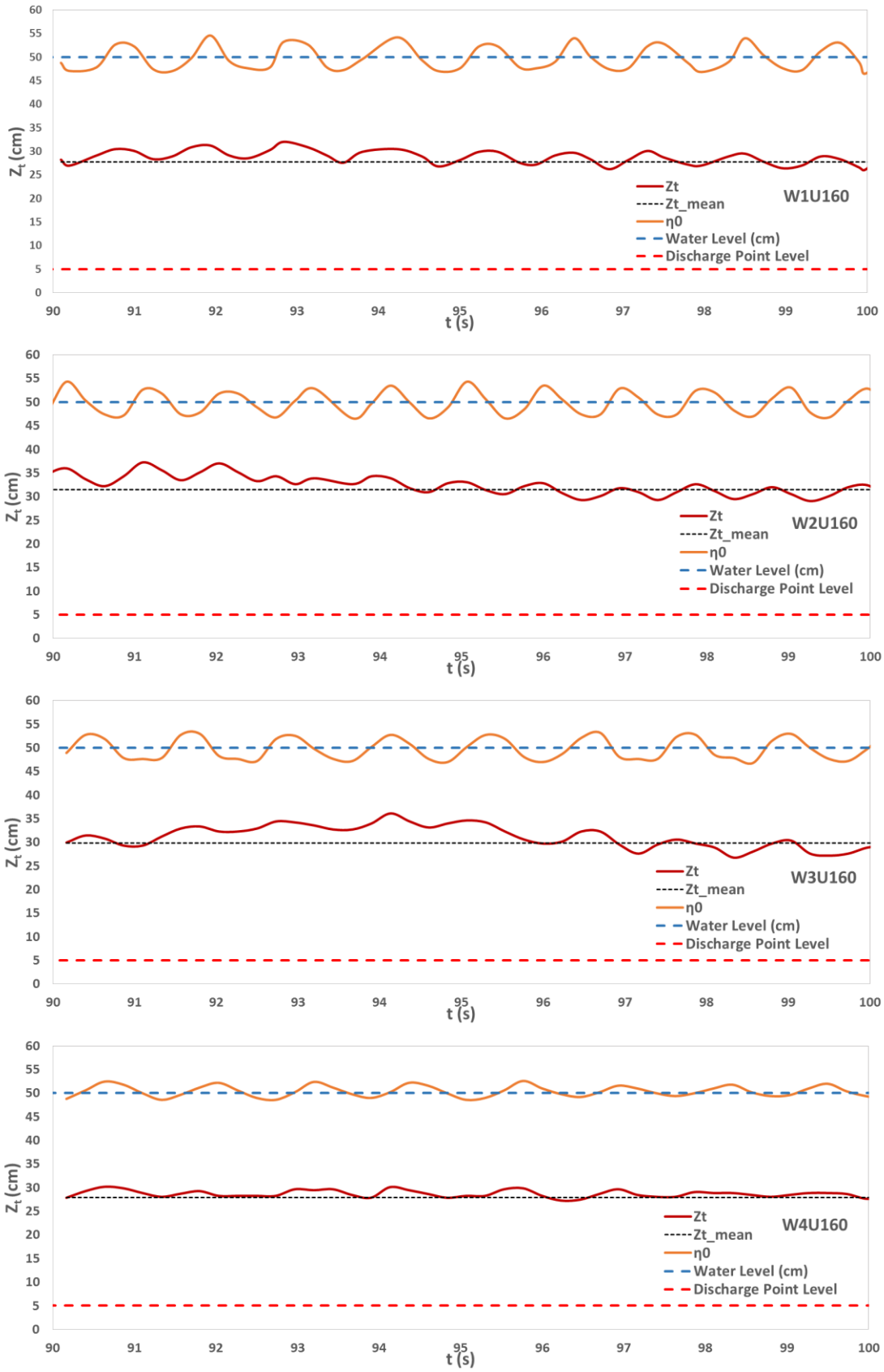
Figure 6.42 : Terminal rise height along wave propagation
(Tests with waves, θ=60°).

144
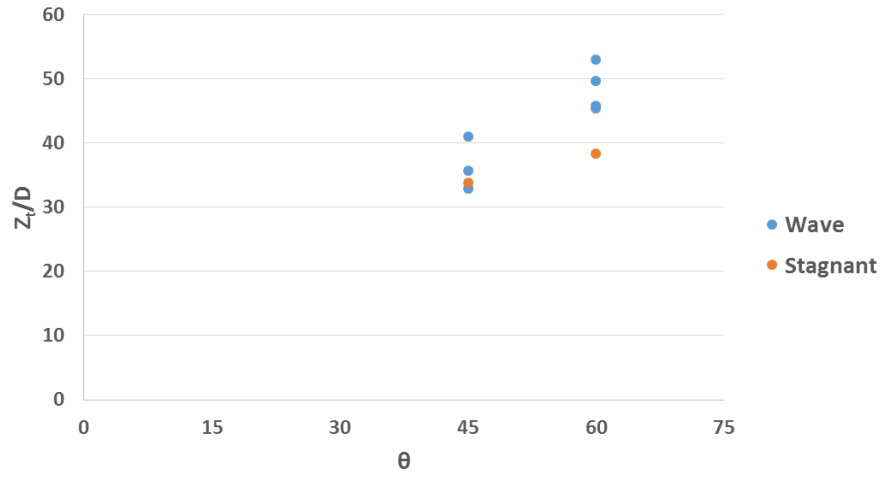
Figure 6.43 : Normalized terminal rise height along discharge angle (θ).
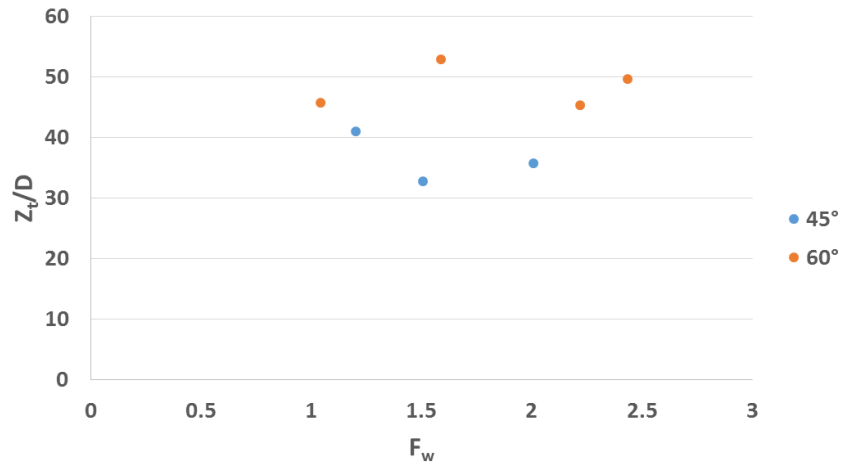
Figure 6.44 : Normalized terminal rise height along wave Froude number (F_w).
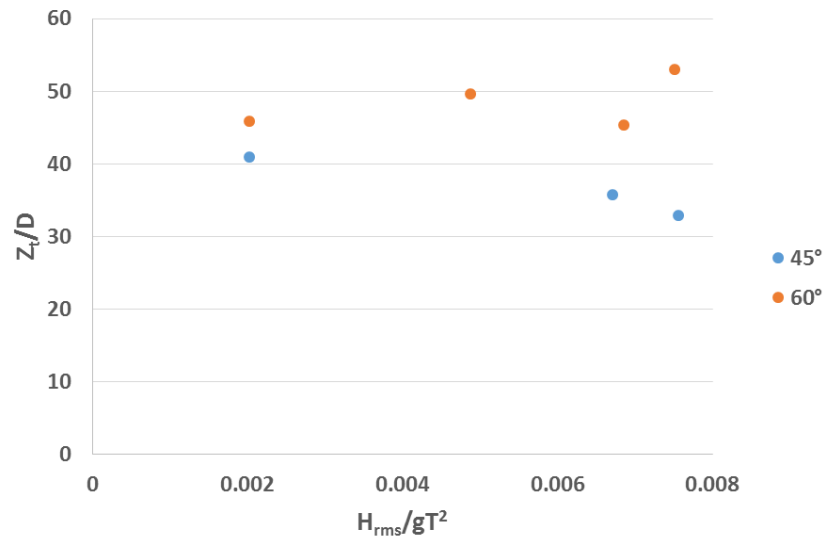
Figure 6.45 : Effect of wave steepness on terminal rise height.

145

Impingement point (X_i)

For the evaluation of impingement point, applied method did not give exact points of impingement point. Due to this reason, time series of impingement point measurements are not presented. However, mean values of detected points for the same duration of time demonstrate conditions for the tests (Table 6.12). In the following figure (Figure 6.46), these values are given for the tests depending on the discharge angle.
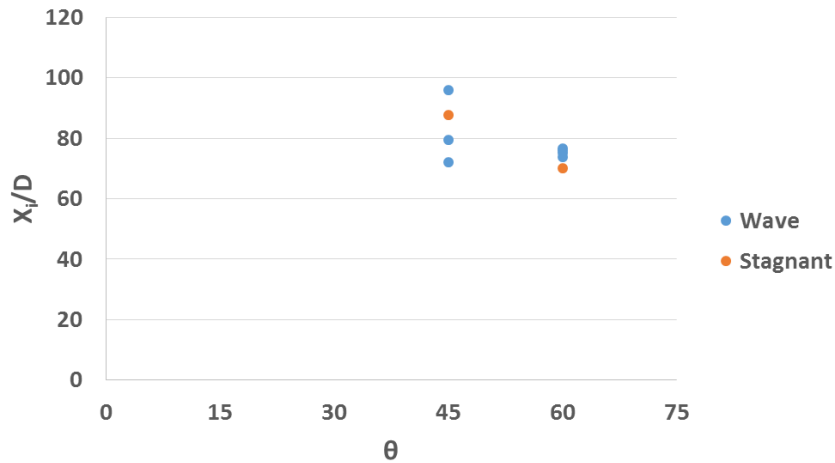
Figure 6.46 : Normalized impingement point distance (X_i).

Phase 2

As it was stated before, in the second phase of image processing, front position of flow (X_e), water surface level at X_e (η) and discharge point (η_0) were the considered parameters.

Propagation of dense layer in transitional zone

In Figure 6.47, flow front position (X_e) time series determined by image processing are given for all of the tests considered under wave conditions. In the graphs time axis shows the time after discharge and started at 25th second for comparison.

146
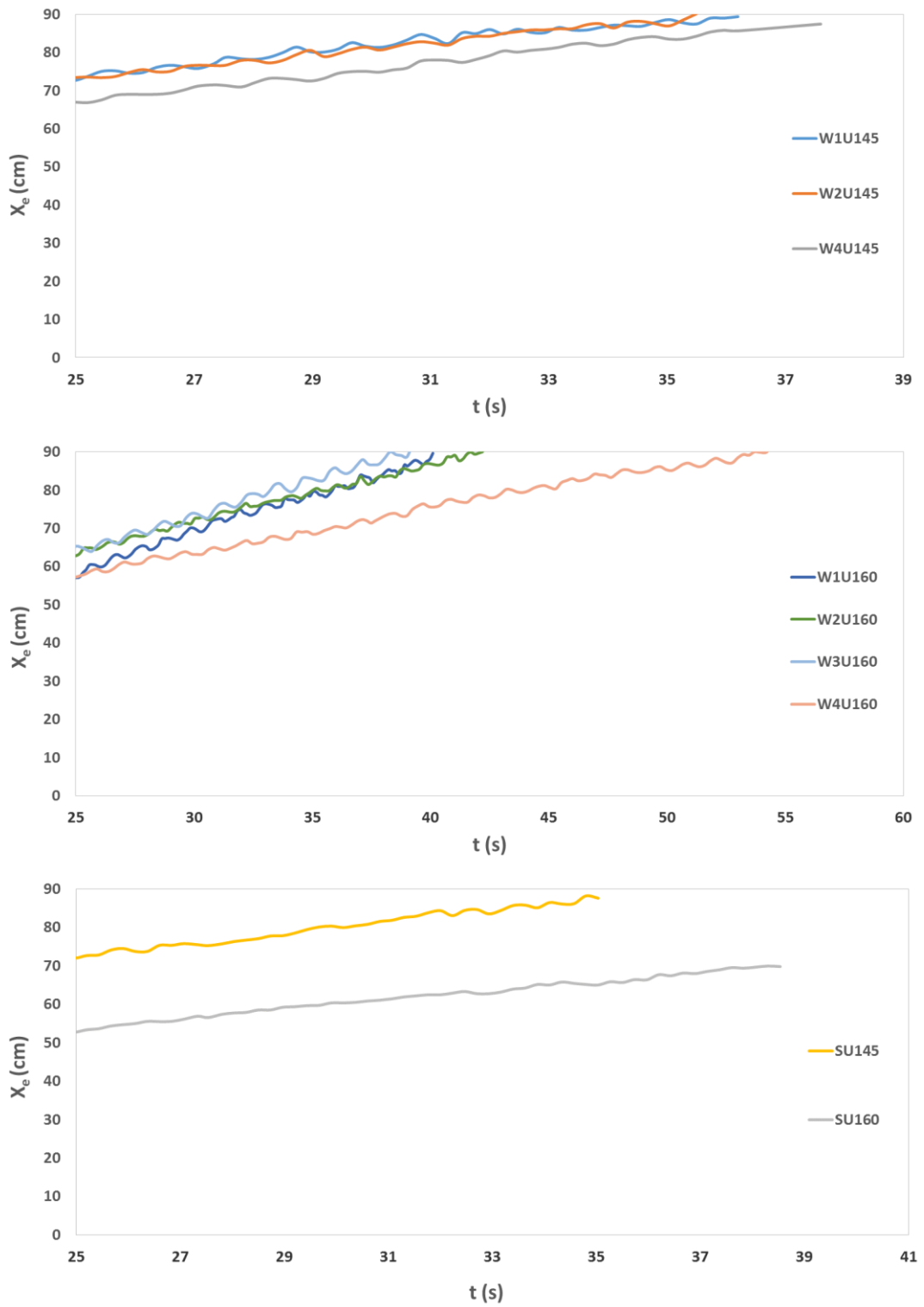
Figure 6.47 : Flow front position in time.

In Figure 6.48, flow front position time series are given in non-dimensional form.
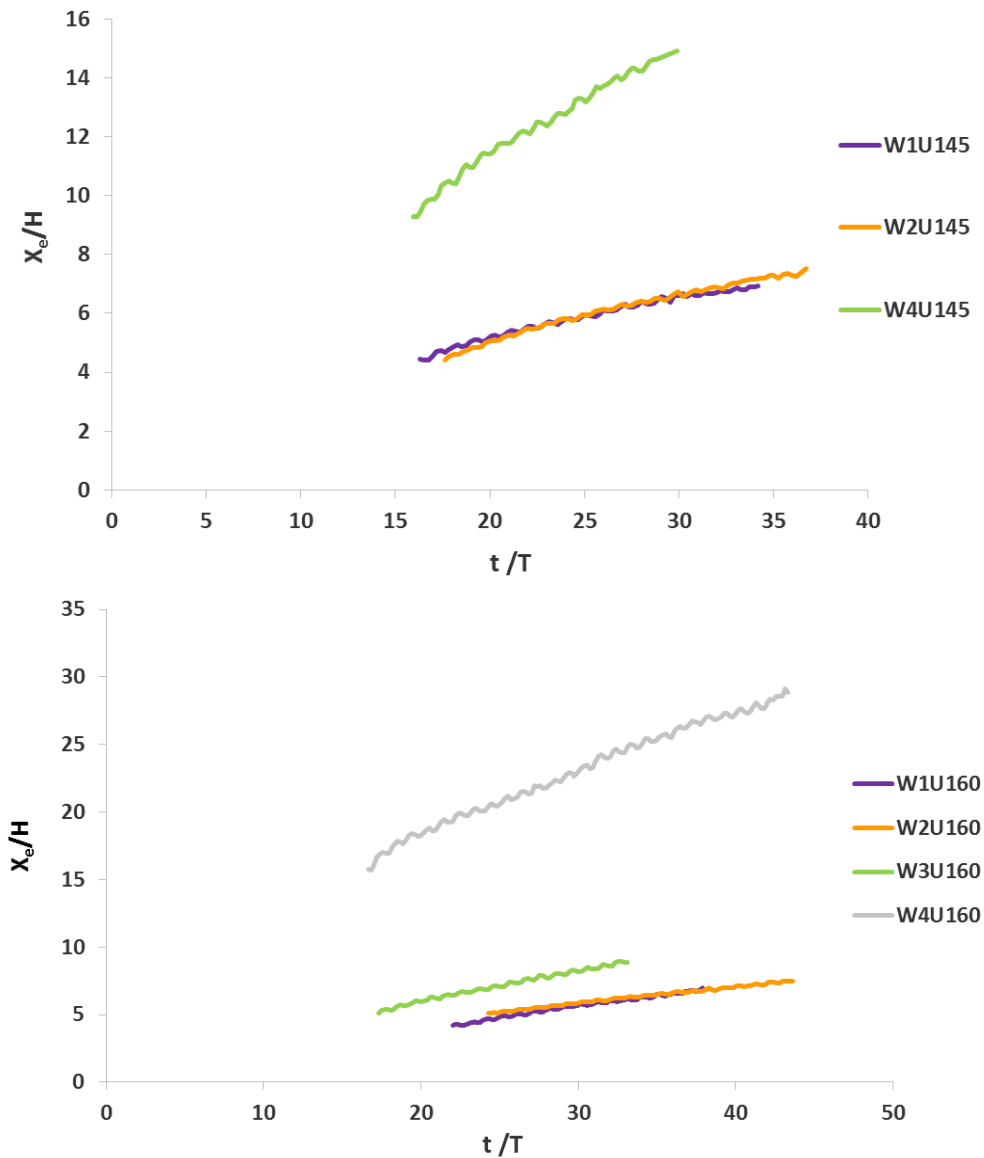
Figure 6.48 : Normalized flow front position with respect to dimensionless time for the tests with waves.

Propagation velocity of flow front (U_L) values were determined as the ratio of propagation distance difference (ΔX_e) to time difference (dt) between each processed image. In Figure 6.49 and 6.50, determined propagation velocity of the tests are given as the time series to be able to compare with the wave propagation. As it can be seen from the figures, started dense current at the bottom propagates with the effects of waves. In Figure 6.51, mean propagation velocity values are plotted against executed wave height values.

148
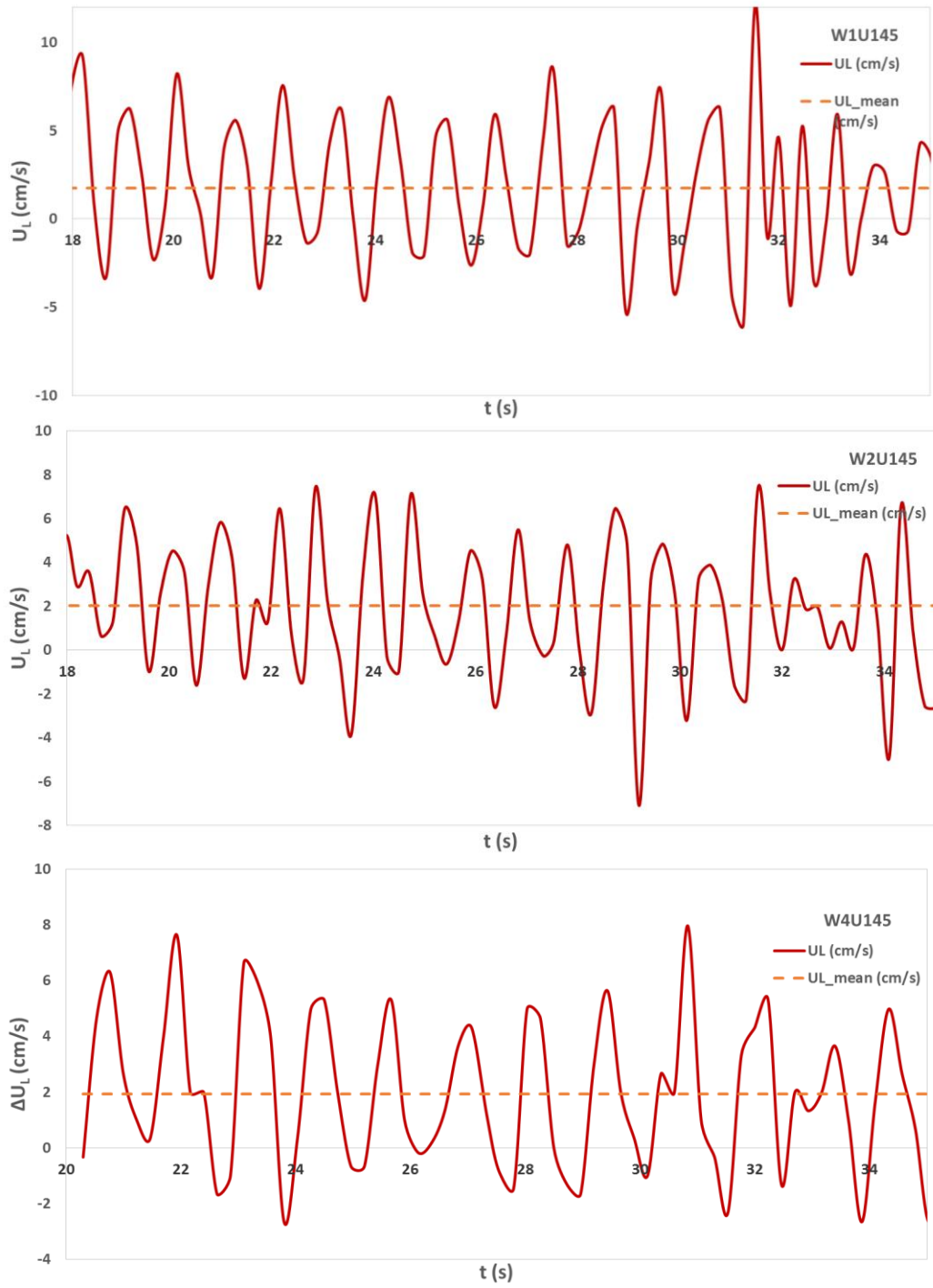
Figure 6.49 : Dense layer propagation velocity in transitional zone
(Tests with waves, θ=45°).
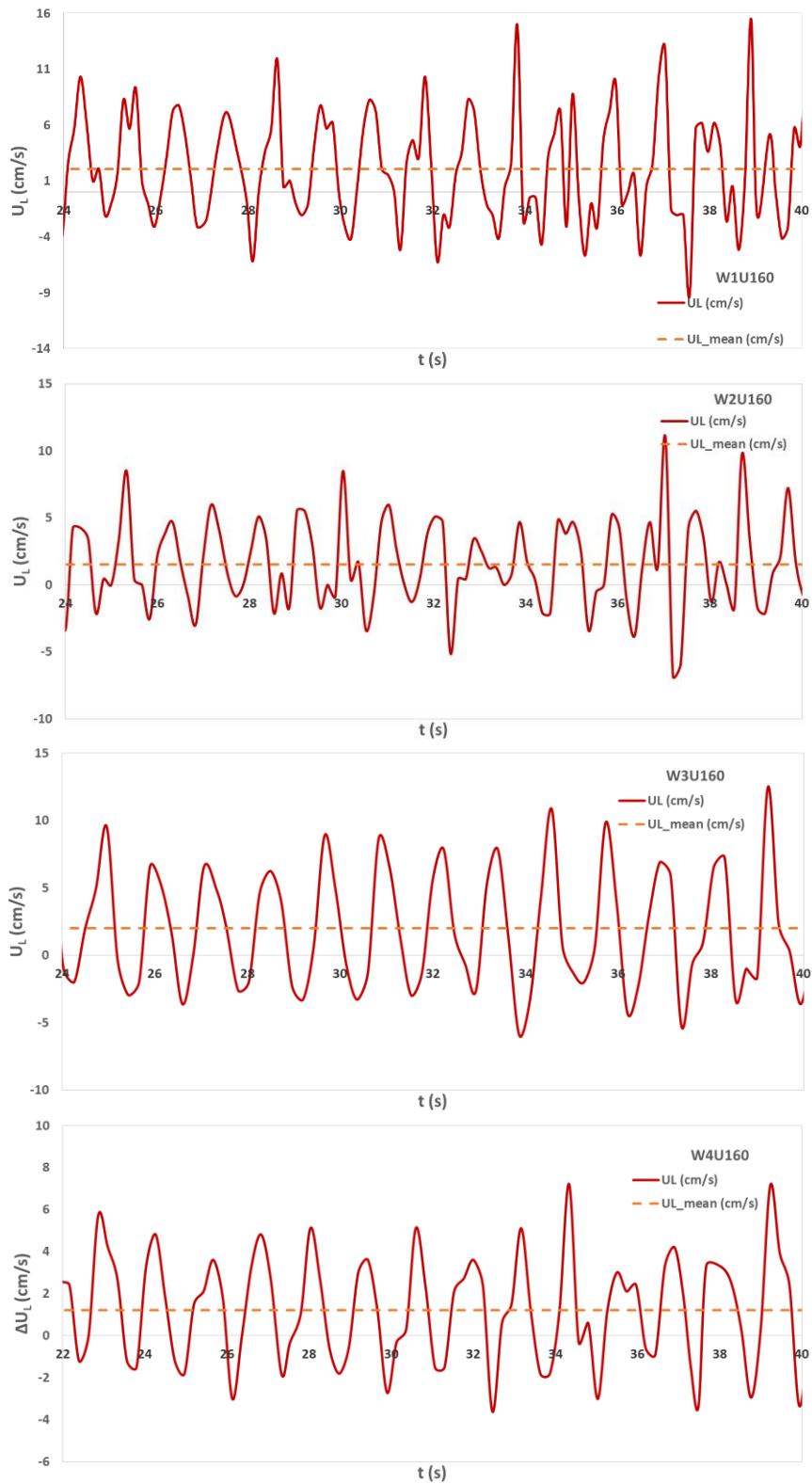
Figure 6.50 : Dense layer propagation velocity in transitional zone
(Tests with waves, θ=60°).
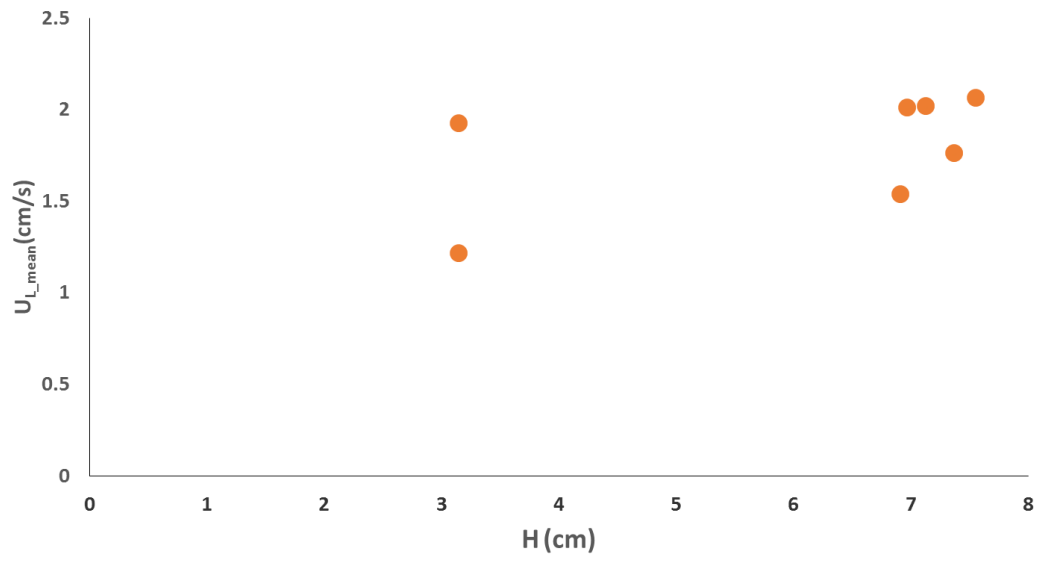
Figure 6.51 : Mean dense layer propagation velocity with respect to wave height.

7. NUMERICAL STUDY AND RESULTS

7.1 Verification of Integral Models For Multiport Brine Discharges

As stated in foregoing chapters, CORJET, UM3 and JETLAG are the most commonly used entrainment models that are used for modelling of brine outfall systems. Due to the rare number of experimental studies of multiport brine discharges, the evaluation of these software in comparison with empirical data does not exist. In this study, these models are verified within the context of port space effect by constituting scenarios of brine outfall systems with multiport diffusers and comparing experimental data.

JETLAG is not included in the results because of simulating multiport jets individually and giving the same results for every scenario executed.

7.1.1 Scenarios

In that chapter, composed scenarios are given with the definition of each input parameter for the simulations. Criteria for each input parameter for modelling scenarios will be discussed mainly classified as effluent parameters, receiving ambient parameters and discharge system parameters, respectively. The parameters for simulations executed are presented at Table 7.1, 7.2 and 7.3.

7.1.1.1 Effluent parameters

- **Effluent Velocity (u_j):** The design criteria for diffuser velocity is that the velocity should be uniform along the diffusers. Also, it should be high enough to prevent accumulation in the discharge pipes and also intrusion of ambient water. Discharge velocity is chosen as 3.24 m/s for the whole simulation cases. Moreover, velocity is an important design parameter, since increasing velocity leads to increase effluent dilution.

- **Effluent salinity concentration (C_0):** Effluent salinity concentration is calculated using the ambient salinity values and formula below (Ladewig & Asquith, 2012):

$$C_{brine} = C_{feed\,water}\left(\frac{1}{1-R}\right) \qquad \text{(7.1)}$$

In that calculation, recovery rate (R) for the RO system is assumed 45% to calculate the salinity of effluent.

- **Effluent density (ρ_0):** Density values for the effluent and receiving environment are calculated using the equation set in El-Dessouky and Ettouney (2002) in which salinity and temperature are the input values to calculate density. For the calculation, effluent temperature assumed same with the ambient water due to the fact that RO is an membrane process.

- **Effluent kinematic viscosity (v):** Effluent kinematic velocity value is calculated using the equation set below (El-Dessouky and Ettouney, 2002) related to dynamic viscosity (μ) calculation in which chosen salinity and temperature values were used.

- **Densimetric Froude Number (F_d):** Densimetric Froude number is chosen as 15 is a typical value for brine outfall systems.

- **Reduced gravitaty (g_0'):** This value is calculated using calculated density values of effluent and receiving environment.

7.1.1.2 Ambient parameters

- **Depth at Discharge (H_A):** The depth at discharge value is taken as 19.2 m which is a constant value for the whole simulations.

- **Ambient Salinity Concentration (C_a):** Ambient salinity concentration values are taken from a measurement data at a point in Aegean Sea (Table 7.1).

- **Ambient Density (ρ_a):** Ambient density is calculated using the same equation for effluents. In that calculation average salinity and temperature of ambient water is taken from example data which is given in Table 7.1.

- **Density Stratification:** Density stratification is an critical parameter for hydrodynamic behavior and mixing of discharged effluents. In this study, a uniform density profile is chosen to be used because of having experimental data without stratification to be used for verification. In Figure 1, density stratification in Aegean Sea from a real measurement data can be seen in density profiles. As it can be seen, it is nearly uniform and close values to data at deepest points are used for the simulations.

- **Ambient Flow Rate (U_A):** In that study, current velocity will be assumed zero to have similar conditions with experimental data.

Table 7.1 : Example temperature and salinity measurements of Aegean Sea.

Depth (m)	Temperature (°C)	Salinity (psu)	Density (kg/m^3)
0.6	22.6048	39.2018	1026.93
1.0	22.6154	39.2081	1026.93
3.3	22.6062	39.1685	1026.90
6.1	22.5315	39.0989	1026.87
9.2	22.3306	38.9445	1026.82
12.1	21.7596	38.9905	1027.82
14.6	21.4013	39.0591	1027.18
16.2	20.8307	38.7268	1027.10
18.5	20.1321	38.8798	1027.42
19.3	19.8303	39.0964	1027.67
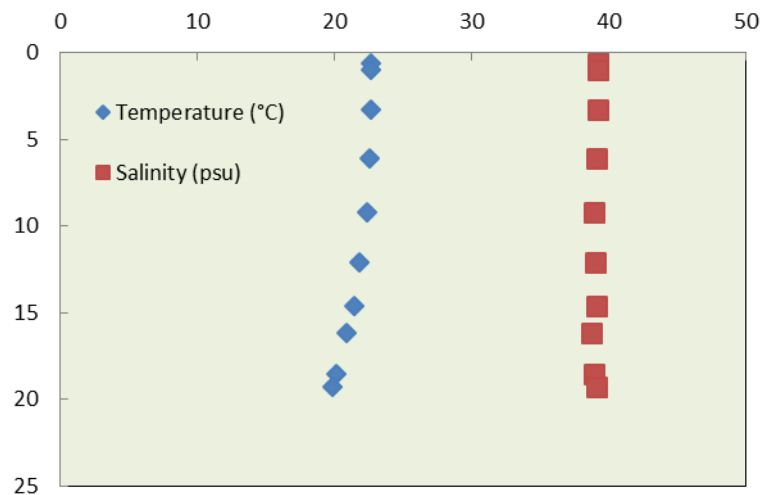
Figure 7.1 : Example temperature and salinity profile of a measurement point at Aegean Sea.

7.1.1.3 Discharge system parameters

- **Diffuser Type:** Diffuser type is chosen as an unidirectional multiport diffuser with equally spaced ports with same diameter. It is the only system that can be modeled by CORJET and UM3.

- **Diffuser length (L_D):** Diffuser length is constant for all scenarios and equal to 200 m.

- **Port diameter (D):** Port diameter is chosen as 0.2 m for the whole simulations.

- **Port orientation:** Vertical angle of discharge (θ) is chosen as 60° for whole scenarios as being the optimum value for negatively buoyant discharges and because it is the only case for which experimental data have been found in the literature.

- **Port height (h_0):** Port height is chosen 0 m compatible with the experimental conditions of verification data that will be used.

- **Port number (n) and Port space (s):** Port number is the number of ports on a multiport diffuser and the port space is the distance between them. These parameters were varied for each scenario due to the fact that effect of port space is the main verification parameter for this study. As stated before, in this study Abessi and Roberts' (2014) experimental work, which includes the range of $0.44 < s/DF_d < 12$, used for verifying the model results. Due to this reason, s/DF_d ratios were chosen in that range except the cases F2S9 and F2S10 which have higher values (Table 7.3).

Table 7.2 : Constant parameters for the scenarios.

Parameter	Value
T (°C)	20
C_a (ppt)	39.0964
C_0 (ppt)	71.084
ρ_0 (kg/m^3)	1052.1
ρ_a (kg/m^3)	1027.7
g_0'	0.2329
u_0 (m/s)	3.24
Q_0 (m^3/s)	1.017 x10^{-1}
F_d	15
ν (m^2/s)	1.11x10^{-6}
H_A (m)	19.2
Port height (m)	0
L_D (m)	200
d_{riser} (m)	0.2
θ (°)	60
U_a (m/s)	0
Stratification	Uniform

Table 7.3 : Variable parameters for the scenarios.

Case No	n	s	s/DF$_d$	Q_T (m^3/s)
F2S1	153	1.32	0.44	1.556 x10^1
F2S2	112	1.80	0.60	1.139 x10^1
F2S3	85	2.38	0.79	8.645
F2S4	68	2.99	1.00	6.916
F2S5	46	4.44	1.48	4.679
F2S6	35	5.88	1.96	3.560
F2S7	15	14.29	4.76	1.526
F2S8	8	28.57	9.52	8.137 x10^{-1}
F2S9	6	40.00	13.33	6.102 x10^{-1}
F2S10	4	66.67	22.22	4.068 x10^{-1}

7.1.2 Results

After constituting scenarios and executing models to be tested, data was generated using scenario input values and empirical equations by Abessi & Roberts (2014). Impact point dilution, impact point location and terminal rise height values were chosen as the parameters to be compared.

Terminal rise height (z_t) is calculated according to formula below in which maximum rise height (z_m) and visual radius (R) obtained from program outputs used. R is taken as double of radial distance (where concentration is 6% of jet centreline, *R=2b*) for CORJET and half of jet diameter (*R=Dia/2*) for UM3 (Palomar et al., 2012b):

$$z_t = z_m + R \qquad\qquad (7.2)$$

In Figure 8.2, simulation results related to impact point dilution (S_i) and port space relation are given in 3 graphs; last two of them are separated parts of the first. As it can be seen from the figure, calculated values according to experimental work, follows a line increasing with increasing port space until $s/DF_d \sim 2$. After this point, S_i values approximate an ultimate value which is the single point region (Figure 7.2a). However, the values for CORJET and UM3 doesn't follow this trend in the plume region ($s/DF_d < 2$) which shows that both of the programmes are not reflecting merging behaviour of jets for this range of port space (Figure 7.2b). For the single point region where the discharged jets are separated ($s/DF_d > \sim 2$), CORJET and UM3 model discharged jets as a single port discharge due to the fact that they are not merging. So, in that graph whole points constitutes a constant value line for each programme (Figure 7.2c). The values of these lines show that both of the programs calculate lower dilution values compared to experimental ones. Indeed if it is looked at the whole range this behaviour is valid for the range of $s/DF_d > 0.8$.
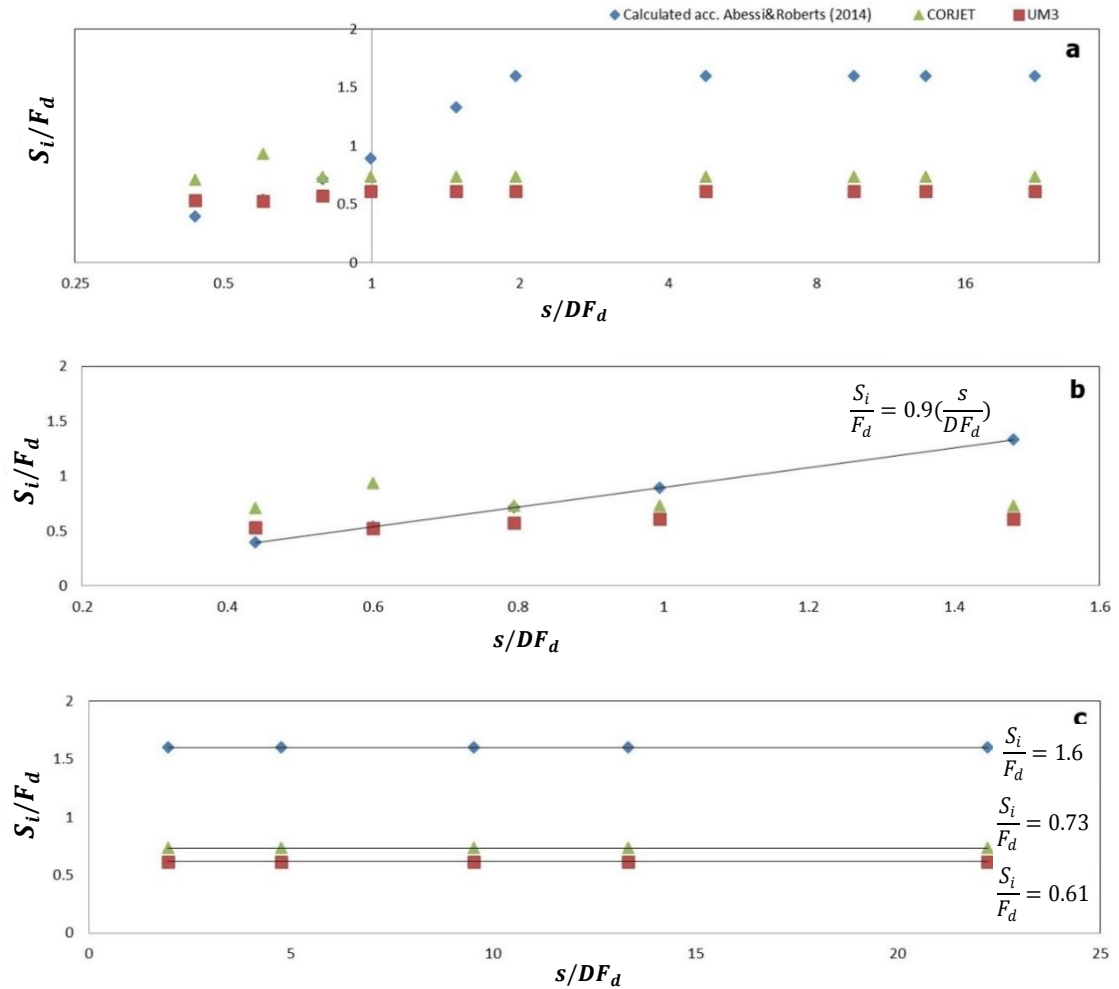
Figure 7.2 : Dilution-port space relation, a) All scenarios, b) Scenarios with
s/DF$_d$<2; c) Scenarios with s/DF$_d$>2.

In Figure 7.3 and 7.4, CORJET and UM3 model results are given with calculated
values for impact point location and terminal rise height and port space relation,
respectively. As mentioned before, it is found out that geometrical characteristics of
discharged dense jets from multiport diffusers follow different trend for closely and
widely spaced situations (Abessi& Roberts, 2014). For closely spaced diffusers, x_i
and y_t values decrease with as the jets get closer (s/DF$_d$<2). (Figure 7.3b, 7.4b). For
further distances, the values are compatible with predicted asymptotic solutions. This
trend is shown as the calculated values according to Abessi and Roberts (2014) in the
figures (Figure 7.3c, 7.4c).
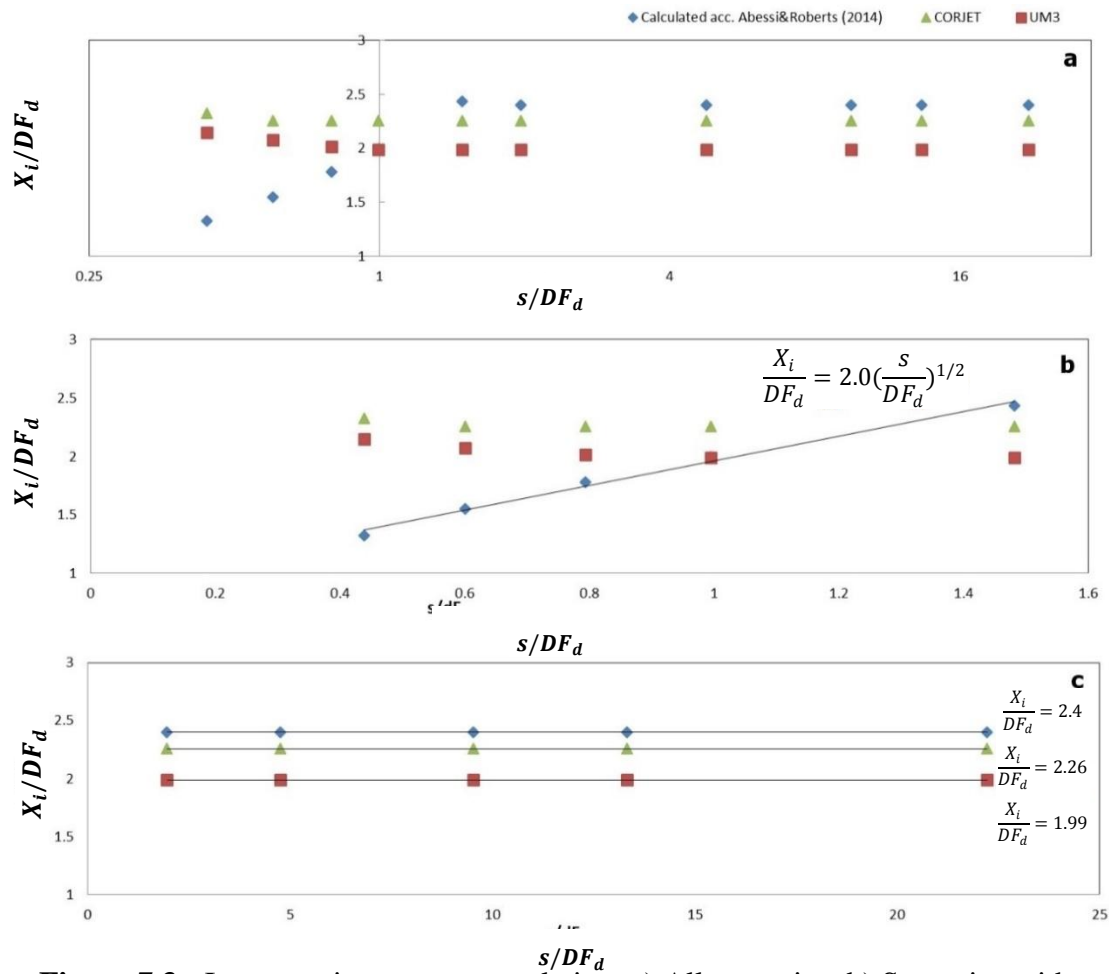
Figure 7.3 : Impact point-port space relation, a) All scenarios, b) Scenarios with s/DF$_d$<2; c) Scenarios with s/DF$_d$>~2.

It is clear in Figure 7.3 and 7.4 that CORJET and UM3 simulations did not reflect jet behavior in line plume region for the geometric characteristics similar to dilution values. It gives higher values for s/DF$_d$<1 and lower values for s/DF$_d$>1, in case of horizontal location of the impact point and as the same for the maximum rise height. As it is shown in the figures, changing port space is almost no effect on the results in that region. In single plume region, both of the programs give results of geometrical features lower compared to calculated ones.
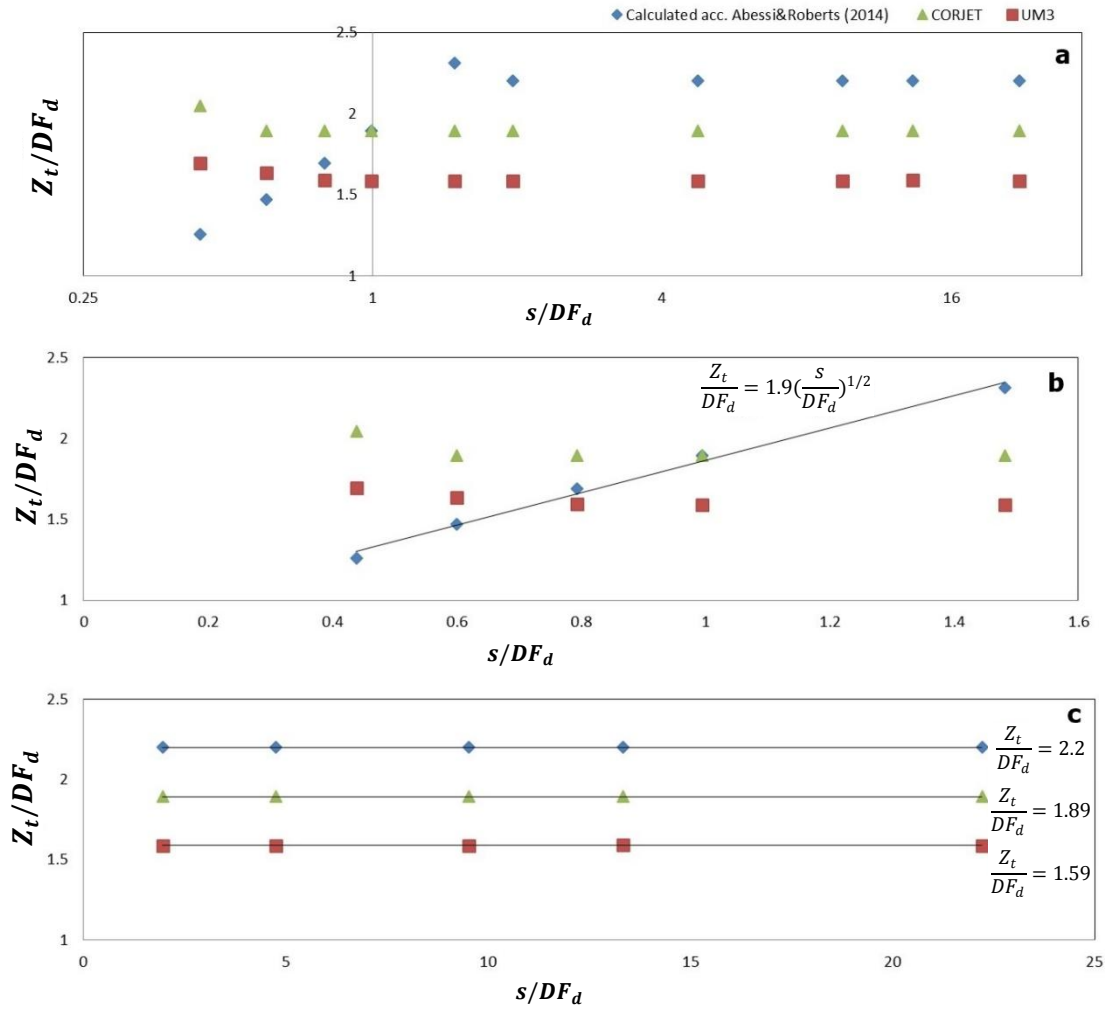
Figure 7.4 : Terminal rise height-port space relation, a) All scenarios, b) Scenarios with s/DF$_d$<2; c) Scenarios with s/DF$_d$>~2.

As the conclusion, numerical results that obtained by commercial integral models UM3 and CORJET are not compatible with experimental data by Abessi and Roberts (2014). However, maybe integral models just need to be modified and can be indeed very useful for prediction of features of brine discharged through unidirectional multiport diffuser systems. If these models are used for simulating unidirectional multiport diffusers, their results are meaningful for port spaces which do not cause merging of jets but it should be taken into consideration that they eventuate in more conservative values of investigated parameters.

7.2 Numerical Modelling of Spreading Gravity Currents

As stated in the previous chapters, discharged brine behaves like an gravity current in the far field region. In this part of the study, executed numerical steady related to spreading gravity currrents is presented. With this study, it was aimed to analyse gravity current behaviour and also produce a practical tool which simply predicts general characteristics of gravity current behaviour on an incline using Boussinesq approximation and steady-state density current assumption. In this context, two Matlab codes were which are capable of solving equations related to spreading of gravity currents by Ellison & Turner (1959) and Garcia (1996) (2-Dimensional) and Alavian (1986) (3-Dimensional) using Runge-Kutta 4th methodology was developed. In following, main equations which are used, scenarios for numerical simulations and results are presented for both of the codes, respectively.

7.2.1 2D Spreading of gravity currents

7.2.1.1 Main equations

Garcia (1996) obtained equations from instantaneous equations governing fluid motion related to 2D spreading of gravity currents by using some assumptions.

A gravity current of cold water flowing into a warmer ambient fluid with a constant density on an incline with the slope of S<<1 was considered (Figure 7.5):
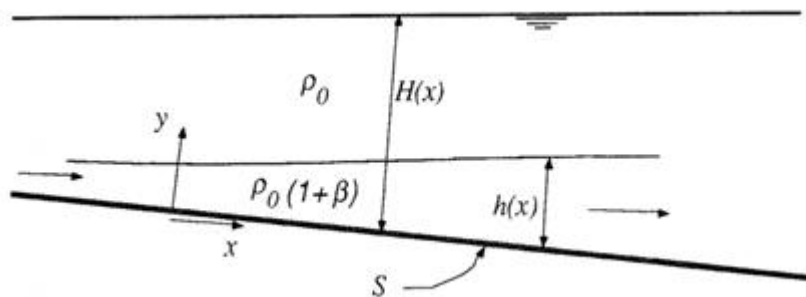
Figure 7.5 : Gravity current propagating over a slope (Garcia, 2006).

Through this process, it was assumed that the thickness of the dense layer is small compared to water depth (h<<H) and the current was steady-state. In addition, Boussinesq and boundary layer approximations, assumption of self-similarity of the sections and neglection of viscous forces were made. For $UBh = U_0 B_0 h_0$ is constant, flow equations as below:

$$\frac{dh}{dx} = \frac{(2E + C_d) - \left(S_1 S_0 + \frac{1}{2} S_2 E\right) Ri}{1 - S_2 Ri} \tag{7.3}$$

$$\frac{h}{3Ri}\frac{dRi}{dx} = \frac{(E + C_d) - \left(S_1 S_0 - \frac{1}{2} S_2 E\right) Ri}{1 - S_2 Ri} = \frac{dh}{dx} - E \tag{7.4}$$

$$\frac{h}{3Ri}\frac{dRi}{dx} = \frac{(E + C_d) - \left(S_1 S_0 - \frac{1}{2} S_2 E\right) Ri}{1 - S_2 Ri} = \frac{dh}{dx} - E \tag{7.5}$$

$$\frac{dU}{dx} = -\frac{U}{3Ri}\frac{dRi}{dx} \tag{7.6}$$

$$\frac{1}{B}\frac{db}{dx} = -\frac{E}{h} \tag{7.7}$$

$$E = f(Ri) \tag{7.8}$$

In these equations, C_d is the friction coefficient, which is assumed as constant, and S_1 & S_2 are shape factors due to non-uniform density distribution and they are defined as below:

$$S_1 = \frac{1}{\left(\frac{\Delta\rho}{\rho_a}\right)_m} \int_0^\infty \frac{\Delta\rho}{\rho_a} dz \tag{7.9}$$

$$S_2 = \frac{2}{\left(\frac{\Delta\rho}{\rho_a}\right)_m h^2} \int_0^\infty \frac{\Delta\rho}{\rho_a} z dz \tag{7.10}$$

Shape factor values were experimentally determined as 0.6-0.9 for S_1 and 0.2-0.3 for S_2 by Ellison & Turner (1959). Alavian (1986) measured shape factors in his experiments as 0.35-0.84 for S_1 and 0.1-0.43 for S_2.

Ri is the Richardson number which is defined as below:

$$Ri = \frac{\Delta\rho}{\rho_a}\frac{gh\cos\theta}{U^2} \tag{7.11}$$

Using the first equation, critical Richardson number (Ri_c), which is the value of Ri making the denominator of the equation zero leading to $\frac{dh}{dx} \approx \infty$ (Garcia, 2006):

$$Ri_c = \frac{1}{S_2} \tag{7.12}$$

According to Ri of the flow compared Ri_c, its behaviour can be defined as subcritical ($Ri > Ri_c$) or supercritical ($Ri < Ri_c$) (Garcia, 2006).

As it was stated before, propagating dense layer reaches to a normal state with a constant Ri through the distance. Following equations for the ultimate Richardson number (Ri_n) is defined as below (Koh, 1981; Garcia, 1996):

$$E_n = E(Ri_n) \approx \frac{dh}{dx} \tag{7.13}$$

$$Ri_n = \frac{E_n - C_D}{0.5 S_2 E - S_1 \tan \alpha} \tag{7.14}$$

Bottom slope (S_0) also determines the flow behaviour. Flow propagating on gentle slope and steep slope are called as subcritical and supercritical flow, respectively. This transition of flow is defined with critic slope parameter (S_{cr}) as below (Garcia, 1996):

$$S_{cr} = \frac{0.5 S_2 E}{S_1} \tag{7.15}$$

In this part of the study, proposed equations by Garcia (1996) were solved with written Matlab code using Runge-Kutta 4th order method. Written code gives variation of Ri, E, U, h, concentration (C) and dilution (D) as the output.

7.2.1.2 Scenarios

Initial density of density current (ρ_0) and ambient water (ρ_a), initial concentration of density current (C_0) and ambient water (C_a), initial flow (Q_0), bottom slope (S_0), discharge width (b_0) and discharge height (h_0) are the input values. In the whole cases of simulation, initial brine salt (C_0) and density (ρ_0) were taken as 71 ppt and 1052 kg/m^3 and ambient salt (C_a) and density (ρ_a) values were taken as 39 ppt and 1025 kg/m^3. S_1 and S_2 values were chosen as 0.8 and 0.3, respectively.

The entrainment equation by Parker et al. (1987) was chosen for the simulations due to the reason of having no usage limit value of Ri. In addition, it was the most proper one when looking at the whole plot lines of entrainment formulas (Figure 5.6).

In Table 7.4, input values of simulated 12 cases are presented.

Table 7.4 : Input values for simulations of 2D numerical modelling of gravity currents.

Case No	C_0	ρ_0	C_a	ρ_a	C_d	b_0	h_0	S_0	U_0 (m/s)	Step size (m)
1	71	1052	39	1027	0.02	10	1	0.005	1	0.05
2	71	1052	39	1027	0.02	10	1	0.01	1	0.05
3	71	1052	39	1027	0.02	10	1	0.05	1	0.05
4	71	1052	39	1027	0.02	10	1	0.1	1	0.05
5	71	1052	39	1027	0.005	10	1	0.15	1	0.05
6	71	1052	39	1027	0.015	10	1	0.2	1	0.05
7	71	1052	39	1027	0.02	10	2	0.05	1	0.05
8	71	1052	39	1027	0.02	10	2.6	0.05	1	0.05
9	71	1052	39	1027	0.02	10	3	0.05	1	0.05
10	71	1052	39	1027	0.02	10	1	0.05	3	0.05
11	71	1052	39	1027	0.02	10	1	0.05	5	0.05
12	71	1052	39	1027	0.02	10	1	0.05	10	0.05

7.2.1.3 Results

Two flow equations were solved with written Matlab code using Runge-Kutta 4th order method as stated before by using the the assumption of constant buoyancy flux equation. Written code gives variation of Ri, E, U, h, concentration (C) and dilution (D) as the output. This programme may be thought as a prediction tool of 2D spreading of gravity currents for a constant current width, taking the end of near field results as the input.

As it can be seen from the plots (Figure 7.6, 7.7 and 7.8), the programme gives the variation of analysed parameters through the distance of propagation. The results are a rough estimation of gravity current spreading for stagnant receiving environment conditions without considering ambient conditions such as waves, currents and bathymetry.

It is necessary to state that the programme is applicable only for supercritical flow conditions which are located in the code defining Ri_c and S_{cr} values. For subcritical flow conditions ($Ri > Ri_c$), the programme is not capable of solving the related equations.

In Figure 7.6, results for Cases 2, 3, 4, 5 and 6 are presented. In these scenarios, changing parameter was only the bottom slope. After running the programme, it was determined that $0<S_0<0.2$ was the range of bottom slope which the programme was succesful to simulate. However, for very low values of S_0 like 0.003, the results were

not good. Thus, it is recommended to use it for bottom slopes which are higher than 0.01.
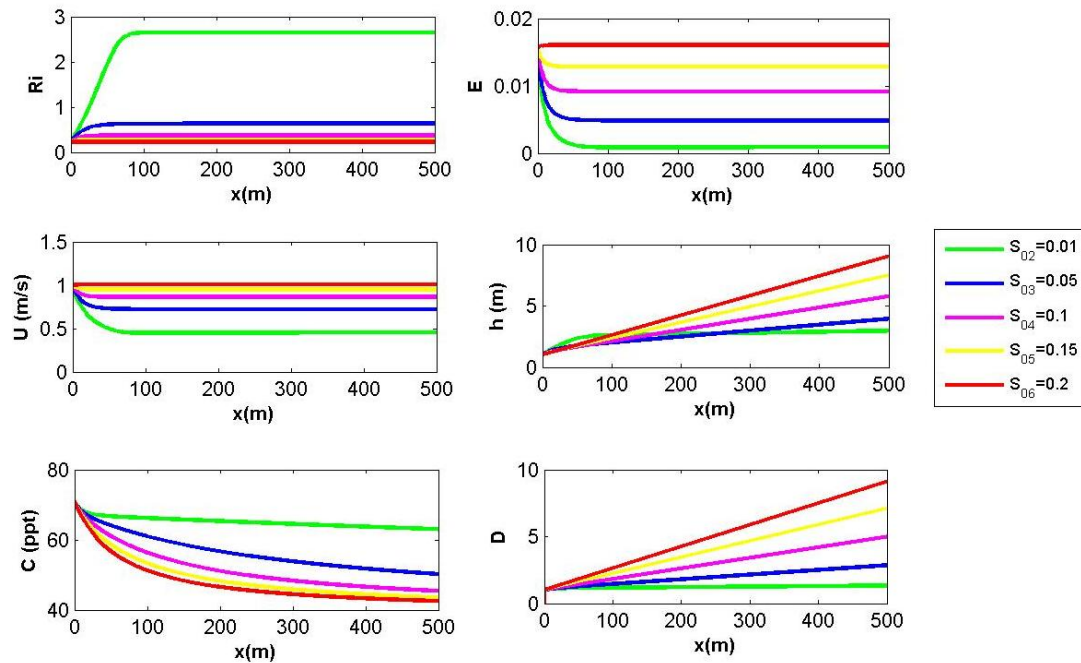
Figure 7.6 : Test plots for various bottom slopes (Cases 2,3,4,5,6).

In Figure 7.7, results for Cases 3, 7, 8 and 9 are presented. In these scenarios, changing parameter was only the initial thickness of gravity current. After running the programme, it was determined that $h_0=2.7$ m was the limit value for this conditions. For the runs with higher initial thickness values, program was not working well.
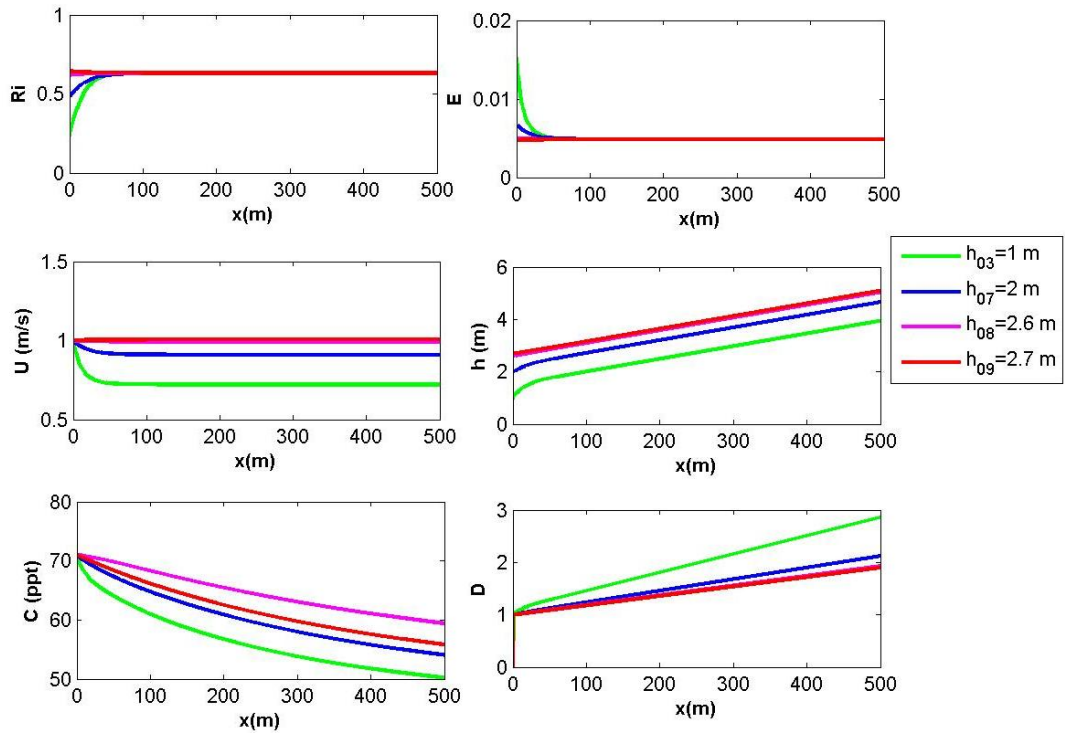
Figure 7.7 : Test plots for various current thicknesses (Cases 3, 7, 8, 9).

In Figure 7.8, results for Cases 3, 10, 11 and 12 are presented. In these scenarios, changing parameter was only the initial velocity of gravity current. After running the programme, it was determined that programme was capable of simulating results for executed scenarios.
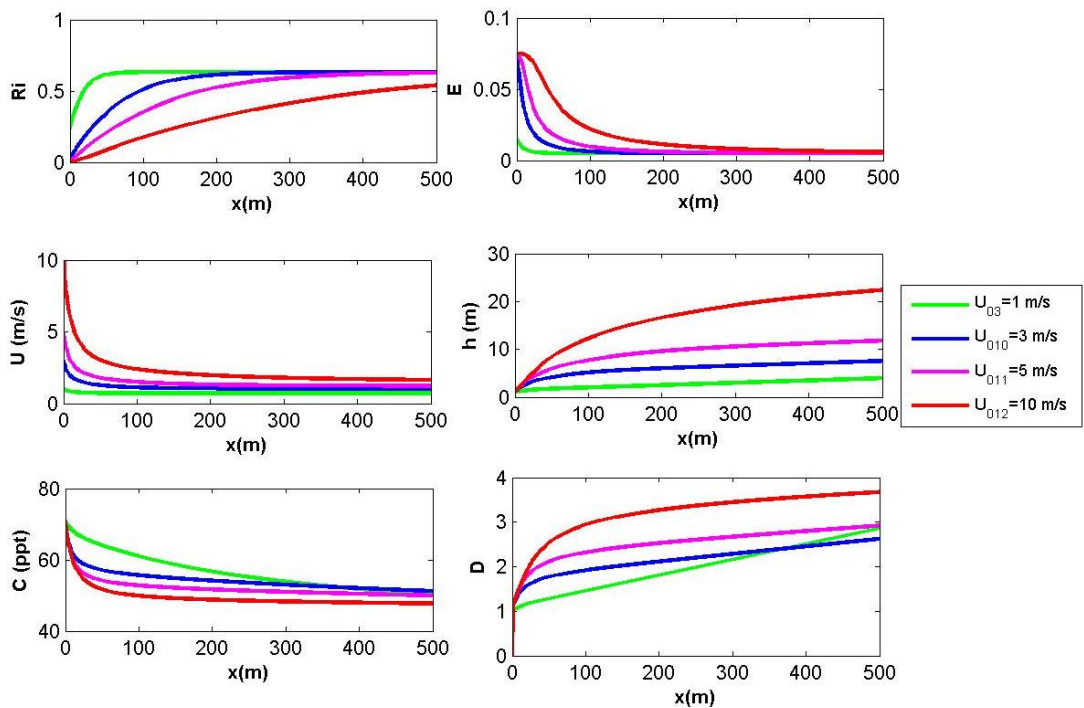
Figure 7.8 : Test plots for various initial velocities (Cases 3, 10, 11, 12).

7.2.2 3D Spreading of gravity currents

7.2.2.1 Main equations

Alavian (1986) developed a model for steady density currents propagating on a slope which requires a constant buoyancy flux (B=Δρ/ρaAU=constant). In their model, entrainment (E) is defined as the entraining water into current from ambient through the upper boundary:

$$\frac{d}{dx}(UA) = EU(b + 2h) \tag{7.16}$$

Here ρ is the mean local density, ρ_a is the ambient density which is assumed constant, $\Delta\rho = \rho - \rho_a$, A is the cross-sectional area of dense layer, U is the mean layer velocity, b is the width and h is the thickness of the layer.

Alavian (1986) defined the momentum equation in the direction of mean motion by the assumption of negligible viscosity difference, Boussinesq approximation and hydrostatic equilibrium of ambient as below:

$$\frac{d}{dx}(U^2A) = S_1 \frac{\Delta\rho}{\rho_a} gA \sin\theta - \frac{1}{2} \frac{d(S_2 \frac{\Delta\rho}{\rho_a} ghA)}{dx} \cos\theta - C_d U^2 b \tag{7.17}$$

In these equations, θ is the angle of incline, $(\Delta\rho/\rho_a)_m$ is the local mean density excess, C_d is the friction coefficient, which is assumed constant, and S_1 & S_2 are shape factors, which are defined as below:

$$S_1 = \frac{1}{(\frac{\Delta\rho}{\rho_a})_m} \int_0^\infty \frac{\Delta\rho}{\rho_a} dz \tag{7.18}$$

$$S_2 = \frac{2}{(\frac{\Delta\rho}{\rho_a})_m h^2} \int_0^\infty \frac{\Delta\rho}{\rho_a} zdz \tag{7.19}$$

As it can be seen, force of gravity (first term in RHS), pressure change due to change in depth (second term in RHS) and friction at the bottom (third term in RHS) are the forces which effect flow behaviour.

Author obtained the following equations of density current motion combining the previous equations:

168

$$\frac{dh}{dx} = \frac{C_d + \left(2 - \frac{1}{2}S_2 Ri\right)E - \left(1 - \frac{1}{2}S_2 Ri\right)\frac{h}{b}\frac{db}{dx} - S_1 Ri \tan\theta}{1 - S_2 Ri} \tag{7.20}$$

$$\frac{h}{3Ri}\frac{dRi}{dx} = \frac{C_d + \left(1 + \frac{1}{2}S_2 Ri\right)E - \left(1 - \frac{1}{2}S_2 Ri\right)\frac{h}{b}\frac{db}{dx} - S_1 Ri \tan\theta}{1 - S_2 Ri} \tag{7.21}$$

$$\frac{db}{dx} \sim 3E \tag{7.22}$$

For 3D gravity currents, Koh (1981) and Garcia(1996) suggested following equations for the ultimate Richardson number, Ri_n.

$$E_n = E(Ri_n) \approx \frac{dh}{dx} \approx \frac{1}{3}\frac{db}{dx} \tag{7.23}$$

$$Ri_n = \frac{\left(\frac{3h}{b} - 1\right)E - C_D}{\left(1 + \frac{3}{2}\frac{h}{b}\right)S_2 E - S_1 \tan\theta} \tag{7.24}$$

Alavian (1986) stated that flows propating on steep slopes (S>1/10) are supercritical which are characterized by reduced lateral spreading due to higher slope values and also interfacial instabilities.

Garcia (1996) defined critic slope parameter (S_{cr}) like this:

$$S_{cr} = \frac{0.5 S_2 E}{S_1} \tag{7.25}$$

In this part of the study, proposed equations by Garcia (1996) were solved with written Matlab code using Runge-Kutta 4th order method. Written code gives variation of Ri, E, U, Q, h, b, concentration (C) and dilution (D) as the output.

7.2.2.2 Scenarios

Initial density of density current (ρ_0) and ambient water (ρ_a), initial concentration of density current (C_0) and ambient water (C_a), initial flow (Q_0), bottom slope (S_0), discharge width (b_0) and discharge height (h_0) are the input values. In the whole cases of simulation, initial brine salt (C_0) and density (ρ_0) were taken as 71 ppt and 1052 kg/m^3 and ambient salt (C_a) and density (ρ_a) values were taken as 39 ppt and 1025 kg/m^3.

The entrainment equation by Parker et al. (1987) was chosen for the simulations due to the reason of having no usage limit value of Ri. In addition, it was the most proper one when looking at the whole plot lines of entrainment formulas (Figure 5.6).

C_d was taken as 0.02. S_1 and S_2 values were chosen as 0.8 and 0.3, respectively.

Table 7.5 : Input values for simulations of 3D numerical modelling of gravity currents.

Case No	C_0	ρ_0	C_a	ρ_a	C_d	b_0	h_0	S_0	U_0 (m/s)	Step size (m)
1	71	1052	39	1027	0.02	10	1	0.005	1	0.05
2	71	1052	39	1027	0.02	10	1	0.01	1	0.05
3	71	1052	39	1027	0.02	10	1	0.05	1	0.05
4	71	1052	39	1027	0.02	10	1	0.1	1	0.05
5	71	1052	39	1027	0.005	10	1	0.15	1	0.05
6	71	1052	39	1027	0.015	10	1	0.2	1	0.05
7	71	1052	39	1027	0.02	10	2	0.05	1	0.05
8	71	1052	39	1027	0.02	10	2.6	0.05	1	0.05
9	71	1052	39	1027	0.02	10	2.7	0.05	1	0.05
10	71	1052	39	1027	0.02	10	1	0.05	3	0.05
11	71	1052	39	1027	0.02	10	1	0.05	5	0.05
12	71	1052	39	1027	0.02	10	1	0.05	10	0.05
13	71	1052	39	1027	0.02	2	1	0.05	1	0.05
14	71	1052	39	1027	0.02	15	1	0.05	1	0.05
15	71	1052	39	1027	0.02	30	1	0.05	1	0.05

7.2.2.3 Results

Three flow equations were solved with written Matlab code using Runge-Kutta 4th order method. Written code gives variation of Ri, E, U, h, b, concentration (C) and dilution (D) as the output. This programme may be thought as a prediction tool of 3D spreading of gravity currents taking the end of near field results as the input.

As it can be seen from the plots (Figure 7.9, 7.10, 7.11 and 7.12), the programme gives the variation of analysed parameters through the distance of propagation. The results are a rough estimation of gravity current spreading for stagnant receiving environment conditions without considering ambient conditions such as waves, currents and bathymetry.

It is necessary to state that the programme is applicable only for supercritical flow conditions which are located in the code defining Ri_c and S_{cr} values. For subcritical flow conditions $(Ri > Ri_c)$, the programme is not capable of solving the related equations.

In Figure 7.9, results for Cases 2, 3, 4, 5 and 6 are presented. In these scenarios, changing parameter was only the bottom slope. After running the programme, it was determined that $0<S_0<0.2$ was the range of bottom slope which the programme was succesful to simulate. However, for very low values of S_0 like 0.003, the results were

not good. Thus, it is recommended to use it for bottom slopes which are higher than 0.01.
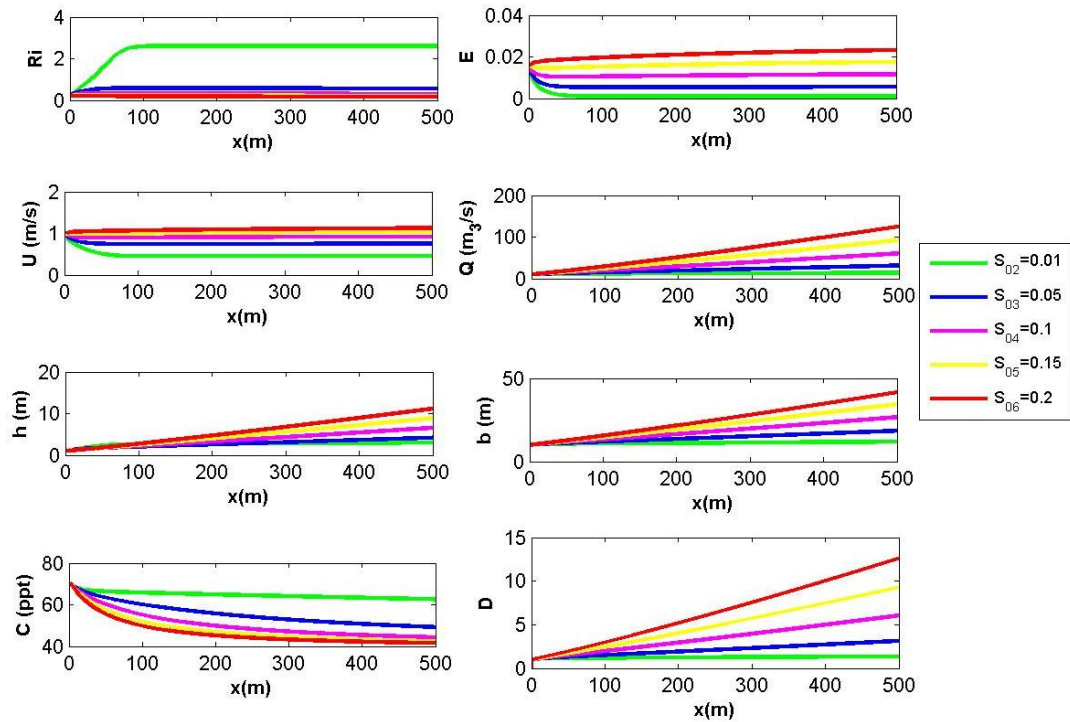
Figure 7.9 : Test plots for various bottom slopes (Cases 2,3,4,5,6).

In Figure 7.10, results for Cases 3, 7, 8 and 9 are presented. In these scenarios, changing parameter was only the initial thickness of gravity current. After running the programme, it was determined that $h_0=2.7$ m was the limit value for this conditions. For the runs with higher initial thickness values, program was not working properly.
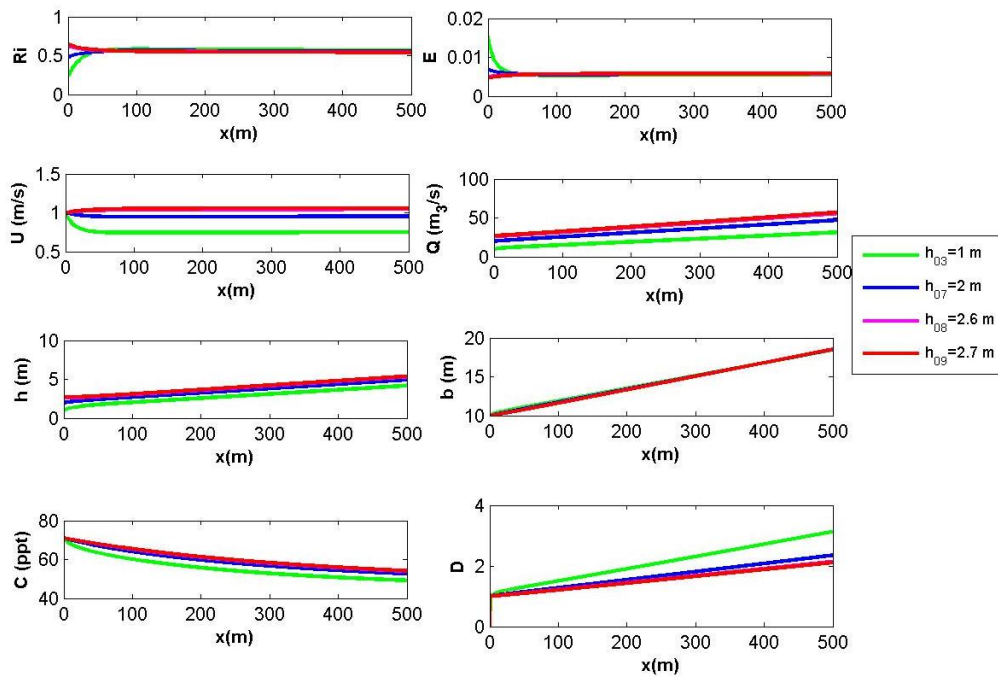
Figure 7.10 : Test plots for various current thicknesses (Cases 3, 7, 8, 9).

Plots of Cases 3, 10, 11 and 12 and Cases 3, 13, 14 and 15 are presented in Figure 7.11 and 7.12, respectively. Plot in Figure 7.11 are the indication of capability of the program for different initial velocity values. It was also seen that the program was successful at simulating results for different initial current width values for executed scenarios.

As the result, it can be concluded that the written programs are capable of presenting general characteristics of gravity currents on inclined bottoms. However, they are not useful for simulating density currents properly and elucidating their exact behaviour in the marine environment. Thus, it can be used as a tool for providing the most basic principles.
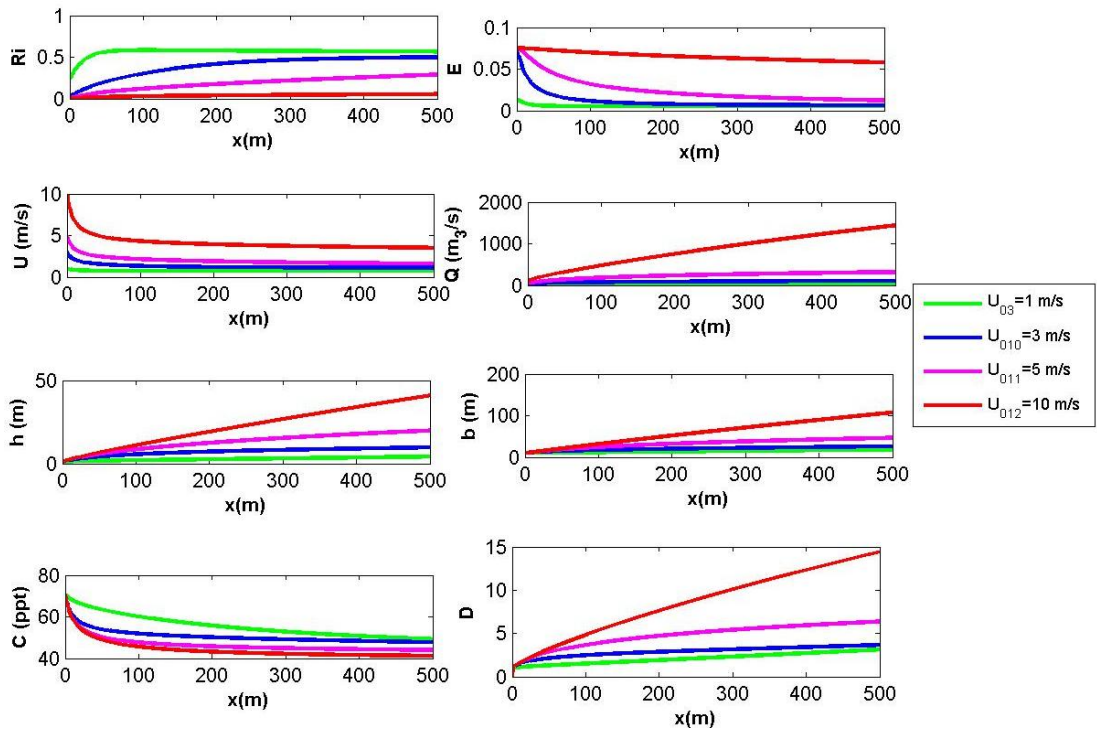
Figure 7.11 : Test plots for various initial velocities (Cases 3, 10, 11, 12).
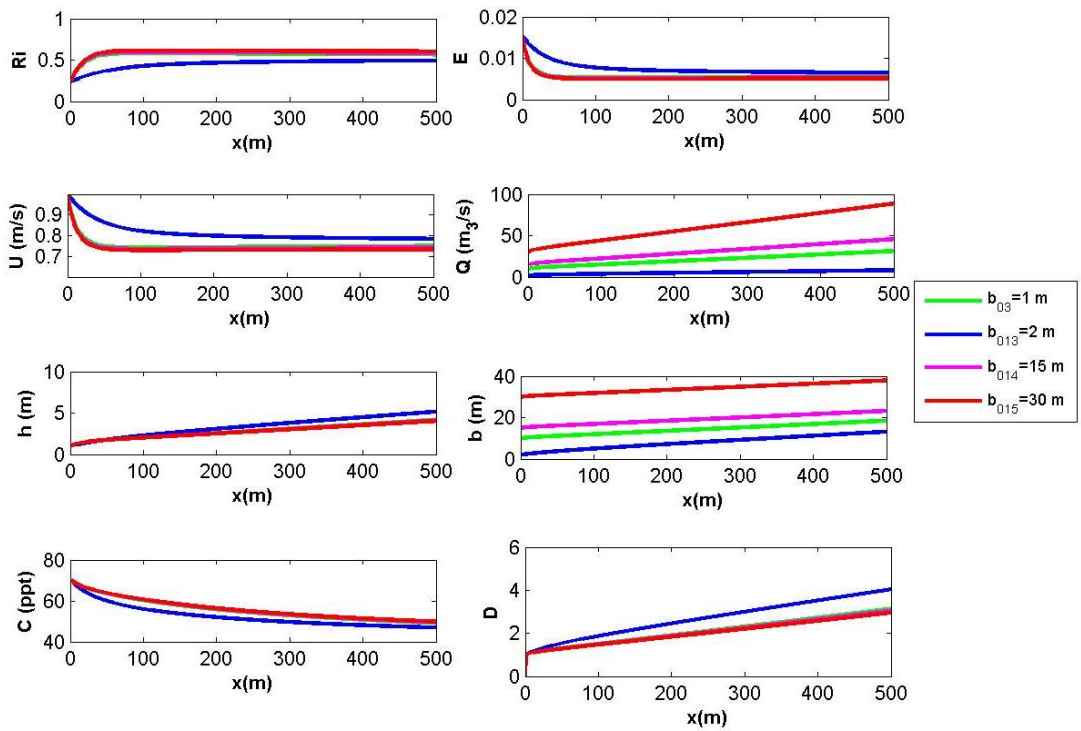
Figure 7.12 : Test plots for various initial widths (Cases 3, 13, 14, 15).

173

8. CONCLUSION AND RECOMMENDATIONS

In the scope of this dissertation, hydrodynamic behaviour of brine discharges in the marine environment was studied by using different methods. The results of this study can be listed as below:

− In the first part of the experimental study, mixing of a stagnant salt layer with the effect of waves was considered. Measured vertical salinity profiles and calculations showed that the external wave energy added to the water column caused rising of potential energy which was observed in the form of thicker salt layers. According to results of limited number of experiments, it was determined that the ratio of potential energy of the mixed water column to generated wave energy has an increasing trend with wave steepness.

− In the second part of the experimental study, a single port, horizontal brine discharge was taken into consideration. It was determined that the wave motion cause oscillation of discharged jet and shifted its impingement point to the bottom compared to stagnant ambient water. Discharged horizontal jet constituted a dense layer at the bottom after its impingement.

− Discharge direction to wave propagation is important for the behaviour of discharged horizontal jet. Cross-sectional areas and propagation of jet was determined by image processing. Propagation rate of dense jet with opposite direction to the wave propagation was higher compared to the case with co-directional discharge. Also, it was determined that the shape of discharged jet was different for these two cases.

− By measuring salinity values at the bottom of the test flume, it was determined that opposite-directional discharge of a horizontal dense jet caused more mixing at the bottom compared to the co-directional discharge case. Also, positive effect of wave action on mixing was obvious compared to stagnant ambient tests.

–   In the third part of the experimental study, inclined dense jet discharge was analysed under regular wave conditions and stagnant ambient. For these tests, two different discharge angles (45° and 60°) were used. Generated waves were transitional Stokes waves with four different wave heights.

–   During the experiments, velocity was measured at terminal rise height of the discharged jets for wave and stagnant conditions. Recorded velocity data was filtered according to correlation values and despiking was applied by a written code using appropriate filters for the tests. Measured horizontal and vertical velocity components showed the effect of wave motion compared to stagnant ambient measurements. Due to the test equipment problems for conductivity measurement for the aim of determining mixing behaviour, further processing of velocity data was abandoned.

–   Observations of the test videos showed that wave motion caused oscillation of discharged jets which was resulted in detention of the jets compared to stagnant conditions. Lateral widths of the jets were bigger at existence of waves that can be qualitatively explained with higher entrainment rates. In addition, outside edges of the jets were more steady for stagnant ambient conditions at the near-field and intermediate regions. Jet deflection at the vicinity of discharge point was inspected which was compatible with previous studies in the literature. This behaviour was more evident for the jets with 60° discharge angle.

–   For the evaluation of experimental videos, image processing study was executed in two parts through which qualitative data was converted into quantitative data. In the first part of the image processing study, terminal rise height (Z_t) and impingement point (X_i) were the considered geometrical parameters of the discharged jet. In the second part, flow front position (X_e) of propagating dense layer was the main parameter studied.

–   Obtained terminal rise height-time series showed that the value of this parameter oscillates along a mean value due to the effect of wave motion in contrast to stagnant ambient discharge. Also, this data together with water surface (η_0)-time series obtained with same method displayed that the discharged jet was moving same phase with the waves. Terminal rise height

values were higher for the tests with 60° discharge angle compared to the ones with 45° discharge angle.

- Image processing for determining the location of impingement point was not so accurate for most of the images taken. Due to this reason, only mean values of this for processable images were obtained.

- Flow front position-time series showed that started dense current at the bottom propagates with the same phase of the wave propagation. In addition, by using this data, propagation velocity of flow front (U_L)-time series were obtained. These plots showed that the wave motion contributes to propagation of dense layer due to its horizontal velocity component at the bottom. This finding was also determined by the relation of mean velocity propagation values of processed images and wave height values.

- In the numerical part of the study, widely used entrainment models (CORMIX, UM3 and JETLAG) for brine discharges evaluated in the context of multiport brine discharges. For this aim, real life desalination discharge scenarios constituted for the simulations. Effluent, ambient and whole of the discharge system characteristics were constant except the space between diffuser ports. For verifying the model results, expected data was produced according to ampiric equations in the literature by using same scenario input parameters. Impact point dilution, impact point location and terminal rise height values were chosen as benchmark parameters. It was observed that JETLAG was simulating multiport jets as they were individual. Due to this reason, it was omitted in the results. After evaluation, it was found out that the other models did not give simulation results which are compatible with experimental data in the literature. Mentioned models give meaningful results in the case of not merging jets with large port spaces between them. However, the results are not consistant with experimental data for closer port spaces that cause merging of discharged jets.

- For simulating spreading of brine in the far-field region, two codes (2D and 3D) that solve related equations with Runge Kutta 4th method were written. For presenting effect of variable parameters, different scenarios were constituted with some constant and variable parameters. With these scenarios,

application ranges of the model for variable parameters were investigated. For solving the equations various assumptions were used to simplfy the equations. Due to this reason, simulations do not reflect real behaviour of the flow and gives a rough estimation of considered parameters. However, it may be used as a practical pre-design tool for predicting various parameters of gravity currents through distance.

Brine discharges can be analyzed in a wide spectrum of topics for a proper management of mentioned wastes. For the future work, it is recommended to expand this study with non-intrusive methods of measuring velocity and concentration fields. In addition, analysing effect of irregular waves may be a good choice for simulating conditions closer to the real life scenarios.

Besides, there is a gap of knowledge related to multiport discharges of brine which is also a wide topic that should be analyzed for various parameters such as different diffuser types and arrangements, ambient conditions and dense jet interaction, etc. In addition, development of existing commercial models for proper simulation of multiport outfalls is required due to increasing number of usage these outfall systems. Besides, studies related to higher computational models would be beneficial for more realistic simulations of these flows.

It is also important to state that brine dispersion should be taken into consideration in the context of environmental impacts especially with field and laboratory studies to establish a guideline for future construction of desalination plants, environmental impact assessment and environmental legislation studies and applications.

REFERENCES

Abessi, O. & Roberts, P. J. (2014). Multiport diffusers for dense discharges, *Journal of Hydraulic Engineering*, *140* (8), 04014032.

Abessi, O, Saeedi, M., Bleninger, T., Davidson, M. (2012). Surface discharge of negatively buoyant effluent in unstratified stagnant water, *Journal of Hydro-environment Research*, *6* (3), 181-193.

Ahmed, M., Shayya, W. H., Hoey, D., Al-Handaly, J. (2001). Brine disposal from reverse osmosis desalination plants in Oman and the United Arab Emirates, *Desalination*, *133* (2), 135–147.

Ahmed, M., Shayya, W. H., Hoey, D., MahendranA., Morris, R., Al-Handaly, J. (2000). Use of evaporation ponds for brine disposal in desalination plants, *Desalination*, *130* (2), 155–168.

Akar, P. J., Jirka, G. H. (1991). CORMIX2: An expert system for hydrodynamic mixing zone analysis of conventional and toxic submerged multiport diffuser discharges. (Report No: PB-93-166924/XAB). Athens, GA: USEPA Technical Report.

Alahyari, A. A. & Longmire, E. K. (1995). Development and structure of a gravity current head, *Experiments in Fluids*, *20* (6), 410-416.

Alavian, V. (1986). Behavior of density currents on an incline, *Journal of Hydraulic Engineering*, *112* (27), 27-42.

Argyrou, M. (1999). Impact of desalination plant on marine macrobenthos in the coastal waters of Dhekelia Bay, Cyprus. Cyprus: Internal Report of Department of Fisheries, Ministry of Agriculture, Natural Resources and Environment.

AWWA (2007). Process Design, Reverse Osmosis and Nanofiltration, AWWA , Manual M46.

AWWA (2011). Desalination of Seawater Manual of Water Supply Practices-M61. American Water Works Association (AWWA), Denver, USA.

Bas, B., Kabdasli, M. S., Erturk Bozkurtoglu, S. N., Seker, D. Z. (2012). Effect of wave direction on discharged brine dilution, *Fresenius Environmental Bulletin*, *21*, No.10a, 3093-3100.

Bas, B., Kabdasli, M. S., Erturk Bozkurtoğlu, S. N. (2011). An experimental study on brine disposal under wave conditions. In E. Rizzuto & C. G. Soares (Ed.) Sustainable Maritime Transportation and Exploitation of Sea Resources'2012. Proceedings of 14th Congress of Intl. Maritime

Assoc. of Mediterranean (IMAM), (pp. 1063-1067). Italy: University of Genova, September 13-16.

Bleninger, T. & Jirka, G. (2008). Modelling and environmentally sound management of brine discharges from desalination plants, *Desalination*, *221* (1-3), 585-597.

Bloomfield, L. J. & Kerr, R. C. (2002). Inclined turbulent fountains, *Journal of Fluid Mechanics*, *451*, 283-294.

Britter, R. E., Simpson, J. E. (1978). Experiments on the dynamics of a gravity current head, *Journal of Fluid Mechanics, 88* (2), 223-240.

Buckee, C., Kneller, B. and Peakall, J. (2009). Turbulence structure in steady, solute-driven gravity currents, In: McCaffrey, W., Kneller, B., Peakall, J., Blackwell (Ed.), *Particulate gravity currents,* (pp. 173-187). Retrieved from: http://onlinelibrary.wiley.com/book/10.1002/9781444304275.

Bleninger, T., Niepelt A., Jirka, G.H. (2009). Desalination Plant Discharge Calculator, *Proc. Intl. Conference and Exhibition on Desalination for the Environment, Clean Water and Energy*, European Desalination Society, Baden-Baden, Germany: 17 - 20 May.

Buros, O.K. (2000). *The ABCs of Desalting*, International Desalination Association (IDA). Retrieved from: http://www.water.ca.gov/pubs/surfacewater /abcs_of_desalting/abcs_of_desalting.pdf.

CEM (2002). Coastal Engineering Manual, U.S. Army Corps of Engineers, Engineer Manual 1110-2-1100, Washington D.C.

Chavand, V., Evenden, C. (2010). Noise assessment of a desalination plant, *20th International Congress on Acoustics 2010*, Sydney, Australia: 23-27 August.

Chen, Y. P. (2006). Three-dimensional modelling of vertical jets in random waves. (Doctor of Philosophy Thesis). The Hong Kong Polytechnic University, Hong Kong.

Chin, D. A. (1987). Influence of surface waves on outfall dilution, *Journal of Hydraulics Engineering*, *113*, 1006-1017.

Chin, D. A. (1988). Model of buoyant jet-surface-wave interaction, *Journal of Waterway, Port, Coastal and Ocean Engineering*, *114* (3), 331-345.

Chang, K. A., Ryu, Y., Mori, N. (2009). Parameterization of neutrallybuoyant horizontal round jet in wave environment, *Journal of Waterway, Port,Coastal, and Ocean Engineering*, *135* (3), 100-107.

Choi, S. U. & Garcia, M. H. (2001). Spreading of gravity plumes on an incline, *Coastal Engineering Journal*, *43* (4), 221-237.

Cenedese, C. & Adduce, C. (2008). Mixing in a density-driven current flowing down a slope in a rotating fluid, *Journal of Fluid Mechanics*, *604*, 369-388.

Chyan, J. M., Hwung, H. H., Chang, Y. H., (1991). Wave effects on the mean flow characteristics of turbulent round jets. *In J. H. W. Lee and Y. K.*

Cheung (Ed.), Proceedings of the 4th Environmental Hydraulics, (pp. 109-114). Balkema, Rotterdam: 15-18 December.

Chyan, J. M. & Hwung, H. H. (1993). On the interaction of a turbulent jet with waves, *Journal of Hydraulic Research*, *31* (6), 791-810.

Chowdhury, M., Testik, F. Y. (2014). A review of gravity currents formed by submerged single-port discharges in inland and coastal waters, *Environmental Fluid Mechanics*, *14* (2), 1-29.

Cipollina, A., Brucato, F., Grisafi, S. N. (2005). Bench-scale investigation of inclined dense jets, *Journal of Hydraulic Engineering*, *131* (11), 1017-1022.

Danoun, R. (2007). Desalination plants: Potential impacts of brine discharge on marine life. (Final Project). The University of Sydney, Sydney.

Darwish, M., Hassabou, A. H., Shomar, B. (2013). Using Seawater Reverse Osmosis (SWRO) desalting system for less environmental impacts in Qatar, *Desalination*, *309*, 113-124.

Davis, L. R. (1999). *Fundamentals of Environmental Discharge Modelling*. New York: CRC Press.

Dean, R. G., Dalrymple, R. A. (1984). *Water Wave Mechanics For Engineers and Scientists*. Englewood Cliffs: Prentice-Hall.

Del-Pilar-Ruso, Y., Carretero, J. A., Casalduero, F. G., Lizaso, J. L. (2007). Spatial and temporal changes in infaunal communities inhabiting soft-bottoms affected by brine discharge. *Marine Environmental Research*, *64* (4), 492–503.

Del-Pilar-Ruso, Y., De-la-Ossa-Carretero, J. A., Loya-Fernández, A., Ferrero-Vicente, L. M., Giménez-Casalduero, F., Sánchez-Lizaso, J. L. (2009). Assessment of soft-bottom Polychaeta assemblage affected by a spatial confluence of impacts: sewage and brine discharges. *Marine Pollution Bulletin*, *58* (5), 776–82.

Dupavillon, J.L., Gillanders, B.M. (2009). Impacts of seawater desalination on the giant Australian cuttlefish Sepia apama in the upper Spencer Gulf, South Australia. *Marine Environmental Research*, *67* (4-5), 207–18.

Doneker, R.L., Jirka, G.H., (2007). CORMIX User Manual: A Hydrodynamic Mixing Zone Model and Decision Support System for Pollutant Discharges into Surface Waters", EPA-823-K-07-001, Dec. 2007. Current Rev. 6.0.0, Updated 04/23/2012.

Einav, R., Hamssib, K., Periyb, D. (2002). The footprint of the desalination processes on the environment, *Desalination*, *152* (1-3), 141–154.

El-Naas, M. H. (2011). Reject Brine Management, Desalination, Trends and Technologies, Michael Schorr (Ed.), ISBN: 978-953-307-311-8, InTech, DOI: 10.5772/13706. Retrived from: http://www.intechopen.com/books/desalination-trends-and-technologies/reject-brine-management.

El-Dessouky, H.T, Ettouney-H.M. (2002). *Fundamentals of Salt Water Desalination*. Amsterdam, The Netherlands: Elsevier.

Ellison, T. H. & Turner, J. S. (1959). Turbulent entrainment in stratified flows, *Journal of Fluid Mechanics*, *6* (3), 423-448.

ERDAS Inc., (1999). ERDAS Field Guide, Fifth Edition, Atlanta, GA.

Etling, D., Gelhardt, F., Schrader, U., Brennecke, F., Kühn, F., Chabert d'Hieres, G., Didelle, H. (2000). Experiments with density currents on a sloping bottom in a rotating fluid, *Dynamics of Atmospheres and Oceans*, *31* (1-4), 139-164.

Falzon, L., Gingell B. (1990). A study of the influence of the effluent from the Tigne RO plant on algae grow. (Dissertation of B.Sc. Degree). Malta University, Malta.

Fernández-Torquemada, Y., Sánchez-Lizaso, J. L., González-Correa, J. M. (2005). Preliminary results of the monitoring of the brine discharge produced by the SWRO desalination plant of Alicante (SE Spain). *Desalination*, *182* (1-3), 385-402.

Fernández-Torquemada, Y. & Sánchez-Lizaso, J. L. (2011). Responses of two Mediterranean seagrasses to experimental changes in salinity. *Hydrobiologia*, *669* (1), 21–33.

Fernandez, R. L., Imberger, J. (2006). Bed roughness induced entrainment in a high Richardson number underflow, *Journal of Hydraulic Research*, *44* (6), 725-738.

Ferrari, S., Querzoli, G. (2006). An experimental study of the interaction between dense sea discharges and wave motion , *4th International Conference on Marine Wastewater Disposal and Marine Environment*, *MWWD 2006*, Antalya, Turkey: 6-10 November.

Firoozabadi, B., Afshin, H., Aram, E. (2009). Three-Dimensional Modeling of Density Current in a Straight Channel, *Journal of Hydraulic Engineering*, *135* (5), 393-402.

Fischer, H. B., List, E. J., Koh, R. C. Y., Imberger, J., Brooks, N. (1979). *Mixing in Inland and Coastal Waters*. New York, USA: Academic Press.

Frenkel, V. S. (2010). Seawater Desalination: Trends and Technologies, Desalination, Trends and Technologies, Michael Schorr (Ed.), ISBN: 978-953-307-311-8, InTech, DOI: 10.5772/13889. Retrieved from: http://cdn.intechopen.com/pdfs-wm/13756.pdf

Frick, W. E., Roberts, P. J. W., Davis, L. R., Keyes, J., Baumgartner, D. J., George, K. P. (2003). Dilution Models for Effluent Discharges (Visual Plumes), *4th Edition*, Georgia, USA.

Gacia, E., Invers, O., Manzanera, M., Ballesteros, E., Romero, J. (2007). Impact of the brine from a desalination plant on a shallow seagrass (Posidonia oceanica) meadow. Estuarine Coastal and Shelf Science, *72* (4), 579-590.

Gaid, K. (2011). A Large Review of the Pre Treatment, Expanding Issues in Desalination, Prof. Robert Y. Ning (Ed.), ISBN: 978-953-307-624-9, InTech, DOI: 10.5772/19680. Retrived from:

http://www.intechopen.com/books/expanding-issues-in-desalination/a-large-review-of-the-pre-treatment.

Garrote-Moreno, A., Fernández-Torquemada, Y., Sánchez-Lizaso, J. L. (2014). Salinity fluctuation of the brine discharge affects growth and survival of the seagrass Cymodocea nodosa, *Marine Pollution Bulletin*, *81* (1), 61–68.

Gordon, H.F., Viscovich, P. G., Thompsn, A. L., Costanzo, S. D., West, E. J., Boerlage, S. F. E. (2012). The effects of Gold Coast desalination plant operations on the marine environment, *IDA Journal of Desalination and Water Reuse, 4* (2), 12-21.

Garcia, M. H. (1996). *Hidrodinamica Ambiental*. Buenos Aires: Universidad Nacional del Litoral.

Garcia, M. H. & Parsons, J. D. (1996). Mixing at the front of gravity currents, *Dynamics of Atmospheres and Oceans*, *24* (1-24), 197-205.

Ger, A. M. (1979). Wave effects on submerged buoyant jets, *Proceedings of 8th Congress of International Association of Hydraulic Research,* (pp. 295-300)*, New Delhi.

Gerber, G. (2008). Experimental measurement and numerical modelling of velocity, density and turbulence properties of a gravity current. (Doctor of Philosophy Thesis). University of Stellenbosch, Matieland.

Gerber, G., Diedericks, G., Basson, G. (2011). Particle image velocimetry measurements and numerical modeling of a saline density current, *Journal of Hydraulic Engineering*, *137* (3), 333-342.

Gleick, P.H., Cooley, H., Wolff, G. (2006). With a grain of salt: an update on saltwater desalination. In: Cooley, H., Gleick, P.H., Katz, D., Lee, E., Morrison, J., Palaniappan, M., Samulon, A., Wolff, G. (Eds.), The World's Water 2006–2007, (pp. 51-89). The Biennial Report on Freshwater Resources. Island Press, Washington, DC: Island Press.

Grace, R. A. (1978). *Marine Outfall Systems: Planning, Design and Construction*. Englewood Cliffs, New Jersey, USA: Prentice Hall.

Hallworth, M. A., Huppert, H. E., Phillips, J. C., Sparks, R. S. (1996). Entrainment into two-dimensional and axisymmetric turbulent gravity currents, *Journal of Fluid Mechanics*, *308*, 289-311.

Hatcher, L., Hogg, Aç J., Woods, A. W. (2000). The effects of drag on turbulent gravity currents, *Journal of Fluid Mechanics*, *416*, 297-314.

Höpner, T. & Windelberg, J. (1996). Elements of environmental impact studies on coastal desalination plants, *Desalination*, *108* (1-3), 11-18.

Hsiao, S. C., Hsu, T. W., Lin, J. F., Chang, K. A. (2011). Mean and turbulence properties of a neutrally buoyant round jet in a wave environment, *Journal of Waterway, Port,Coastal, and Ocean Engineering*, *137* (3), 109-122.

Huppert, H. E. & Simpson, J. E. (1980). The slumping of gravity currents, *Journal of Fluid Mechanics*, *99*, 785-799.

Hughes, S. A. (1993). *Physical Models and Laboratory Techniques In Coastal Engineering, Advanced Series On Ocean Engineering*. World Scientific Publishing.

Hwung, H. H., Chyan, J. M., Chang, C. Y., Chen, Y. F. (1994). The dilution processes of alternative horizontal buoyant jets in wave motions, In B. L. Edge (Ed.), *Proceedings of International Conference On Coastal Engineering*, Kobe, Japan: 23-28 October.

IDA (2011). International Desalination Association (IDA) Worlwide Desalting Plant Inventory.

IDA (2012). International Desalination Association (IDA) Worlwide Desalting Plant Inventory.

Islam, M. A. & Imran, J. (2010). Vertical structure of continuous release saline and turbidity currents, *Journal of Geophysical Research*, *115* (C08), 1-14.

Ismail, N. M. & Wiegel, R. L. (1981). Opposing wave effect on momentum jets spreading rate, *Journal of Waterway, Port,Coastal, and Ocean Engineering*, *109* (4), 465-483.

Jibril, B. E. Y. & Ibrahim, A. A. (2001). Chemical conversions of salt concentrates from desalination plants. *Desalination*, *139* (1-3), 287–295.

Jirka, G. H. & Akar, P. J., (1991). Hydrodynamic classification of submerged multiport-diffuser discharges, *Journal of Hydraulic Engineering*, *117* (9), 1113-1128.

Jirka, G. (2008). Improved discharge configuration for brine effluents from desalination plants, *Journal of Hydraulic Engineering*, *134* (1), 116-120.

Kenna, E. N., Zander, A. K. (2000). *Current Management of Membrane Plant Concentrate*, American Water Works Association.

Keulegan, G. H. (1958). The motion of saline fronts in still water. (Report No: 55831). National Breau of Standards, Twelfth progress report on model laws for density currents.

Kikkert, G. A., Davidson, M. J., Nokes, R. I. (2007). Inclined negatively buoyant discharges, *Journal of Hydraulic Engineering*, *133* (5), 545-554.

Kneller, B., Bennett, S., McCaffrey, W. (1999). Velocity structure, turbulence and fluid stresses in experimental gravity currents, *Journal of Geophysical Research*, *104* (C3), 5381-5391.

Koh, R. C. Y. (1981). Buoyancy driven gravitational spreading, *Coastal Engineering*, *15,* 2965-2975.

Koole, R., Swan, C. (1994). Measurements of a 2-D non-buoyant jet in a wave environment, *Coastal Engineering*, *24* (1-2), 151-169.

Kuang, J., Hsu, C. T., (1998). Experiments on 2D-submerged vertical jets with progressive surface waves, In A.W. Jayawardena, J.H.W. Lee, Z.Y. Wang (Ed.), *Proceedings of 2nd International Symposium On Environmental Hydraulics,* (pp. 155-160). Hong Kong, China: 16-18 December.

Ladewig, B., Asquith, B. (2012). *Desalination Concentrate Management*. Springer Publishing.

Lai, C. C. K., Lee, J. H. W. (2012). Mixing of inclined dense jets in stationary ambient, *Journal of Hydro-environment Research*, *6* (1), 9-28.

Lam, K. M. & Xia, L. P. (2001). Unsteady effluent dispersion in a round jet interacting with an oscillating cross-flow, *Journal of Hydraulic Engineering*, *130* (7), 667-677.

Latorre, M., (2005). Environmental impact of brine disposal on Posidonia seagrasses, *Desalination*, *182* (1-3), 517–524.

Lattemann, S., Höpner, T. (2003). *Seawater Desalination: Impacts of Brine and Chemical Discharge on the Marine Environment*. Balaban Desalination Publications.

Lattemann, S. & Höpner, T. (2008). Environmental impact and impact assessment of seawater desalination, *Desalination*, *220* (1-3), 1–15.

Lee, J. H. W., Chu, V. (2003). *Turbulent Jets and Plumes-A Lagrangian Approach*, Kluwer Academic Publishers.

Levy, J. L., Stauber, J. L., Jolley, D. F., (2007). Sensitivity of marine microalgae to copper: the effect of biotic factors on copper adsorption and toxicity, *The Science of the Total Environment*, *387* (1-3), 141–54.

Lin, Y-C., Chang-Chien, G-P., Chiang P-C., Chen, W-H., Lin, Y-C. (2013). Potential impacts of discharges from seawater reverse osmosis on Taiwan marine environment, *Desalination*, *322*, 84–93.

Lin, J., Hsiao, S., Hsu, T., Chang, K. (2013). Buoyancy effect on turbulent round jet under regular waves, *Journal of Waterway, Port, Coastal, and Ocean Engineering*, *139* (3), 190-208.

Lin, M.-H., Lee, C.-H., Lin, Y.-C., Yang, K.-H. (2011). Potentially toxic trace elements accumulating in marine sediment and bivalves in the outfall area of a desalination plant, *Desalination and Water Treatment*, *25* (1-3), 106-112.

Lin, J. F., Hsiao, S. C., Hsu, T. W., Chang, K. A. (2011). Experimental study of a negatively buoyant horizontal jet in wave environment, *Proceedings of the ASME 2011 30th International Conference On Ocean, Offshore and Arctic Engineering, OMAE 2011,* Rotterdam, The Netherlands: June 19-24.

Lior, N. (2013). *Advances in Water Desalination*. Hoboken, New Jersey, USA: Wiley.

Malcangio, D., Petrillo, A. F. (2011). Brine Outfalls: State of the Art, Expanding Issues in Desalination, Prof. Robert Y. Ning (Ed.), ISBN: 978-953-307-624-9, InTech, DOI: 10.5772/22722. Retrieved from: http://www.intechopen.com/books/expanding-issues-in-desalination/brine-outfalls-state-of-the-art.

Mani, J. S. (2012). *Coastal Hydrodynamics*. New Delhi: India PHI Learning Private.

Marugán-Cruz, C., Rodríguez-Rodríguez, J., Martínez-Bazán, C. (2009). Negatively-buoyant starting jet, *Physics of Fluids*, *21* (117101),1-14.

Marti, C. L., Antenucci, J. P., Luketina, D., Okely, P., Imberger, J. (2011). Near field dilution characteristics of a negatively buoyant hypersaline jet generated by a desalination plant, *Journal of Hydraulic Engineering*, *37* (1), 57-65.

Martin, J. E. & Garcia, M. H. (2009). Combined PIV/PLIF measurements of a steady density current front, *Experiments in Fluids*, *46* (2), 265-276.

Miller, B. (2011). Design of large desalination discharges with multiple jets, *International Symposium on Outfall Systems*, Mar del Plata, Argentina: 15-18 May.

Mok, K. M., Leong, K. K., Yeh, H. (2003). Experimental observations of the flow structures at gravity current fronts, *International Conference on Estuaries and Coasts,* Hangzhou, China: November 9-11.

Mok, K. M., Leong, C. S., Hoi, K. I., Yeh, H. (2011). The impact of a gravity current with a vertically mounted circular cylinder, *International Conference on Computer and Communication Devices, ICCCD 2011,* Bali Island, Indonesia: 1-3 April.

Mori, N. & Chang, K.A. (2003). Experimental study of a horizontal jet in wavy environment, *Journal of Engineering Mechanics*, *129* (10), 1149-1155.

Mossa, M. (2004). Behaviour of nonbuoyant jets in a wave environment, *Journal of Hydraulic Engineering*, *130* (7), 704-717.

Nemlioglu, S. & Roberts, P. J. W. (2006). Experiments on Dense Jets Using Three-Dimensional Laser-Induced Fluorescence (3DLIF), *4th International Conference on Marine Waste Water Disposal and Marine Environment, MWWD 2006,* Antalya, Turkey: 6-10 November.

Palomar, P. & Losada, I. J. (2011). Impacts of Brine Discharge on the Marine Environment. Modelling as a Predictive Tool, Desalination, Trends and Technologies, Michael Schorr (Ed.), ISBN: 978-953-307-311-8, InTech, DOI: 10.5772/14880.

Palomar, P., Lara, J. L., Losada, I. J., Rodrigo, M., Alvárez, A. (2012a). Near field brine discharge modelling part 1: Analysis of commercial tools, *Desalination*, *290*, 14-27.

Palomar, P., Lara, J. L., Losada, I. J., Rodrigo, M., Alvárez, A. (2012b). Near field brine discharge modeling part 2: Validation of commercial tools, *Desalination*, *290*, 28-42.

Papakonstantis, I. G., Christodoulou, G. C., Papanicolaou, P. N. (2011a). Inclined negatively buoyant jets 1: geometrical characteristics, *Journal of Hydraulic Research*, *49* (1), 3-12.

Papakonstantis, I. G., Christodoulou, G. C., Papanicolaou, P. N. (2011b). Inclined negatively buoyant jets 2: concentration measurements, *Journal of Hydraulic Research*, *49* (1), 13-22.

Parsons, J. D. & Garcia, M. H. (1998). Similarity of gravity current fronts, *Physics of Fluids*, *10* (12), 3209-3213.

Payo, A., Cortés, J. M., Antoranz, A., Molina, R. (2010) Effect of wind and waves on a nearshore brine discharge dilution in the east coast of Spain, *Desalination and Water Treatment*, *18*, (1-3), 71-79.

Peters, W. D., Venart, J. E. S. (2000). Rough-surface gravity current flows, *10th International Symposium of Application of Laser Techniques to Fluid Mechanics*, Lisbon, Portugal: July 10-13.

Pincince, A. B., List, E. J. (1973). Disposal of brine into an estuary, *Journal of Water Pollution Control Federation*, *45* (11), 2335-2344.

Rajagopalan, K. (2011). *Membrane Desalination, Drinking Water Treatment: Focusing on Appropriate Technology and Sustainability (Strategies for Sustainability),* In Ray Chittaranjan & Jain Ravi (Eds.), Springer.

Rajaratnam, N. (1979). *Turbulent Jets*. Amsterdam, The Netherlands: Elsevier.

Raluy, R. G., Serra, L., Uche, J. (2004). Life-cycle assessment of desalination technologies integrated with energy production systems, *Desalination*, *167*, 445–458.

Raluy, G., Serra, L., Uche, J. (2006). Life cycle assessment of MSF, MED and RO desalination technologies, *Energy*, *31*, (13), 2361–2372.

Raventos, N., Macpherson, E., Garcia-Rubies, A. (2006). Effect of brine discharge from a desalination plant on macrobenthic communities in the NW Mediterranean, *Marine Environmental Research*, *62* (1), 1–14.

Ravizky, A. & Nadav, N. (2007). Salt production by the evaporation of SWRO brine in Eilat : a success story, *Desalination*, *205,* 374–379.

Riera, R., Tuya, F., Sacramento, A., Rodriguez, M., Monterroso, O. (2011). The effects of brine disposal on a subtidal meiofauna community, *Estuarine, Coastal and Shelf Science*, *93* (4), 359–365.

Roberts, P. J. W. & Toms, G. (1987). Inclined dense jets in flowing current, *Journal of Hydraulic Engineering*, *113* (3), 323-341.

Roberts, P. J. W., Ferrier, A., Daviero, G., (1997). Mixing in inclined dense jets, *Journal of Hydraulic Engineering*, ASCE, *123* (8), 693-699.

Roberts, P. J. W., Salas, H. J., Reiff, F. M., Libhaber, M., Labbe, A., Thomson, J. C. (2010). *Marine Wastewater Outfalls and Treatment Systems*. London, UK: IWA Publishing.

Ruiz-Mateo, A., Antequera, M., González, M. (2008). Physical modelling of brine discharges to the sea, *5th International Conference on Marine Waste Water Discharges and Coastal Environment*, *MWWD 2008*, Dubrovnik: October 27-31.

Sadiq, M., (2002). Metal contamination in sediments from a desalination plant effluent outfall area, *Science of The Total Environment*, *287* (1-2), 37–44.

Seil, G. J. & Zhang, Q. (2010). CFD modelling of desalination plant brine discharge systems, *Journal of the Australian Water Association*, *37* (6), 79-83.

Sethi, S., Walker, S., Drewes, J., Xu, P. (2006). Existing & emerging concentrate minimization & disposal practices for membrane systems, *Florida Water Resources Journal*, *58* (6), 38-48.

Shao, D. D., Law, A. W. K., Li, H. Y. (2008). Brine discharges into shallow coastal waters with mean and oscillatory tidal currents, *Journal of Hydro-environment Research*, *2*, 91-97.

Shao, D. D. & Law, A. W. K. (2010). Mixing and boundary interactions of 30° and 45° inclined dense jets, *Environmental Fluid Mechanics*, *10* (5), 521-553.

Shao, D. D. & Law, A. W. K. (2011). Boundary impingement and attachment of horizontal offset dense jets, *Journal of Hydro-environment Research*, *5* (1), 15-24.

Shiau, B.-S., Yang, C-L., Tsai, B-J. (2007). Experimental observations on the submerged discharge of brine into coastal water in flowing water. ICS 2007 (Proceedings), *Journal of Coastal Research*, Special Issue *50***, 789-793.

Shuto, N. Ve Ti, L. H. (1974). Wave effects on buoyant plumes, *Proceedings of 14th International Conference of Coastal Engineering*, ASCE (pp. 2199-2209). Copenhagen: 24-28 June.

Simpson, J. E. & Britter, R. E. (1979). The dynamics of the head of a gravity current advancing over a horizontal surface, *Journal of Fluid Mechanics*, *94*, 477-495.

Socolofsky, S. A., Jirka, G. H. (2005). Mixing and Transport Processes in the Environment, CVEN 489-501: Lecture Notes, Texas A&M University, Coastal and Ocean Engineering Division.

SOL-BRINE (2012). Development of an advanced, innovative, energy autonomous system for the treatment of brine from seawater desalination plants, LIFE+Environment project: LIFE 09 ENV/GR/000299. Deliverable 1.1: Report on the evaluation of existing methods on brine treatment and disposal practices.

Talavera, J. L. P. & Quesada-Ruiz, J. J. (2001). Identification of the mixing processes in brine discharges carried out in Barranco del Toro Beach , south of Gran Canaria (Canary Islands), *Desalination, 139* (1-3), 277–286.

Tam, Y. F. B. (2005). Experimental study of vertical jets in JONSWAP random waves. (Master of Philosophy Thesis). The Hong Kong Polytechnic University, Hong Kong.

Tanino, Y., Nepf, H., Kulis, P. (2005). Gravity currents in aquatic canopies, *Water Resources Research*, *41* (12), 1-9.

Tarrade, L., Miller, B. and Smith, G. (2010). Physical modelling of brine dispersion of desalination outfalls, *6th International Conference on Marine Wastewater Discharges, MWWD 2010*, Langkawi: 25-29 October.

Tian, X., Roberts, P. J. W., (2003). A 3D LIF system for turbulent buoyant jet flows, *Experiments in Fluids*, *35*, 636-647.

Tomasko, D.A., Blake, N.J., Dye, C.W. & Hammond, M.A. (1999). Effects of the disposal of reverse osmosis seawater desalination discharges on a seagrass meadow (Thalassia testudinum) offshore of Antigua, West Indies In S.A. Bortone (Ed.), *Seagrasses: Monitoring, Ecology, Physiology and Management* (pp. 99-112). Boca Raton, Florida: CRC Press.

Tokyay, T., Constantinescu, G., Meiburg, E. (2012). Tail structure and bed friction velocity distribution of gravity currents propagating over an array of obstacles, *Journal of Fluid Mechanics*, *694*, 252-291.

Tokyay, T., Constantinescu, G. (2012). Lock-exchange gravity currents with small volume of release propagating over bottom-mounted obstacles, *XIX International Conference on Computational Methods in Water Resources, CMWR 2012, University of Illinois,* Urbana-Champaign: 17-21 June.

Turner, J. S. (1966). Jets and plumes with negative or reversing buoyancy, *Journal of Fluid Mechanics*, *26* (4), 779-792.

UNESCO (1981). The Practical Salinity Scale 1978 and the International Equation of State of Seawater 1980. UNESCO Technical Papers in Marine Science 36.

Ungarish, M. (2009). *An Introduction to Gravity Currents and Intrusions*. Boca Raton, FL: Chapman and Hall/CRC.

Url-1 <http://www.westernro.com/uncategorized/what-is-reverse-osmosis-2/> , erişim tarihi 02.07.2014.

Url-2 <http://www.tampabaywater.org/tampa-bay-seawater-desalination-plant.aspx> erişim tarihi 02.07.2014.

Url-3 < http://www.iucnredlist.org/details/153534/0>, erişim tarihi 02.09.2014.

Url-4<http://blog.energyrecovery.com/wp-content/uploads/2013/10/Barcelona-desalination-plant-aerial-view.jpg>, erişim tarihi 08.10.2014.

Url-5 <http://www.abb.com>, erişim tarihi 08.10.2014.

Url-6<http://desalination.edu.au/wp-content/uploads/2013/01/Binningup-January-2013-Water-Corp-CB1_20591.jpg>, erişim tarihi 08.10.2014.

Url-7<http://he.wikipedia.org/wiki/%D7%A7%D7%95%D7%91%D7%A5:Ashkelon_Desalination_Plant.jpg>, erişim tarihi 08.10.2014.

Url-8 <www.cormix.info>, erişim tarihi 12.05.2013.

Url-9 <http://upload.wikimedia.org/wikipedia/commons/e/e0/Water_wave_theories.svg>, erişim tarihi 25.11.2014.

Url-10 <http://www.photoscape.org/ps/main/index.php>, 25.11.2014.

U.S. Department of the Interior (2003). Desalting Handbook for Planners, 3rd Edition. (Report No. 72). Virginia: U.S. Department of the Interior, Desalination and Water Purification Research and Development

Program, Bureau of Reclamation, Technical Service Center, Water Treatment Engineering and Research Group Technical Report.

Valero, F., Barceló, A. and Arbós, R. (2011). *Electrodialysis Technology - Theory and Applications, Desalination, Trends and Technologies,* Michael Schorr (Ed.), ISBN: 978-953-307-311-8, InTech, DOI: 10.5772/14297. Retrivied from: http://www.intechopen.com/books/desalination-trends-and-technologies/ electrodialysis-technology-theory-and-applications.

Vafeiadou, P., Papakonstantis, I., Christodoulou, G. (2005). Numerical simulation of inclined negatively buoyant jets, *The 9th International Conference on Environmental Science and Technology*, Rhodes Island, Greece: September 1-3.

Van der Merwe, R., Röthig, T., Voolstra, C., Ochsenkühn, M. ., Lattemann, S., Amy, G. L. (2014). High salinity tolerance of the Red Sea coral Fungia granulosa under desalination concentrate discharge conditions: an in situ photophysiology experiment, *Frontiers in Marine Science*, *1*, 1–8.

Vanhems, C. (1992). Critical Review of Desalination Concentrate Disposal to Surface Water, U.S.A.

Vaselali, A. & Vaselali, M. (2009). Modelling of brine waste discharges spreading under tidal currents, *Journal of Applied Sciences*, *9* (19), 3454-3468.

Voutchkov, N. (2011). Overview of seawater concentrate disposal alternatives, Desalination, *273* (1), 205-219.

WaterUse Assosciation (2011). Seawater Concentrate Management, White Paper.

Wells, M., Cenedese, C., Caulfield, C. P. (2010). The relationship between flux coefficient and entrainment ratio in density currents, *Journal of Physical Oceanography, 40* (12), 2713-2727.

Whiting, R. (2012). *Seawater Reverse Osmosis* [PowerPoint slides]. Retrieved from: http://www.slideshare.net/texasnetwork/seawater-reverse-osmosis-swro-the-basics.

WL│Delft Hydraulics, ENVECO S. A., D. Argyropoulos & Associates (2004). Implementation of Articles 5 & 6 of the Water Framework Directive 2000 / 60 / EC, Volume 3, Analysis of Pressures (Contract No: 39/03/61).

Yaghubi, S., Abbaszadeh, S., Golchoubian, P., Afshin, H., Firoozabadi, B. (2013). Experimental investigation of the effect of two consecutive obstacles on turbidity current, *1st International Conference on Environmental Science and Technology,* Nevşehir, Turkey: June 18 – 21.

Yongping, C. (2006). Three-dimensional modelling of vertical jets in random waves. (Doctor of Philosophy Thesis). The Hong Kong Polytechnic University, Hong Kong.

Yoon, S. J. & Park, G. S. (2011a). Impact of desalination byproducts on marine organisms: A case study at Chuja Island Desalination Plant in Korea, *Desalination and Water Treatment*, *33* (1-3), 267–272.

Yoon, S.J., Park, G.S. (2011b). Ecotoxicological effects of brine discharge on marine community by seawater desalination, *Desalination and Water Treatment*, *33* (1-3), 240–247.

Younos, T. (2005). Environmental issues of desalination, *Journal of Contemporary Water Research & Education*, *132*, 11-18.

Zeitoun, M. A., Reid, R. O., McHilhenny, W. F., Mitchell, T. M. (1970). Model studies of outfall systems for desalination plants. Part III Numerical simulations and design considerations. (Report No: 804). Washington, DC.: Office of Saline Water, U.S. Dept. of Interior, Research and Development Progress Report.

Zimmerman, R. (1999). The Larnaca seawater desalination plant. Environmental Impact Assessment Report.

APPENDICES

APPENDIX A: Processed Images: Phase 1

APPENDIX B: Processed Images: Phase 2

Figure A.1 : Processed images: Phase 1 (Test W1U145).
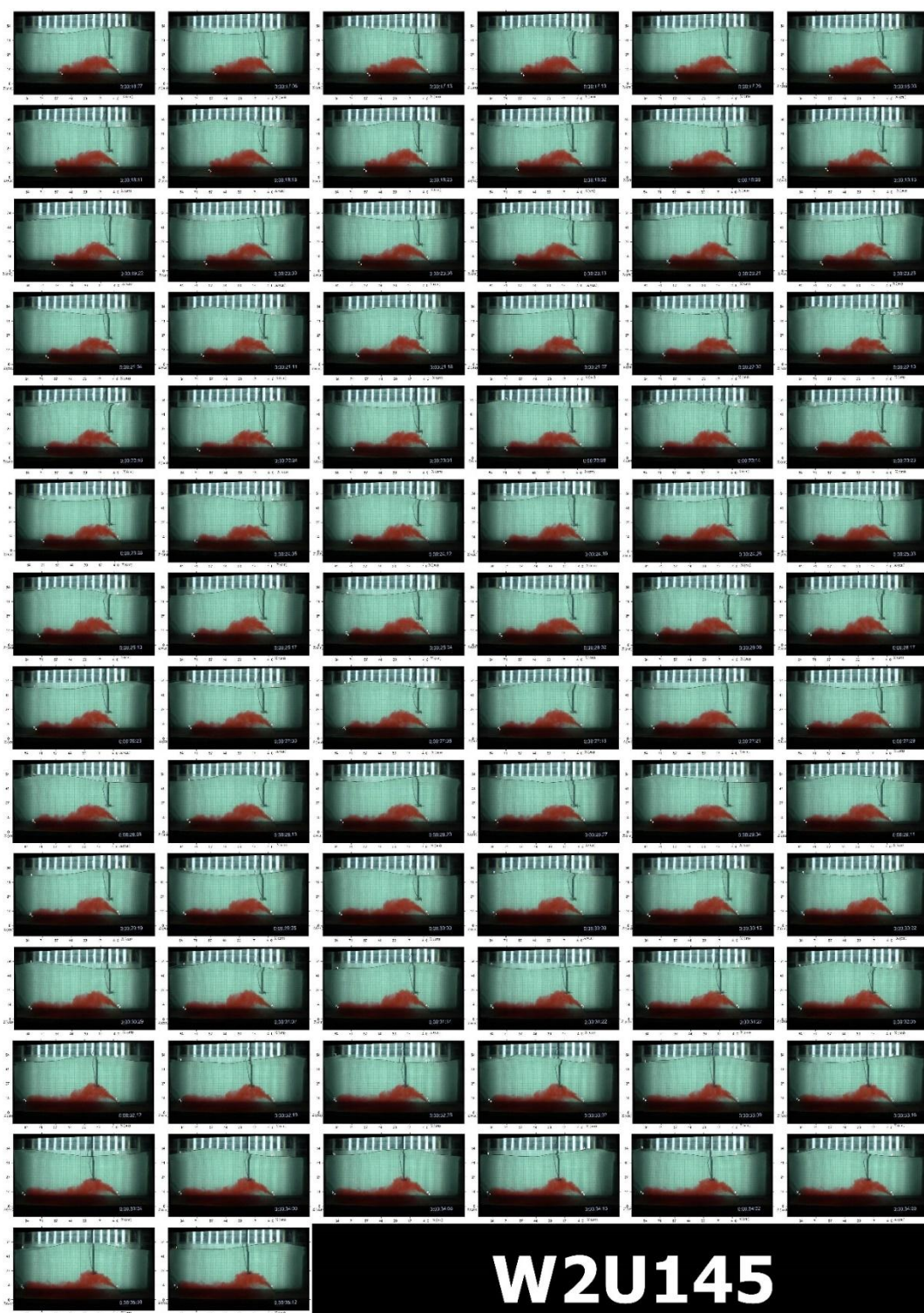
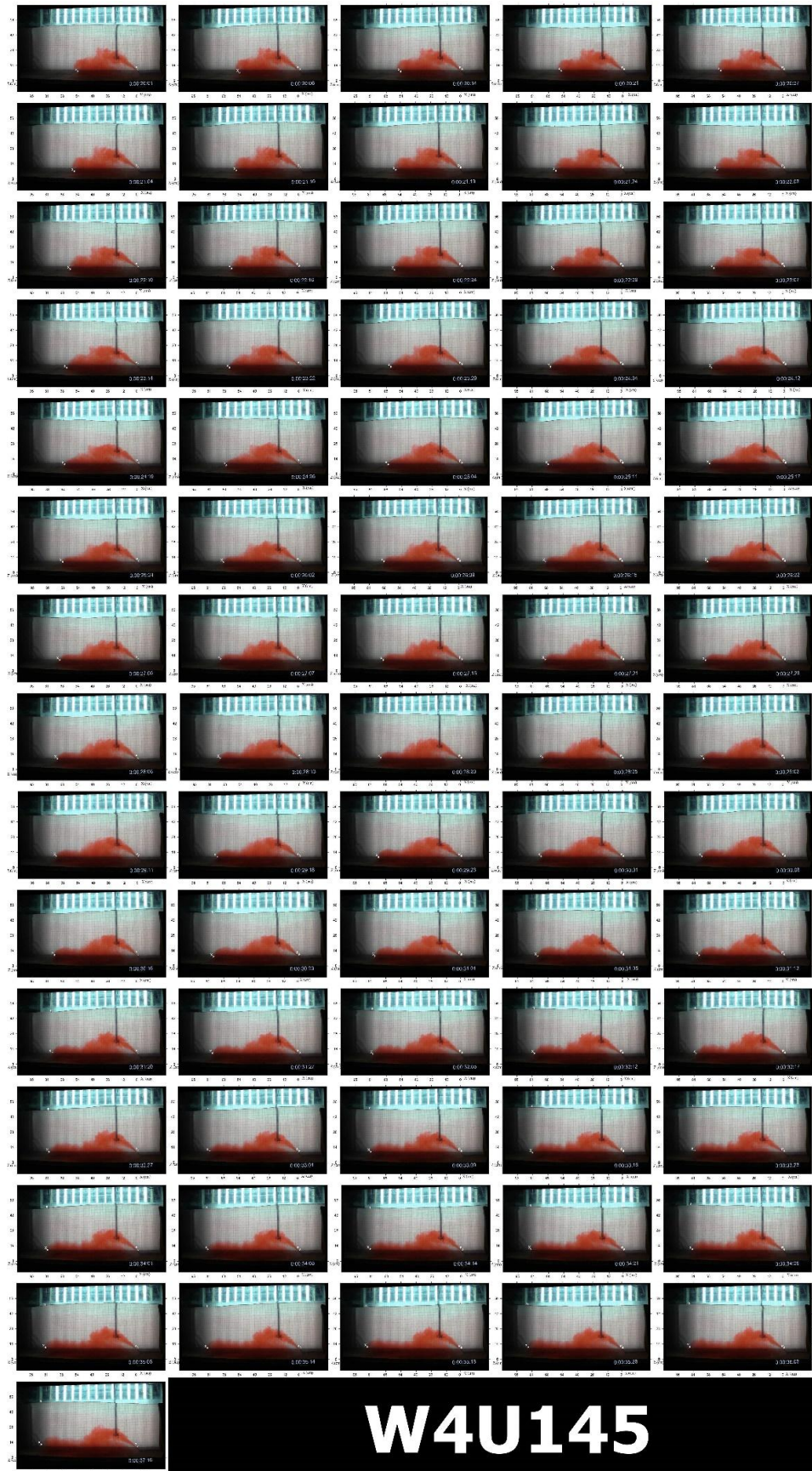**Figure A.2 :** Processed images: Phase 1 (Test W2U145).
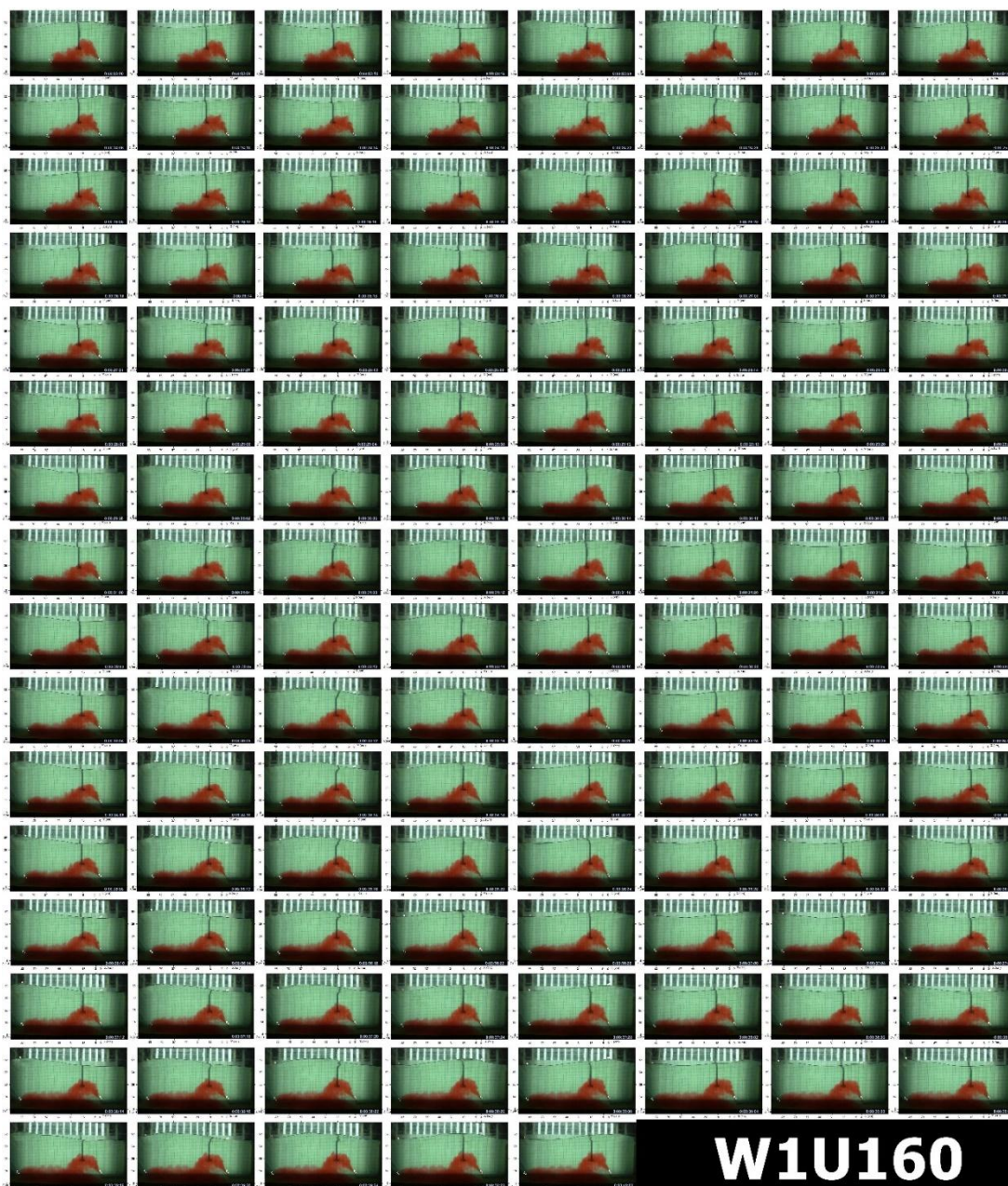
Figure A.3 : Processed images: Phase 1 (Test W4U145).

Figure A.4 : Processed images: Phase 2 (Test W3U160).
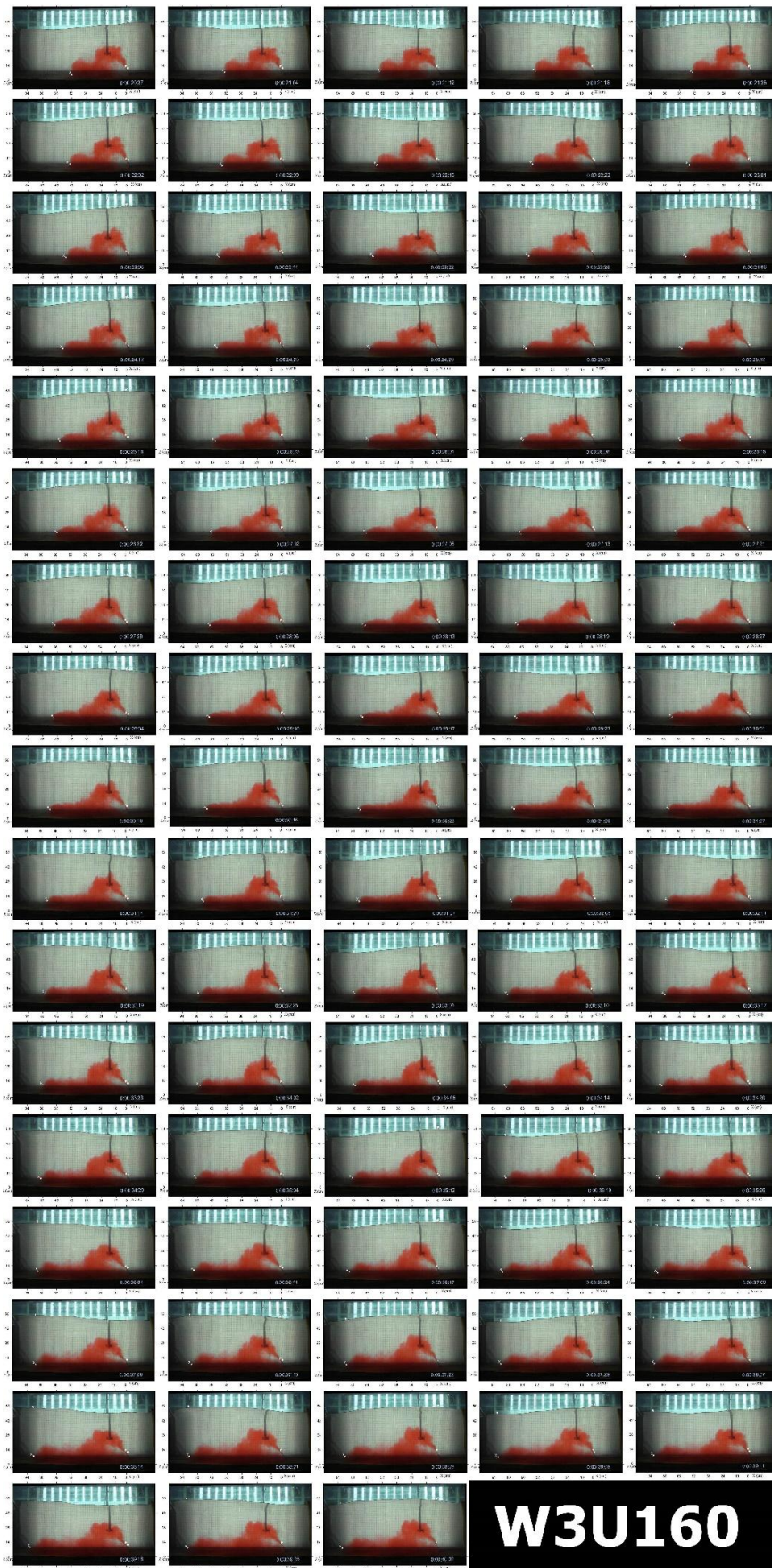
Figure A.5 : Processed images: Phase 1 (Test W2U160).

199

Figure A.6 : Processed images: Phase 1 (Test W3U160).

Figure A.7 : Processed images: Phase 1 (Test W4U160).
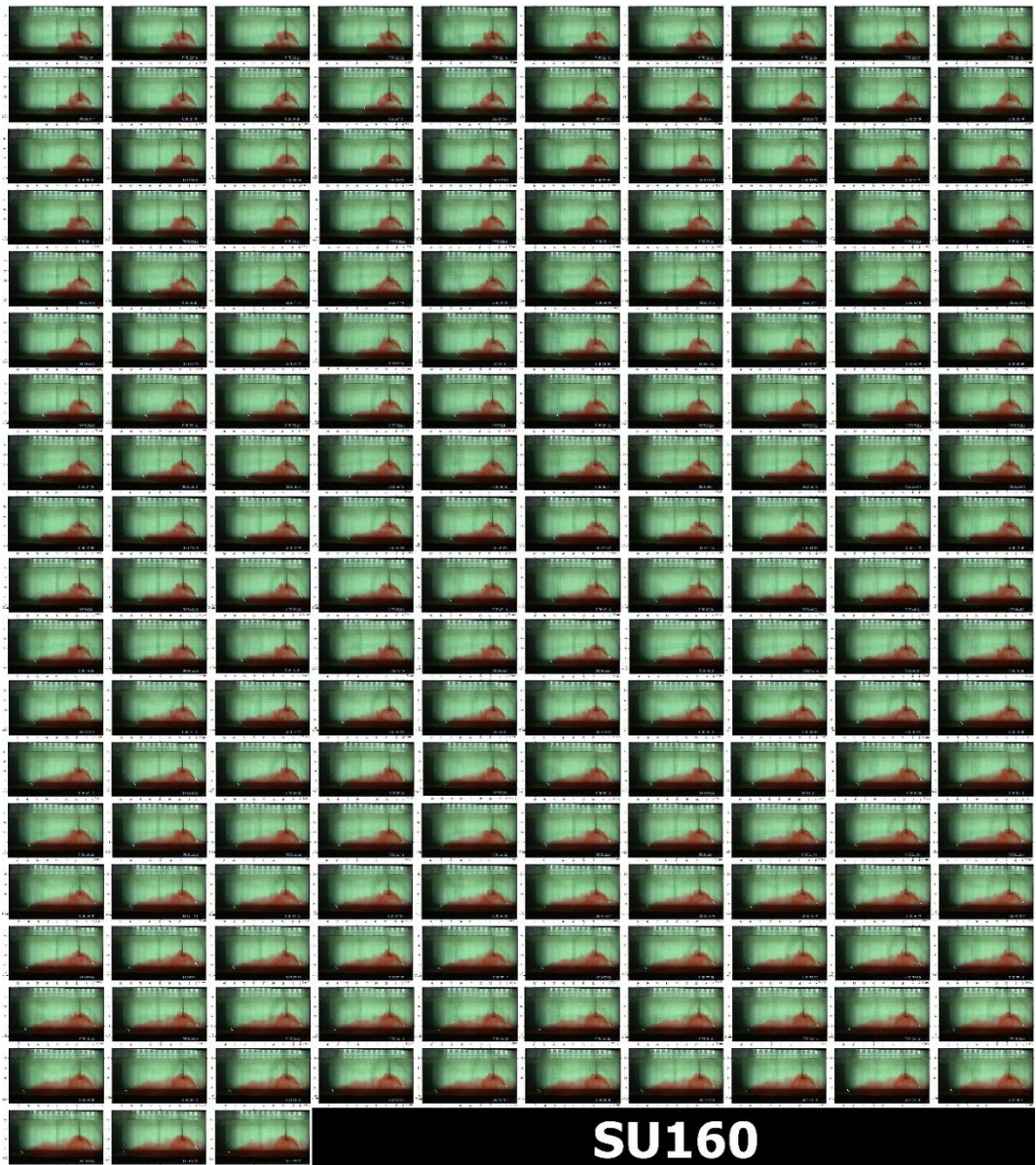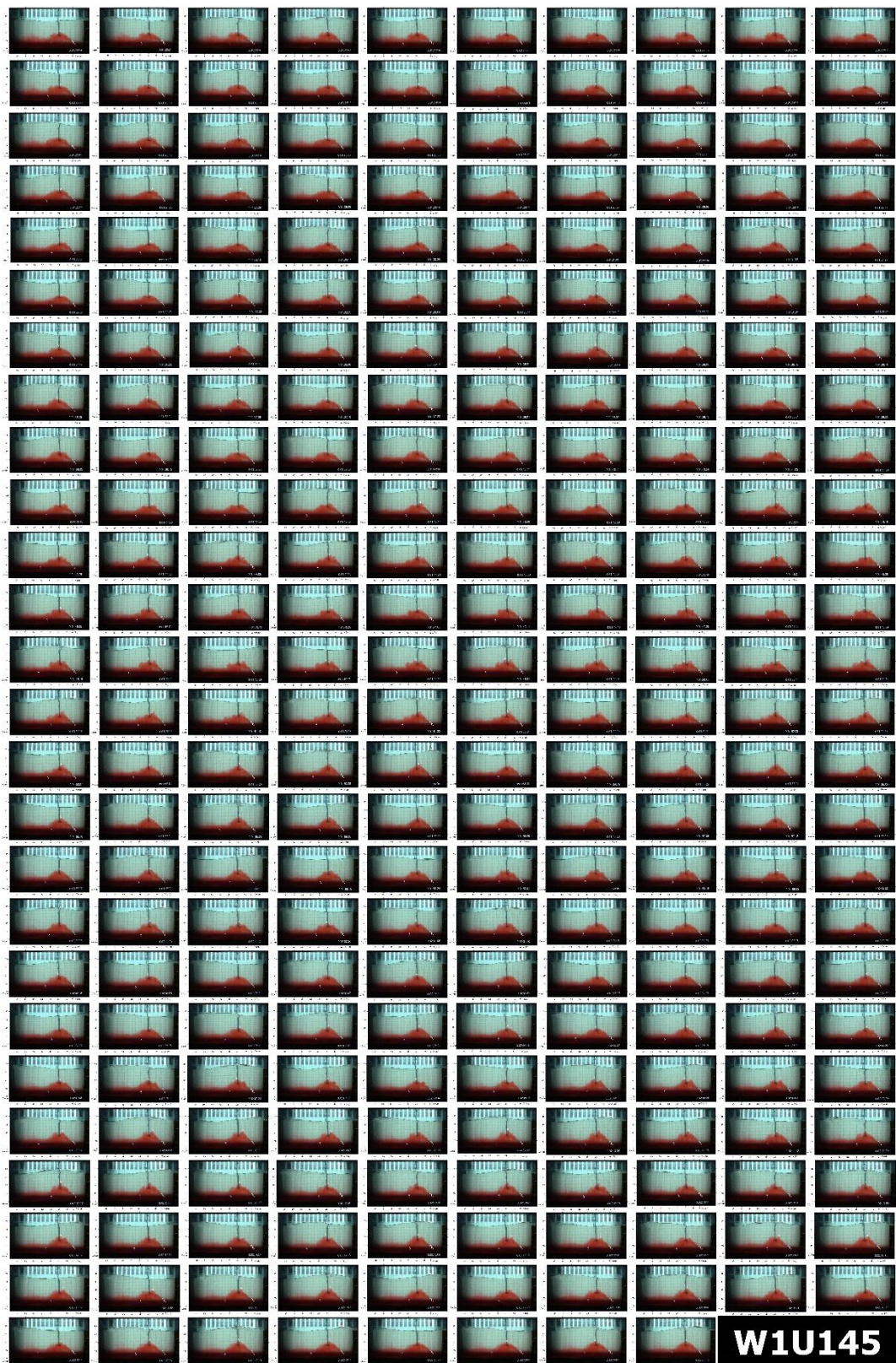
Figure A.8 : Processed images: Phase 1 (Test SU145).

Figure A.9 : Processed images: Phase 1 (Test SU160).

Figure B.1 : Processed images: Phase 2 (Test W1U145).

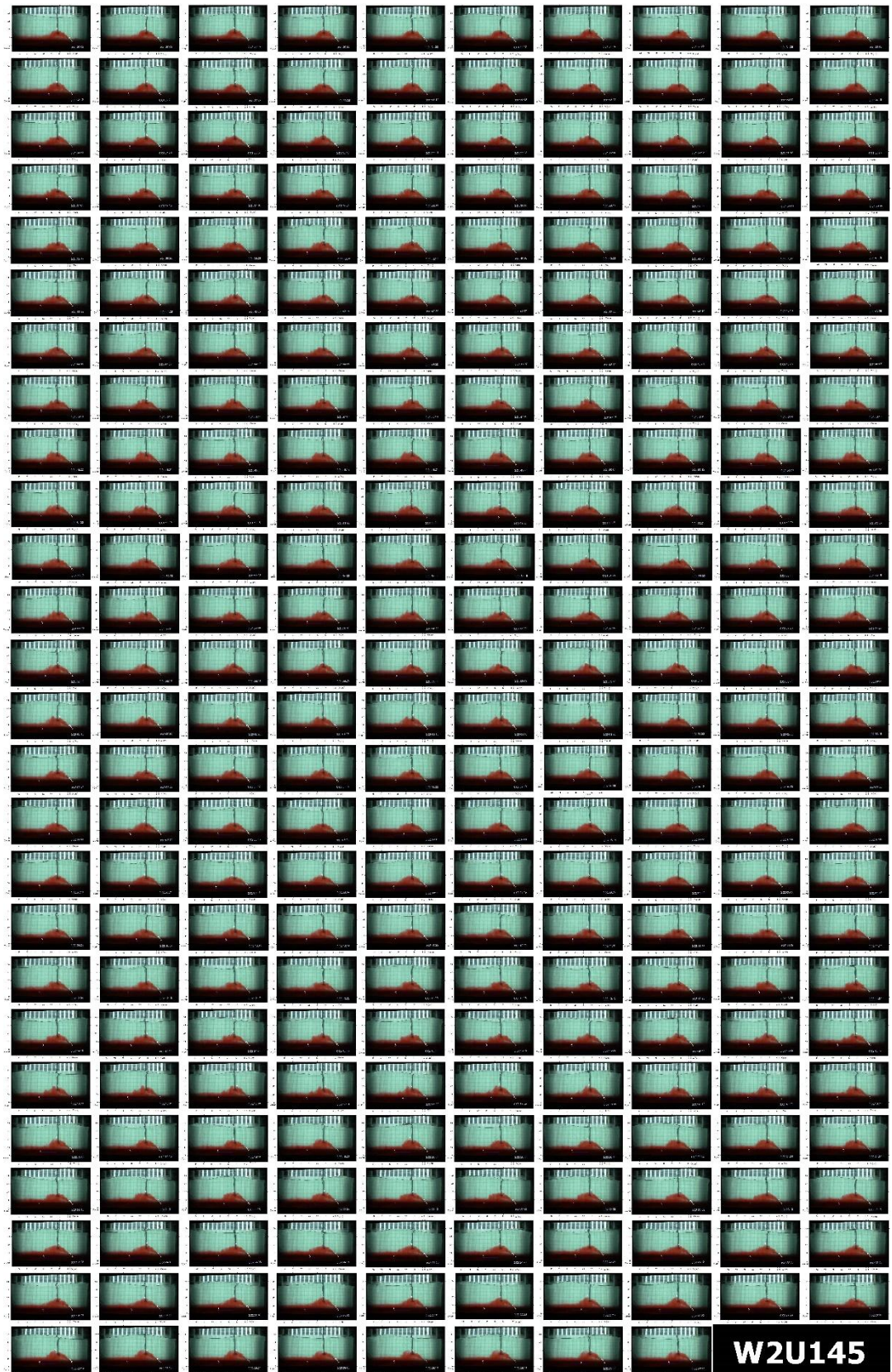**Figure B.2 :** Processed images: Phase 2 (Test W1U160).

Figure B.3 : Processed images: Phase 2 (Test W2U145).

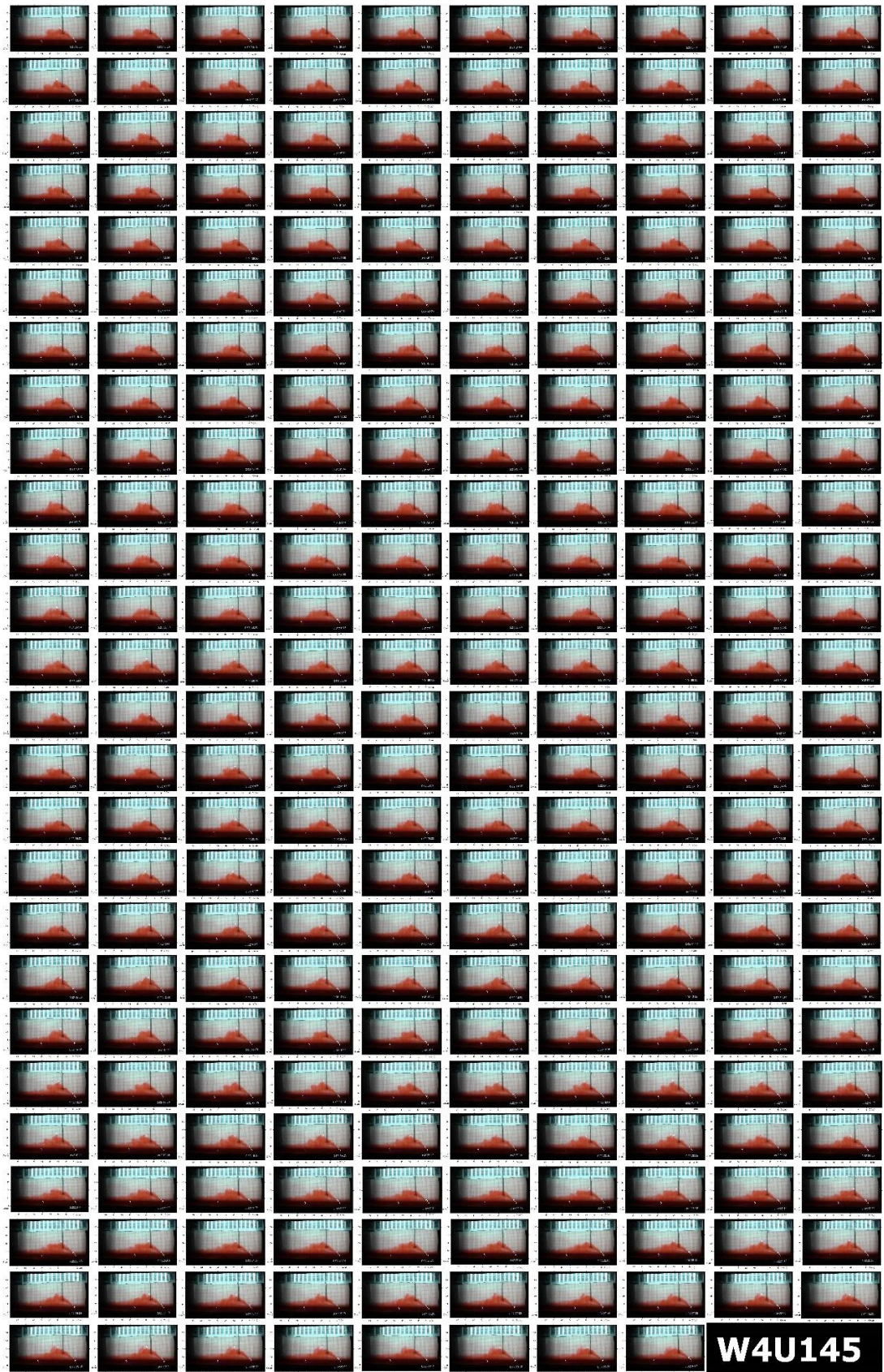**Figure B.4 :** Processed images: Phase 2 (Test W3U160).

208

Figure B.5 : Processed images: Phase 2 (Test W4U145).

Figure B.6 : Processed images: Phase 2 (Test W4U160).

Figure B.7 : Processed images: Phase 2 (Test SU145).

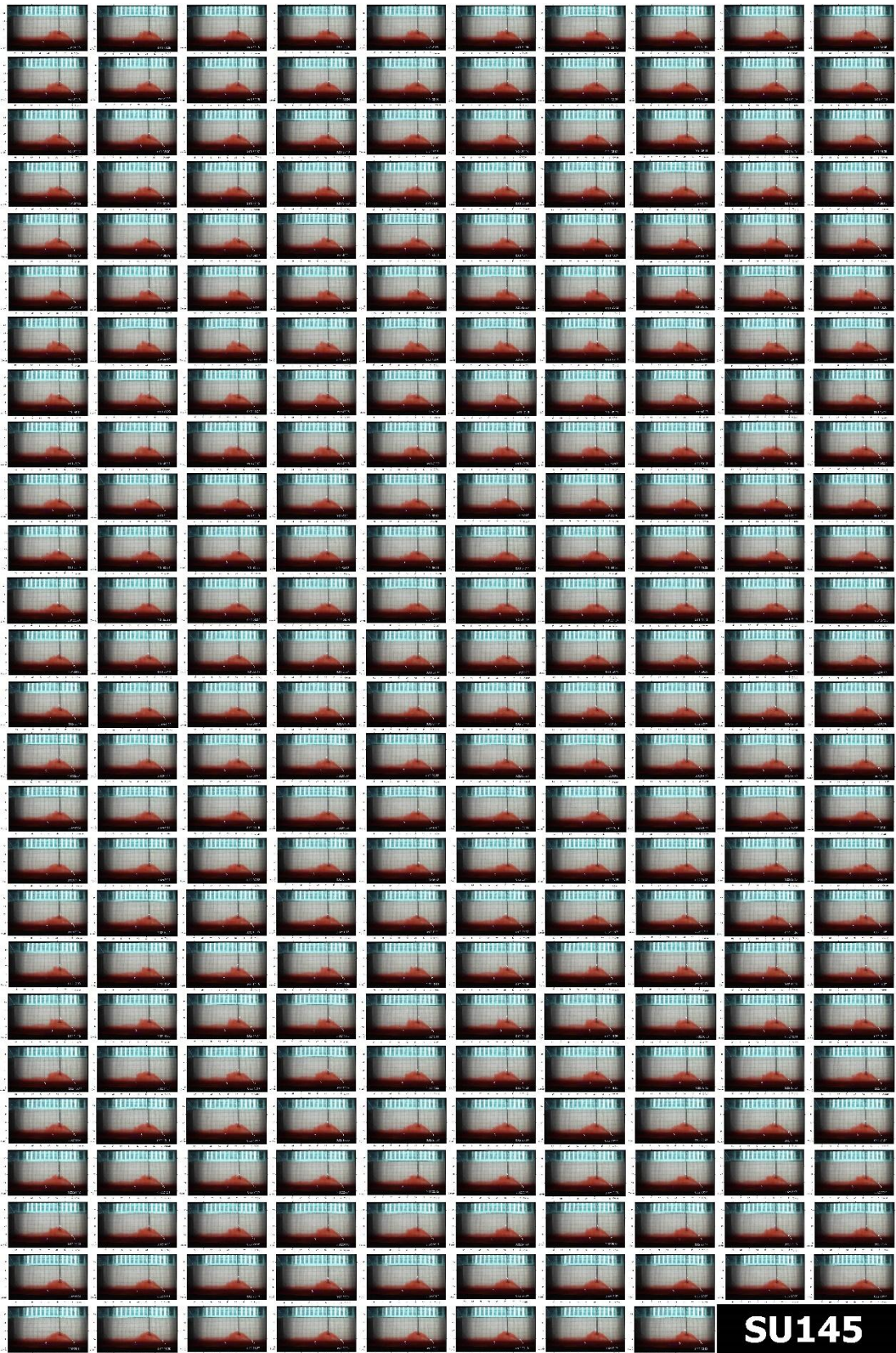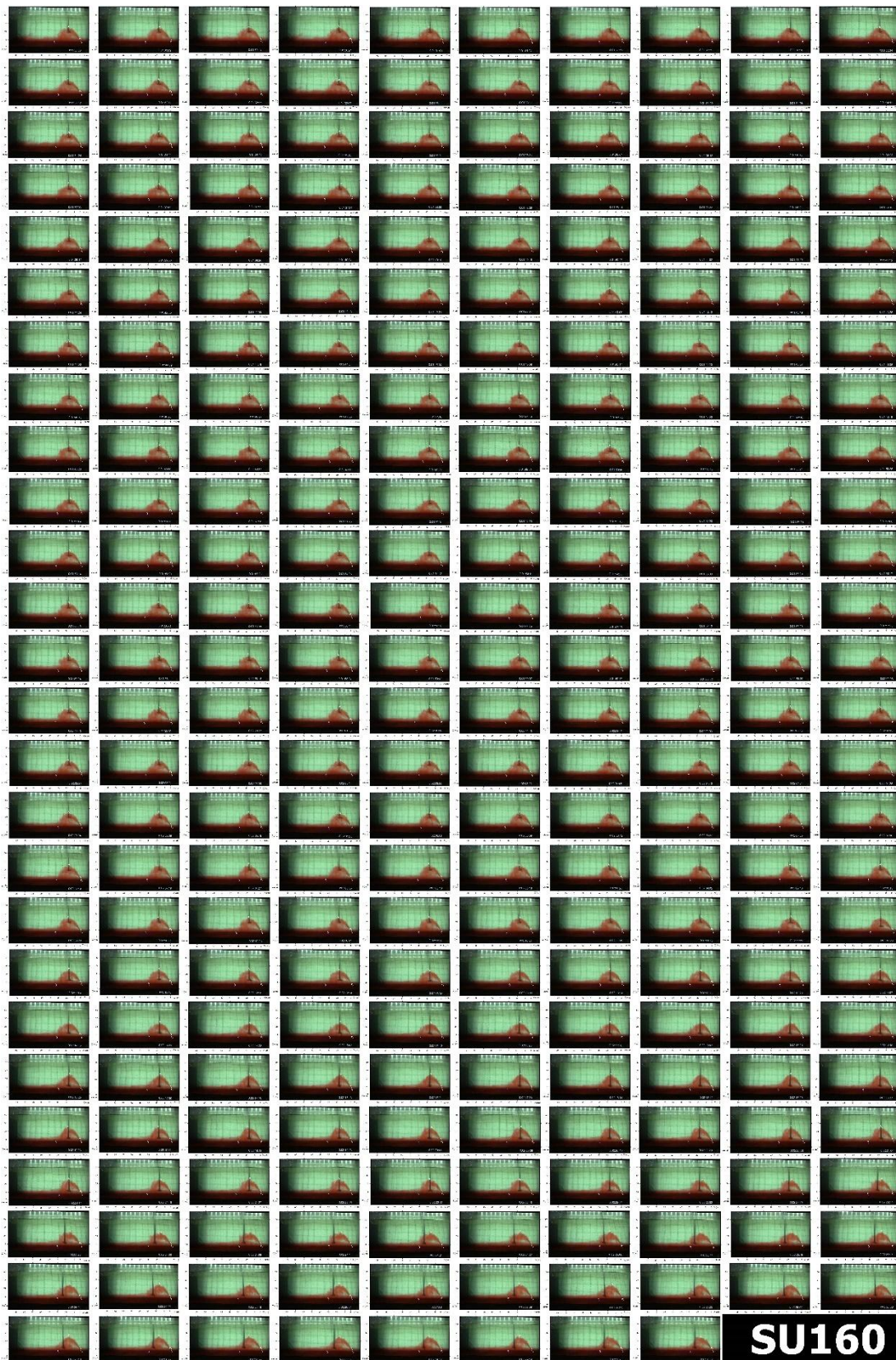**Figure B.8 :** Processed images: Phase 2 (Test SU160).

CURRICULUM VITAE

Name Surname: Bilge Baş

Place and Date of Birth: İstanbul/11.01.1981

E-Mail: basb@itu.edu.tr ; bilgebas81@gmail.com

B.Sc.: ITU Environmental Engineering

M.Sc.: ITU Coastal Sciences and Engineering

Professional Experience and Rewards:

- 2013-2014 (1 year): Visiting PhD Student
  University of Cantabria, Environmental Hydraulics Institute (IH Cantabria), Spain.
- 2009-2014: Research Assistant
  ITU Faculty of Naval Architecture & Ocean Engineering
- 2005-2009: Researcher/ ITU Coastal Science and Engineering Research Group (CSERG)

2013: Tubitak 2214 International Doctoral Research Fellowship Programme
2013: International Research Fellowship of Tinçel Education and Cultural Foundation
2011: Research Assistant & PhD Student Fellowship of Vehbi Koç Foundation

List of Publications and Patents:

Journals:

Kabdasli, M. S., Kacmaz, E., **Bas, B.**, Oguz, E., Bagci, T. (2010). An oil spill distribution study in an industrial coastal zone, *Fresenius Environmental Bulletin*, **19,** No.9a, 1935-1945.

International Conference Papers:

Bagci, T., Elginoz Yasa, N., **Bas, B.**, Oğuz, E., Akgul, M. A., Yuce, A., Kabdasli, S., (2009). An experimental study on geotextile usage for protection of scour under submarine pipelines, 13th Congress of Intl. Maritime Assoc. of Mediterranean IMAM 2009, 12-15 October, Istanbul, Turkey.

National Conference Papers:
Kirca, V.S.O., Elginoz, N., Civak, G., Ozkan, E., **Bas, B.**, Kabdasli, S. (2014). Today and future of multi-purpose offshore platforms in European seas: The Mermaid Project, 8th National Coastal Engineering Symposium, 7-9 November, Istanbul (in Turkish).

Kabdasli, M. S., Kacmaz, E., Elginoz Yasa, N., **Bas, B.**, Koroglu, A., (2008). Examining Coastal Area Usage Diversities and Resulted Problems in The Bosphorus. VII. National Conference of Turkey's Coastal and Marine Areas, 27th-30rd May 2008, Ankara (in Turkish).

Bas, B., Kabdasli, S., Yuce, A. (2007). "Examining Impacts of Tsunamis on Caisson and Rubble Mound Breakwater Experimentally", 6th National Coastal Engineering Symposium, 25th-28th October, Izmir, (in Turkish).

Baş, B., Olmez, T., Tunay, O., Kabdasli, I., Kabdasli, S., (2007). Pollution Profile and Waste Minimization Study For A Shipyard, 6th National Coastal Engineering Symposium, 25th-28th October, Izmir (in Turkish).

Olmez, T., **Bas, B.**, Tunay, O., Kabdasli, I., Kabdasli, S., (2007). Pollution Profile and Waste Minimization Study For A Marina", 6th National Coastal Engineering Symposium, 25th-28th October, Izmir, (in Turkish).

Elginoz Yasa, N., Kabdasli, M. S., **Bas, B.**, Yagci, O., (2007). "Examining The Impact of Submerged Plants to Wave Characteristics", 6th National Coastal Engineering Symposium, 25th-28th October, Izmir (in Turkish).

PUBLICATIONS/PRESENTATIONS ON THE THESIS

- **Bas, B.**, Kabdasli, M. S., Erturk Bozkurtoglu, S. N., Seker, D. Z. (2012). Effect of wave direction on discharged brine dilution, *Fresenius Environmental Bulletin*, 21, No.10a, 3093-3100.

- **Bas, B.**, Kabdasli, M. S., Erturk Bozkurtoglu, S. N. (2011). An experimental study on brine disposal under wave conditions. *14th Congress of Intl. Maritime Assoc. of Mediterranean (IMAM)*, September 13-16, Genova, Italy.

- **Bas, B.**, Kabdasli, M. S., Erturk Bozkurtoglu, S. N., Seker, D. Z. (2011). Brine dilution under codirectional wave attacks. *16th International Symposium on Environmental Pollution and its Impact on Life in the Mediterranean Region, (MESAEP)*, September 24-27, Ioannina, Greece.